POLITECNICO
MILANO 1863

SCUOLA DI INGEGNERIA INDUSTRIALE
E DELL'INFORMAZIONE

MPC comparisons for residential HVACs and parametric optimization of compact DEC system

Department Of Energy
Doctoral Programme in Energy and Nuclear Science and Technology

Author: **Ettore Zanetti**

Student ID: 10391315
Supervisor: Prof. Marcello Aprile
Tutor: Prof. Livio Mazzarella
PhD Cycle: XXXIV

Acknowledgements

First, I would like to acknowledge my thesis advisor Professor Marcello Aprile. I would like to express my deepest gratitude for his guidance throughout my years in the research group, as a student, then a researcher and then again as a PhD student, it has been an incredible journey that would not have been possible without him as a mentor. I am also extremely happy and honored to be the first supervised student since he got his professorship. Then I want to express my deepest thanks to my PhD tutor, Professor Livio Mazzarella, who was always there to help me shape the direction of my research work and give deep and meaningful feedback. I am also extremely grateful to my day-to-day mentor and supervisor, PhD Rossano Scoccia, who I must thank for the constant support and feedback. My journey in research would probably not have started without seeing the contagious passion and enthusiasm that Rossano showed me before starting the PhD, and the wonderful research group he coordinates, the "Veluxiani". I would like to thank all of them starting from the former members, Marica and Davide to Rossella, Mohammad, Giulia, Paola and Letish, for these wonderful years together. I would like to thank all the professors and researchers that helped me throughout my PhD by sharing their knowledge and expertise. David Blum and Donghun Kim for their continuous support during my exchange period at LBNL. Francesco Casella for all our chats on numerical simulation and modelling, and my thesis reviewers Alberto Leva and Marco Simonetti for helping me putting the finishing touches to my dissertation. Then I would like to acknowledge the head of the whole research group Professor Mario Motta to thank him for the support throughout this whole endeavor and for creating such a wonderful working environment in the ReLab research group that I consider an extended family, and I would also like to thank all its members for the support and assistance during the long days of experiments. Talking about family, words cannot express how thankful I am to my wife Thao. Her contagious passion for science, drive and hard work, honesty and generosity has been an inspiration and motivation for me to always to overcome any obstacles and reach the end of my PhD and improve as an individual. Finally, I will switch to Italian. Grazie a tutti i miei famigliari e amici che mi hanno sostenuto, supportato e sopportato durante questi anni di studio. Per concludere, grazie mamma e papà per tutto il supporto che mi avete dato durante questi anni. Mi avete dato la possibilità di studiare e poter esplorare tutte le mie passioni, permettendomi di arrivare fino a questo risultato. Grazie con tutto il cuore, non potrei desiderare niente di diverso.

Abstract

Reducing energy consumption and increasing renewable penetration are necessary to mitigate climate change and achieve sustainability goals. In the building sector, HVAC systems (heating ventilation and air conditioning) account for 20% of the primary energy consumption in developed countries. Furthermore, demand, especially cooling in developing countries, could increase by up to 50% by 2050. Most of the cooling is carried out by electrical chillers further straining the power grid. Thermally activated Desiccant Evaporative Cooling (DEC) systems have become a possible alternative. However, traditional DEC systems are bulky and not suitable for residential applications. Compact DEC systems are being developed, but research is still needed. This thesis aims to study and optimize a compact DEC system named FREESCOO numerically and experimentally. This specific DEC and in general HVAC systems can benefit from advanced control, since it can help reduce discomfort, running cost and environmental impact. Advanced control, including Model Predictive Controllers (MPC) have a large variety of possible formulations even for the same HVAC system. This left a gap in literature on the influence of each formulation and solver choice. Furthermore, MPC is mainly studied for commercial buildings because in general it is not economically favorable for residential buildings. The aim is to analyze common MPC formulations to find the most suitable methodology and find a way to improve the local controller in a residential scenario using know how coming from an off-line MPC. The case study analyzed is a two-room apartment in Milan that uses floor heating coupled with a heat pump for heating and FREESCOO together with a district heating for cooling. 250 data points were collected for two FREESCOO iterations and a 2D finite volume model was calibrated and validated with less than 6% NRMSE. Then, optimizing phases times thermal COP was increased by 20% for the cooling season. MPC comparisons lead to the conclusion that nonlinear MPCs do not bring benefit at the cost of longer computational time and more instability in the convergence. Lastly, using the MPC results pre-on and pre-off parameters were found to deal with floor heating high thermal inertia reducing by 90% discomfort in the heating season.

Keywords: HVAC, optimal control, DEC, MPC comparison, residential

Sommario

Ridurre il consumo energetico ed aumentare la penetrazione di rinnovabili è necessario per mitigare il cambiamento climatico e ranggiungere i target di sostenibilità. Gli HVAC consumano il 20 % dell'energia primaria nei paesi sviluppati. Inoltre, la domanda potrà aumentare del 50 % entro il 2050, specialmente di raffrescamento in paesi in via di sviluppo. La maggior parte del raffrescamento è fatta con condizionatori elettrici che appesantiscono ulteriormente la rete elettrica. I condizionatori dessicanti evaporativi (DEC) attivati termicamente possono essere un'alternativa. Purtroppo, i DEC tradizionali sono ingombranti e difficilmente integrabili in realtà residenziali. Si stanno studiando DEC più compatti, ma ulteriore ricerca è necessaria. La tesi si pone l'obiettivo di studiare ed ottimizzare un sistema DEC compatto chiamato FREESCOO da un punto di vista numerico e sperimentale. Questi DEC e i sistemi HVAC più in generale beneficiano dal controllo avanzanto, che permette di ridurre l'impatto ambientale, i consumi ed il discomfort. Ci sono molte formulazioni per il controllo avanzato e predittivo (MPC) anche per lo stesso HVAC. Per questo motivo, c'è un vuoto in letteratura sull'influenza di ogni formulazione e scelta di risolutori. Inoltre, gli MPC sono maggiormente studiati per grossi edifici commerciali. Il secono obbiettivo è pertanto analizzare diverse formulazioni MPC per trovare la migliore e in seguito trovare un modo per migliorare la performance del controllore locale utilizzando i risultati di un ottimizzazione offline. Il caso studio scelto è un bilocale a Milano che utilizza pavimento radiante per riscaldamento accopiato ad una pompa di calore e FREEESCO con teleriscaldamento per raffrescamento. 250 punti di funzionamento sono stati raccolti per due iterazioni di FREESCOO e un modello 2D a volumi finiti è stato validato sperimentalmente con un NRMSE minore del 6 %.Ottimizzando i tempi di ciclo il COP termico è migliorato del 20 % per la stagione di raffrescamento. Comparando le diverse formulazioni MPC è emerso che gli MPC non lineari non portano benifici ma aggiugono tempo computazionale ed instabilità. Si sono ricavati preaccensione e prespegnimento usando i risultati da MPC per minimizzare l'effetto dell'inerzia termica del pavimeno radiante riducendo il discomfort del 90 % per la stagione di riscaldamento.

Parole chiave: HVAC, controllo predittivo, condizionatore dessicante evaporativo

Contents

1 | Introduction

1.1. Energy background

Energy plays a key role in modern society and more is needed to increase the worldwide standard of living to an acceptable level. However, the increasing demand for energy is in contrast with the sustainability goals to mitigate the climate change effect. Therefore, particular focus should be put on the development of the more energy hungry sectors. The building sector is one of the largest energy consumers, in particular, heating and cooling systems account for 20% of primary energy consumption and a comparable amount of carbon dioxide emissions in Major Economic Forum (MEF) countries [1]. If no action is taken to improve energy efficiency in the building sector, energy demand is expected to rise by 50 % by 2050 [2]. Therefore, energy efficiency, net zero energy buildings and low-carbon technologies will play a crucial role in the energy transition needed to make the change happen [3].

1.1.1. Cooling issue

A large portion of this energy consumption increase is due to cooling needs in developing countries and the rise of the average temperature due to climate change [4]. The majority of the cooling is carried out by vapour compression systems that run mainly on electricity increasing the strain on the power grid. Therefore, alternatives that do not run mainly on electricity are needed.

In the last decade, Desiccant Evaporative Cooling (DEC) systems have become a possible alternative to traditional vapour compression based air conditioning systems, heat pumps, and chillers, as shown by [5]. These systems are based on the physical principles of evaporative cooling and desiccant dehumidification of air. In the evaporative part of the system a stream of air can be cooled by direct or indirect evaporation. In the case of direct evaporation, the air stream is cooled by water injection. This adiabatic process will lower the dry bulb temperature while increasing the relative humidity, so the drier the air stream at the beginning, the more cooling potential is available. In indirect evaporative cooling, an air to air heat exchanger is present where one stream is cooled by the direct evaporation process and the other stream is cooled via a heat exchanger. In solid DEC systems, the dehumidification of air via the adsorption process is usually carried out using the so called desiccant wheels coated by adsorption material (e.g. silica gel, lithium chloride) [6]. Two air streams go through the component at the same time, namely the regeneration and humid air streams, allowing the device to function continuously. However adsorption processes realized by means of desiccant rotors have the disadvantage of the carrying over the adsorption heat, with a consequent negative impact on the overall system performance. Furthermore, with the desiccant rotor technology, it is not possible to acquire a high adsorption capacity in the desiccant materials, since the rotor coating cannot be too thick. Lastly this kind of system is usually employed for non residential application due to space constraints. [7] provides an extensive review on the latest developments for solid DEC systems, highlighting novel concepts using fixed bed technology. Potentially, fixed bed configurations could be used for smaller scale buildings and even apartments. However, the compactness of the fixed beds also makes the heat exchanger work in a transient intermittent operation, which is much harder to properly control with respect to a traditional rotary system.

1.1.2. Control issue

These novel DEC systems and HVAC (Heating Ventilation and Air Conditioning) systems in general can benefit from advanced control strategies, since they can help reduce environmental impact, reduce running costs, and increase comfort conditions. There are several approaches that can be defined as advanced control for the building sector. The state of the art of existing technology consists mostly of Rule Based Controllers (RBC), based on a set of hysteresis and Proportional Integral Derivative (PID) for each piece of equipment in the HVAC. Consequently, a custom heuristic RBC, a fuzzy controller, or an auto-tuning PID can be considered advanced control for the building sector. However, these are all feedback controllers that can only act upon a signal coming from the building. This approach works well when the response of HVAC is quick as for air based system. However, when considering a concrete core floor heating system, fairly common in low consumption buildings in Europe because it allows the use of lower grade heat, the dynamic response can be delayed by hours. Furthermore, today there is a need to deal with the increasing number of renewables present in the electrical grid and production demand mismatch. Buildings can be part of the solution, as they are large energy consumers and theoretically their thermal mass can be used to shift their demand [8]. However, this is not possible with traditional controllers, a promising approach to solve all these issues are Model Predictive Controllers (MPC) [9], since they can help increase renewable penetration by unlocking load flexibility potential in buildings [10, 11] and deal with slow HVAC dynamics [12, 13]. Model Predictive Controllers (MPC) [14–16], use a model of the building and its HVAC system together with forecasts of the boundaries (weather, occupancy, setpoint, ...) in order to estimate the thermal behavior of the building and the HVAC system. Then they can find the most suitable control trajectory through an optimization process to achieve a certain objective that can be comfort, energy reduction, maximization of local renewable self consumption or apply demand response strategies.

In general a multitude of modeling approaches can be found in literature for the MPC formulation and numerical implementation even for identical HVAC systems. One reason is that MPC itself has different theoretical approaches, such as centralized versus distributed, or stochastic versus deterministic. Furthermore, the objective and constraints of the MPC can be formulated in different ways regarding the quantification, relative importance, and limitations of the performance indicators (e.g., energy use, carbon emissions, energy cost, load flexibility, thermal comfort).

Then, each component of the HVAC can be modeled in several ways, leading to a delicate balance between accuracy in the prediction, robustness, and computational requirements. For example, the COP (Coefficient Of Performance) of an heat pump is a complex function of at least load ratio, external, and supply temperatures. So, changing only the COP formulation from a constant value to a function of external and supply temperature can increase the accuracy of the prediction at the cost of increasing the nonlinearity of the objective function, which can decrease the robustness to find an optimal solution and increase computational requirements. Furthermore, physical control inputs (e.g., percent valve position) can be used as optimal control variables directly, though this could result in a formulation that includes nonlinearity and integer variables, leading to a Mixed Integer NonLinear Programming (MINLP) problem. On the other hand, heat flow rates could be selected as optimal control variables. In this case, the resulting problem could result in a linear or quadratic programming, which exhibits better mathematical properties (e.g., numerical efficiency and convexity). However, converting the optimal control trajectory into useful physical control inputs for the HVAC system becomes more difficult as the system complexity increases. As a consequence, a significant amount of time could be spent iterating to identify the most suitable optimization formulation for each HVAC system. Lastly, advanced control cannot be used directly in a small residential case study. The reason is the cost of the implementation. A potential solution could be the use of a cloud solution, where all the computations can be implemented. However, a real time implementation depends on the availability of the web communication and increases the safety risks [17]. A good compromise could be to extrapolate useful rules from offline optimization run on the cloud and do a sporadic re tuning process of the local micro controller that does not strain the communication system. Furthermore, this solution could be implemented in a lot more existing households with ease of implementation such as a firmware update of the micro controller.

1.2. Literature review

This section shows that state of the state of the art of predictive control in sub section 1.2.1 and shows the application gap that this thesis is trying to fill. In sub section 1.2.2 is shown a review on the compact DEC system FREESCOO and its possible application to a residential case study is discussed.

1.2.1. Model Predictive Control

A lot of the text in this section belongs to the manuscript [18], where I am the first author, a draft is attached to Appendix A. [19] does an extensive review on advanced predictive controllers for building types, highlighting the benefit of each approach and leading to the conclusion that potentially MPC can have the best performance for commercial buildings where the economy of scale is sufficient to justify setup and running costs. For the residential case instead cheaper solutions that require less computational power and setup time are to be preferred. This aligns with the idea of implementing a cloud based solution that can be employed for several houses, increasing the economy of scale and reducing the final implementation costs. The first step is to identify the correct MPC methodology to apply to the case study.

[14, 20] provide a comprehensive review on building MPC literature. From their studies it emerges that a lot of work has been done to try and address the benefit and applicability of different MPC formulations.

Considering MPC architecture and theoretical approach, [21, 22] compare centralized and distributed MPC architectures, highlighting that distributed approaches have slightly worse comfort and energy saving performance but better computational time. [23–26] compare deterministic versus robust or stochastic MPC, showing that stochastic or robust have a better performance in high uncertainty scenarios and comparable in others. Rather than focusing on architecture and theoretical approach, [27, 28] instead analyse the MPC problem formulation focusing on different cost function and constraints, assessing which formulations are more robust and computationally efficient, but limiting their analysis to Linear Programming (LP), Quadratic Programming (QP) and Mixed Integer Linear Programming (MILP).

Considerable effort was also put into analyzing different building envelope thermal modeling approaches. [29] compared several black box and grey box model structures for modeling the building envelope systems and concluded that black box models are more computationally efficient for larger case studies but become less reliable for longer prediction horizons. [30] analyzed the effects of grey box model order on the performance of MPC for concrete core activated buildings. [31] also shows that model order has a strong influence on the model quality. Furthermore, [31] identified seven factors that play an important role in the building envelope model accuracy. [32, 33] show that a purely physical driven white box approach can be viable in certain building types.

Less comprehensive work is available on comparison about HVAC modeling and optimal control variable choice and their impact on the resulting MPC formulation. [34] performed an extensive analysis on the impact of different COP formulations in the MPC problem leading to linear programming and nonlinear programming problems, highlighting the potential benefit of a nonlinear formulation. [35] compares a linear time invariant MPC, a linear time variant and a nonlinear MPC in a case study with a heat pump and domestic hot water. The results show that the nonlinear solution is the best one, but the linear time variant gets close and remains more robust. In both [34, 35] cases, binary variables are not taken into account, avoiding mixed integer nonlinear programming formulations, which arise fairly commonly when dealing with HVAC systems. Indeed, I did not find any study comparing MINLP with other formulations, only [36] introduces a custom MINLP solver comparing with Bonmin [37] for a solar thermal system. Furthermore, it is especially hard to cross compare different works due to lack of common case study and common metrics. Therefore, there is a need of a comprehensive comparison between different formulations even on the same case study that will allow to choose the most suitable MPC methodology.

1.2.2. FREESCOO desiccant evaporative cooling system

One of the novel concepts mentioned in [7] is FREESCOO. FREESCOO is an acronym that stands for FREE Solar COOling [38]. It is a compact solar powered DEC air conditioning system that can dehumidify, cool, and heat thermal zones for the residential and commercial sectors. FREESCOO was developed by Solarinvent, a startup created in Italy at the beginning of 2014 [39]. [40] highlights the major benefits of fixed bed heat exchangers and in particular the FREESCOO solution with respect to a traditional desiccant rotor based DEC system:

- higher dehumidification rate because the adsorption material is continuously cooled during adsorption phase;
- higher storage potential thanks to the higher mass of silica gel present in the device. This allows the system to be used also as an energy storage, regenerating it at a more convenient time and using it when the user needs cooling;
- adsorption and regeneration processes occur at different times, allowing more flexibility in tuning the dehumidification rate and heat input leading to higher thermal COP.

The last version of FREESCOO mentioned in [40] is coupled with a solar thermal panel to get the heat needed for the regeneration of the silica gel bed. Unfortunately solar thermal installations saw a drop in the last decade mainly due to the increasing competition of photovoltaic (PV) systems. One of the main reason is the massive installation of PV systems that happened after 2006 due subsidies in Europe that contributed to a fast growth of the technology and a large economy of scale reducing their price. However, in recent years low temperature district heating systems are seen as possible alternative to conventional district heating systems [41]. Working at lower temperatures allows them to integrate the renewable energy share of the network, such as solar thermal farms [42], waste heat [43] and large ground source heat pumps [44]. Furthermore, climate change caused Summers to be hotter in Norther European countries to the point where a cooling system is required and district heating systems are fairly widespread. FREESCOO is an ideal solution for this type of district network because it is designed to have a low regeneration temperature, around 60-65 (°C), close to the one of the district and the big mass of the adsorption bed can be used to conveniently accommodate the energy flexibility required by the district network. Furthermore, it solves a traditional problem of district heating networks allowing for an extensive use of the network during the summer, making the district more competitive year round. Furthermore, decoupling FREESCOO from the local solar thermal system allows for a more compact device that can be installed in an apartment rather than a single family house and can be more price competitive. Lastly, an advantage with respect to vapour compression split systems is that FREESCOO can treat external air, so it can also be used as an Air Handling Unit (AHU) addressing Indoor Air Quality (IAQ).

1.3. Thesis objectives

To address the points raised in the literature review this PhD thesis has three main objectives:

1. contribute in developing a new version of FREESCOO device that will be cheaper, more compact and that works with district heating;
2. compare different MPC formulations to partially fill the literature gap, while trying to find a general methodology applicable to a wide array of residential HVACs;
3. find a way to extrapolate useful parameters from the optimization process that can be used directly in residential micro controllers.

1.3.1. FREESCOO device development

About Objective 1, this thesis work helped Solarinvent with the development of a new FREESCOO device. In particular, I focused on modeling and analysis of the compact cooled adsorption heat exchanger, that is the core component of the device. The main activities carried out were:

- develop numerical simulation models to address the theoretical performance of the heat exchanger;

- carry out experiments on the heat exchanger to asses the real performance and validate the numerical model;
- develop a reduced order model for FREESCOO heat exchanger that can be used for optimization purposes to improve FREESCOO control.

1.3.2. MPC comparison and assessment

About Objective 2, this work tries to partially fill the literature gap by applying a number of MPC optimal control problem formulations and optimization solvers to a relatively common building HVAC system as case study. The idea is to focus on two issues that could cover a broad range of HVAC systems: 1) nonlinearity arising from the estimation of the heat pump COP and 2) binary on-off physical control inputs for distribution circuit valves. Then as an emission system a floor heating system wil considered. As mentioned in 1.1.2 floor heating systems are beneficial to increase energy efficiency of the HVAC system. However they can suffer from high thermal inertia and applying a MPC to mitigate the impact of floor heating on thermal comfort. This HVAC configuration is present in a lot of hydronic systems in Europe and the methodology applied to a specific case study could be extended to similar ones (boiler instead of heat pump, radiators instead of floor heating).

Depending on the approach to model these two issues, the resulting optimization problem formulation can be a QP, Non linear Programming (NLP), or MINLP. Each formulation encompasses a trade-off between accuracy in the prediction, robustness to find an optimal solution, and computational requirements. With these issues in mind, the goals are:

- show all the challenges faced using different modelling approaches;

- understand the benefits of increased prediction accuracy from increased model complexity and compare with the resulting losses in robustness and added computational requirements;
- survey available optimization solvers of each problem formulation, especially novel MINLP specific solvers, on a typical building HVAC optimal control problem;
- deduce which approach is more suitable in terms of Key Performance Indicators (KPI) and detailed time series analysis.

1.3.3. Rule based controller parameter extrapolation

the objective is to find useful parameters to implement in the respective micro controllers using the output of the best MPC formulation and the parametric optimization on the reduced order model for FREESCOO :

- An important characteristic of standard floor heating systems is the high thermal inertia which causes a delay between the heat supply and the response in the internal air temperature. For concrete core radiant floors this has been estimated to be 1 to 3 hours [45].This slow response can create underheating or overheating issues and consequent discomfort and/or waste of energy. The optimal control trajectory found by the MPC algorithm will take into account the disturbances forecasts and buildings dynamics to avoid both underheating and overheating. The objective will be to extrapolate useful parameters from the MPC optimal control trajectory to increase the comfort conditions, while keeping a similar energy input and cost;
- FREESCOO is a transient device, where the heat exchanger runs an adsorption phase followed by a regeneration phase. To guarantee a continuos operation two heat exchangers are present. The phases timings affect the average power output of the system. In general

a higher regeneration time, keeping fixed the adsorption time leads to an increase in average power output at the cost of lower thermal COPs. Vice versa a shorter regeneration cycle leads to lower average power outputs at the benefit of increased thermal COP. The ideal scenario is to increase the energy performance while keeping comfort. This means matching the cooling demand from the building with the average power output of the DEC system. Therefore the work will focus on tuning FREESCOO cycle times.

2 | General framework

2.1. Framework description

Starting from the objectives stated in Section 1.3, the overall framework of the thesis work can be summarized in Figure 2.1.

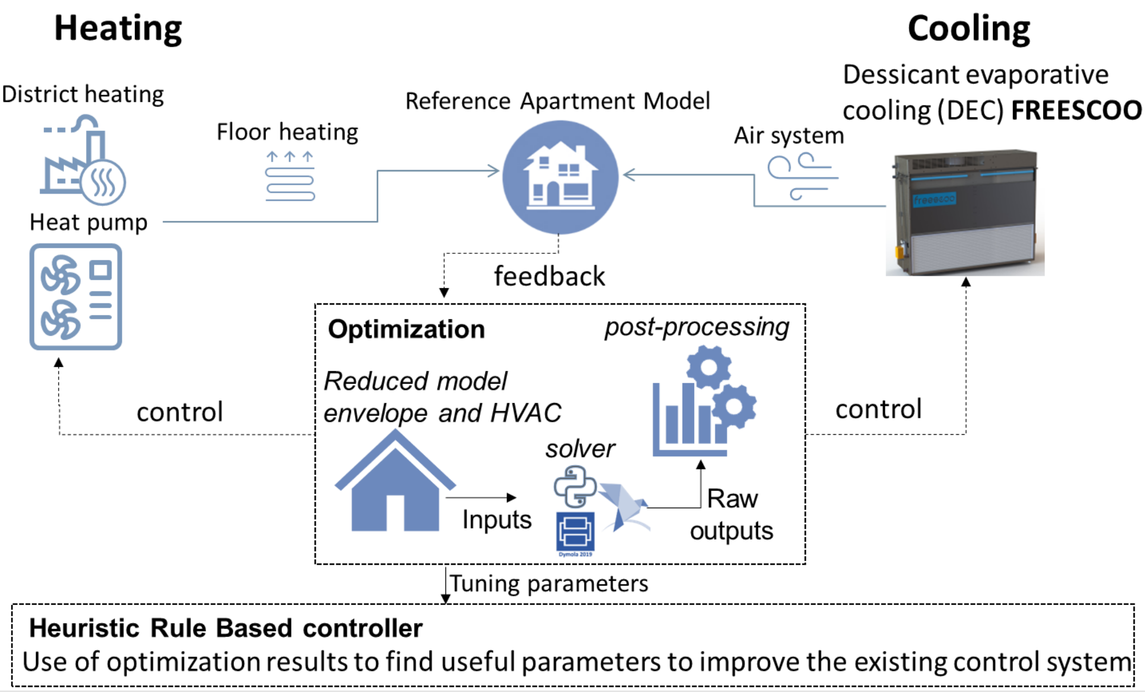

Figure 2.1: General framework of the thesis. Detailed modelling of the building and HVAC components, optimal control and parameter optimization, Heuristic rule based controller definition. Solid lines correspond to physical connection (i.e. HVAC components to building), dashed lines correspond to digital signals exchange

The diagram showed in Figure 2.1 is quite complex and in the bullet points below each element was addressed.

- The first element is the reference apartment model to be used for the whole analysis. This thesis work will consider a residential case study since one of the objectives is to improve existing micro controllers using the results of predictive control. The choice of an apartment instead of a terrace was mostly due to reasoning that district heating systems are present mostly in urban areas and serve condos.
- The second elements are the emission systems. For heating, a floor heating system was chosen over a radiator because it can be more problematic in terms of achieving comfort and control. However, needing a lower supply temperatures to work properly it makes it easier to integrate with low temperature district heating, renewables and heat pumps. Furthermore, the reference MPC formulation obtained at the end of Chapter 5 can be used also if dealing with a radiator system. For cooling, one of the objective of the thesis is to develop a novel compact DEC system so the emission system considered is air based.
- The third elements are the generation systems. For heating an heat pump was used to carry out the MPC formulation study because of the increased complexity in the optimization function given by taking into account the heat pump COP. Furthermore, the MPC formulation found can be extended to a district heating by changing the electricity price with the district price and putting the $COP \simeq 1$. In the same way it could be extended to a case study with a boiler by switching the COP for the boiler efficiency η. In regards to cooling the generation system used is the novel DEC system FREESCOO coupled with low temperature district heating for the regeneration process.
- The fourth element is the chosen HVAC optimization method to reduce consumption, improve comfort and unlock building flexibility potential. Core elements of the optimization are the reduced order models of the envelope and HVAC considered, the solver and the post

processing algorithm that interfaces with the detailed reference apartment model or with an apartment existing in a real building. For the heating case, the objective of the thesis is to compare several MPC formulations coupled with different solvers, find the most suitable one that can be generalized to similar HVAC systems. Then find a way to indirectly use these results to find key parameter to improve on the reference apartment baseline controller.

For the cooling case the objective is to optimize FREESCOO key control parameters, namely the cycle phase times, to adjust the power output with respect to the demand and maximize he thermal COP. Applying the same MPC real time methodology would be very impractical due to the extremely nonlinear, transient and integer (on-off) behaviour of FREESCO meaning that the results found would be far from a theoretical global optimum. Instead by using the reduced order model of the FREESCOO heat exchanger, for the sake of computational time, it is more robust to directly carry out a parameter optimization of the cycle phases times parameters used in the FREESCOO device.

- The last element is the assessment of the performance for the Heuristic Rule Based controller in both heating and cooling scenarios, once the parameters are determined to assess the performance improvement with respect to the baseline controllers.

2.2. Simulation and optimization tools

To carry out all the objectives shown in 2.1 careful considerations were done to assess the best tools to be used in this PhD thesis and that could be also easily extended to different case studies. The requirements and the solution found are summarized in Figure 2.2

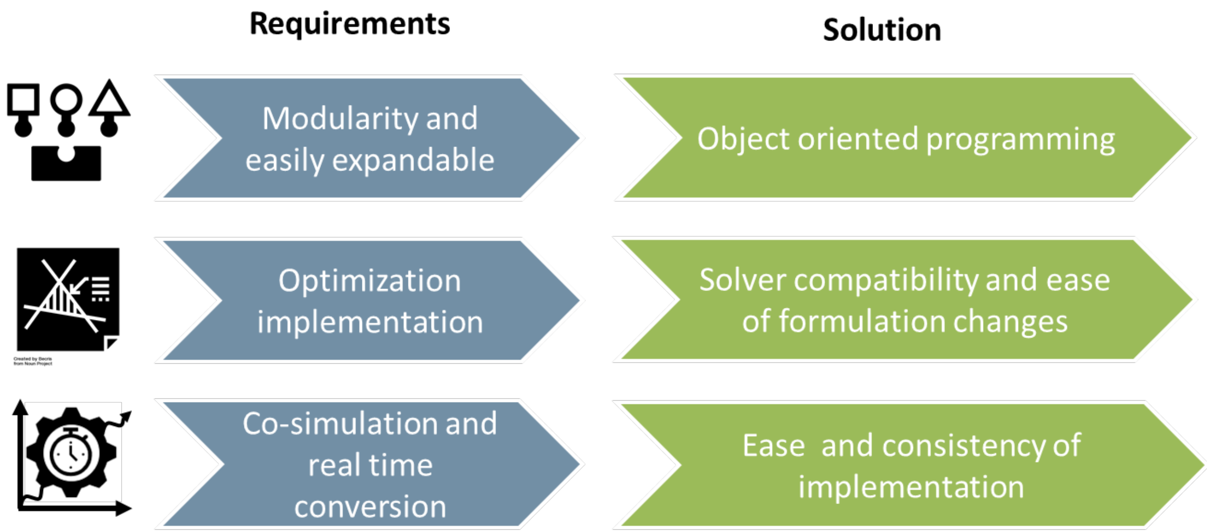

Figure 2.2: Summary of simulation and optimization tools assessment in terms of requirements and solution identified

The first requirement is that to extend the results of the PhD thesis to different case studies the simulation tool should allow models to be modular, easily expandable and customizable. However, the level of detail of the envelope and HVAC modelling should be similar to the state of the art modelling software such as E+ [46], TRNSYS and IES – VE [47] [48]. Furthermore, the development and integration of custom models, like for the FREESCOO device heat exchanger, should be as straightforward as possible. Both E+ and IES-VE do not satisfy this first requirement, since the development and integration of custom components is not straightforward. TRNSYS allows a more streamline process to develop custom components called "types", however modifying existing models is not easy if not impossible such as for the building model Type56b, which for all intents and purposes can be considered a black box for the user. Furthermore, in all this cases the physical and the numerical simulation models coincide, meaning that the modeller does not just have to write the mathematical equations describing the physical process under analysis, but also the numerical approach used to solve those equations. In this way if a different or new solution algorithm has to be tried, the whole model needs to be rewritten. This leaves room for more errors, fragmentation of the same model and more difficulty in implementing faster and more efficient computational algorithms (i.e. parallelizzation, multi rate solvers). The solution I identified to this problem is the use of object oriented programming for the handling of cyberphysical systems coupled with symbolic acausal modelling because it allows to solve both problems at the same time [49]. Firstly by having an object oriented language, different instances of the same component (i.e. heat pumps) can be derived from a single reference object making the whole modelling process more robust. Then with the use of acasual and symbolic modelling the user needs to write only the system of equations making up the physical object that has to be modelled [49]. Then the compiler with the user preference will convert the overall system of equations into its numerical form using different solvers to find the solution. Among the programming languages implementing this logic the most successful to date is the Modelica programming language [50], which implements all the aforementioned features, namely object orientation, acasual and symbolic modelling. Then, most Modelica tools allow to use the same models to be used for parameter optimization by leveraging symbolic manipulation and calculating explicit Jacobians, useful in the Newthon's method for the calculation of the global optimum. For the cooling case the optimization was carried out using the native interior point optimizer for parameter optimization of Dymola. Dymola is a commercial modeling and simulation environment based on the Modelica language. Lastly, a large open source community using Modelica in the building sector lead to the development of several Building and HVAC libraries such as the IBPSA Modelica library [51], the Buildings [52] and the IDEAS [53]. The core components of these libraries will be used in the development on the case study models for the reference apartment. I actively participated in the development of some IBPSA models, in particular I developed the test suite for the weather BESTEST comparing the weather simulation performance of several building simulation software [54].

The second requirement is that several MPC formulations and optimization solvers have to be tested. Therefore the tool used has to be able to easily couple different solvers to the optimization problem definition. Furthermore, since several formulations need to be implemented the tool should allow to easily switch between them with minimal changes to guarantee the robustness of the approach, and than to possibly expand the formulations to different case studies. Several tools are available, however the two most commonly used up to date are CasaDi [55] and Pyomo [56]. Both allow to use the standard solver interface AMPL [57], which allows interface the most common solvers. The main differences between CasaDi and Pyomo are that, the first is implemented with C++ and only recently a Python interface has been released making it easier to use and co-simulate with other simulation software. Pyomo instead is natively developed as a Python interface, furthermore it is structured as an object oriented tool where each optimization problem can be characterized as an object making it easier and more robust to apply changes to test different formulations of the same problem. For this reason Pyomo was chosen to carry out the MPC formulations comparisons.

The tested solvers are SCIP [58], Baron [59], Bonmin [37] for the MINLP problem class. These MINLP solvers are among the best performers according to [60], which analyzed their performance on a set of 335 convex MINLP problems and included both open source and commercial solvers. IPOPT [61] is among the most used NLP solvers and so it was chosen for the NLP and QP problems.

The last requirement is that the reference apartment developed in Modelica and the MPC formulations developed in Pyomo have to be coupled in a co-simulation environment. For this purpose, the tool used must take the

Modelica models developed and easily interface them with the optimal control algorithms in terms of input-output. Furthermore it should also provide consistent boundary conditions forecasts for the optimization and a result analysis in terms of Key Performance Indicators (KPI). The software BOPTEST [62], that I helped beta test during a one year exchange period, responds to all this requirements by wrapping the Modelica models into an Application Programming Interface (API) that can be easily coupled via a Python script. Furthermore, it provides as output a standard subset of KPIs, including thermal discomfort, energy consumption, cost of the energy and computational time ratio. In this way, it will be possible to consistently compare all the MPC formulations on the same emulator and highlight the pros and cons of each approach.A more detailed explanation of the co-simulation is given in Section 5.3.

2.3. Case study selection

Starting with the building envelope model, the chosen case study is a two room apartment in the south of Milan. It is part of the European Climate-KIC co-financed project Merezzate+. It was chosen for the availability of monitored data for the validation of the building fabric model and for the availability of a cloud communication infrastructure that allow in future works to implement this thesis results in some test apartments micro controllers. Furthermore, a low temperature 4^{th} generation district heating and FREESCOO are also part of the project and the final iteration of the FREESCOO device is installed in some of the apartments. The low temperature 4^{th} district helps increasing the overall efficiency of the district [63] by reducing distribution losses and pumping costs of the network for the same energy supplied, FREESCOO is designed to work with such temperatures. Differently from the actual Merezzate+ case study, the thesis case study scenario employs an heat pump as generation system for heating to carry out the MPC comparison analysis. The reason is that heat pumps are more complex than a district heating, since the heat pump COP is a complex function of partial load and external and supply temperatures, providing a wider range of MPC formulations as explained in the previous section. Furthermore, the results and conclusion can be easily extended to the case study with only the district heating. So in Figure 2.4 is shown the HVAC scheme for the MPC formulation analysis in the heating scenario. A summary of the building district, the apartment and the generation technologies employed is given in Figure 2.3.

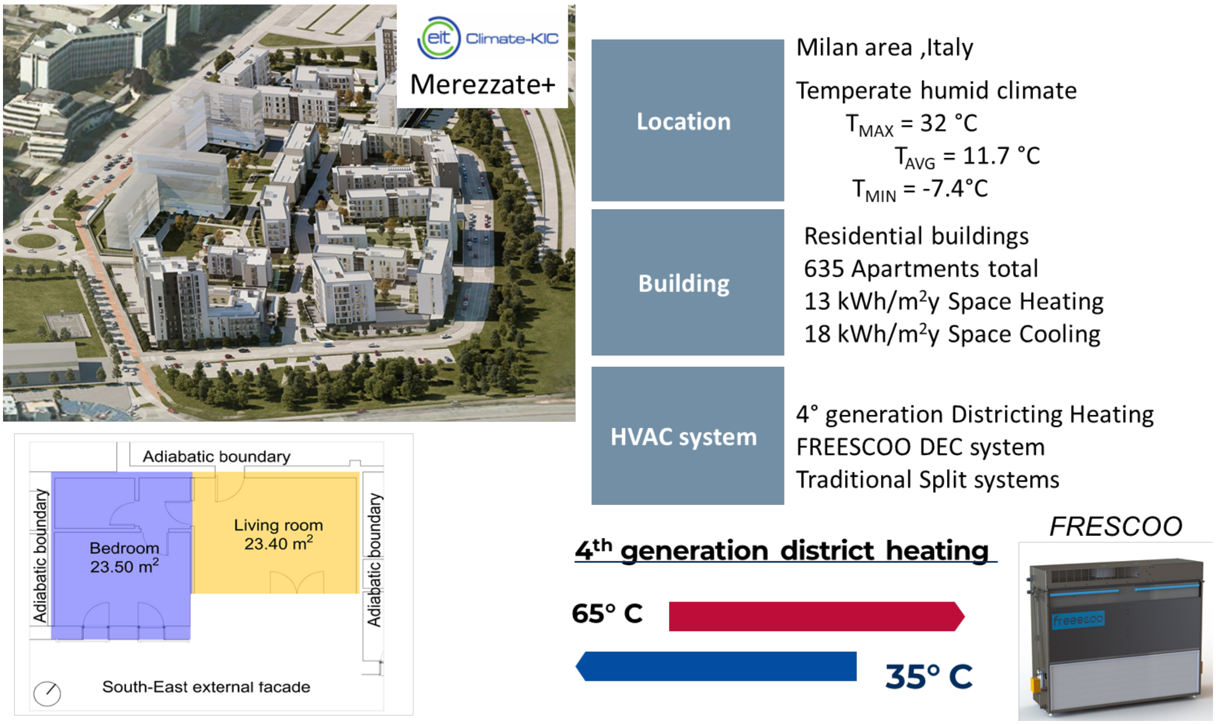

Figure 2.3: Merezzate+ district summary, on the left a render of the district, on the right a summary of Milan weather, apartment consumption and HVAC

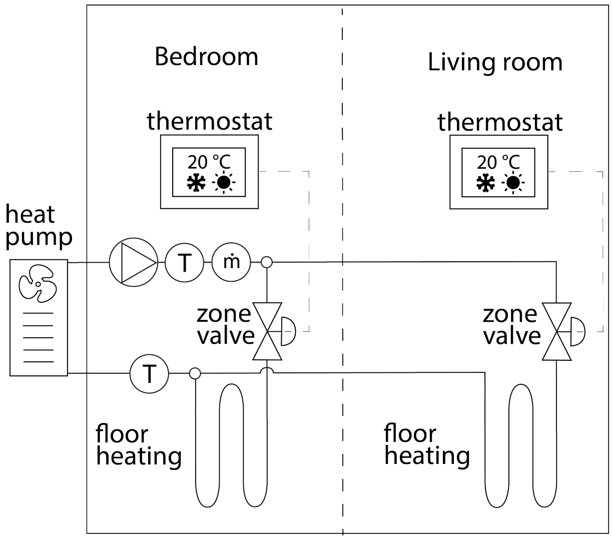

Figure 2.4: Two room apartment HVAC scheme for MPC analysis in heating operation mode

Despite its simplicity, the case study includes the most common HVAC hydronic system components, thus allowing the authors to apply several optimal control models leading to different problem classes to be solved: QP, NLP and MINLP.

The detailed emulator model for the apartment and the HVAC system was developed in Modelica using the IBPSA 3.0 (master branch commit 8a0d2372) [51], Buildings 8.0 (master branch commit 69bb7cf6) [52] and IDEAS 2.1 (master branch commit 5c8f4a93) [53] libraries.

For the cooling case study instead, FREESCOO is used as air conditioner coupled with the District Heating (DH) for the regeneration as shown in 2.5.

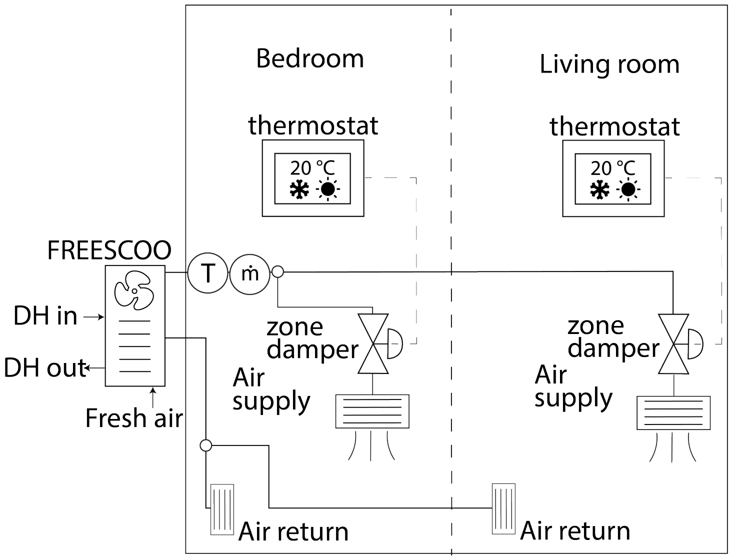

Figure 2.5: Two room apartment HVAC scheme for FREESCOO analysis in cooling and dehumidification operation mode

In this case the same Modelica libraries Buildings and IBPSA based envelope model was used. Furthermore, a Modelica library named FREESCOO was developed throughout the PhD work that includes, a 2-D model of the FREESCOO heat exchanger, a reduced order model for parameter optimization and a model of the whole FREESCOO device.

3 | The case study of Merezzate+

In this chapter the case study of the PhD thesis is layed out in detail. Section 3.1 reports the apartment envelope in terms of description, simulation modelling and calibration. Then the HVAC system used for the heating case study the heating and cooling cases studied are explained more in detail.

3.1. Envelope model

The envelope model is described first in terms of physical and geometrical properties in Sub section 3.1.1. Then in terms of boundary conditions taken from the Milan typical year weather in Sub section 3.1.2,occupational schedules and internal gains. Finally a brief showcase of the Modelica Buildings implementation is shown including a calibration process carried out from experimental data obtained in Merezzate in Sub section 3.1.3.

3.1.1. Physical and geometrical properties

In Figure 3.1, a schematic of the apartment is presented. In general the apartment can be considered a well insulated heavy construction. A brief summary of the physical and geometrical properties is given in Table 3.10. For a more detailed showcase, the properties of each wall highlighted in the figure are shown in Table 3.1 for the external wall, 3.2 for the internal partitions, 3.3 for the elevator separator, 3.5 for the ceiling and 3.6 for the floor properties. All the layers are defined from the external surface to the internal surface. For the nomenclature,N is the layer position,

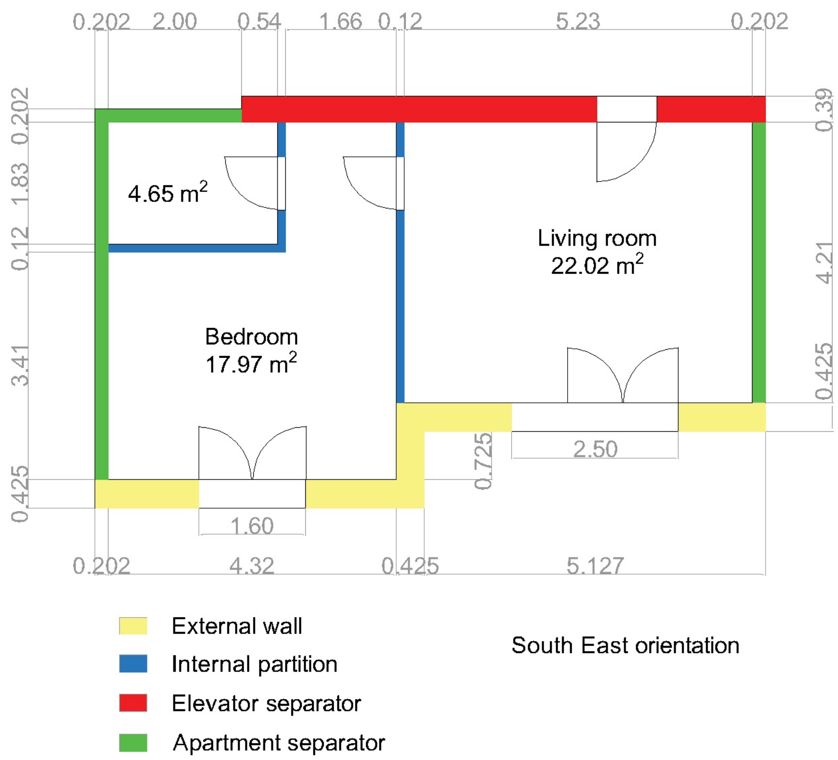

Figure 3.1: Case study apartment scheme

$x(m)$ is the thickness of the layer, Description stands for the material type, $k(W/m/K)$ is the thermal conductivity, $c(J/kgK)$ is the specific heat capacity, $d(kg/m^3)$ is the density, abs_{IR} and abs_{Sol} are the long wave and short wave absorption coefficients respectively.

Table 3.1: External wall properties

N	Description	x (m)	k (W/(mK))	c (J/kgK)	d (kg/m^3)	absIR (-)	absSol (-)
1	Exterior plaster	0.005	0.3	840	1300	0.9	0.6
2	EPS 120 thermal insulation panel	0.1	0.034	1250	23	-	-
3	Masonry brick	0.3	0.207	840	750	-	-
4	Gypsum plaster	0.02	0.57	1000	1300	0.9	0.6

Table 3.2: Internal partition properties

N	Description	x (m)	k (W/(mK))	c (J/kgK)	d (kg/m^3)	absIR (-)	absSol (-)
1	Gyproc Duragyp panel	0.0125	0.25	1000	1025	0.9	0.6
2	Plasterboard panel	0.0125	0.25	1000	710	-	-
3	Glass wool insulation panel	0.07	0.04	840	40	-	-
4	Plasterboard panel	0.0125	0.25	1000	710	-	-
5	Gyproc Duragyp panel	0.0125	0.25	1000	1025	0.9	0.6

Table 3.3: Elevator shaft partition properties

N	Description	x (m)	k (W/(mK))	c (J/kgK)	d (kg/m^3)	absIR (-)	absSol (-)
1	Gypsum plaster	0.02	0.57	1000	1300	0.9	0.6
2	Concrete	0.3	2.15	880	2400	-	-
3	Glass wool insulation panel	0.045	0.038	1030	13	-	-
4	Plasterboard panel	0.0125	0.25	1000	710	-	-
5	Gyproc Duragyp panel	0.0125	0.25	1000	1025	0.9	0.6

Table 3.4: Apartments separator wall properties

N	Description	x (m)	k (W/(mK))	c (J/kgK)	d (kg/m^3)	absIR (-)	absSol (-)
1	Gyproc Duragyp panel	0.0125	0.25	1000	1025	0.9	0.6
2	Plasterboard panel	0.0125	0.25	1000	710	-	-
3	Glass wool insulation panel	0.07	0.04	840	40	-	-
4	Plasterboard panel	0.0125	0.25	1000	710	-	-
5	Glass wool insulation panel	0.07	0.04	840	40	-	-
6	Plasterboard panel	0.0125	0.25	1000	710	-	-
7	Gyproc Duragyp panel	0.0125	0.25	1000	1025	0.9	0.6

Table 3.5: Ceiling properties

N	Description	x (m)	k (W/(mK))	c (J/kgK)	d (kg/m^3)	absIR (-)	absSol (-)
1	Ceramic tiles	0.015	1	840	2300	0.9	0.6
2	Concrete slab with additive	0.064	1	880	1800	-	-
3	Expanded polystyrene	0.026	0.034	1300	25	-	-
4	Isover fonasoft	0.006	0.113	2100	450	-	-
5	Light substrate	0.105	0.1	1200	400	-	-
6	Reinforced concrete (1% steel)	0.23	2.3	1000	2300	-	-
7	Gypsum and sand plaster	0.2	0.8	1000	1600	0.9	0.6

Table 3.6: Floor properties

N	Description	x (m)	k (W/(mK))	c (J/kgK)	d (kg/m^3)	absIR (-)	absSol (-)
1	Gypsum and sand plaster	0.2	0.8	1000	1600	0.9	0.6
2	Reinforced concrete (1% steel)	0.23	2.3	1000	2300	-	-
3	Light substrate	0.105	0.1	1200	400	-	-
4	Isover fonasoft	0.006	0.113	2100	450	-	-
5	Expanded polystyrene	0.026	0.034	1300	25	-	-
6	Concrete slab with additive	0.064	1	880	1800	-	-
7	Ceramic tiles	0.015	1	840	2300	0.9	0.6

For the glazing systems there is one window in each room. They are two double panel windows and a detailed description of glazing system properties are reported in Tables 3.7 and 3.8.

Table 3.7: Glazing systems dimensions

Thermal zone	height (m)	length (m)
Living room	2.35	2.5
Bedroom	2.35	1.6

Table 3.8: Glazing systems optical properties

N	Descripti	x (m)	k (W/mK)	tauSol (-)	rhoSol (-)	tauIR (-)	absIR (-)
1	Glass	0.003	1	0.6	0.075	0	0.84
2	Air	0.013	-	0.6	-	-	-
3	Glass	0.003	1	0.6	0.075	0	0.84

Lastly the floor heating system needs to be characterized. The active layer of the floor heating is $N = 4$ in the floor stratigraphy in Table 3.6, meaning that it is placed under a concrete layer and can be considered a high mass floor heating system. Two heating circuits per room are present, the properties of the circuit pipes are shown in Table 3.9.

Table 3.9: Floor heating pipes properties

Name	Value
Outer Diameter (m)	0.017
Inner Diameter (m)	0.015
Roughness (m)	7E-06
Density (kg/m^3)	983
Thermal conductivity (W/mK)	0.4
Circuit pipe distance (m)	0.1

3.1.2. Boundary conditions

In this section are reported the boundary conditions used for the simulations carried out in most of the heating and cooling scenarios. In terms of weather a typical year, TMY3, in Milan was considered.In Figures 3.2, 3.3 and 3.4 of the typical year, Milan can be considered a continental temperate humid climate. The maximum $T_{DryBulb}$ is 32 (°C), the minimum is -7.4 (°C) and the average 11.7 (°C).

The other boundary conditions, including occupation, setpoint schedules for heating and cooling, sensible heat gains and latent heat gains considered are summarized in Table 3.10, The setpoint and occupation profile come from the hypothesis of a two working people that go to work during the week from 8 a,m, to 20 p.m and stay at home during the weekend. The internal gains were obtained from the ASHRAE standard 90.1 for low consumption buildings and the UNI/TS-11300-1:2014.

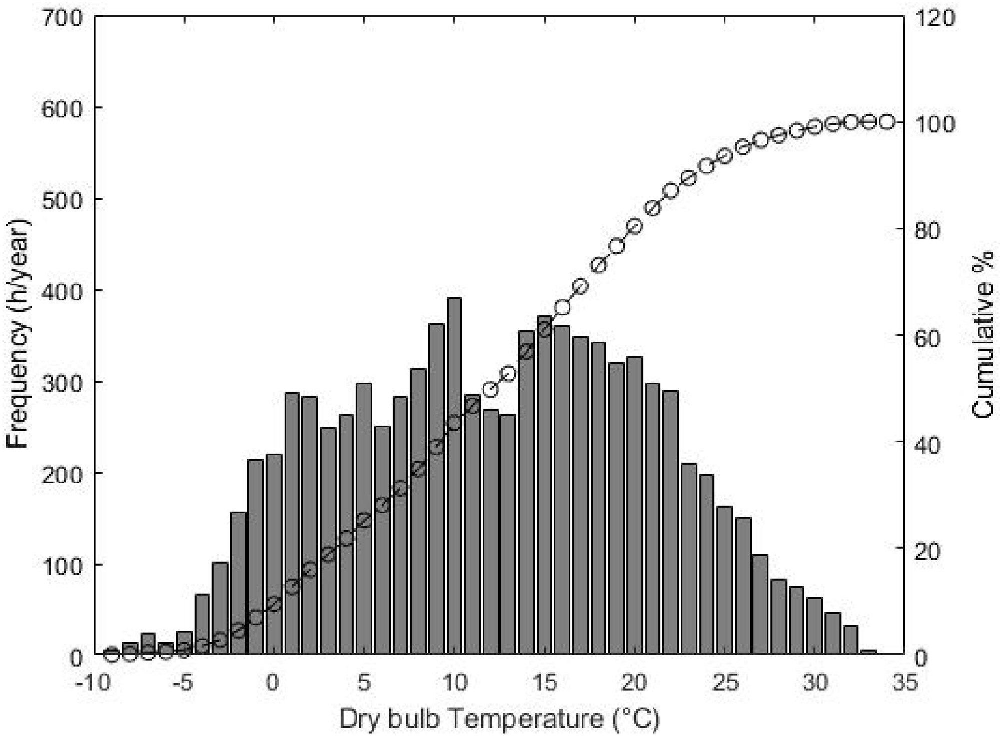

Figure 3.2: Dry bulb temperature yearly frequency for Milan typical year weather data

Table 3.10: Apartment properties

Total surface	44.5 (m^2)
Total Volume	30.3 (m^3)
Total window area	8 (m^2)
External surface area to volume ratio	0.25 (1/m)
Average external transmittance	0.46 ($W/(m^2/K)$)
heat pump nominal capacity	5 (kW)
Occupation period	from 20 p.m. to 8 a.m. for weekdays and occupied during the weekends
Heating setpoint Cooling setpoint	21 (°C) Setpoint and 18 (°C) Setback 26 (°C) Setpoint and 28 (°C) Setback
Total sensible loads	300 (W) when occupied
Total latent loads	80 (W) when occupied

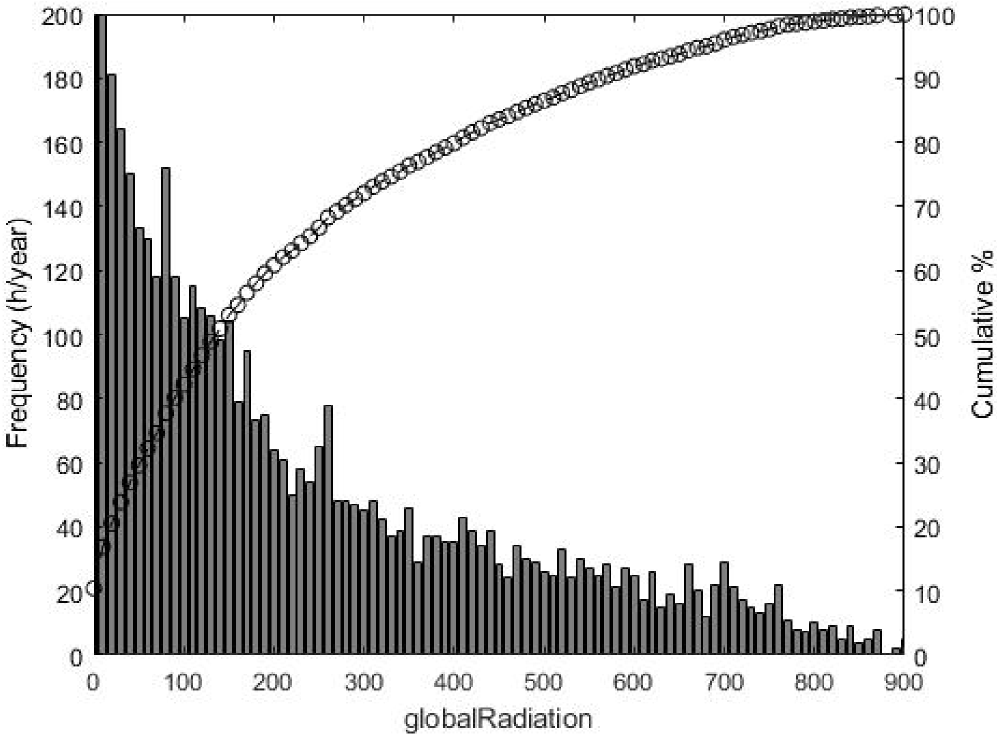

Figure 3.3: Global horizontal radiation yearly frequency for Milan typical year weather data

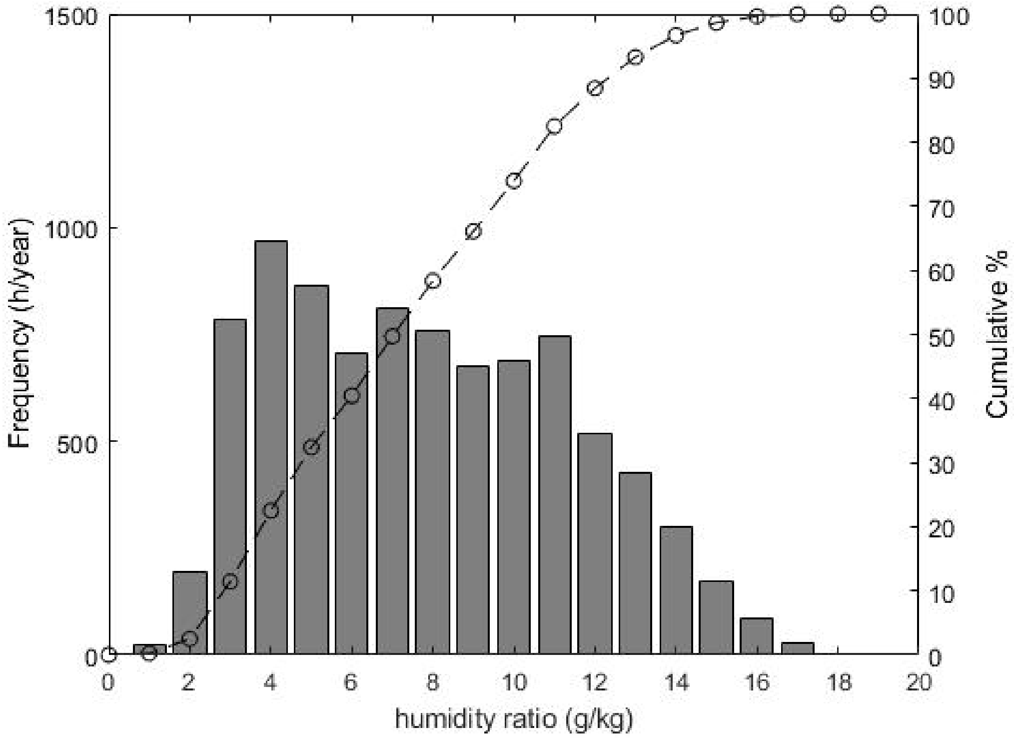

Figure 3.4: Humidity ratio yearly frequency for Milan typical year weather data

3.1.3. Detailed model and calibration

From the available properties and boundary conditions a suitable two thermal zone model was developed using the Modelica Buildings library, a screenshot of the Buildings Modelica envelope model is shown in Figure 3.5.

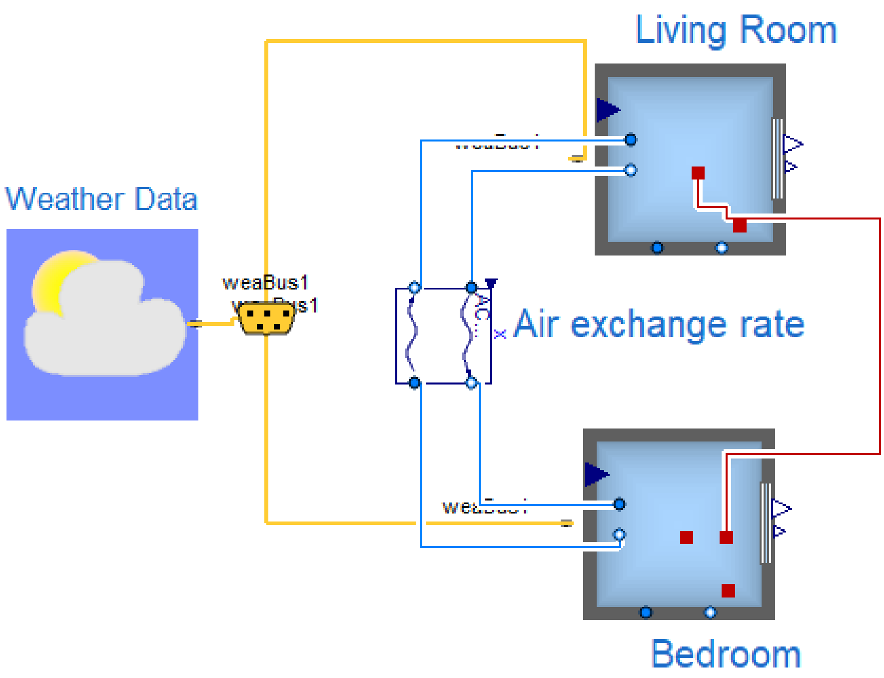

Figure 3.5: Two room apartment modelled using the Modelica Buildings library.On the left the weather data reader (yellow lines connect the boundaries to the thermal zones) and on the right the two thermal zones coupled with both a thermal connection between the shared wall (red line) and an aeraulic connection through the air exchange model (blue lines).

For more details on the modelling principles behind the Thermal zone model for the Buildings library the reader can check [64]. The floor heating model instead comes from TRNSYS 17 model [47]. The two zone apartment model was calibrated and validated using experimental data coming from a two week free-floating experiment carried out between August and September 2020 in a two room apartment belonging to the Merezzate+ project. The weather data for the boundary condition comes from a local Arpa Lombardia weather station, and the radiation and cloud coverage comes from the CNR weather forecast service. The indoor conditions were measured using a globo thermometer show in Figure 3.6.

Figure 3.6: Indoor globo thermometer positioned in the center of the living room. The two pictures are the two sides of the empty living room. The instrument accuracy is ± 0.23 (°C)

The calibration process involved the tuning of four parameters. The overhang shading effect that was approximated as a constant shading of 30 % from the sun entering the room and hitting the exterior wall, the offset between the local external temperature and the wind speed with respect to those available from Arpa Lombardia, namely 1.5 (°C) and 0.5 (m/s) Lastly the infiltration rate which was increased by 10 % with respect to the nominal value to reach 0,2 (vol/h) with respect to the total apartment volume of 30.3 m^3. The calibration process was carried out using the Dymola internal model calibration tool. The comparison between the experimental data and the simulation data for the living room in a validation period, not considered during the calibration, are shown in Figure 3.7.

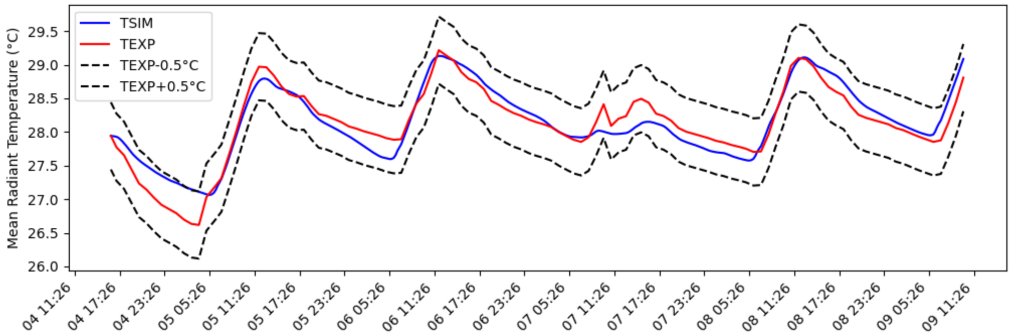

Figure 3.7: Validation simulation of living room mean radiant temperature where the globo thermometer was positioned. On x-axis the time and on the y-axis the mean radiant temperature for a week free floating experiment in September. TSIM corresponds to the simulation temperature and TEXP corresponds to the experimental measurement done with a globo thermometer. The dashed lines represent a ± 0.5 (°C), that accounts for all the possible experimental errors including instrument, forecasts and positioning

As shown in the validation figure, the mean radiant temperature in the simulations follows pretty well the experimental values with Normalized Mean Square Error (NRMSE) of 2 %.

3.2. Heating HVAC model

For the heating case the thermal zones are connected to an hydronic system modeled using Modelica as well. In particular the Buildings and IDEAS libraries have been used. In Figure 3.8 a diagram view of the Modelica model is shown.

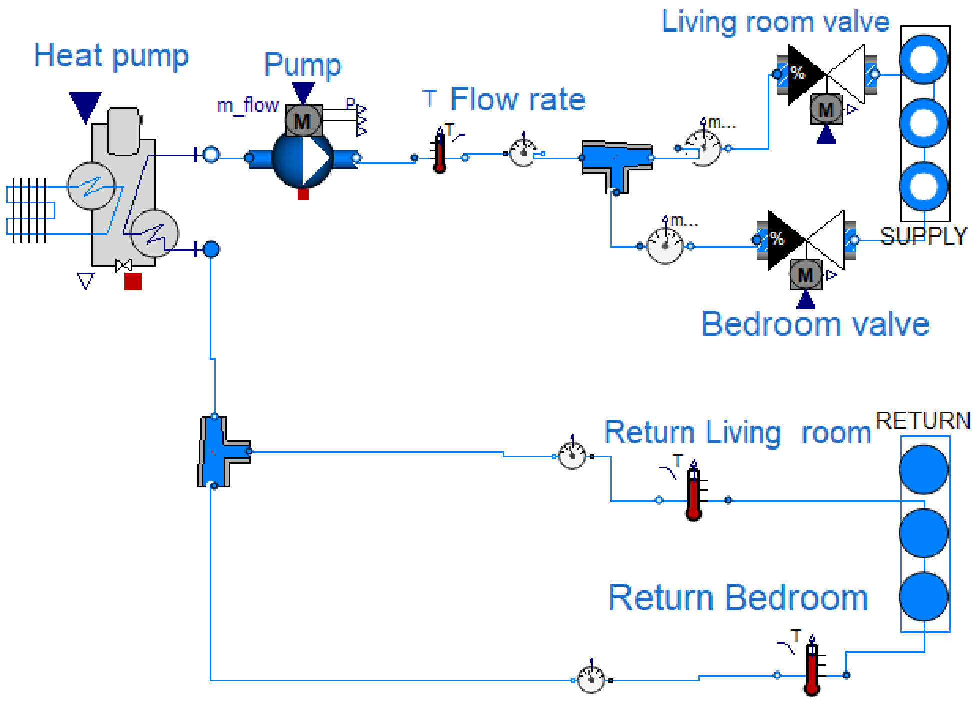

Figure 3.8: Diagram view of the hydronic circuit model. The blue lines can be imagined as physical water pipes connections, then zone valves, junctions, temperature and mass flow rate sensors are also present.

As mentioned in the Introduction an heat pump was considered instead of the district heating to give more flexibility and generality to the solution of the MPC comparison.The heat pump model is a dynamic performance map model taken from the IDEAS library with the default performance map and nominal power of 5 (kW). The reference heat pump is a Daikin Altherma and the performance map is shown in Figure 3.9,

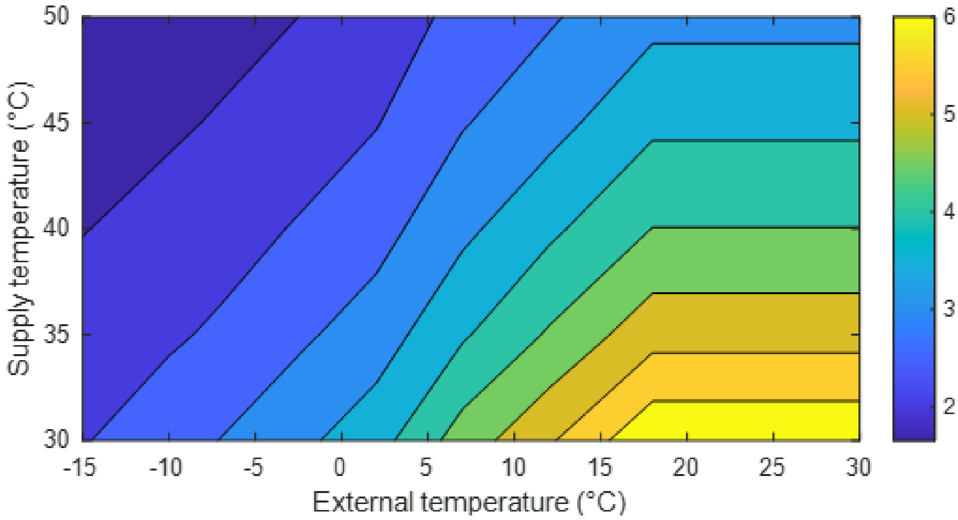

Figure 3.9: Daikin Altherma performance map. on x-axis the external temperature, on y-axis the supply temperature. The color indicates the value of the COP

The pump is an ideal constant head pump that provides the nominal flow rate to each thermal zone when on, that is, 1240 (l/h) for each thermal zone according to the design values from the apartment drawings. The circuit valves for the floor heating zone were modeled after the two-way valves of Modelica Buildings. They can be considered on/off valves without flow modulation capabilities. In the hydronic circuit are present temperature sensors, thermometer symbol, and mass flow rate sensors, clock symbol, also taken from the Modelica Buildings. Lastly, the junctions and pipes are all considered adiabatic, and the models come from the Modelica Buildings library. The supply and return ports are connected to the fluid terminals of the floor heating in their respective thermal zones.

3.3. Cooling HVAC model

For the cooling case the thermal zones air fluid nodes are connected to the FREESCOO device. In 3.10, a Modelica diagram view of the FREESCOO device is shown. The highlights are the two heat exchangers described below. The prehumidifier for the evaporative cooling side and the rehumidifier to bring the air at the outlet of the adsorption to nominal conditions of RH, that is, around 60%. The last elements are the air to water heat exchanger to warm the external air used for regeneration and the hot water coming from the district heating system modeled as a constant heat source at 60 (°C) since we are dealing with a 4^{th} generation district heating. The two heat exchanger models are explained in detail in Chapter 4, while all the other elements are taken from the Modelica Buildings library.

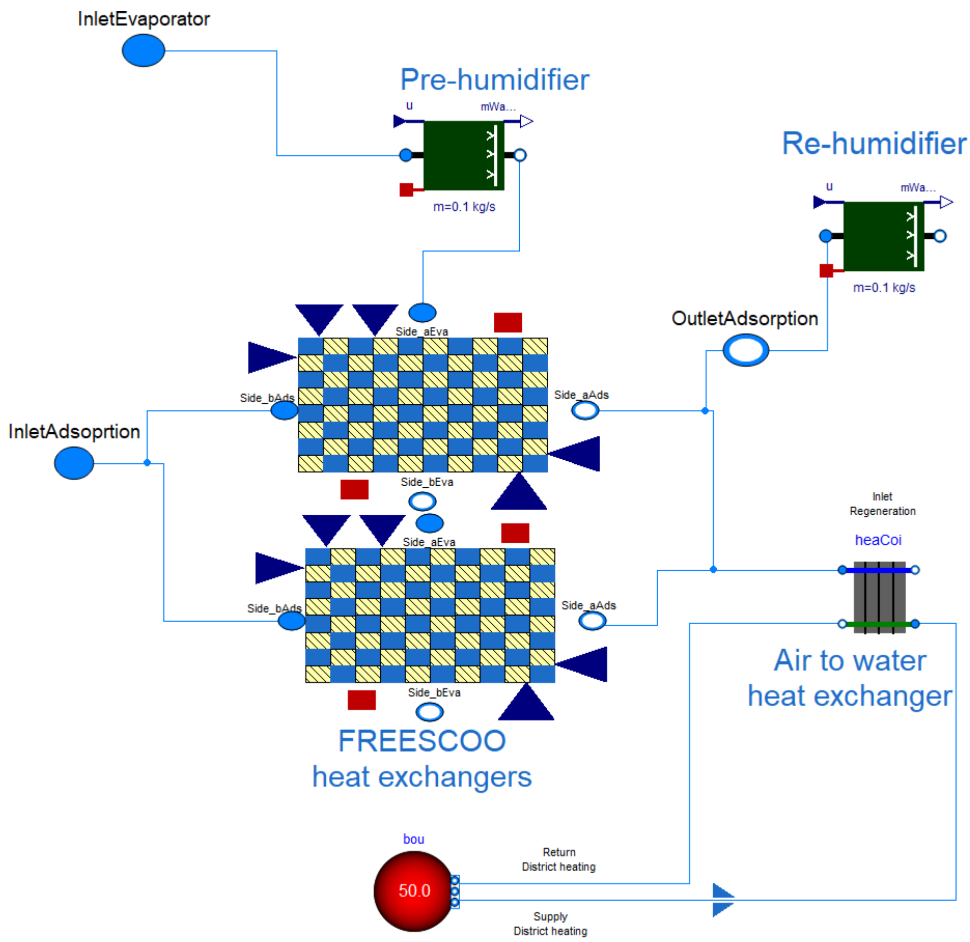

Figure 3.10: Diagram view of the FREESCOO device that includes the two heat exchangers, the humidifier for the evaporation side, the rehumidifier to reach temperature and humidity setpoints after the adsorption phase and the air to water heat exchanger for regeneration purposes

4 | FREESCOO design and optimization

This Chapter showcases the work carried out in the development of the latest version of the FREESCOO device with a particular focus on the indirectly evaporative cooled heat exchanger. Section 4.1 explains the general working principle of the FREESCOO device and heat exchanger in detail. Section 4.2 presents the experimental studies carried out by me in collaboration with Solarinvent and the ReLab research facility. Section 4.3 shows the post processing and analysis of the experimental data, addressing the found issues. Section 4.4 presents the physical modeling of the FREESCOO heat exchanger and the development of a custom Modelica library, "FREESCOO2D". Section 4.5 shows the calibration and validation of the FREEESCOO 2-D heat exchanger model based on the experimental results. Section 4.6 shows the development of a reduced order model of FREESCOO using the simulation output of the detailed 2D model. Finally in Section 4.7 the reduced order model is used to run a parametric optimization on the phases times.

4.1. FREESCOO concept

FREESCOO is a DEC system based on a compact fixed bed so that it can be installed in smaller spaces with respect to traditional rotary DEC systems like residential apartments. It works both as an air conditioner and AHU. The core component of FREESCOO is an air to air heat exchanger, where on one side we have supply air flowing on top a silica gel adsorption bed and on the other process air getting cooled through a direct evaporation process. Then this air stream will remove the heat generated by the adsorption process on the other side of the heat exchanger. When the adsorption bed is saturated the regeneration process is carried out by process air heated up by an air to water heat exchanger, where the hot water comes from the district heating. To guarantee a continuous operation two of these heat exchanger are used sequentially, while one is in adsorption phase the other one is in regeneration or precooling. In Figure 4.1 a graphical representation of the various processes is shown.

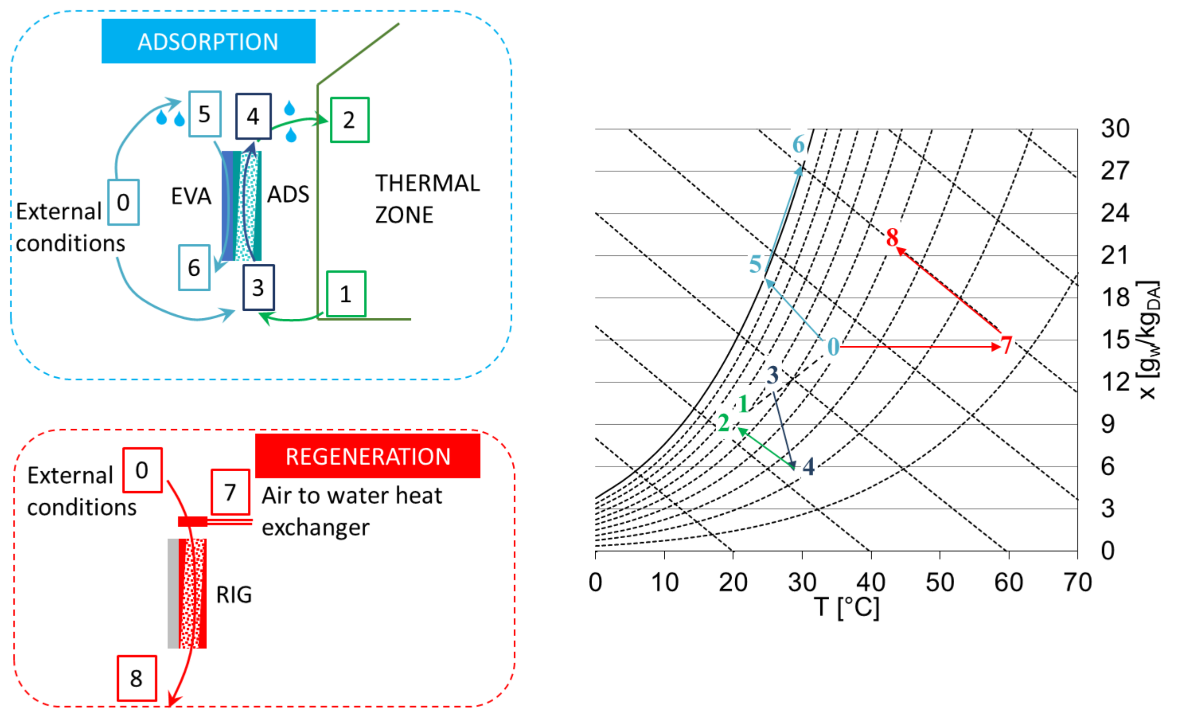

Figure 4.1: 1) blue quadrant shows the adsorption process 2) red quadrant shows the regeneration process 3) Right diagram shows transformations of the external and process moist air on a Mollier moist air psychrometric chart

The various phases shown in Figure 4.1 are described below:

Adsorption:

- (0-5) direct evaporative cooling of the process air. The external air

(0) passes through a sprinkler system that will bring it close to the wet bulb temperature (5)

- (5-6) heat exchange of the process air with the supply air, while being kept at wet bulb temperature by the water flow coming from the sprinklers and dropping in the evaporator channels until the outltet (6);
- (1-3) mixing of the supply air (1) with the external air (0) for air change purposes;
- (3-4) adsorption of the supply air moisture content by the fixed bed of silica gel and simultaneous heat exchange with the process air;
- (4-2) direct evaporative cooling of the supply air to reach the desired temperature and humidity levels;

Regeneration:

- (0-7) heating of the external air in an air-to-water heat exchanger (HX). The required energy for this step can come from solar, geothermal or waste heat source or as in this case study from a low temperature district heating;
- (7-8) desorption of the moisture trapped in the silica gel bed.

Precooling:

- (0-6) after the regeneration phase, before a new adsorption phase can start the heat exchanger is cooled down by turning on only the fan driving the process air.

Starting from the FREESCOO general concept and previous version of the heat exchanger coupled with solar thermal I contributed in the testing and evaluating of three new heat exchanger concepts summarized in Figure 4.2.

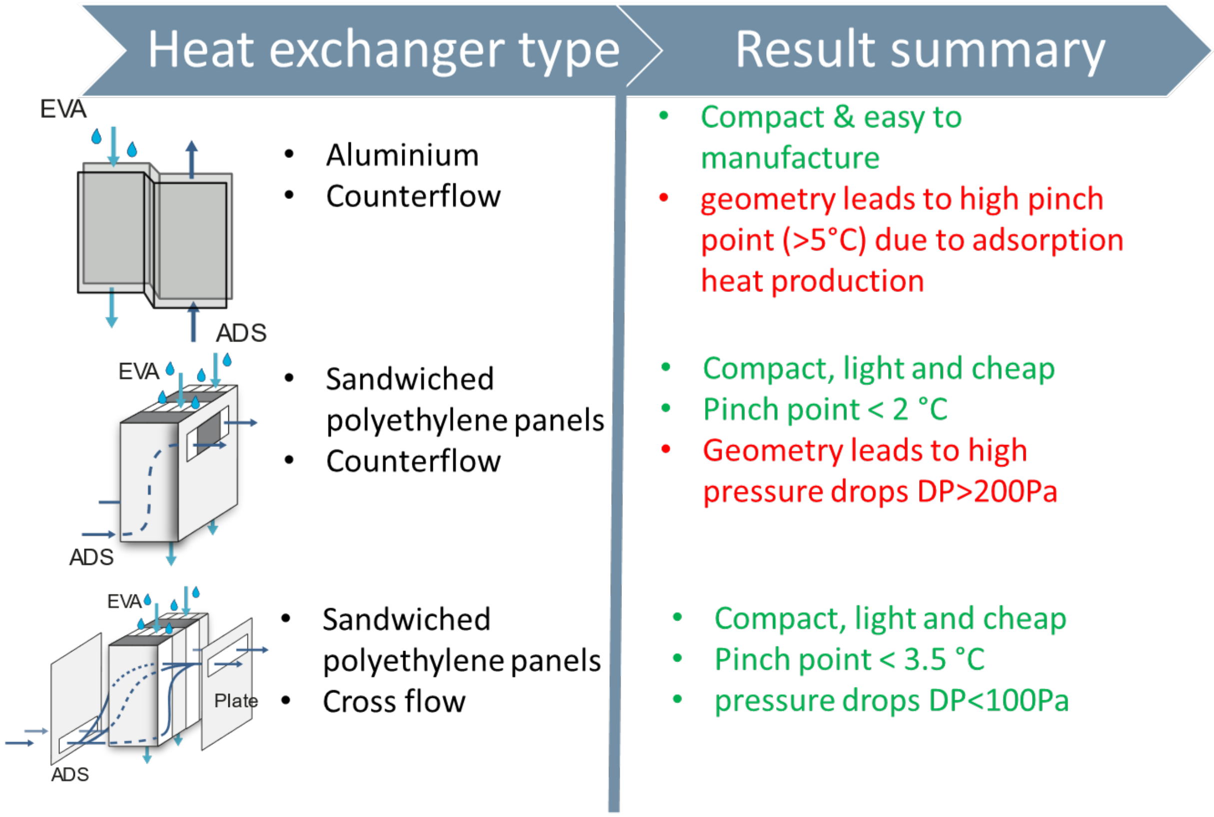

Figure 4.2: Freescoo heat exchanger tested concepts

The evaluation was carried through numerical analysis and experimental campaigns, at Solar Invent for the first concept and at ReLab [65] for the remaining two.

1. In the first concept the heat exchanger is composed by a series of bent aluminium plates so that they can be stacked on top of each other, while leaving enough space for the air to flow and pack the silica gel. This configuration is adopted because the final device should be as flat as possible so that it could be potentially be integrated into a building facade. The nominal dimension of the exchanger is 750 x 300 x 250 (cm) and the FREESCOO system has two heat exchangers to guarantee a continuous operation. This means that staking too many plates on top of each other or making them too thick would be very expensive and make the device impractically heavy. However,

this lead to a poor heat transfer between the two side because all the adsorption heat has to transfer by conduction in the smaller section of the plates. This lead to a pinch point between the potential wet bulb temperature and supply air that was on average close to the maximum cooling potential of the external air given normal summer conditions in Milan.

2. The first concept was abandoned in favour of a series of polyethylene panels sandwiched together. The plastic heat exchanger solved most of the problems of the previous iteration making it cheaper, lighter and with a much better heat transfer capacity. However, the silica gel was tightly packed in between the sandwich panels at the point that the heat exchanger on the supply air side would behave as a porous media. In fact, the measured pressure losses during experiments were too high at nominal air flow rates considering the average cooling power at nominal conditions,namely 1500 (W), with an airflow of 500 (kg/h) and pressure drops up to 250 (Pa).

3. The last and final iteration of the heat exchanger is identical to the second one. However the supply side of the heat of exchanger was opened, as shown in Figure 4.2, leaving the air enough space to pass in a cross flow configuration rather than a counter flow one. This lead to a drastic reduction in pressure losses at nominal condition, while the heat transfer capabilities were still between acceptable boundaries.

4.2. Experimental campaign

As explained in Section 4.1, I analyzed the last two iteration of the heat exchanger in the ReLab facility. The experiments were conducted in ReLab (www.relab.polimi.it) using the two calorimeters shown in Figure 4.3.

Figure 4.3: ReLab 50 (kW) calorimeters to simulate external and internal environments

The calorimeters and their measurement instrumentation are certified according to the EN 17025. All the instrumentation is connected to the control panel inside the chambers and then the digital signal travels from the acquisition system to the computer interface on the left. The acquisition time step of the calorimeter is 2 (s).

In order to the test the heat exchanger an aluminum test rig was developed and built around the heat exchanger; they are both shown in Figure 4.4. The purpose of the test rig is to provide all the necessary components that normally would be present in the final unit, such as the sprayed cold water for the evaporative cooling, the air-to-water heat exchanger to warm up the regeneration air and a system of shutters to redirect the air during the different phases (adsorption and regeneration).

Figure 4.4: 1) on the left the test rig that contains the heat exchanger the humidifier and the air to water heat exchanger, 2) in the center the tested air to air heat exchanger, 3) on the right the test rig attached to the measuring tubes and the two fans

In order to provide the airflow rate and measure it the test rig was connected via flexible air ducts to the fans. Furthermore, measuring tubes containing temperature, humidity and pressure probes were placed at all the outlets of the heat exchanger. A schematic of the connections and all the measurements points is shown in Figure 4.5.

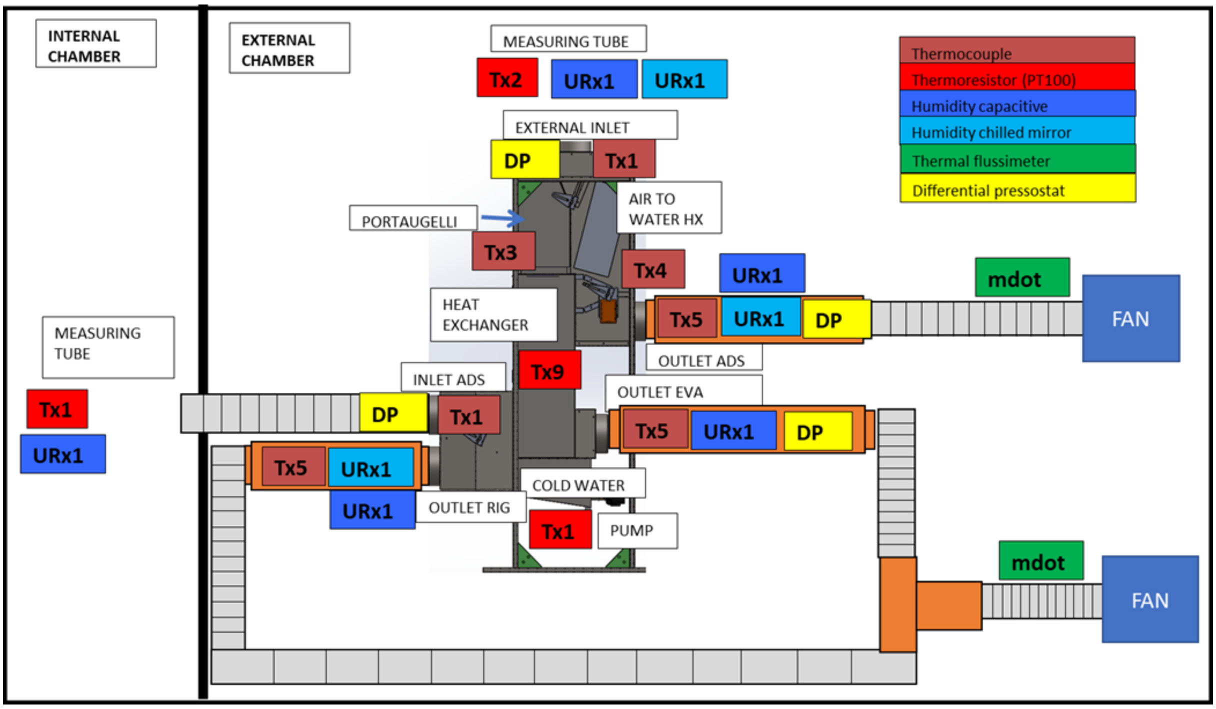

Figure 4.5: Test rig configuration in the climatic chambers including measurement points and sensors

There are redundant measurements of humidity and temperature at almost every inlet and outlet besides for the internal chamber inlet. For the water uptake estimation (the amount of water adsorbed by the silica gel bed), the measurements needed are the air mass flow rate, the inlet and outlet humidity ratios and the heat exchanger internal temperatures. There is a total of nine thermal resistors inside the heat exchanger placed along the height of the heat exchanger and along the flow direction, in Figure 4.6 a drawing of the position for each thermal resistor is shown.

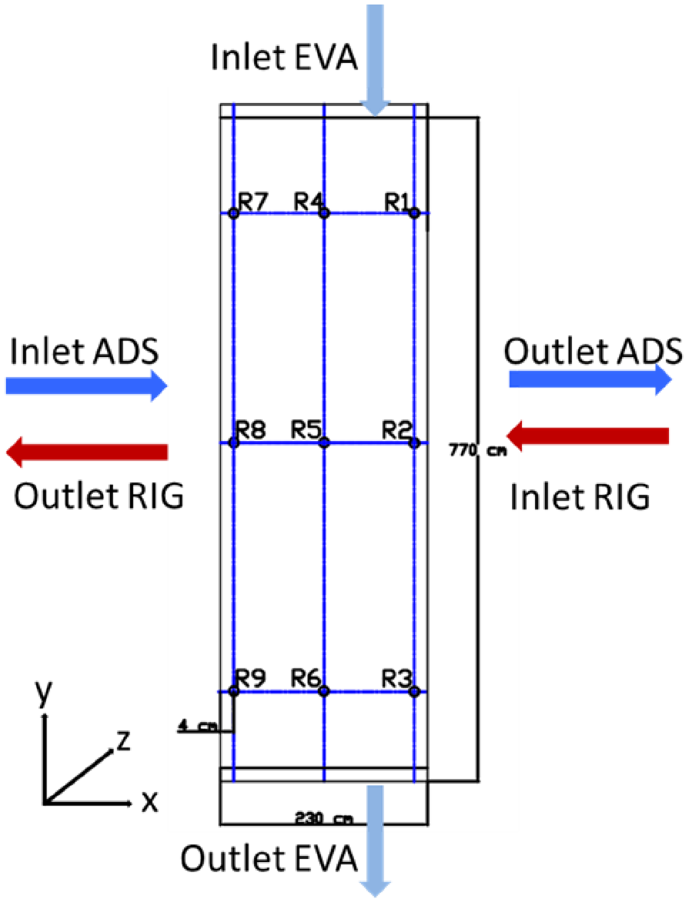

Figure 4.6: Thermal resistances positions inside the heat exchanger, view is from a cross section of the heat exchanger as highlighted by inlets and outlets

The thermal resistances are placed along the x and y direction, while with respect to z they are placed around the center of the heat exchanger since we assume that the flow distribution will be equal along the z direction. Furthermore, they are not all on the same plate to avoid disturbing too much the air flow. They are glued on the internal surface of the heat exchanger between the heat exchanger and the silica gel pad.

In Table 4.1 is reported a brief list of all the measurement instruments needed for the water uptake estimation, in terms of variable measured, accuracy and response time.

Table 4.1: Sensors summary

	brand	Measure	Accuracy	Response time
Thermal	PT100	T (°C)	$\pm(0.15 + 0.002T)$ (°C)	< 10 (s)with air flow 1 (m/s)
Capacitive hygrometer	EE31	RH (%)	$\pm(1.4 + 0.01mv)$ (%)	<15 (s) with air flow 1 (m/s) and constant T
chilled mirror	OptiDew	T (°C)	±0.2 (°C)	1 (°C/s)
chilled mirror	S800	T (°C)	±0.1 (°C)	1 (°C/s)
Thermal flux meter	Proline t-65	$\dot{m}$(kg/s)	±1.5(%)	<30 (s)

A summary of the experimental campaign is reported in the bullet points below:

- around 100 tests for the second heat exchanger and 150 for the third one were conducted. That corresponds to 28 complete cycles for the second heat exchanger and around 43 cycles for the third heat exchanger. Each cycle condition was repeated at least three times to minimize the influence of the previous cycles since the FREESCOO system is always in transient condition.
- 3 external conditions to simulate late spring early autumn and summer $T_{wetbulb} = 20, 23, 26(°C)$ and $T_{drybulb} = 28, 30(°C)$
- 3 room conditions $T_{room} = 24, 26, 30(°C)$ and $RH = 60(\%)$ to simulate 2 comfort condition and a ventilation scenario (all supply air is taken from external environment)
- 12 combinations of flow $\dot{Q}_{flow} = 40, 60, 80, 100(\%)$ of nominal value 550 (kg/h) for ADS and RIG, 360 (kg/h) for EVA
- 3 cycle times for Adsorption (ADS), Regeneration (REG) $= 40, 30, 18(min)$

4.3. Data analysis

All the data was post processed using Matlab and Python scripts. Additional variables were also calculated starting from the available measures such as humidity ratios $x(kg_w/kg_{da})$ and enthalpies $h(kJ/kg)$ using the moist air equations available on the ASHRAE handbook [66]. For the uncertainty analysis of derived measurements the uncertainty was calculated as follows. Assuming that z (final quantity that we want to estimate) is a function of n quantities $x1, x2, ..., xn$ or written in the form $z = z(x1, x2, ..., xn)$, the uncertainty of z, that we can call u_c can be estimated according to the uncertainty propagation principle. Under the assumption that $x1, x2, ..., xn$ are not correlated between each other u_c can be calculated according to Equation 4.1.

$$u_c^2 = \sum_{i=1}^{n} (\frac{\partial z}{\partial x_i})^2 u^2(x_i) \tag{4.1}$$

The partial derivatives of z with respect to $x1, x2, ..., xn$ represent the sensitivity coefficients that have to be calculated in the operating point for each xi, while $ux1, ux2, ..., uxn$ are the uncertainties related to $x1, x2, ..., xn$. Furthermore, under the assumption that $ux1, ux2, ..., uxn$ are random errors that follow a t-student distribution, the sample size N>60 for stationary measurements, while for the dynamic measurements we have just one sample every 2 (s), considering the time constants of the sensor we could say that we can take a point ever 10 (s) leading to N=5 and we want a 95 % chance that the real value of z will lie between the mean value of z and its error band we can estimate the extended uncertainty value $Uc = kuc$, where k will be $k = 2$ for $N > 60$ and $k = 12.706$ for $N = 1$.

From a first analysis of the data and the experimental setup few things were noticed:

- the thermocouple at the inlet of the adsorption bed gives a slightly higher value with respect to the PT100 used at the entrance of the flexible tube. from spot measurements it does not seem that the air stream heats up while going through the flexible tube (it's insulated). So the sensor measurement was disregarded;
- the thermal resistors used for measuring the internal heat exchanger temperature were glued between the plastic and the silica gel layer. This probably affected their deformation capacity, affecting the change in the resistance value due to temperature changes. So these measures are to be considered mostly qualitative;
- chilled mirrors are preferred to capacitive hygrometers for humidity measurements thanks to their higher precision. Furthermore, the thermal inertia of the measuring tube and the sensor metal tip impacted T and consequently also RH.

In order to use the data to validate the model a study to evaluate the measurement delay was conducted. In Figure 4.7 all the measuring tubes previously attached to the test rig were connected to each other. Looking at the scheme the x-axis coordinate shows the position with respect to the tube inlet. The designation "xN" tells how many instruments of the same type are present in the same tube section. The tubes are numbered 1 to 4 from the inlet of the first tube.

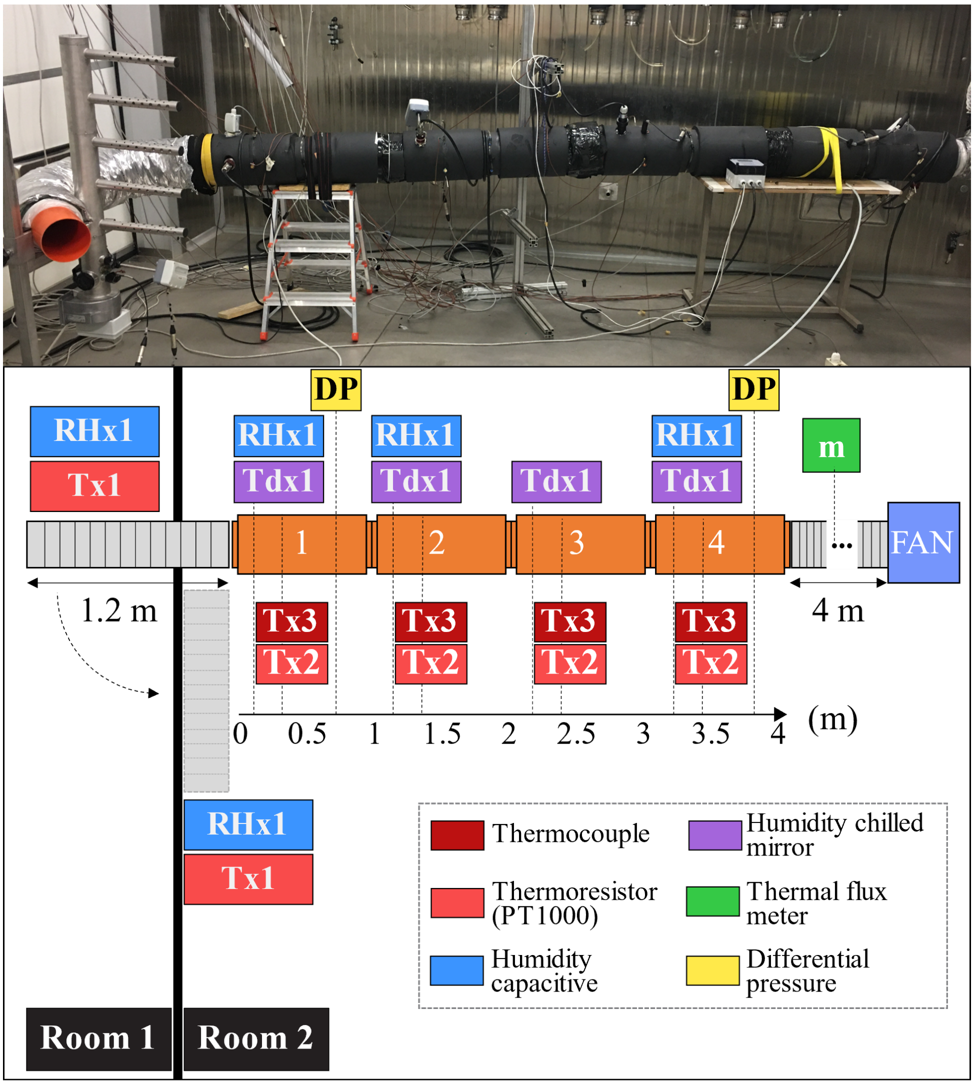

Figure 4.7: 1) the top figure is reported a picture of the experimental setup, 2) the bottom figure is a scheme with all the measurement points and sensors the xN indicates the number of that specific instrument.

The climatic chambers are also provided with an absolute barometer used to adjust for ambient pressure together with the differential pressure sensors. The experiments were designed as a series of step changes between the conditions of the two rooms. As shown in Figure 4.7, the experimental setup is installed in climatic Chamber 2. There is a small aperture between the two chambers where the end of the flexible channel can tightly fit. Two lab technicians were able to move the flexible end of the tube from one measuring point in a chamber to the other in around 1 second, while also sealing or opening the aperture between the two climatic chambers, the fan would suck air inside the duct until a steady state is reached. A total of twelve step change experiments were conducted considering different relative humidity, temperatures, and flow rate as shown in Table 4.2:

Table 4.2: Sensors delay experiments, 1 and 2 indicate Room 1 and 2 as in Figure 4.7

Name	**T2 (°C)**	**RH1(%)**	**T1 (°C)**	**RH2(%)**	$\dot{m}$ **(kg/h)**
A (1→2)	20 ± 0.2	60 ± 3	20 ± 0.5	20 ± 1.5	100 ± 2
B (2→1)	20 ± 0.2	60 ± 3	20 ± 0.5	20 ± 1.5	100 ± 2
C (1→2)	20 ± 0.2	60 ± 1.5	20 ± 0.5	20 ± 1.5	360 ± 6
D (2→1)	20 ± 0.2	60 ± 1.5	20 ± 0.5	20 ± 1.5	360 ± 6
E (1→2)	20 ± 0.2	60 ± 1.5	20 ± 0.5	20 ± 1.5	550 ± 8
F (2→1)	20 ± 0.2	60 ± 1.5	20 ± 0.5	20 ± 1.5	550 ± 8
G (1→2)	20 ± 0.2	20 ± 1.5	20 ± 0.5	20 ± 1.5	130 ± 2.2
H (2→1)	20 ± 0.2	20 ± 1.5	30 ± 0.5	20 ± 1.5	100 ± 2
I (1→2)	20 ± 0.2	20 ± 1.5	30 ± 0.5	20 ± 1.5	550 ± 8
L (2→1)	20 ± 0.2	20 ± 1.5	30 ± 0.5	20 ± 1.5	550 ± 8
M (1→2)	20 ± 0.2	20 ± 1.5	30 ± 0.5	20 ± 1.5	360 ± 6
N (2→1)	20 ± 0.2	20 ± 1.5	30 ± 0.5	20 ± 1.5	360 ± 6

The first column indicates the name of the experiment which corresponds to the capital letter, while $i \rightarrow j$ corresponds to the direction of the step, the tube is moved from chamber i to chamber j. The variable values inside the tables are the mean value of the variable $\pm$ two times the standard deviation for each experiment. Starting from these experimental data an inverted feedback loop transfer function model, in Figure 4.8, was developed to reconstruct the delayed signals. For a detailed explanation of the modelling process I published the results in the manuscript [67], attached to the thesis in Appendix B, furthermore the figures present in this chapter also come from the manuscript.

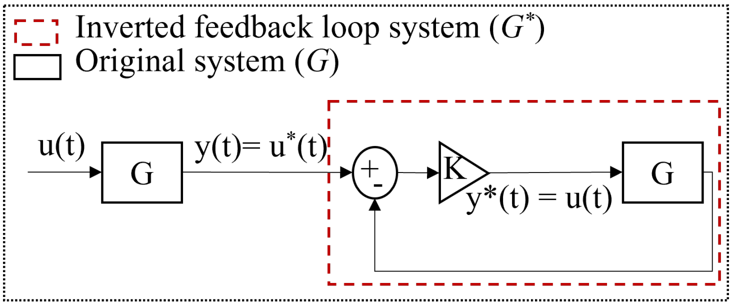

$$G^*(s) = \frac{K}{1 - KG(s)} = \frac{K}{1 + K\frac{zeros}{poles}} = \cdots$$
$$= \frac{Kpoles}{poles + Kzeros}$$

Figure 4.8: Scheme of the inverted transfer function for signal reconstruction, G is the transfer function emulating the behaviour of the sensor and $G*$ is the inverted transfer function to reconstruct the signal

$u^*(t)$ corresponds to the measure read by the sensor, $y^*(t)$ is the output of the feedback loop and corresponds to the reconstructed signal $u(t)$ and G^* corresponds to the inverted transfer function. In Figure 4.9 is shown the output of the sensor model G vs experimental data and then the output of the inverted model G^*.

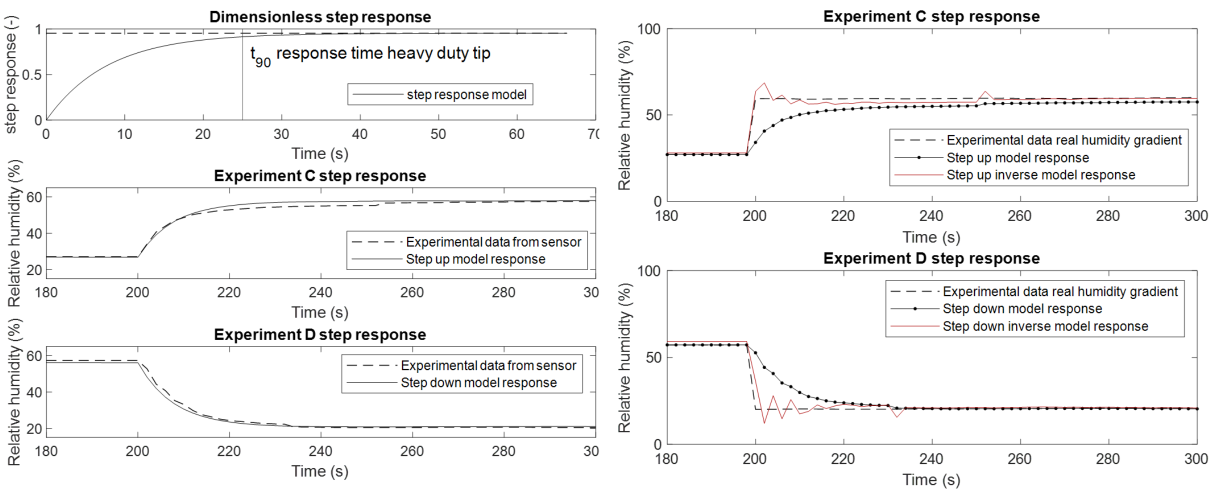

Figure 4.9: 1) on the left the sensor model that mimics the delayed signal, 2) on the right the reconstructed signal starting from delayed data.

The inverse model can accurately reconstruct the original data for the step change. However, it does introduce some small nonphysical oscillations in the humidity signal due to noise amplification, which can be filtered out with a noise rejecting filter such as a moving average or a Savitzky-Golay filter [68]. Despite the noise introduced the NRMSE for both experiments are below the sensor tolerance being 0.9 (%) for experiment C and 1.4 (%) for experiment D. It is also interesting to notice at 255 (s) for experiment C and 235 (s) for experiment D the fact that if the sensor input presents some small noise, it will be amplified by the inverse model. This further confirms the necessity to properly pre-process the data before applying the inverse model and apply the noise rejection filter afterwards. To show the capability of the modelling approach let's consider a synthetic humidity profile:

$$RH = 20sin(\frac{\pi}{60}t) + 40 \pm \mathcal{N}(0, 4)\ (\%) \tag{4.2}$$

Where RH is the real relative humidity, t is the time in seconds and $\mathcal{N}$ is a white noise that adds ± 2 (%) on the variability of the actual value.

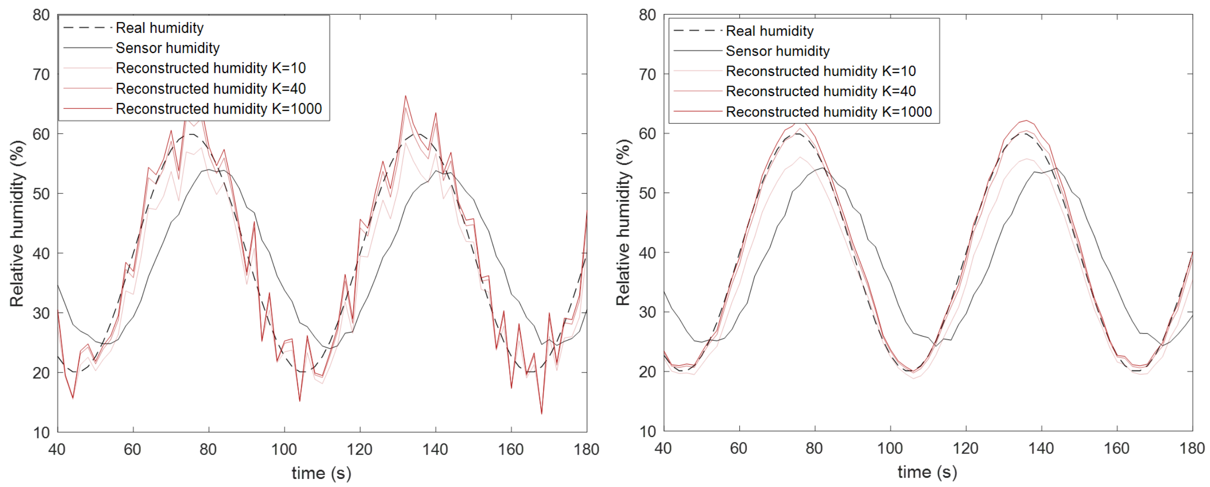

Figure 4.10: 1) On the left the signal reconstruction without filtering, 2) On the right the reconstructed signal with a Savitzky-Golay filter applied

The figure above shows the importance of filtering the data and also the choice of the feedback gain K, where a trade off between reconstructing the signal and sensitivity to measure uncertainty has to be done. In fact

In this case the RMSE for K = 10 becomes 3.4 (%), 1.06 (%) for K = 40 and 9.6 for K = 1000. The experimental data used for the validation and calibration of the FREESCOO model were all post processed trying to find a suitable profile reconstruction.

4.4. FREESCOO 2-D heat exchanger model

Beside the experimental campaign also a 2-D model of the final iteration of the heat exchanger and then of the whole FREESCOO model were developed and included in a custom Modelica Library "FREESCOO2D", that will be published on Github. The reason is to use it to run monthly simulations for the whole cooling season estimating the performance of the device in the two room apartment case study. The model should be able to represent the useful heat rate of the heat exchanger (ADS heat rate) and the bed dynamics, meaning how much time does it take to fill the silica gel bed with moisture and then how much time does it take to regenerate it. The first step is to verify the cross flow and porous media hypothesis. In order to do so a 3-D Computational Fluid Dynamics (CFD) model of one of the heat exchanger plates and the metal casing was done using the software Fluent ®. In Figure 4.11 a screenshot of the velocity contours in Fluent are shown.

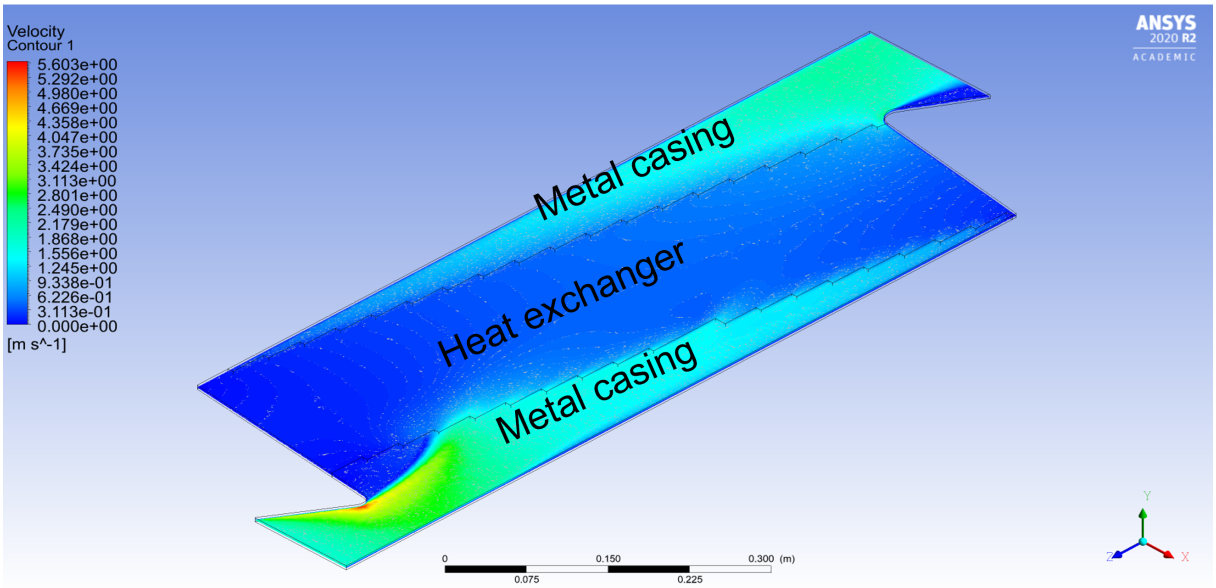

Figure 4.11: 3-D CFD model of plate and metal casing for heat exchanger. the air enters from bottom right and goes out from top left.

The heat exchanger was modelled as a porous media where the viscous resistances were found using as inputs the experimental data where the air flow and pressure losses for the Ergun equation [69]. The temperature was considered constant at 40 (°C), so only forced flow dynamics were modelled with no heat transfer. Then a grid analysis study was conducted to check that the solution will be invartiant with respect to grid size as shown in Figure 4.12.

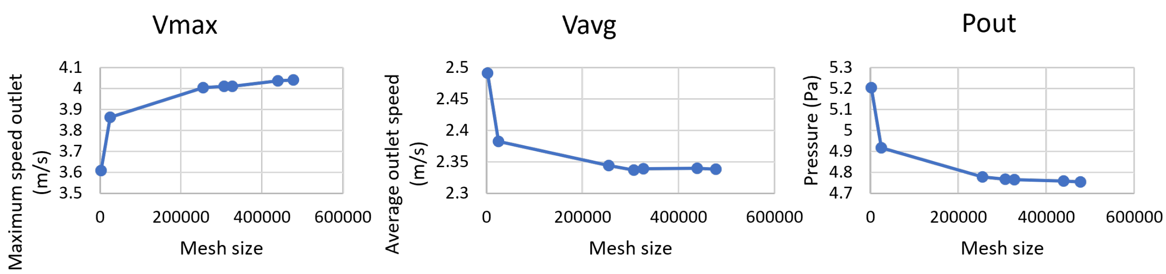

Figure 4.12: 1) maximum speed at outlet of mesh, 2) average speed at the outlet 3) absolute pressure outlet.

Then a simulation was run verifying that residuals ($< 10^{-6}$), continuity

($< 10^{-4}$) and mass balance ($< 10^{-8}$) had reasonable values. A 2-D velocity profile of the plane cutting the middle section was extracted from Fluent and post processed in Matlab. In Figure 4.13 is shown the the velocity profile inside the heat exchanger at the nominal flow rate conditions for the device 550 (kg/h).

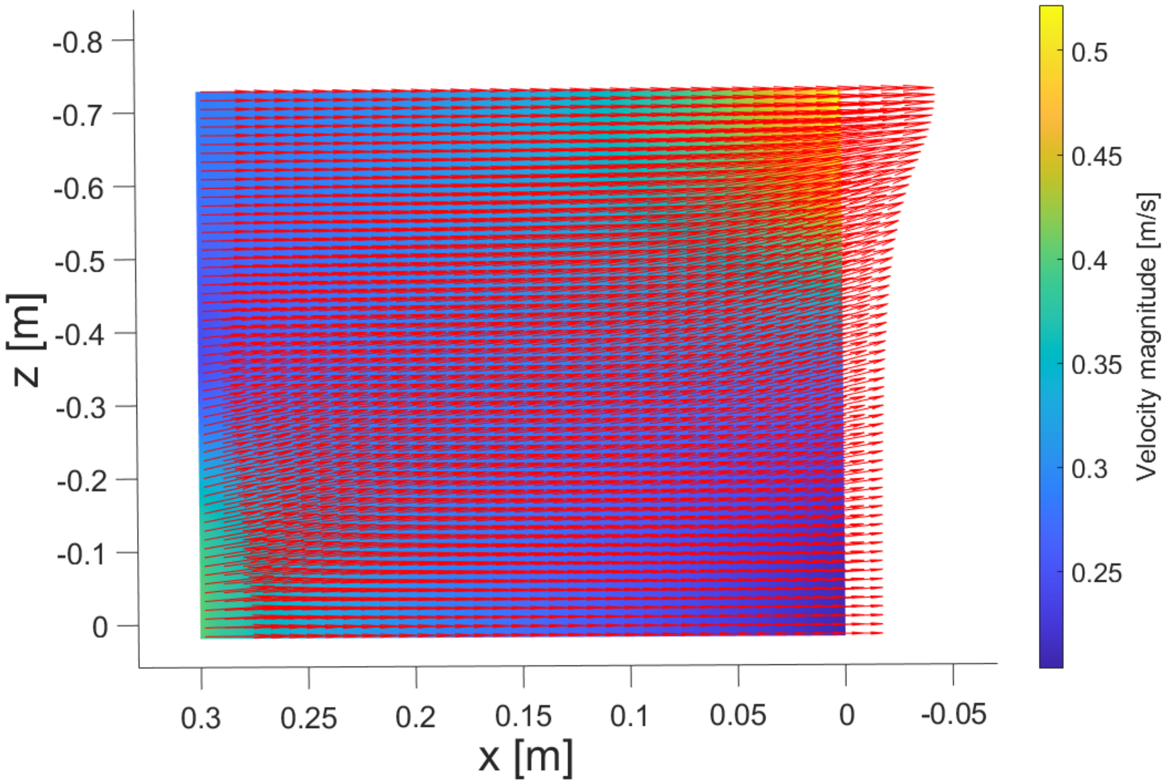

Figure 4.13: velocity profile inside the mid section of the heat exchanger (evaporator air flow top to bottom and adsoprtion flow left to right).

Looking at the figure above it shows that the vertical component of the velocity is smaller than the horizontal one meaning that the heat exchanger will work almost in a cross flow configuration. Under the assumption that the fluidodynamics are decoupled from the thermodynamics happening inside the heat exchanger the velocity profile could be used as input for the thermal 2-D model of FREESCOO.

The 2-D model of the FREESCOO heat exchanger was developed using

Modelica so that it could be used together with the two room apartment model. A specific library called "FREESCOO2D" was developed making it compatible with the fluid models available in the IBPSA and Buildings libraries. The following hypothesis were used in the development of the model:

- the heat transfer, temperature and velocity distribution across the plates is considered uniform. So only one plate was modelled;
- the heat exchanger is cross flow, no vertical fluxes were assumed along the vertical axis for the adsorption side;
- there is a continuos stream of water recirculating inside the evaporator kept at the outlet EVA air wetbulb temperature that allows the air to remain around the wetbulb temperature and also contributes to the sensible heat exchange;
- the thermal symmetry is not done considering the half plates because the silica gel is glued only on one side of the plate. So the control volume was taken as a full polyethylene panel plus the the space between two panels that makes the adsorption side and their surfaces were considered connected for the plate to plate conduction. In Figure 4.15 a visual representation shows the two sides and how they are connected.

Below is reported a description of all the components.

FREESCOO heat exchanger

The heat exchanger is modelled as a finite volumes 2-D component that divides the area in which EVA and ADS airflows exchange heat in a grid of ‘m x n’ elements, where m is the number of nodes in the horizontal or x axis (flow direction of adsorption) and n is the number of nodes in the vertical or y axis (flow direction of evaporator). It has an inlet and outlet for both EVA and ADS sides. The mass flow rate profiles inside are determined by a matrix of digital inputs, ADS and EVA have respectively one input for the velocity on the x-axis and the y-axis. Lastly two heatports to access the internal temperatures of the heat exchanger are available, a schematic of the heat exchanger and its internal diagram view are reported in Figure 4.14.

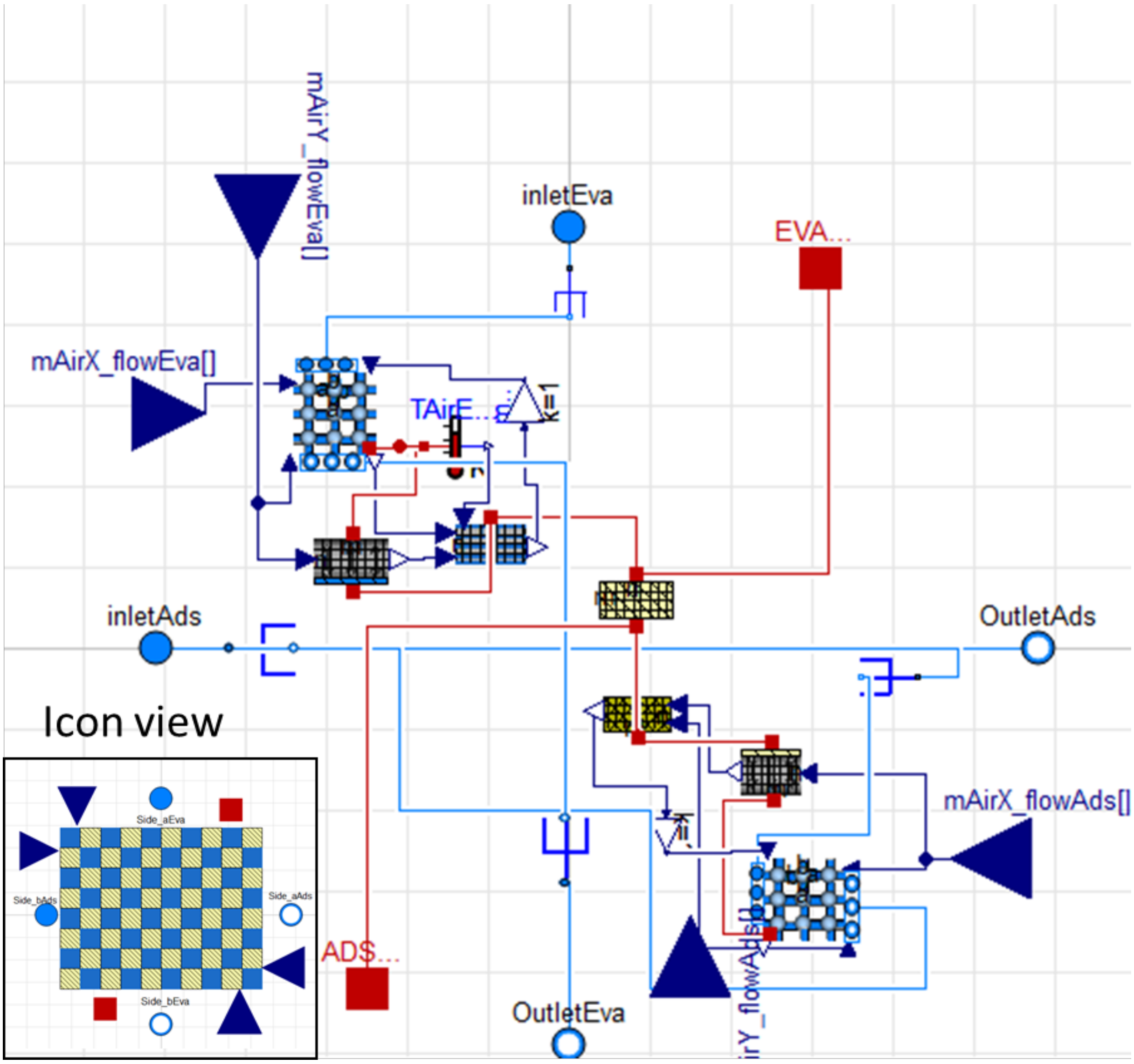

Figure 4.14: 1) on the left FREESCOO heat exchanger 2-D model wrapper 2) FREESCOO 2-D model diagram view. This image shows all the components that are explained throughout the section. As a brief introduction on the top left there is the evaporator side made up of the control volumes, convection and plate models. In the middle the conduction model and in the bottom right the adsorption side of the heat exchanger with air volume, convection and plate models. The light blue lines are fluid connections (moist air transport equations), the blue lines are are digital exchanged signals) and the red lines are heat transfer between parts.

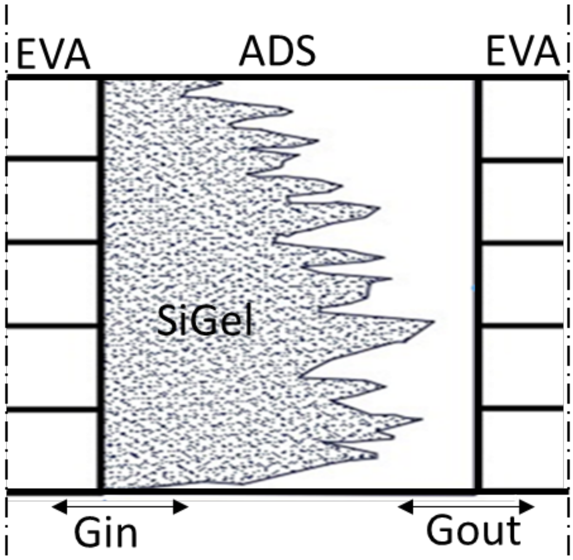

Figure 4.15: Single plate heat transfer connection. Silica gel is present only on one side of the of the channel, so thermal symmetry is achieved by cutting in half the evaporator channel. *Gin* is the trasmittance considering silica gel and plate thickness, while *Gout* only considers plate thickness, the total trasmittance *Gtot* is the equivalent parallel of *Gin* and *Gout*

The components inside the heat exchanger model are:

1. air volumes network, for both EVA and ADS, called 'airVolNetEva' and 'airVolNetAds', respectively.
2. convection model for the EVA, called 'convection2DFreescooEva'.
3. convection model for the ADS, called 'Convection2DFreescooAds'.
4. conduction model between EVA and ADS side for the HX plate, called 'Conduction2D'.
5. heat exchanger Evaporation plate model, called 'EvaPlate2D'.
6. heat exchanger Adsorption plate model, called 'AdsPlate2D'.

Air volumes network model

This component divides the air volume present in the corresponding side (EVA or ADS) of the HX plate in a m x n grid. In Figure 4.16 are reported the icon and diagram view of the air volumes network models.

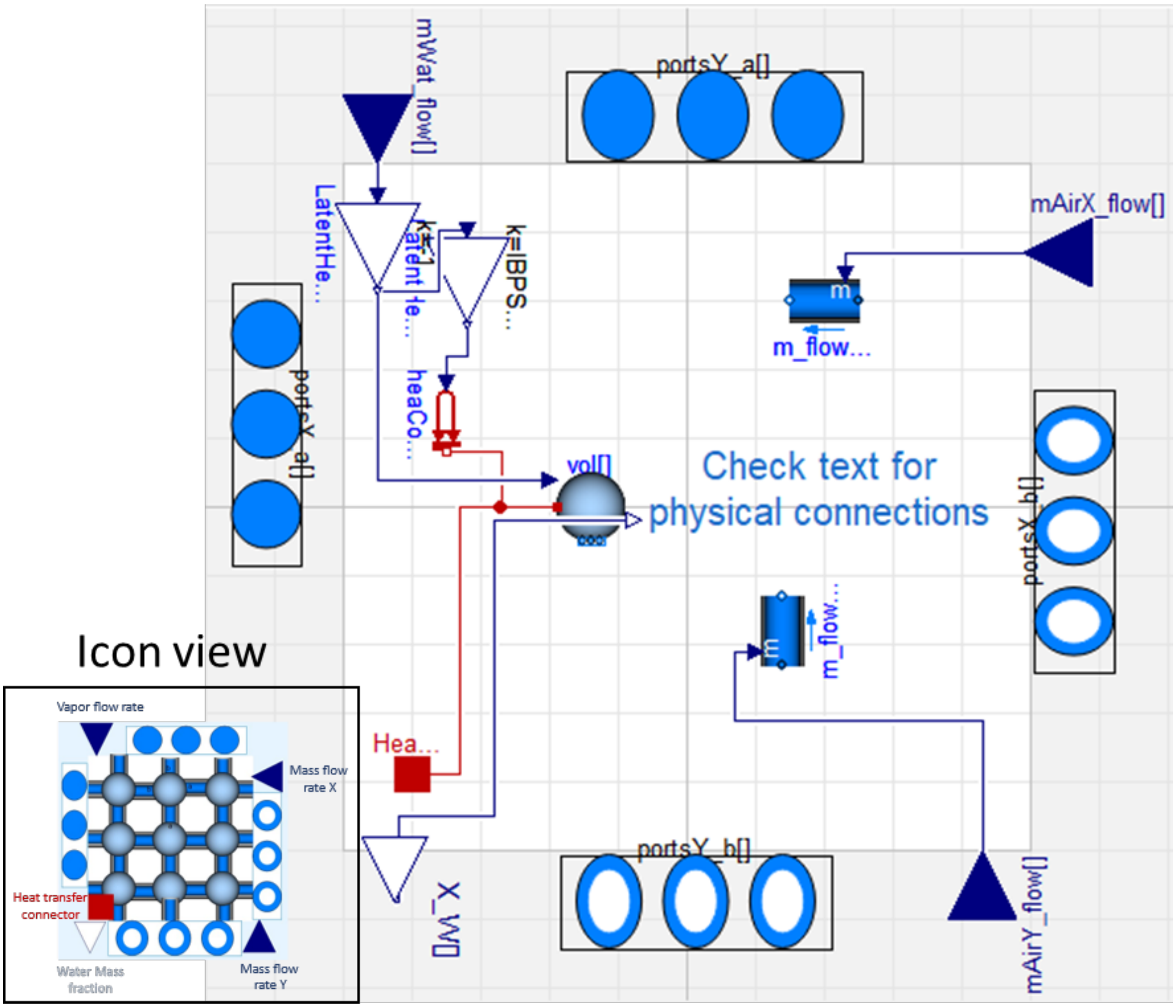

Figure 4.16: 1) Icon for air volumes model 2) Air volumes model diagram view

As it can be seen in the diagram view, this component has vector flow inlets (solid blue circles) and outlets (blue border and white interior circles) in the x and y directions, whose mass flow rates are controlled by the real input matrices values (dark blue solid triangles) 'mAirXflow' and 'mAirYflow'. the single humid air volume and imposed mass flow rates models come from the Modelica Buildings library and use the ASHRAE book of fundamental equations for the moist air state equations. The connections between the arrays of single volume models (light blue lines) are made in the textual view so they are not visible from the diagram view. The air volume net component has one more matrix real input value ‘mWatflow’ that connects an external water mass flow rate evaporating to the air volumes. Furthermore, the latent heat of evaporation related to the water exchange in the the air volume is added or removed to the air volumes heat ports. The heat ports are also extended at the boundary of the air volume network model to allow heat transfer between the air volumes and the respective heat transfer models. Finally, the mass fraction of water with respect to the total air X_W (kg_w/kg_{tot}) is extended as an output to determine the rate of mass transfer in the plate model. Mass fraction is used instead of humidity ratio because moist air is treated as a binary fluid mix in Modelica.

Convection model for Evaporator side

The Evaporator (EVA) convection model uses the air mass flow rates at each volume to determine the local heat and mass transfer coefficients. In Figure 4.17 is shown the model Icon.

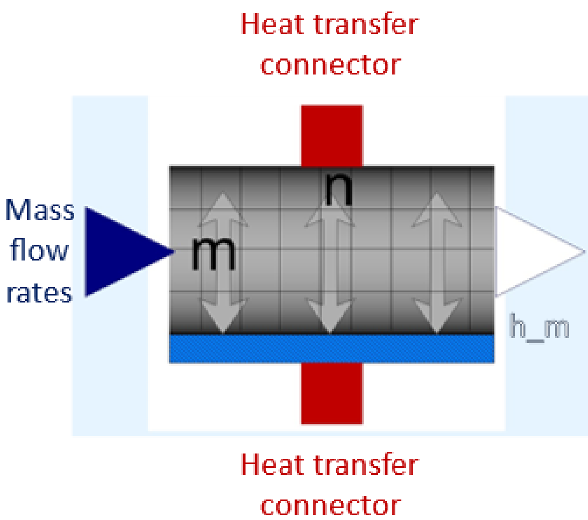

Figure 4.17: Evaporator convection model icon

The real input matrix is the mass flow rate at each volume, from this the Yovanovich correlation for non circular ducts [70] is used to determine the local heat transfer coefficient. Then, using Lewis analogy the local mass transfer correlation is found and used as output for the model. The two heat ports connect on one side to the air volume network and on the other to the EVA plate model. The local heat transfer coefficient correlation is shown below:

$$h_c = \frac{Nu\lambda_a}{D_{eq}}\ (W/m^2/K) \tag{4.3}$$

Nu is the Nusselt number, λ_a is the air thermal conductivity and $D_{eq} = \sqrt{A_{cross}}$ is the equivalent diameter and A_{cross} is the cross section area of the channel. The expression for Nu is reported in the equation below:

$$Nu = \left[\left(\frac{f(Pr)}{\sqrt{y^*}} \right)^m + \left(c_3^5 \left(\frac{f(Re_{\sqrt{A_{cross}}})}{y^*} \right)^{5/3} + c_1^5 \left(\frac{f(Re_{\sqrt{A_{cross}}})}{8\sqrt{\pi}\epsilon^{-0.3}} \right)^{5/3} \right)^{m/5} \right]^{1/m} \tag{4.4}$$

where $y^* = \frac{y}{D_{eq}Re_{\sqrt{A}}Pr}$ is the dimensionless position for the developing flow. y is the axial coordinate of the flow (y axis for the heat exchanger). $\epsilon = height/length$ is the aspect ratio of the cross-section. $Re_{\sqrt{A}}$ is the Reynolds number with respect to D_{eq}. $C_1 = 3.84$ is an experimental constant under the assumption of uniform flux, $C_3 = 0.501$ is another experimental constant under the assumption of uniform flux. $m = 2.27 + 1.65Pr^{(1/3)}$ is a correlation parameter. $f(Pr)$ 4.5 is a function of the Prandtl number.

$$f(Pr) = \frac{0.886}{\left[1 + (1.909Pr^{1/6})^{9/2}\right]^{2/9}} \tag{4.5}$$

$f(Re_{\sqrt{A}})$ 4.6 is a function of the Reynolds number

$$f(Re_{\sqrt{A}}) = \left[\left(\frac{12}{\sqrt{\epsilon(1+\epsilon)} \left(1 - \frac{192\epsilon}{\pi^5} tanh\left(\frac{\pi}{2\epsilon}\right)\right)} \right)^2 + \left(\frac{3.44}{\sqrt{y^*}} \right)^2 \right]^{1/2} \tag{4.6}$$

Convection model for Adsorption side

The Modelica structure of the convection model for the Adsorption side (ADS) is identical with respect to the EVA model, in Figure 4.18 the icon is shown. However, since the plate on the ADS side behaves like a porous media the correlation from [71] was implemented.

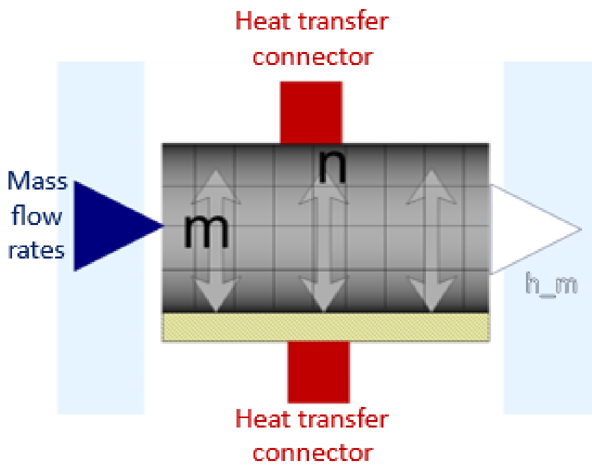

Figure 4.18: Adsorption convection model icon

The local heat transfer correlation is given by the equation below:

$$h_c \frac{D}{\lambda_a} = 1 + \frac{4(1-\epsilon_p)}{\epsilon_p} + 0.5(1-\epsilon_p)^{0.5} Re_D^{0.6} Pr^{0.5} \tag{4.7}$$

where $Re_D = (1-\epsilon_p)Re$ is the the Reynolds number adjusted for the particle diameter and $\epsilon_p = 1 - \frac{D^2}{Z}$ is the porosity, $D(m)$ is the average particle diameter and $Z(m)$ is the height of the channel.

Evaporator plate model

The Evaporator plate is made up a series of rectangular channels as shown in 4.15. The EVA plate model has one matrix real inputs with the air temperature to calculate the saturation condition at air temperature and one with the humidity ratio and mass transfer coefficient to calculate the water mass transfer between plate and air volume. The real output is the vapor flow rate and there is an heat port to connect the plate to the convection model. In Figure 4.19 the model Icon is reported.

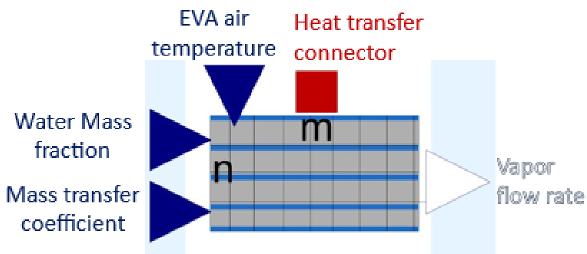

Figure 4.19: Evaporator plate model icon

The plate as the air volumes is discretized in a 2-D nxm grid. The energy balance coming out of the spatial discretization is reported below:

$$C\frac{\partial T(x,y)_{i,j}}{\partial t} = g_x(\Delta T_x^- + \Delta T_x^+) + g_y(\Delta T_y^- + \Delta T_y^+) + \dot{Q}_{in,i,j} + \dot{m}_{w,i,j}h_{fg} + \dot{m}_{lw}cp_lw(T_{w,i-1,j} - T_{i,j}) \tag{4.8}$$

where $C(kJ/K)$ is the polyethylene plate heat capacity, $g_i(W/K)$ is the thermal conductance $g_x = \lambda_{plate}t_{plate}\frac{Y}{n}(\frac{X}{m+1})^-1$ and $g_y = \lambda_{plate}t_{plate}\frac{X}{m}(\frac{Y}{n+1})^-1$, λ_{plate} is the thermal conductivity of the plate, t_p is the plate thickness, X and Y are the length and height of the plate. ΔT_i are the temperature differences $\Delta T_x^- = T_{i,j-1} - T_{i,j}$, $\Delta T_x^+ = T_{i,j+1} - T_{i,j}$,$\Delta T_y^- = T_{i-1,j} - T_{i,j}$, $\Delta T_y^+ = T_{i+1,j} - T_{i,j}$. $\dot{Q}_{in}(W)$ is the heat balance at the heat port given by the convection with the EVA air the conduction with the ADS side of the plate. $\dot{m}_w(kg/s)$ is the evaporated or condensed water mass flow rate and h_{fg} is the water latent heat of evaporation. $\dot{m}_{lw}$ is the liquid water flow rate in each along the plate, cp_{lw} is the liquid water specific heat and $T_{w,i,j}$ is the liquid water temperature.

the mass balance is shown below:

$$\dot{m}_w = A_{wetting}h_{mass,i,j}(x_{air,i,j} - x_{sat,i,j}) \tag{4.9}$$

Where $A_{wetting}(m^2)$ is the wet area with respect to the total plate area, which is calculated as the internal surface of the rectangular duct resulting from the discretization process plus the area of all the channel separators in between.

$$A_{wetting} = f_{aw}\left(2\frac{XY}{mn} + 2nChan\frac{Y}{mn}t_p\right) \tag{4.10}$$

where f_{aw} is the ratio between the total area and the wet area, this parameter will be used to calibrate the model. $nChan$ is the total number of channels in the plate. ρ_{air} is the air density. $x_{air,i,j}(kg_w/kg_{da})$ is the air humidity ratio and $x_{sat,i,j}$ is the saturation humidity ratio calculated at the plate temperature.

Adsorption plate model

The adsorption plate Modelica model structure is identical to the EVA model, in Figure 4.19 the icon of the Modelica model is reported. Differently from the evaporator side, there are no channels instead the the space between two plates is filled with silica gel.

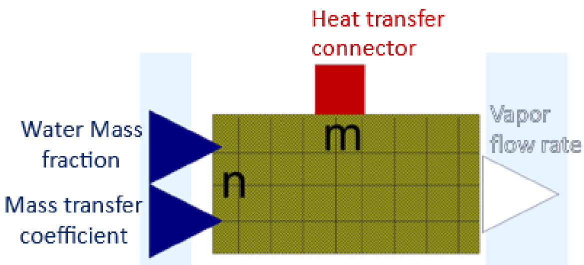

Figure 4.20: Evaporator plate model icon.

Below is reported the energy balance for the ADS plate:

$$C\frac{\partial T(x,y)_{i,j}}{\partial t} = g_x(\Delta T_x^- + \Delta T_x^+) + g_y(\Delta T_y^- + \Delta T_y^+) + \dot{Q}_{in,i,j} + \dot{m}_{w,i,j}q_{ads,i,j} \tag{4.11}$$

C is the lumped capacity of the polyethylene plate and silica gel. In the same way g_i is the thermal conductance of the plate plus the silica gel. q_{ads} (J/kg_w) is the adsorption or desorption specific heat. The value is similar to the latent heat of vaporization of water. However, using the expression from [6] grey box model, it can be modelled as a function of the silica gel water uptake W (kg_w/kg_{sigel}), that is the mass of water contained in the silica gel. The expression is reported below:

$$q_{ads}(kJ/kg_w) = \begin{cases} -12400W_{i,j} + 3500 if W \leq 0.05 \\ -1400W_{i,j} + 2950 if W \geq 0.05 \end{cases} \tag{4.12}$$

the adsorbed or desorbed water flow rate $\dot{m}_w(kg/s)$ is similar to the one on the evaporation, but instead of having the saturation humidity ratio x_{sat} as function of the plate there is the equilibrium humidity ratio x_{eq}. x_{eq} is not only a function of the plate and silica gel temperature but also a function of the water uptake W. The expression for x_{eq} is taken from ashrae and is:

$$x_{eq} = \frac{0.622 RH_{eq} P_{vs_{eq}}}{101325 - RH_{eq} P_{vs_{eq}}} \tag{4.13}$$

$P_{vs_{eq}}$ is the saturation pressure and is calculated according to the Ashrae correlation present in the book of fundamentals. Rh_{eq} is a function of the temperature and the water uptake W. In Figure 4.21 the relative humidity RH_{eq} is plotted against water uptake W for different values of temperature.

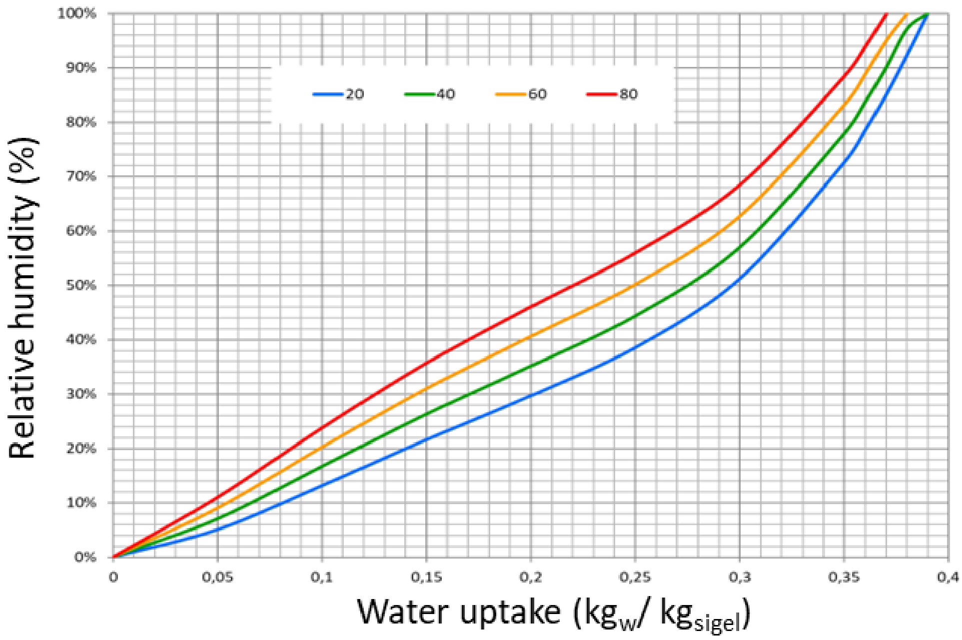

Figure 4.21: Equilibrium relative humidity plotted against the water uptake (adsorption bed humidity) for different temperatures (°C).

From the data points available in Figure 4.21 a correlation as function of both temperature and water uptake was calculated:

$$\begin{aligned} RH_{eq,i,j} = &-a_0 W_{i,j}^3 T_{i,j} + a_1 W_{i,j}^2 T_{i,j} + a_2 W_{i,j} T_{i,j} \\ &-a_3 T_{i,j} + a_4 W_{i,j}^3 - a_5 W_{i,j}^2 - a_6 W_{i,j} + a_7 \end{aligned} \tag{4.14}$$

The last equation needed is to calculate the dynamic balance of the water uptake W, which is shown below:

$$\rho_{sigel} A_{wetting} t_{sigel} \frac{W_{i,j}}{dt} \tag{4.15}$$

where ρ_{sigel} is the dry silica gel density, $A_{wetting}$ is the active area of silica gel, it is calculated as the total area multiplied by a calibration factor $f_{awsigel}$.

Conduction model

This model describes the conduction heat transfer between the EVA and ADS side of the plate. The Modelica Icon is reported in Figure 4.22. This model has only two heatports that connect on one side to the ADS part of the plate and on the other to the EVA side.

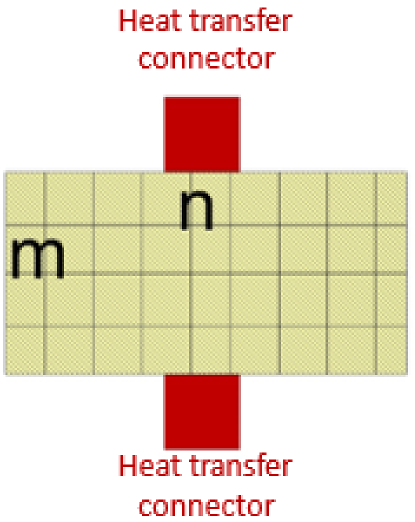

Figure 4.22: Plates conduction model icon

Looking at 4.15 the conduction phenomena occurs on two sides,the internal where the silica gel is glued and the external where there is no silica gel. Therefore the balance equation would be:

$$\dot{Q} = (G_{int} + G_{out})A_{cond}(T_{EVA,i,j} - T_{ADS,i,j})\ (W) \tag{4.16}$$

Gint and *Gout* are considered in parallel and therefore the total trasmittance will be the summation of the two contributions. $G_{int}\ (W/m^2/K) = \frac{1}{\frac{3t_{plate}}{4\lambda_{plate}} + \frac{0.5t_{sigel} - 0.5t_{plate}}{\lambda_{sigel}}}$ is the internal conductance, and the external conductance $G_{out} = \frac{1}{\frac{t_{plate}}{2\lambda_{plate}}}$. λ_i are the thermal conductivities and $A_{cond} = XY\ (m^2)$ In Figure 4.23 there is a scheme that shows the discretization used to lump the plate and silica gel masses of the various volumes.

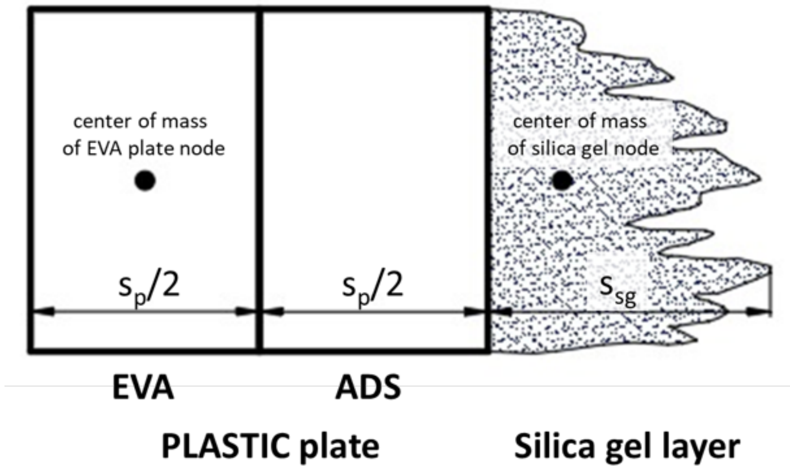

Figure 4.23: Plate conduction discretization method, mass lumped in the center of mass

4.5. 2-D heat exchanger calibration and validation

In order to test the response of the model to the conditions that the experimental heat exchanger was subjected, it was necessary to create a test scenario in Dymola. The diagram view of the test model is shown in Figure 3.17.

In this test, boundary conditions were added (solid blue vessel icons), together with temperature (thermometer icons), specific enthalpy, mass flow rate and mass fraction (all clock-like icons) sensors. Also, timetables that read the temperature, mass fraction and mass flow rate inputs from the chosen experimental values and temperature sensors for collecting the HX plate temperature (2 groups of 9 thermometers) in both sides and in the same location as the thermal resistors placed in the tested HX. Finally, a humidifier is added to the inlet of the EVA with a control system that sets the temperature difference between inlet and outlet of the humidifier to a fixed value, in order to simulate the direct evaporative cooling that the corresponding airflow undergoes.

For the regeneration phase, the RIG flow goes in a direction that is opposite to the one that the ADS flow has to maximize the regeneration process, so this also had to be considered when creating the timetable input (called ADSRIG). In this case, the mass flow for the RIG time steps were assigned a negative value, and the model did not need to be changed since it was designed for having flow in any direction. Similarly for the boundary conditions, they act as input or output depending on the directions of the flow. The sensors have the same capabilities of bidirectional flow as the multimode HX model.

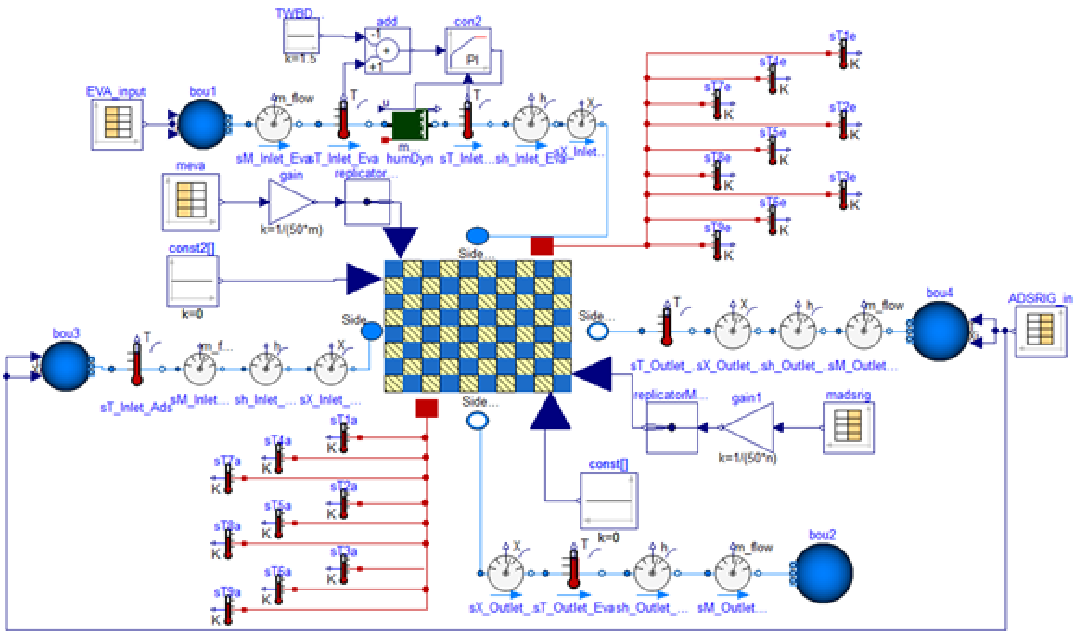

Figure 4.24: diagram view of the test model with heat exchanger and boundary conditions.

Convergence analysis

For the convergence analysis, constant inputs we applied to all the components of the model, in terms of temperature, mass fraction and mass flow rate for 5000 (s). In Table 4.3 below are reported the boundary conditions tested.

Table 4.3: Boundary condition grid sesitivity

Parameter	Value	Units
	ADS	
Inlet temperature	26.0	(°C)
Inlet water mass fraction	0.01251	(kgw/kgtot)
Total mass flow rate	0.0993	(kg/s)
	EVA	
Inlet temperature	33.8	(°C)
Inlet water mass fraction	0.01608	(kgw/kgtot)

Starting from this boundary conditions different test at different n and m values were tried. Table 4.4 reports a summary of the results.

Table 4.4: summary results grid sensitivity

m	n	Tot. no. of elements	Size x elem (cm)	Size y elem (cm)	Area elem (cm^2)	Simulation time (s)
3	9	27	7.67	8.33	63.89	25
9	27	243	2.56	2.78	7.10	1600
18	54	972	1.28	1.39	1.77	3600
24	72	1728	0.96	1.04	1.00	8700
27	81	2187	0.85	0.93	0.79	16000
30	90	2700	0.77	0.83	0.64	30000

The grid sensitivity estimation of the model was checked on the temperature and overall heat and mass exchanged, calculated on inlet and outlet conditions, at the end of the simulation for both the ADS and EVA. A summary of all the comparisons is reported in Tables 4.5, 4.6 and 4.7.

Table 4.5: summary results grid sensitivity T_{ADS} and T_{EVA} outlet at the end of simulation

m	n	T_{ADS} out last (°C)	% Δ previous grid	% Δ 30x90 grid	T_{EVA} out last (°C)	% Δ previous grid	% Δ 30x90 grid
3	9	24.84	-	6.59	23.29	-	0.77
9	27	25.97	4.56	2.33	23.18	0.49	0.27
18	54	26.33	1.37	0.99	23.14	0.16	0.12
24	72	26.44	0.43	0.57	23.13	0.05	0.07
27	81	26.52	0.33	0.24	23.12	0.04	0.03
30	90	26.59	0.24	-	23.12	0.03	0.03

Table 4.6: summary results grid sensitivity Q_{ADS} and Q_{EVA} outlet at the end of simulation

m	n	Q_{ADS} (kJ)	% Δ previous grid	% Δ 30x90 grid	Q_{EVA} (kJ)	% Δ previous grid	% Δ 30x90 grid
3	9	8810	-	9	-8812	-	9
9	27	9198	4.4	5	-9200	4.41	5
18	54	9489	3	2	-9497	3.16	2
24	72	9650	2.34	0.9	-9653	2.34	0.9
27	81	9710	0.6	0.3	-9715	0.6	0.3
30	90	9739	0.3	-	-9745	0.3	-

Table 4.7: summary results grid sensitivity M_{wADS} water and M_{wEVA} outlet at the end of simulation

m	n	M_{wADS} (kg)	% Δ previous grid	% Δ 30x90 grid	M_{wEVA} (kg)	% Δ previous grid	% Δ 30x90 grid
3	9	-2.271	-	7.30	2.591	-	12.67
9	27	-2.169	4.5	2.48	2.420	6.6	5.23
18	54	-2.139	1.4	1.05	2.368	2.14	2.98
24	72	-2.129	0.44	0.60	2.329	1.64	1.29
27	81	-2.122	0.34	0.26	2.299	1.27	1.29
30	90	-2.117	0.26	-	2.292	0.28	-

The acceptable trade off between computational time, thinking that two of this models will have to run for a whole month in parallel in the FREESCOO device, a total number of elements around 1000 was chosen. This will lead to errors < 1 % for temperature and water balances and $<$2% for the heat balances.

Calibration results

As mentioned in the previous section the 2-D model should be able to catch the supply heat rate dynamics, meaning the useful cooling effect, and the silica gel bed dynamics, meaning the water mass flow adsorbed and desorbed by the bed. For this reason the calibration process was conducted on an experiment where a complete adsorption starting from unknown conditions was done, then a complete regeneration and finally another complete adsorption. Figure 4.25 shows the simulated versus experimental results for the behaviour of the heat exchanger in terms of cumulative heat for each phase amd cumulative water mass exchanged. Then also the boundary conditions in terms of air flow rates, inlet temperatures and inlet humidity ratios for ADS,RIG and EVA are shown.

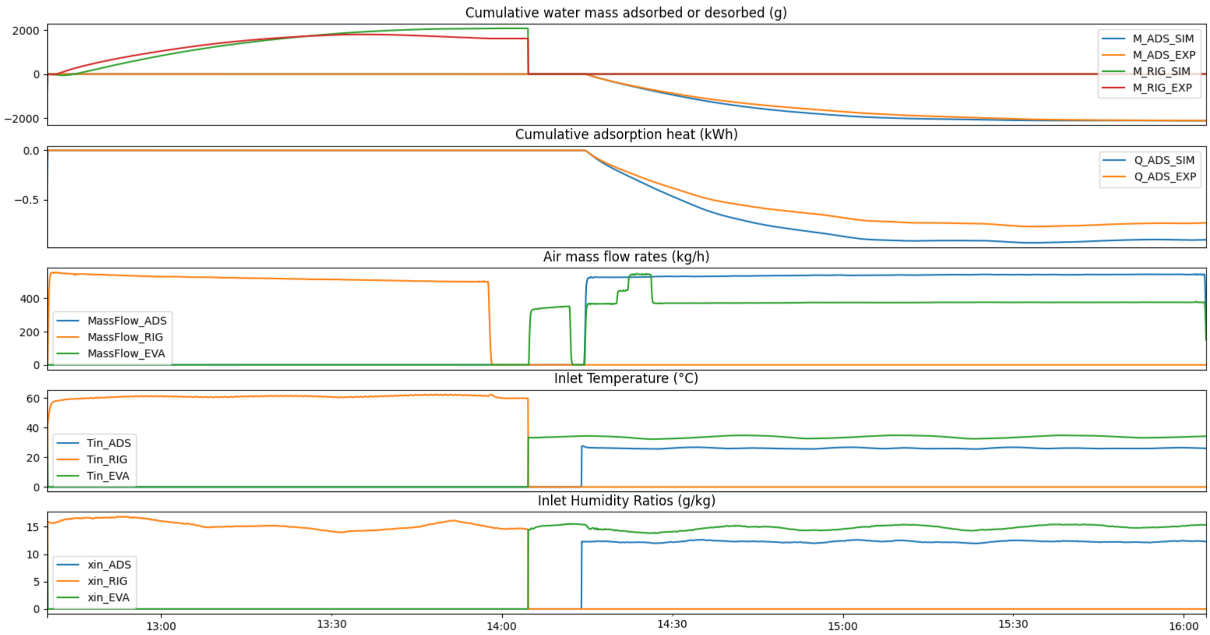

Figure 4.25: 1) comparison cumulative water balance RIG and ADS (bed dynamics); 2) comparison cumulative heat balance ADS (useful heat); 3) inlet temperature boundary conditions; 4) inlet Humidity Ratios boundary conditions for pre-calibrated model.

Looking at the simulation output before the calibration process the issues found are reported below. At the beginning of the regeneration phase the outlet air temperature increased quicker for the simulation than the experiment. This is due to the delayed thermal response of the measuring system introduced by the measuring tubes thermal inertia. Using the process mentioned in the previous section a suitable sensor "model" that reproduces the thermal inertia was identified and applied to the modelica model. Furthermore, at the end of the regeneration the outlet temperature of the simulation is lower than experimental value. Since this is a long complete regeneration in theory the outlet temperature should be very similar to the inlet temperature and slightly lower due the device thermal losses. However, the experimental regeneration temperature is 2 (°C) higher with respect to to the inlet. This suggests that there is an underestimation in the inlet air temperature, which is probably due to the thermocouple measuring the air tempereration inside the air to water heat exchanger to be not properly insulated. By adding a constant temperature offset to the inlet experimental temperature and the sensor model that takes into account the thermal dynamics of the measuring tube the chart in Figure 4.26, shows a much better agreement between the experimental and simulated values.

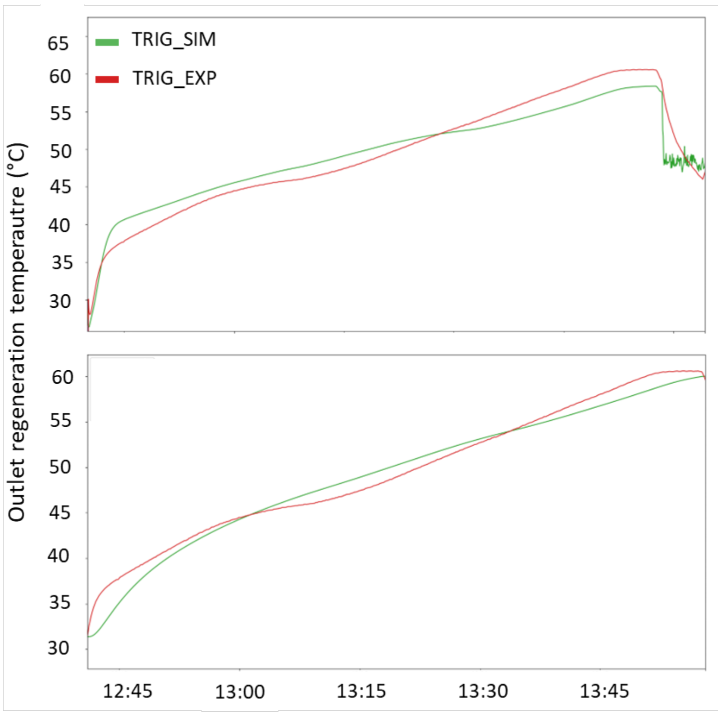

Figure 4.26: outlet regeneration temperature (°C) for simulation (SIM) and experiments (EXP): 1) Results before calibration process; 2) Results after calibration process.

In Figure 4.28 it can be noticed that the outlet ADS temperature in the experiment is consistently higher than the simulation. There are multiple reasons for this. In this simulation the f_{aw} parameter was chosen as 0.8, meaning that 80 % of the heat exchanger area was considered uniformly wet on the EVA side. However, the final value of the parameter after calibration was 0.05 meaning that only 5 % of the heat exchanger EVA surface is actually wet. This stems from the fact that the internal area of the EVA side is made up of the total area of the channels present in the polyethylene panel, which is much larger than the actual wet area. Furthermore, the sprinklers do not wet the whole surface evenly as shown in Figure 4.27.

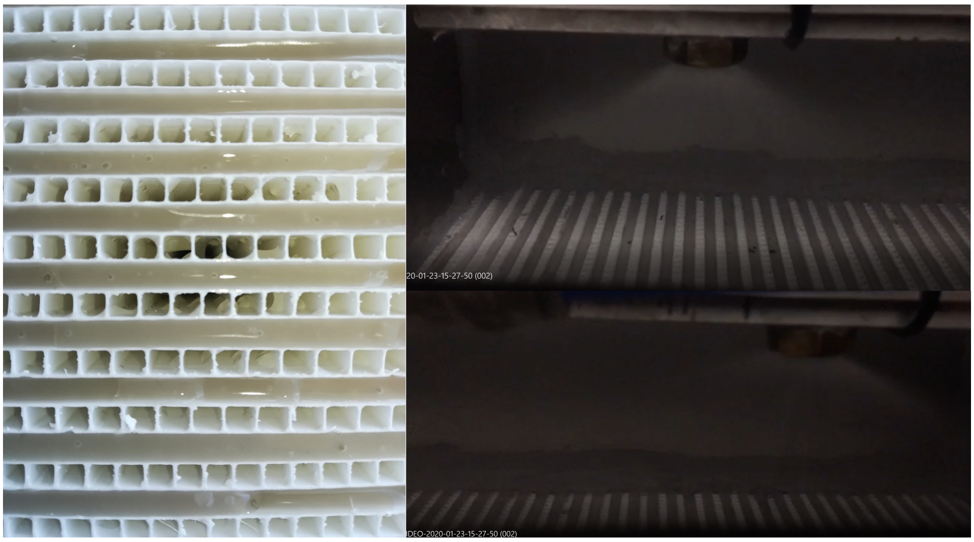

Figure 4.27: showcase on wettability of the EVA side. 1) portion of the EVA channels after turning on sprinklers; 2) showcase of sprinklers capability.

Then also in this case a sensor model that takes into account the dynamics of the measuring tube was considered.

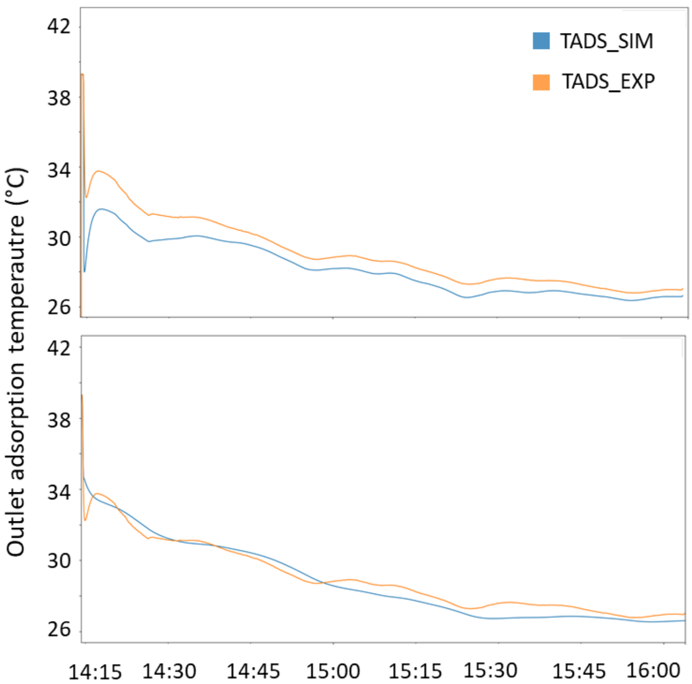

Figure 4.28: outlet Adsorption temperature for simulation in blue (sim) and experiments in orange (exp): 1) results before calibration process, 2) results after calibration process.

After tuning this parameters using the Dymola calibration toolbox the calibrated model results are shown in Figure 4.29.

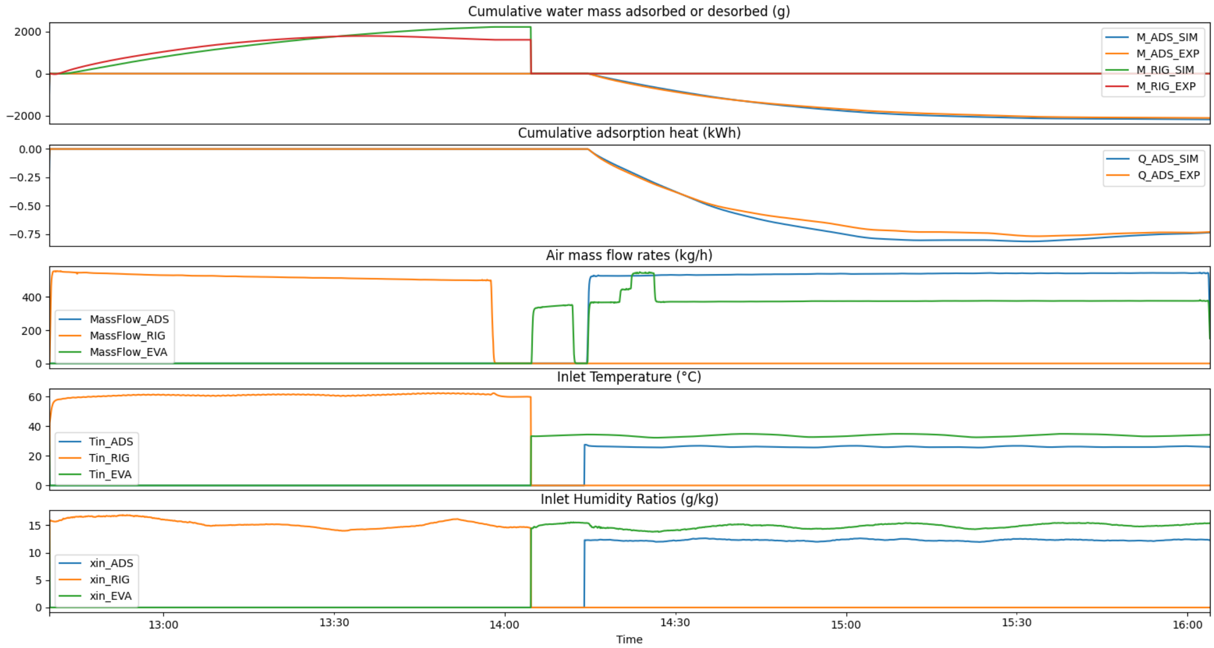

Figure 4.29: 1) comparison cumulative water balance RIG and ADS (bed dynamics); 2) comparison cumulative heat balance ADS (useful heat); 3) inlet temperature boundary conditions; 4) inlet humidity ratios boundary conditions for calibrated model;

By looking at 4.29 after the calibration process it can be seen that the simulation reflects better the experimental values. However, looking at the first chart and in particular at the regeneration side cumulative water desorbed, it can be seen that the simulation still overestimate the value with respect to the experiment. This is due to the fact that the humidity ratio for at the outlet of the regeneration was measured using only a relative humidity sensor. The reason is that the chilled mirror underwent a long cleaning cycle during the experiment and its data are not usable. Therefore it is reasonable to assume that the simulation gives a number close to the actual amount of water regenerated. This hypothesis is reinforced by the fact that we are considering a complete cycle (complete adsorption, complete regeneration, complete adsorption) and the total amount of adsorption water matches between simulation and experiment, and is around

2 (kg). At the same time the amount of water desorbed at the end of the regeneration phase for the simulation is also around 2 (kg). The couple of percentage difference can be attributed to the hysteresis effect taking place in the silica gel.

Validation results

in Figures 4.30 and 4.31 is show the validation of the calibrated models for different sets of experiments. The initialization of the calibrated model internal temperatures and water uptakes for the different experiment was found using the Dymola state estimator.

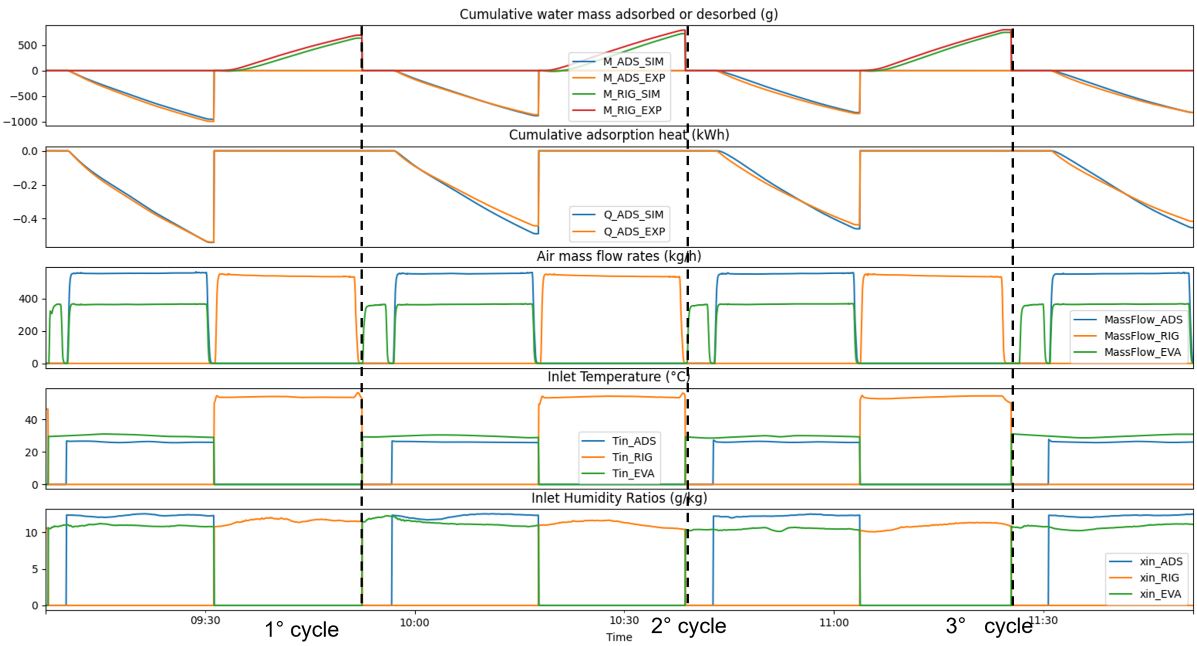

Figure 4.30: 1) comparison cumulative water balance RIG and ADS (bed dynamics) 2) comparison cumulative heat balance ADS (useful heat) 3) inlet temperature boundary conditions 4) inlet humidity ratios boundary conditions.

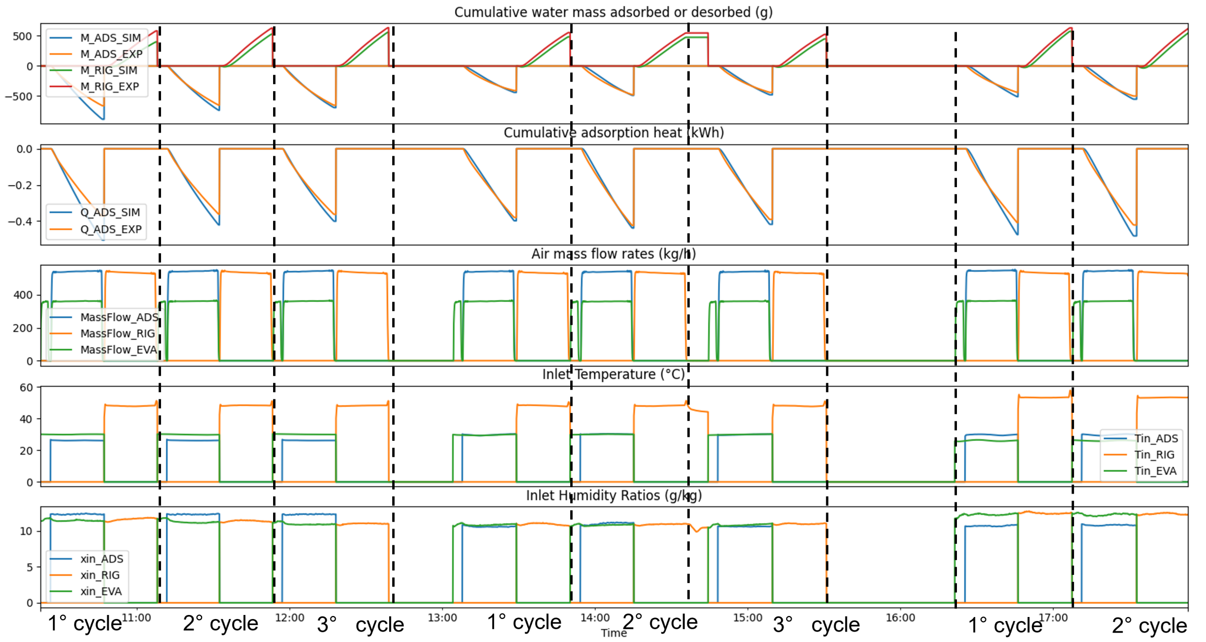

Figure 4.31: 1) comparison cumulative water balance RIG and ADS (bed dynamics); 2) comparison cumulative heat balance ADS (useful heat); 3) inlet temperature boundary conditions; 4) inlet humidity ratios boundary conditions

Looking at the time series data in Figures in 4.30 and 4.31, the calibrated model performs well both regarding the cooling heat rate and the water balance on the bed in different boundary conditions and cycles times. The average NRMSE on the cumulative cooling heat for all the experiments conducted is below 5% and for the water loading balance is below 4%.

4.6. Heat exchanger reduced order model

In order to carry out the parameter optimization a suitable low order model has to be trained using data from the 2-D model. The reason is that the 2-D model is too complex to be used for a two week parameter optimization. In Figure 4.32 is shown a figure of the reduced order The reduced order model equations and variables are explained below:

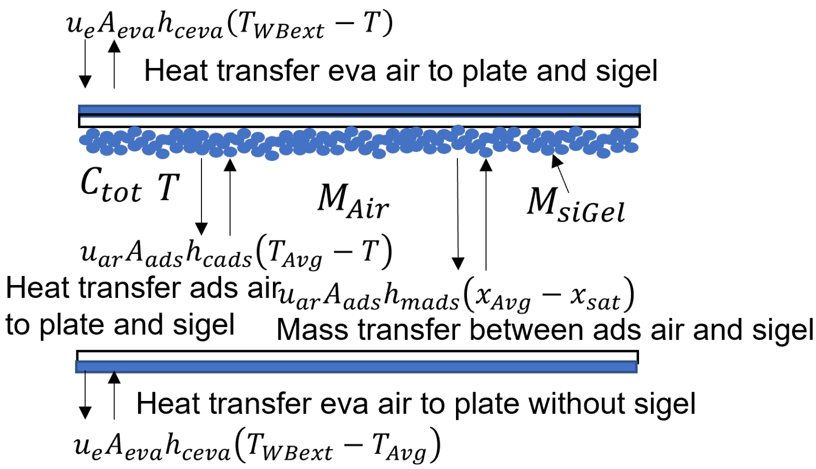

Figure 4.32: reduced order model configuration for FREESCOO.

Describing the variables shown in the figure: u_e $(-)$ is the control variable, 0 if there is no air flow on the evaporative side, 1 otherwise. u_{air} $(-)$ is the control variable, 1 when there is adsorption air flow, 0 viceversa. A_{eva} (m^2) is the evaporative side heat exchange area. A_{ads} (m^2) is the adsorption side heat exchange area. h_{ceva} $(W/m/K)$ is the convective heat transfer coefficient between evaporative side air stream and plate. $h_{cads}(W/m/K)$ is the convective heat transfer coefficient between adsorption side air stream and the silica gel plate node. T_{WBext} (K) is the external wet bulb temperature. T_{avg} (K) is the average adsorption air temperature between inlet and outlet. T (K) is the average temperature of plate and silica gel. C_{tot} is the combined heat capacity of plate and silica gel. M_{Air} is the mass of dry air present in the adsoprtion side of the heat exchanger. M_{siGel} is the mass of dry silica gel. h_{mads} $(W/m^2/K)$ is the mass transfer coefficient between adsorption air and plate , silica gel node. $x_{avg}(kg_w/kg_{dair})$ is the average adsorption air humidity ratio, while $x_{sat}(kg_w/kg_{dair})$ is the saturation humidity ratio at the interface. x_{sat} is calculated using an isotherm taken from the 2-D model. In this model the temperature is assumed to be constant at 40 (°C) to simplify the RH isotherm relationship so RH is:

$$RH = 0.0078 - 0.06W + 24W^2 - 124W^3 + 204W^4 \tag{4.17}$$

T_{avg} and x_{avg} are calculated instead as linear relationships between air inlet and outlet conditions:

$$\begin{aligned} T_{avg} &= \alpha T_{Air} + (1-\alpha) T_{AirIn} \ (K) \\ x_{avg} &= \beta x_{Air} + (1-\beta) x_{AirIn} \ (kg_w/kg_{dair}) \end{aligned} \tag{4.18}$$

T_{Air} (K) is the outlet adsorption air temperature, while T_{AirIn} (K) is the inlet adsorption air temperature. x_{AirIn} (kg_w/kg_{dair}) is the inlet adsorption air humidity ratio, while x_{Air} (kg_w/kg_{dair}) is the outlet adsorption air humidity ratio.

The equations building up the model are reported below:

$$M_{siGel}\frac{dW}{dt} = u_{air}A_{ads}h_{mads}(x_{Avg} - x_{sat}) \ (kg/s) \tag{4.19}$$

this equation represent the water mass balance of the silica gel. W $(kg_w/kg_{drysigel)}$ is the average water load of the whole heat exchanger.

$$M_{siGel}\frac{dW}{dt} + M_{Air}\frac{dx_{Air}}{dt} = \dot{m}_{Air}(x_{Airin} - x_{Air}) \ (kg/s) \tag{4.20}$$

This equation shows the overall water balance of the control volume made up by silica gel node and adsorption air node. M_{siGel} is the silica gel mass, M_{air} is the air node mass and $\dot{m}_{Air}$ is the adsorption air mass flow rate.

$$\begin{aligned} C_{tot}\frac{dT}{dt} &= u_e A_{eva} h_{ceva}(T_{WBext} - T) + \\ u_{ar}A_{ads}h_{cads}(T_{avg} - T) &+ u_{ar}A_{ads}h_{mads}(x_{avg} - x_{sat})\dot{q}_{ads} \ (W) \end{aligned} \tag{4.21}$$

This equation represent the energy balance for the silica gel and plate node.

$\dot{q}_{ads}$ (W/kg_w) is the latent adsorption heat rate.

$$C_{tot}\frac{dT}{dt} + C_{Air}\frac{dh_{Air}}{dt} = u_e A_{eva} h_{ceva}(T_{WBext} - T_{avg}) + u_e A_{eva} h_{ceva}(T_{WBext} - T) + \dot{m}_{Air}(h_{AirIn} - h_{Air})\ (W) \tag{4.22}$$

This equation represent the energy balance for the overall control volume. C_{Air} (J/kgK) is the adsorption air heat capacity. h_{AirIn} (J/kgK) is the inlet adsorption air enthalpy, while h_{Air} (J/kgK) is the outlet air enthalpy calculated as function of T and x via $h = cp_a T + x(cp_v T + \delta h_{lat})$. All the parameters present in this model were initialized starting from the available physical and geometric parameters of the heat exchanger. Using the Dymola calibration toolbox the model was then calibrated using the 2-D model output from the experiment shown in 4.25. The validation was then carried out using the data from 4.30. The simplified model on the validation results shows a NRMSE of 16% for the adsorption heat balance considering an average between all cycles and 15% for the water mass balance.

4.7. FREESCOO phase times optimization: cooling scenario

This Section reports the results coming from the simulation of the apartment in the cooling scenario,from 1^{st} of May to 30^{th} of September, using the detailed heat exchanger model explained in Section 4.4 for the FREESCOO device, comparing the baseline FREESCOO controller phase times with the optimal phase times. The optimal phase times were found exchanging the detailed 2-D FREESCOO heat exchanger model with the reduced order model explained in Section 4.6 to run the optimization.

4.7.1. Baseline and parameter optimization

As mentioned in previous sections the FREESCOO device is a transient DEC system and therefore the useful cooling power when keeping constant the air flow rates is determined by the adsorption and regeneration cycling times. Before showing the parameter optimization process in Figure 4.33 the baseline controller implemented in the cooling scenario Modelica model is shown.

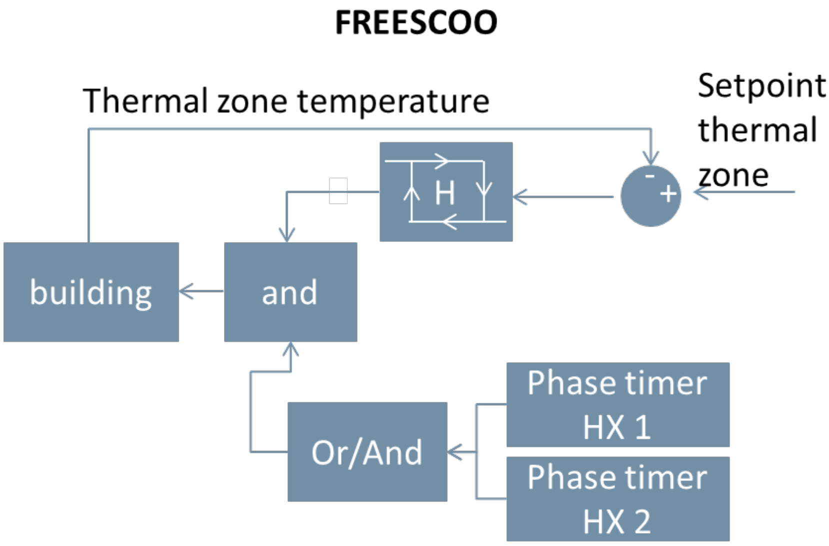

Figure 4.33: Control scheme for the cooling system in the Modelica model.

The baseline controller is made up of two parts. A thermostat for each thermal zone that has an hysteresis controller with an offset of 0.4 (°C) and a phase timer for each heat exchanger present in the FREESCOO device. The phase timer has an internal clock that starts a pre cooling and adsorption phase once the thermostat in one of the thermal zones requires a cooling action, after the adsorption time the heat exchanger goes into regeneration mode. The two heat exchanger are used sequentially to allow for a continuous cooling operation. In Figure 4.34 is reported the outlet temperature on the ADS / RIG side of the heat exchanger for a sample cycle of the FREESCOO heat exchanger starting with a regeneration phase, precooling and then adsorption.

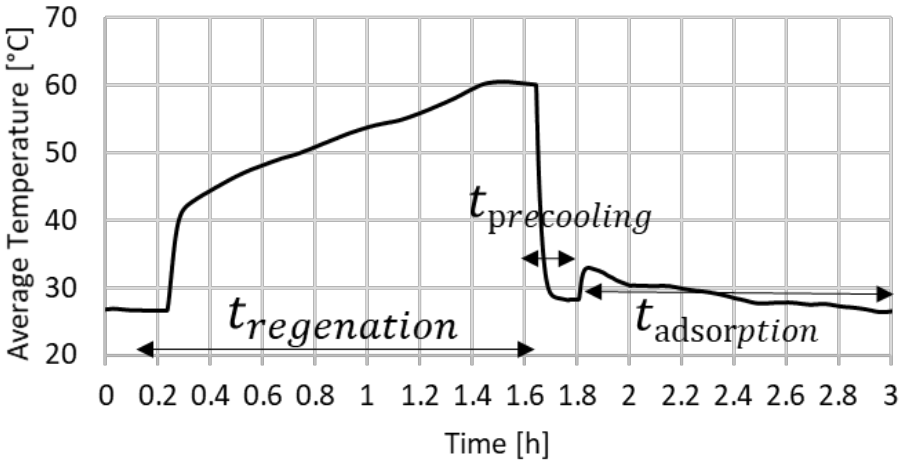

Figure 4.34: Typical cycle of the FREESCOO heat exchanger. On the x-axis the time in hours is shown, on the y-axis the average temperature (°C) of the heat exchanger is shown. $t_{regeneration}$ is the regeneration time, $t_{precooling}$ is the precooling time and $t_{adsorption}$ is the adsorption time.

The default values of the FREESCOO device come from the experiments conducted on the test bench shown in the previous section and are assumed as $t_{regeneration} = 1800$ (s), $t_{precooling} = 160$ (s) and $t_{adsorption} = 1800$ (s). Using Dymola parameter optimization toolbox coupled with the interior point solver IPOPT and the reduced order model of FREESCOO developed in the previous section new phase times parameters $t_{regeneration}$ and $t_{adsorption}$ were found. The optimization was a multi objective optimization run for two weeks per month for the whole cooling season from 1^{st} of May to 30^{th} of September. Two weeks were chosen as a trade off between getting a large enough number of data points for the optimization and a large enough amount of validation days afterwards. The optimization objectives were the minimization of temperature mismatch between setpoint and room air temperature for both thermal zones, regeneration overall thermal energy input and overall electrical consumption of the FREESCOO device. The priority in terms of weighting parameters for the optimization was given to the temperature mismatch.

4.7.2. Optimal phase times results

The summary of the monthly new values for the regeneration time $t_{regeneration}$ and adsorption time $t_{adsorption}$ are reported in Table 4.8, the training period was from the 10^{th} to the 24^{th} for each month.

Table 4.8: regeneration and adsorption optimized cycle times.

Months	$t_{adsorption}$ (s)	$t_{regeneration}$ (s)
May	3000	1000
Jun	2200	1100
Jul	1800	1400
Aug	1700	1600
Sep	2600	1050

Looking at Table 4.8 it is clear that in the warmest months the overall cycle frequency reduces and the difference between regeneration and adsorption reduces. This is consistent with intuition that making shorter cycles and longer regenerations leads to a higher mean thermal cooling power needed to cope with the cooling demand in the hottest months. The opposite can be said instead for late spring in May or September.

In Table 4.9 are reported the KPI results for the cooling season simulation in the baseline case and in the case with optimized cycle times. For this simulation the 2-D calibrated model of the FREESCOO heat exchanger was used. The KPIs analyzed are the thermal discomfort calculated as shown in the previous sections. The hygrometric discomfort calculated as in the number of hours where the humidity ratio is above the threshold value of 10.5 (g_w/kg_{dair}) in the thermal zones. The cooling thermal energy is the overall cooling energy provide to the thermal zone and calculated as $Q_{cool} = \int_{t_0}^{t_f} (\dot{m}_{ads}(h_{outads} - h_{inads}))dt$, where t_0 (s) is the start time of the simulation, t_f (s) is the stop time, $\dot{m}_{ads}$ (kg/s) is the adsorption air flow rate, h_{outads} $(J/kg/K)$ is the adsorption outlet enthalpy from FREESCOO and h_{inads} $(J/kg/K)$ is the inlet adsorption air enthalpy. The thermal COP is calculated as the ratio between the overall cooling energy provided Q_{cool} divided by the regeneration heat $Q_{reg} = \int_{t_0}^{t_f}(\dot{m}_{reg}cp_{air}(T_{inreg} - T_{ext}))dt$, where $\dot{m}_{reg}(kg/s)$ is the regeneration air flow rate, cp_{air} $(J/kg/K)$ is the air specific heat, T_{inreg} (°C) is the inlet regeneration temperature and T_{ext} (°C) is the ambient temperature. The electrical Energy Efficiency Ratio (EER) is calculated as the ratio between Q_{cool} and the overall electrical power consumed by FREESCOO. Starting from experimental data and the fan datasheets the electrical consumption of FREESCOO is calculated as $P_{el} = \int_{t_0}^{t_f}(P_{base} + k_{fan}(f(\dot{m}_{ads}) + f(\dot{m}_{reg}) + f(\dot{m}_{eva})))dt$, where P_{base} is the baseline electrical consumption when the device is turned on due to onboard electronics and water pump, k_{fan} is the fan characteristic parameter given in the datasheet together with the polynomial function of the air mass flow rate $f(\dot{m}_{air})$.

Table 4.9: KPI results for cooling scenario for baseline and in the case of optimized cycling parameters

Variables	baseline	improved pars
Temperature mismatch (Kh)	24	26 (+8%)
Humididity ratio mismatch (h)	7	7.6 (+8%)
Cooling thermal energy (kWh)	301	303 (+1%)
Thermal COP (-)	0.63	0.81 (+22%)
Electrical EER (-)	10.2	10 (-2%)

Looking at the KPI results there is a marginal increase in terms of temperature and humidity ratio mismatch, 8% with respect to the baseline. However, the absolute values remain quite small,less than 0.2 K on average per occupied hour, meaning that thermal and hygrometric comfort are achieved for most of the occupied hours. As expected the thermal COP improves with the new parameters by 22%, while keeping an almost identical EER meaning that in general the FREESCOO device was turned on for the same amount of time in the baseline and improved parameter cases. This means that passing from the baseline to the improved parameter case the time the adsorption is carried out for the majority of the time and the reduction in cooling power does not affect the comfort. Figure 4.35 shows a sample day in July comparing the baseline solution with respect to the improved parameter solution.

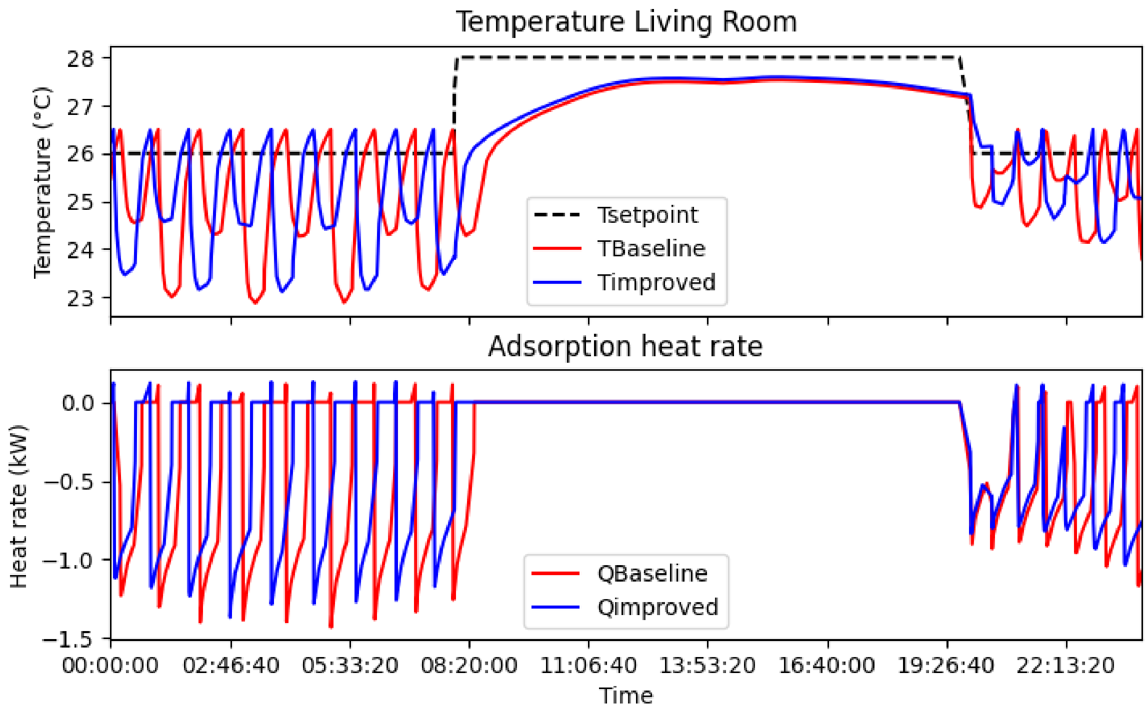

Figure 4.35: simulation of one day in July for the cooling scenario comparing the FREESCOO baseline controller and the improved controller. For both plots in the x-axis is shown the time for the day. The blue line corresponds to the results of the improved controller, the red to the baseline and the black dashed line to the setpoint. The top chart shows the air temperature in the living room on the y-axis, while the bottom chart shows the adsorption cooling heat rate.

Looking at Figure 4.35, it can be seen that the room temperature is always lower than the setpoint plus the 0.4 (°C) hysteresis and that the average adsorption heat rate is lower in the improved case. However, it's also clear that a lot of the time FREESCOO cools the internal air below the setpoint value minus the hysteresis value. There are three main reasons for this behaviour. The first one is that to avoid to many on and offs of the FREESCOO device, it will work for a minimum amount of time before switching off set to 10 (min). The second reason is that the FREESCOO controller has only an hysteresis controller and the air flow rate is kept constant at nominal value. The third reason is that the apartment model was calibrated when empty, meaning that the capacity of the air node is low and probably the result would be different with the addition of furniture that would increase the heat capacity of the room.

5 | MPC comparisons and rules extrapolation

This Chapter reports the work carried out that makes the effort to compare different Model Predictive Control (MPC) solvers and formulations and extrapolate a possible general strategy and solver approach for similar HVAC systems. This part of the work was submitted as a separate journal paper [18], see attached pre-print at the end of the manuscript. In Section 5.1 are presented the theoretical approaches used to derived the reduced order model for the optimization. In Section 5.2 are presented all the formulations used including additional constraints and solver choices. Finally, in the Results section 5.4 are presented a summary of KPI and detailed time series analysis results. In Section 5.5 the analysis of the MPC trajectory and parameter extrapolation is reported.

5.1. MPC reduced order model theoretical approaches

The core component of the MPC is the building and HVAC models used for the prediction, that can range from a purely numerical black-box such as Artificial Neural Networks (ANN) to detailed physical models called white box. The advantages of the first approach are that the preliminary knowledge on the building and HVAC systems does not have to be known a priory and the model is very lightweight and can be computed very quickly. The disadvantage is that a lot of good quality data is required to train data driven black box models and that traditional optimization techniques using model derivatives to estimate the optimal control trajectory cannot be used. The opposite is true for the white box modelling approach. In this case, more preliminary data is required (e.g. building plans, geometry, physical properties), but less data are needed for the calibration phase. However, these models tend to be computationally expensive and too complex to be used directly into an optimization engine. The best of both worlds is a grey box approach, such as [72] where a Resistance Capacitance (RC) electrical thermal analogy model was used. In these way the model retains a physical meaning, requiring some preliminary knowledge on the building and less data for the training process than for a black box model, whilst being more lightweight and suitable for the optimization process than a white box model. So, I identified a grey-box model based on resistance capacitance analogy using the Matlab identification toolbox [73] to be used within the MPC controller. Different combinations of number of Resistances (R) and Capacities (C) were tried leading to a 7R3C scheme that was adopted for each thermal zone (Figure 5.1). The three capacities are related to the room temperature T_r, wall temperature T_w and floor temperature T_f. Resistances connect the capacity nodes to each other and furthermore, two resistances connect C_r and C_w to the external temperature T_{ext}. The wall has a resistance that connects also with the sky temperature T_{sky}. The sky temperature allows the low order model to better treat the radiative heat exchange with the external environment, especially in the presence or absence of clouds. Lastly, the capacitances of the rooms are connected to each other as a proxy for air exchange between the two thermal zones. The solar heat source $\Phi_s(W/m^2)$ is the hemispherical global radiation hitting the external walls and windows. It is split by the coefficients a and c between the wall and the floor and multiplied respectively by the opaque area A_{wall} and the windows area A_{win}. a and c are tuning parameters that can be assumed as proxy of absorptance and trasmittance. Φ_{int} (W) are the internal gains split in sensible and radiative thermal power by the parameter b. The sensible part goes to the room capacitance C_r and radiative goes to the wall capacitance C_w. Lastly, the heat flow rate on the floor heating system is shown in the figure as $\Delta\dot{H} = \dot{H}_{out} - \dot{H}_{in}$. It is modelled in four different ways, depending on the optimization formulation being tested:

1. linear formulation where the optimal control variable for $\Delta\dot{H}$ is the heat flow $\dot{Q}$
2. Linear formulation where the optimal control variable for $\Delta\dot{H}$ is the supply temperature T_{in} with a constant flow rate equal to the nominal value $\dot{m}_{fnom}$
3. nonlinear formulation where the optimal control variables for $\Delta\dot{H}$ are the valve position u_i [0;1] with $u_i \in \mathbb{R}$ multiplied by $\dot{m}_{fnom}$ and the supply temperature T_{in}
4. Mixed Integer Nonlinear formulation where the optimal control variables for $\Delta\dot{H}$ are the valve position u_i [0;1] with $u_i \in \mathbb{Z}$ multiplied by $\dot{m}_{fnom}$ and the supply temperature T_{in}

Furthermore, for the formulations using the supply temperature T_{in} a control variable, there is a need to estimate the outlet temperature T_{out} to calculate the heat flow rate in the floor. Therefore, a linear relationship to correlate the outlet temperature from the floor heating circuit T_{out} to the inlet T_{in} and floor T_f temperatures is introduced:

$$T_{out} = w_f T_{in} + (1 - w_f) T_f \tag{5.1}$$

The assumption behind this linear relationship is that water mass flow rate $\dot{m}_{floor}$ is constant so that the heat transfer coefficients remain constant. This assumption is valid for this case study since the zones valves can only be open or closed and do not provide variable flow control.

Since the training of RC models is not the focus of the present work, the identification procedure is briefly reported. The capacities and resistances of the model were trained using two weeks of free floating data, where the boundary conditions were derived from a synthetic profile obtained through a Fourier analysis of the typical year data [74]. In this way all the major frequency components are present. An additional week of data where the heating system is on is used to find the weighting parameter w_f. The result of the identification leads to a NRMSE of 18% for the whole heating season, in Milan from the 15^{th} of October to the 15^{th} of April, in open loop simulation.

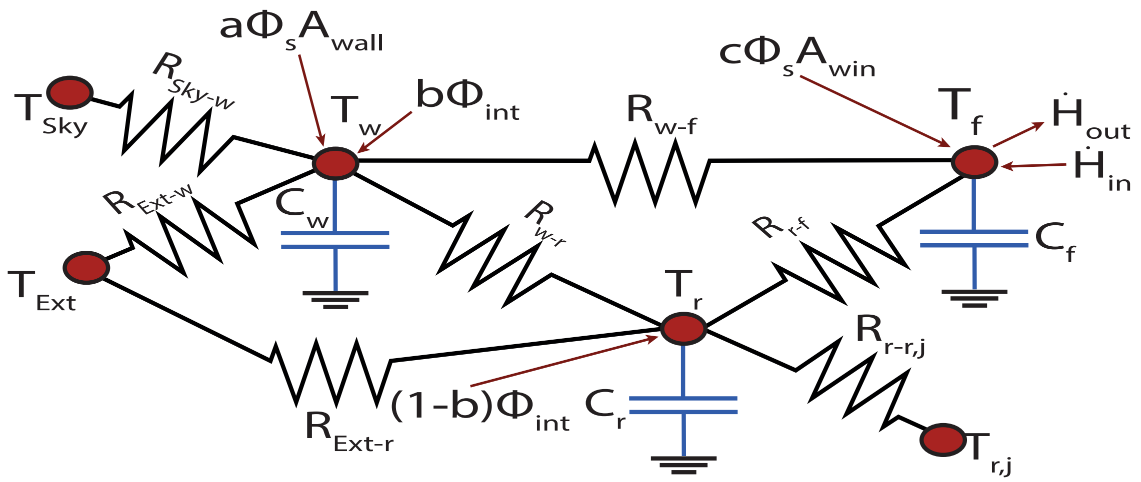

Figure 5.1: Thermal zone reduced order model, the red dots are the temperatures, the blue parallel lines are the capacitors associated wit the temperature states, the resistances are the thermal resistances between the temperatures and the red lines indicate a heat flow into the node.

5.2. MPC used formulations

The reduced order model problem can range from linear to nonlinear mixed integer thanks to the different formulations for the optimal control variables. Furthermore, nonlinearity due to additional constraints and objective function needs to be added to characterize the final MPC problem class.

Table 5.1: MPC states and disturbances

Control horizon	24 (h)
Time step	15 (min)
Solution update	Every time step
Discretization	Direct collocation
States (x)	T_{rliv} $(°C)$: $(-\infty, +\infty)$ T_{fliv} $(°C)$: $(-\infty, +\infty)$ T_{wliv} (°C) : $(-\infty, +\infty)$ T_{rbed} $(°C)$: $(-\infty, +\infty)$ T_{fbed} $(°C)$: $(-\infty, +\infty)$ T_{wbed} $(°C)$: $(-\infty, +\infty)$
Disturbances	T_{ext} $(°C)$: $(-\infty, +\infty)$ T_{sky} $(°C)$: $(-\infty, +\infty)$ T_{setliv} $(°C)$: $(-\infty, +\infty)$ T_{setbed} (°C) : $(-\infty, +\infty)$ $\dot{Q}_{rad}(kW)$: $[0, max]$ $\dot{Q}_{intliv}(kW)$: $[0, max]$ $\dot{Q}_{intbed}(kW)$: $[0, max]$ p_e(€) : $(constant)$

Table 5.1 contains all the common elements across the formulations, including dynamic states, disturbances and implementation choices. In the table only the final choice for control horizon and time step is shown. However, four different control horizons were tried for the optimal control problems from 6 up to 72 (h). Considering that we are dealing with deterministic forecasts, in theory the longer the prediction horizon, the better will be the solution. However, this comes at an increased computational time. The final choice was 24 (h) since longer times did not show any improvement on the KPIs. This time aligns with the fact that we are dealing with a heavy construction and a floor heating with a high thermal inertia. The suitable time step is also affected by the slow dynamics of the floor heating. Bringing it below 15 (min) did not give any significant benefits. The MPC solution is updated at every time step, so every 15 (min). To convert the optimal control problem into a programming problem, a direct collocation method [75] was implemented in the Pyomo problem statement. Direct collocation means that the time dependant optimal control problem was

Table 5.2: MPC controls, constraints and objectives

Control (u)	u1	$\delta_{liv,bed}\ (°C):\ (-\infty,+\infty)$
	u2	$T_{in}(°C):\ [T_{mix}, T_{inmax}]$
	u3	$u_{liv,bed}(-):\ \{0,1\} \in \mathbb{Z}$
	u4	$u_{liv,bed}:\ [0,1] \in \mathbb{R}$
	u5	$u_{liv,bed} = 1$
	u6	$\dot{Q}_{liv,bed}(kW):\ [0, max]$
Constraints (c)	c1	Comfort constraint $T_{r,liv,bed}(t) - T_{set,liv,bed}(t) + \delta_{liv,bed}(t) \geq \varepsilon$
	c2	Maximum heat flow rate $1/(1-w_f)\dot{Q}_{liv,bed}(t) \leq \dot{m}_f c_w(T_{inmax} - T_{f,liv,bed}(t))$
	c3	Mixing constraint $T_{in} \geq T_{mix} = \dfrac{u_{liv}T_{f,liv} + u_{bed}T_{f,bed}}{(u_{liv}+u_{bed})}$
Objective function	J_{tot}	Objectives (j) $min(J_{tot} = \int_{t_0}^{t_f}\sum_{i=1}^{N} k_i j_i dt)\ with\ 0 \leq k_i \leq 1$
	j1	Energy cost QP $J_{en} = p_e \dfrac{(\Delta\dot{H}_{liv}(t) + \Delta\dot{H}_{bed}(t))}{COP(T_{ext})(t)}$ (€)
	j2	Energy cost NLP $J_{en} = p_e \dfrac{\Delta\dot{H}_{liv}(t) + \Delta\dot{H}_{bed}(t)}{COP(T_{ext}, T_{in})(t)}$ (€)
	j3	Temperature mismatch $J_{com} = \delta^2(t)\ (K^2h)$
	j4	Frequency switching $J_{swi} = \dfrac{du_{liv}}{dt}^2 + \dfrac{du_{bed}}{dt}^2\ (-)$
	j5	Binary constraint $J_{bin} = u_{liv}(1-u_{liv}) + u_{bed}(1-u_{bed})\ (-)$

discretized into a subset of problems, one for each time step where the control can be considered constant in my approximation. The six states include all the temperatures in both thermal zones and the disturbances are the same as reported in the previous section plus the two room set points and the energy price p_e.

Table 5.2 reports all the control variables, constraints and objectives functions utilized in the different formulations. Each problem formulation will have a subset of these as shown in Table 5.3. Starting explaining Table 5.2 elements from the optimal control variables, $u1$ is an auxiliary variable that is coupled with the constraint $c1$ and the objective $j3$. Looking at the constraint $c1$, δ will be higher than zero if the room temperature T_r is lower than the setpoint temperature T_{set}, so by including δ^2 in the objective that needs to be minimized, the solver is forced to keep T_r higher than the setpoint temperature. The other control variables are related to the heat flow rate in the floor and are explained in section in the previous section. $u2$ is the supply temperature and can go from the the maximum temperature fixed at 45 (°C) to avoid high temperatures in the floor, to a minimum temperature, defined as the adiabatic mixing temperature in constraint $c3$. The formulation of $c3$ comes from a local energy and mass balance at the return outlet of the floor heating system under the assumption that the nominal flow rate is the same for all the circuits. $T_{f,liv,bed}$ is the floor temperature and $u_{liv,bed}$ is the floor heating circuit valve control. $u3$ are the valve controls under the assumption that the valve can continuously modulate the flow from totally closed to totally opened. $u4$ are the valve controls under the assumption that the valve can only be fully closed or fully open like in the case study emulator model. $u5$ are the valve controls under the assumption that the valve is kept always open and the modulation is done only on the supply temperature T_{in}. Finally, $u6$ considers as optimal control variable the heat flow rate directly in the floor that can go from zero to a maximum value determined by constraint $c2$.

The heat flow rate constraint $c2$ limits the maximum heat flow rate linearly with the floor temperature as a function of the maximum supply temperature T_{inmax} and the weighting parameter w_f. This constraint helps modelling the behavior of the floor slab, where the higher the floor temperature the lower is the heat rate at constant supply temperature. In the constraints section of the table are reported $c1, c2$ and $c3$ that are coupled with the relative optimal control variables as explained above.

In the last section of the table are presented all the objectives that can make up the the overall objective to be minimized by the solver. The final objective function J_{tot} to be minimized is the sum of different objectives each weighted by a k_i parameter, where i corresponds to a specific objective. The weighting parameters k_i are needed to balance the impact of each objective on the total objective function j_{tot}.To find the best values of k_i several iterations of the parameters were tried to balance the weights, while giving priority to the comfort constraint. The objectives $j1$ and $j2$ are the energy cost and are calculated as the energy price p_e multiplied by the total heat flow rate provided by the heat pump , $\Delta\dot{H}_{liv}(t)+\Delta\dot{H}_{bed}(t)$, divided by the heat pump COP. The COP is a function of the external temperature $\mathrm{COP}(T_{ext})$ for $j1$, so the underlying problem remains quadratic. In $j2$ it becomes a function of external and supply temperatures $\mathrm{COP}(T_{ext}, T_{in})$, so the optimization problem becomes non linear because a control variable is present in the denominator of a fraction. $j3$ is the temperature mismatch between the room temperature T_r and the setpoint T_{set} and works as a comfort proxy. The frequency switching objective $j4$ is the sum of the squared valve controls derivatives. This objectives serves the purpose of penalizing undesirable sudden changes in the control variables. The binary constraint forces u_{liv} and u_{bed} to be either close to 0 or 1 to avoid having increasing the value of the objective function. The reasoning behind this constraint is to approximate a mix integer nonlinear problem, while keeping it continuous nonlinear. However, care should be taken when initializing this optimization problem because the introduction of the binary constraint causes a big discontinuity in the solution space.

Starting from Tables 5.1 and 5.2 several MPC formulations can be defined ranging from linear with a quadratic objective to mixed integer nonlinear. Table 5.3 reports the MPC formulations coupled with the solvers and relative options used for the study.

Table 5.3: MPC problem statement.

Tag	Formulation	Problem type	Solver	Tolerance	Initialization	Post process	Subsolvers
MPC1	$\delta_{liv/bed}$, $\dot{Q}_{liv/bed}$, C_{comf}, C_{Qmax}, $j_{COP,L}$, j_{comf}, j_{switch}	QP	IPOPT	10^{-6}	Free-floating	$\dot{Q}_i$ conversion into u_i and $T_{in,set}$	MA57
MPC2	$\delta_{liv/bed}$, T_{in}, u_{open}, C_{comf}, C_{Tmin}, $j_{COP,NL}$, j_{comf}, j_{switch}	NLP	IPOPT	10^{-6}	Free-floating	conversion of u_i from T_{in} and T_{in} $= T_{in,set}$	MA57
MPC3	$\delta_{liv/bed}$, T_{in}, u_R, C_{comf}, C_{Tmin}, $j_{COP,NL}$, j_{comf}, j_{switch}	NLP	IPOPT	10^{-6}	Free-floating	round u_i and T_{in} $= T_{in,set}$	MA57
MPC4	$\delta_{liv/bed}$, T_{in}, u_R, C_{comf}, C_{Tmin}, $j_{COP,NL}$, j_{comf}, j_{switch}, j_B	NLP	IPOPT	10^{-6}	Free-floating	$T_{in} = T_{in,set}$	MA57
MPC5	$\delta_{liv/bed}$, T_{in}, u_B, C_{comf}, C_{Tmin}, $j_{COP,NL}$, j_{comf}, j_{switch}	MINLP	Bonmin-BB	10^{-4}	MPC3 sol	$T_{in} = T_{in,set}$	CBC, IPOPT
MPC6	$\delta_{liv/bed}$, T_{in}, u_B, C_{comf}, C_{Tmin}, $j_{COP,NL}$, j_{comf} ,j_{switch}, j_B	MINLP	Bonmin-BB	10^{-4}	MPC4 sol	$T_{in} = T_{in,set}$	CBC, IPOPT
MPC7	$\delta_{liv/bed}$, T_{in}, u_B, C_{comf}, C_{Tmin}, $j_{COP,NL}$, j_{comf}, j_{switch}, j_B	MINLP	Bonmin-Hyb	10^{-4}	MPC4 sol	$T_{in} = T_{in,set}$	CBC, IPOPT
MPC8	$\delta_{liv/bed}$, T_{in}, u_B, C_{comf}, C_{Tmin} ,$j_{COP,NL}$, j_{comf}, j_{switch}	MINLP	Baron	10^{-4}	MPC3 sol	$T_{in} = T_{in,set}$	CPLEX, IPOPT
MPC9	$\delta_{liv/bed}$, T_{in}, u_B, C_{comf}, C_{Tmin}, $j_{COP,NL}$, j_{comf}, j_{switch}, j_B	MINLP	Baron	10^{-4}	MPC4 sol	$T_{in} = T_{in,set}$	CPLEX, IPOPT
MPC10	$\delta_{liv/bed}$, T_{in}, u_B, C_{comf},C_{Tmin} ,$j_{COP,NL}$, j_{comf}, j_{switch}, j_B	MINLP	SCIP	10^{-4}	MPC4 sol	$T_{in} = T_{in,set}$	CPLEX, IPOPT

Table 5.3 shows ten MPC formulations that were tested. The Tag column reports the formulation names. The Formulation column shows the corresponding optimization variables, constraints and objectives described in Table 5.2. Note that the auxiliary variable δ, the temperature constraint C_{comf}, the temperature mismatch j_{comf}, and the switching objective j_{switch} are present in all formulations. The Problem Type column reports the optimization problem type for each MPC formulation, which can be either

QP, NLP or MINLP. The Solver column shows the solver chosen, including the MINLP handling algorithm option if present. The Tolerance column is the solver tolerance which was determined through a parametric study as a compromise between quality of the solution and computational time for each solver. The Initialization column defines how the optimization problem variables were initialized. Free-floating initialization means that a simulation is run using the reduced order model subject to the same boundary conditions, as in the forecasts used for the optimal control, with the floor heat flow rate set to zero. In other formulations, a slightly randomized solution of a different MPC formulation is used as initialization as indicated. The Post Process column shows the steps needed to convert the optimal control trajectory into the physical control inputs used in the emulator model. The Subsolvers column refers to the solvers used by the solver indicated in the Solver column. Another parameter not included in the table is the Timeout. It corresponds to the maximum time between each control horizon optimization and was fixed at two minutes for all formulations as a compromise between giving the solvers enough time to converge to a solution and the overall computational time.

Below, a summary for each MPC formulation presented in Table 5.3 is provided:

- MPC1: This formulation uses heat flow rates directly as optimization variables $\dot{Q}_{liv/bed}$, and $j_{COP,L}$ as the energy objective. In this way the final constraints are linear in optimization variables, and the objective function is quadratic, making a QP problem. The solver of choice for the QP was IPOPT with the linear subsolver MA57. The tolerance was set to 10^{-6} from the default value of 10^{-8} and the timeout time to 120 $[s]$, and the initialization is free-floating. Some post processing is required to convert the optimal control trajectory into the physical control variables used in the emulator. If $\dot{Q}_{liv/bed}$ is higher than a threshold value, equivalent to the minimum cutoff power of the heat pump set as 20 % of the nominal value 800 [W], the valves $u_{liv/bed}$ will be opened else they remain closed. The supply temperature setpoint is calculated using the previous step return temperature plus the delta given by $\dot{Q}_{liv/bed}$.

- MPC2: This formulation uses the supply temperature as an optimization variable T_{in}, while the circuit valves remain always open u_{open}, and $j_{COP,NL}$ is used for the energy objective. Together with the linear radiant floor heat modeling approach (see point 2) in Section 5.1, the final constraints are linear in optimization variables, and nonlinear in the objective due to the presence of COP as a function of the supply temperature T_{in}, making an NLP problem. The solver of choice for the NLP problem was IPOPT with the linear subsolver MA57. The tolerance was set to 10^{-6} from the default value of 10^{-8} and the timeout time to 120 [s], and the initialization is free-floating. A post process is required to convert the optimal control trajectory into the physical control variables used in the emulator. If the supply temperature T_{in} is higher than a threshold value, the valves $u_{liv/bed}$ will be opened, else they remain closed.

- MPC3: Compared to MPC2, this MPC does not assume the circuit valves are fully open. Instead, it relaxes the on/off binary constraints to a real number set u_R as mentioned in the third bullet item in Section 5.1 and in Table 5.2. The final problem formulation is nonlinear in terms of constraints and optimization variables due to the multiplication between supply temperature and valve control. The objective is also nonlinear due to the presence of COP as a function of the supply temperature T_{in} and the multiplication of two optimization variables in the heat flow rate calculation. The added nonlinearity of MPC3 compared to MPC2 makes the problem nonconvex because the solver can change T_{in} or u_R to modulate the heat flow rate, making the process of finding a global optimum harder. Solver settings were identical to MPC2. MPC also needs to convert the optimal control trajectory into the physical control variables used in the emulator. If the circuit valve $u_{liv/bed}$ value is higher than a threshold value. the valves $u_{liv/bed}$ will be opened, else they remain closed.

- MPC4: This formulation is identical to MPC3, apart from the addition of the binary objective j_B. The idea behind j_B is to force u_R to be either closed $u_R = 0$, or open $u_R = 1$, by penalizing all solutions that modulate the flow rate in a continuous manner. This allows for a smaller control space by reducing the optimal operating range of the zone valves. This will serve as an NLP approximation of an MINLP formulation, corresponding to actual physical control variables of the emulator.

- MPC5: This formulation is the same as MPC3 but replacing the continuous relaxation (u_R) with the binary constraint (u_B). In this way the final problem formulation is mixed integer nonlinear due to the multiplication between continuous supply temperature and on/off valve control variables, making a MINLP problem. The additional complexity of MPC5 compared to the previous QP and NLP formulations requires a dedicated MINLP solver. The solver of choice for MPC5 was BONMIN-BB. CBC was used as MIQP subsolver and IPOPT as NLP solver. The tolerance was set to 10^{-4} from the default value of 10^{-6} and the timeout time to 120 $[s]$. The initialization is done by taking the solution of MPC3 after rounding the values of $u_{liv/bed}$. The MINLP solution can be directly applied to the emulator with no need for post processing of the solution.

- MPC6: This formulation is identical to MPC5 apart from the addition of the binary objective j_B and the initialization done with MPC4 solution. The rationale is similar as in the transition from MPC3 to MPC4. However, instead of a single NLP problem, it is extended to all subsets of NLP problems generated by the MINLP solver.

- MPC7: This formulation is identical to MPC6, where a different MINLP algorithm option was used for the Bonmin solver BONMIN-Hyb.
- MPC8: This formulation is identical to MPC5, where a different MINLP solver was used named Baron. The MIQP solver is CPLEX and the NLP solver is IPOPT.
- MPC9: This formulation is identical to MPC8 with the addition of the binary constraint j_B.
- MPC10: This formulation is identical to MPC9 with the difference that the MINLP solver of choice was SCIP.

5.3. Co-simulation setup.

All the elements shown in previous sections are coupled in a co-simulation. The optimal control routine runs on the Python toolbox Pyomo [56] and the detailed emulator model is wrapped in a Docker container using the BOPTEST software [62]. A schematic representation of the co-simulation is given in Figure 5.2.

Going more into the details of the co-simulation environment, all the cases mentioned in Table 5.3 were directly implemented in Python using a concrete instance modeling feature of Pyomo. The solvers were compiled externally and coupled with Pyomo using the AMPL interface. Finally, the Kalman filter from [76] was used to update the states of the reduced order model at each time initialization.

BOPTEST provides an easy to use API interface that allows the optimiza-

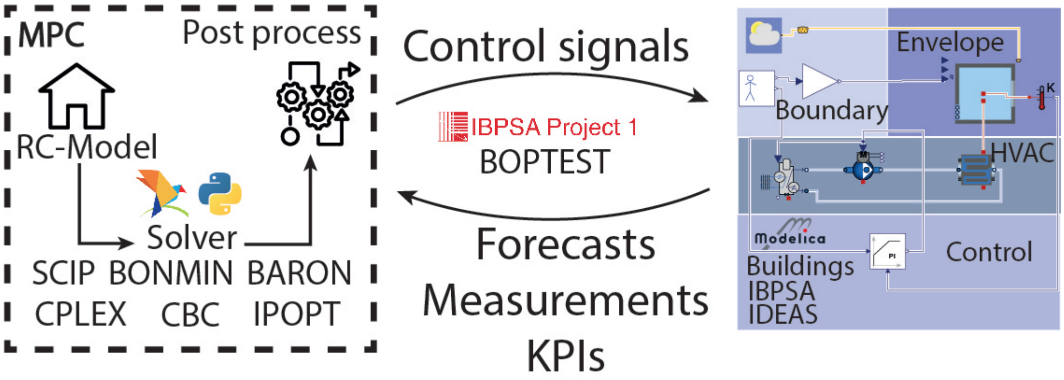

Figure 5.2: co-simulation setup,on the left the optimization environment in Python-Pyomo, on the right the detailed Modeica building and HVAC models and in the middle the software BOPTEST that allows the signal exchange, provides forecasts and KPIs

tion scripts to manipulate the control variables of the detailed model, access sensor data and access forecasts and the KPIs calculated by BOPTEST. The control variables are the supply temperature setpoint and the zone valve open or closed signal. The forecasts are the disturbance variables reported in Table 5.1 and are considered deterministic, meaning that the same disturbances will also be used in the emulator model. The measurements are the room temperature, the water supply temperature and the return temperature from each zone, and are used by the Kalman filter to estimate the initial value of room, wall and floor temperature for each zone. To estimate the performance of each MPC formulation, BOPTEST can calculate many KPIs, though this work considers the thermal discomfort, computational time ratio and energy cost . Furthermore, three additional KPIs were used to evaluate the performance of these MPC formulations, namely the total computational time of the MPC (s) solver, the thermal energy used, the control arc length and the number of MPC solver time-out or error events occurred throughout the evaluation period. The equations and descriptions are reported in Table 5.4, and the description of the variables is reported below. Only valid solutions are used to update the MPC control trajectory. Time-out solutions are valid most of the time, a solution is considered valid if the variables values are within the bounds, however,

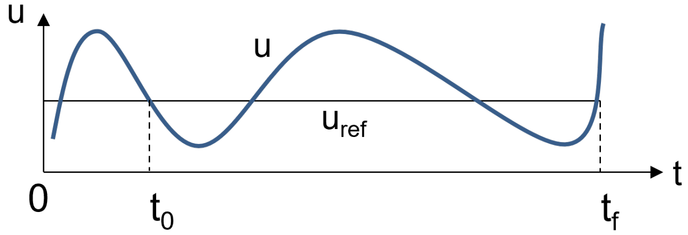

Figure 5.3: On the y-axis is the value of the control variable u and u_{ref} is the reference value kept as constant. On the x-axis is time with the evaluation period taken from t_0 to t_f.

it may be not fully converged, meaning that constraints may not be completely satisfied. Instead, solutions with a error in the solver status are discarded. In this case the solution at the previous time step is used until a new valid solution is found. All the simulations were carried out on a Linux Ubuntu 18 laptop with 16GB of RAM and an Intel(R) Core(TM) i7-8650U CPU @ 1.90GHz. All the solvers have multi thread capability so up to 8 threads were used for the simulations.

Table 5.4: BOPTEST and MPC specific KPIs

Name	Description	Equation	Type
K_{dis}	Discomfort	$\frac{\sum_{z=1}^{N}\int_{t_0}^{t_f} max(T_{set}(t)-T_r(t),0)dt}{N}$ (Kh/zone)	BOPTEST
K_{timr}	Computational time ratio	$\frac{\sum_{k=1}^{M}\frac{\delta T_k}{\delta t_k}}{M}$ (-)	BOPTEST
K_{cost}	Energy cost	$\frac{\int_{t_0}^{t_f} p_{el}\frac{\dot{Q}_{tot}(t)}{COP(t)}dt}{A_{tot}}$ (€ /kWh)	BOPTEST
K_{en}	Thermal energy supplied	$\frac{\int_{t_0}^{t_f}\dot{Q}_{tot}(t)dt}{A_{tot}}$ (kWh /m^2)	case study specific
K_{ttot}	Total computational time	(s)	case study specific
K_{err}	Solver errors or time-outs	(-)	case study specific
K_{conlen}	Control arc length	$\frac{\int_{t_0}^{t_f}\sqrt{1+(\frac{du}{dt})^2}dt}{\int_{t_0}^{t_f}\sqrt{1+(\frac{du_{ref}}{dt})^2}dt}$ (-)	case study specific

Regarding Table 5.4: in the discomfort KPI definition (K_{dis}), T_r (K) is the room operative temperature and T_{set} (K) the heating setpoint, N is the total number of zones, t_o and t_f are the initial and final time of the evaluation period; in the computational time ratio KPI definition (K_{timr}), $\delta T_k(s)$ is the MPC computational time at step k, M is the number of control steps and $\delta t_k(s)$ is the time interval of control step k; in the cost KPI definition (K_{cost}), p_{el} (€/kWh) is the electricity price considered as constant, equal to 20 (€/kWh), Q_{tot}(kWh) is the total energy supplied by the heat pump and A_{tot} (m^2) is the total floor area of the apartment. Q_{tot} (kWh) is also used to calculate the thermal energy KPI K_{en}; lastly, a new KPI is introduced in this manuscript called control arc length (K_{conlen}). The goal of the latter KPI is to showcase the amount of frequency switching for the control system throughout the evaluation period. So, K_{conlen} is the ratio between the length of the actual control trajectory versus a fictional reference trajectory u_{ref} that consider the control variable u to be constant for the evaluation period. A visual representation is given in Figure 5.3.

5.4. Results and conclusions

The evaluation period is the month of January. It is taken as representative for the whole heating season because similar conclusions can be drawn from the rest of the heating season. The MPC control trajectory is updated every time step, 15 (min), while the control horizon considered is 24 (h). The resulting optimization problem will be calculated for 2976 times and each iteration has around a 1000 constraints, 600 optimization variables for the linear problems and 1200 for the nonlinear problems. In the first Subsection 5.4.1, BOPTEST and custom KPIs are compared to have an overview of all the different formulations. In the second Subsection 5.4.2, a detailed analysis on the time series results is carried out to better explain some of the differences found in the KPIs. In Sub-section 5.4.3 a summary of the results and a justification for the best MPC formulation are given.

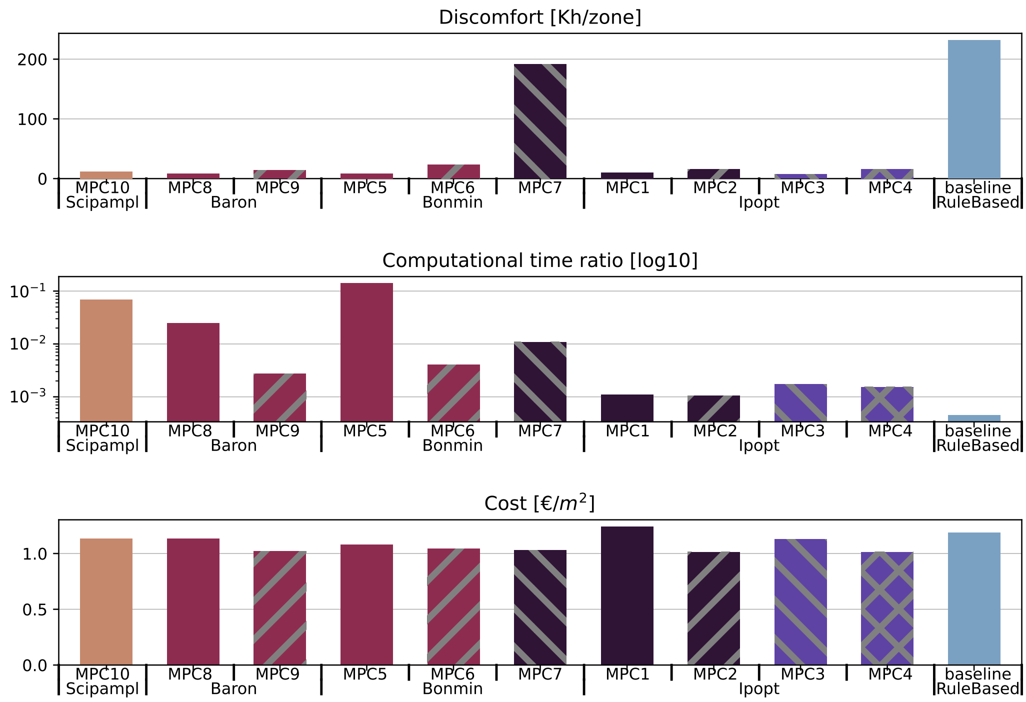

Figure 5.4: BOPTEST KPIS for the month of January 1) Thermal discomfort K_{dis}, 2) Computational time ratio K_{timr} in logarithmic scale, 3) Cost K_{cost}, the KPI description is presented in 5.4 . The results are shown for all the MPC combinations explained in 5.3

5.4.1. Key Performance Indicators comparison

Figures 5.4 and 5.5 report the KPI results calculated by BOPTEST and post processing specific to this study as described in Table 5.4.

Looking at the discomfort KPIs K_{dis} in Figure 5.4 most of the formulations outperform the rule based controller, defined in Section 5.5.1 with more than 90% decrease in discomfort. The main reason is the ability to compensate for the delayed response of the floor heating system as shown in the various time series plots Figures 5.6,5.7 and 5.8. In fact the MPC turns on the system before the change of setpoint, bottom plot, that leads to the room temperature being close to the setpoint in the transition time step, top plot. This is true for most formulations apart from the baseline, however, the MPC7 solution using Bonmin with the Hybrid method leads

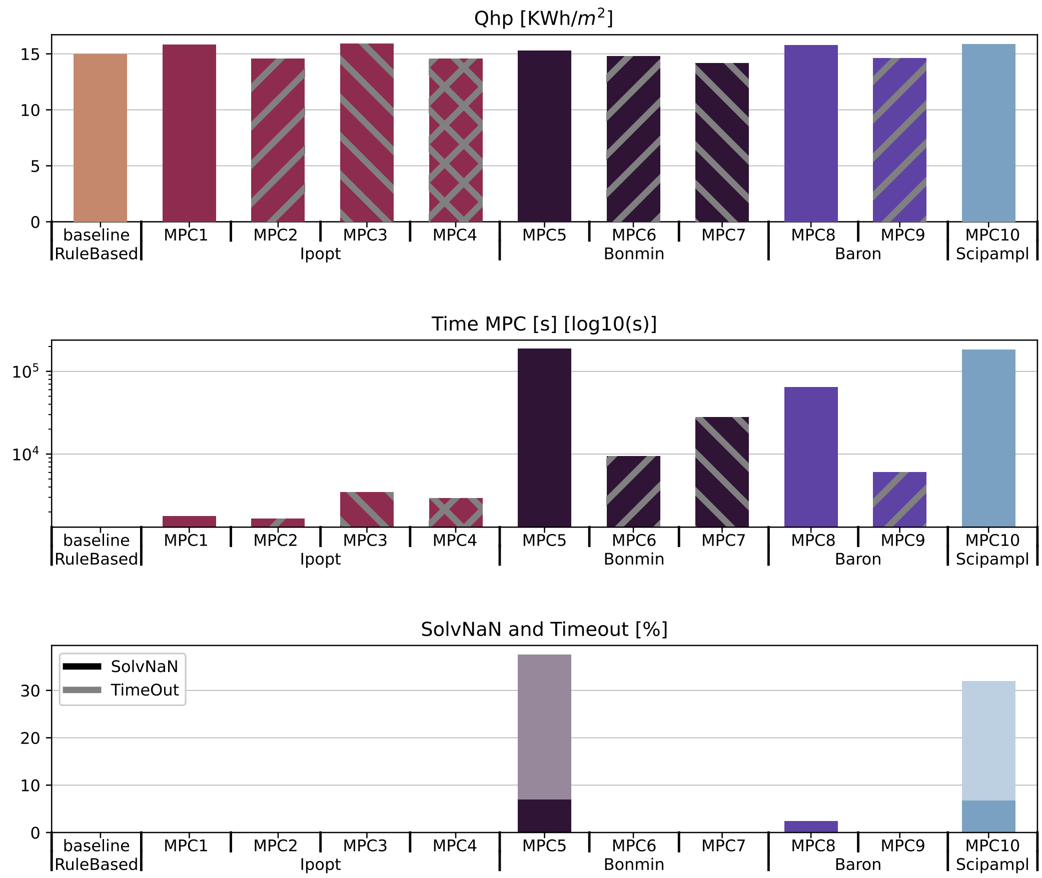

Figure 5.5: MPC specific for the month of January KPIs: 1) Thermal heating power per square meter K_{en}; 2) total computational time in logarithmic scale K_{ttot}; 3) Total number of solver time out or error status K_{err}, the KPI description is presented in 5.4. The results are shown for all the MPC combinations explained in 5.3.

to discomfort similar to the baseline controller. I managed to make the MPC7 formulation work properly, the results are similar to MPC6 and not shown in the chart, however, it required a lot of manual tuning in the comfort constraints and solver internal options (MINLP approximation relaxation, integer tolerance) to guide the solution. This highlights the fact that Bonmin-Hyb is probably not robust enough for this type of problem.

Looking at the computational time ratio K_{timr} in Figure 5.4 and total computational time K_{ttot} in Figure 5.5 the obtained trend is as expected with simpler formulations being faster than the more complex ones. However, all the MPC formulations have a K_{timr} value much lower than one, meaning that in theory they could all be used for a real time application where the MPC control is updated every 15 (min). Looking at a relative comparison of the computational time K_{ttot}, MPC1 and MPC2, the QP formulations, take between 15 and 20 (min), in the chart around $1e03$ (s), to run for all the 2976 optimization iterations, so on average from 0.3 to 0.4 (s) per control horizon optimization. MPC3 and MPC4, the NLP formulations, take between 50 and 60 (min), in the chart around $3e03$ (s) , so on average from 1 to 1.3 (s) per control horizon optimization. The remaining MINLP formulations instead take from 1 (h) 40 (min), in the chart $6e03$ (s) up to 2 (d) and 5 (h), in the chart $1.9e05$ (s), so on average from 2 (s) to 64 (s) per control horizon optimization. This big variation in computational time for the MINLP problems, MPC5 to MPC10, shows that each solver or formulation has a bigger impact on the reliability of the solver-formulation combination. In fact, as shown in Figure 5.5 MPC5 using Bonmin as solver but with the formulation without binary objective $j5$ and MPC10 using $j5$ in the formulation, but SCIP as solver have longer computational time, due to having a lot of errors or timeouts in the solutions for around 30 % of the iterations, meaning that the MINLP solvers are struggling to find a proper solution. Furthermore, SCIP was not able to find a solution without the $j5$

binary objective, and in general all the MINLP solvers benefit from the introduction of $j5$ in terms of reliability and computational time. This, could be explained by the fact that by introducing $j5$, each NLP approximation of the MINLP is itself an approximation of a MINLP problem.

The last KPIs to look at are the thermal energy (K_{en}) in Figure 5.5 and the energy cost (K_{cost}) in Figure 5.4. About K_{en}, all the formulations and the baseline are within 6 % of each other, with MPC2, MPC4, MPC6, MPC7 and MPC9 being marginally better than the baseline and MPC1, MPC3, MPC8 and MPC10 being marginally worse. When looking at cost however, MPC1 is the worst performer with 5 % increase with respect to the baseline, while MPC2, MPC4, MPC6 and MPC9 show the best performance with a 13 % decrease in cost with respect to the baseline. The main difference in performance is due to the fact that MPC1 considers the COP only as a function of the external temperature because the supply temperature is not available, while the other formulations use the supply temperature as a control variable and have a COP also as a function of the supply temperature, allowing for a more efficient use of the heat pump. From these KPIs, though, it is not clear why the MPC2, MPC4, MPC6 and MPC9 seem to outperform the other nonlinear formulations. For that, we must consider a more detailed analysis of time series data, see next subsection.

5.4.2. Typical day analysis

Looking at the charts in Figures 5.6,5.7 and 5.8, when comparing the thermal power distribution, bottom charts, of MPC2, MPC4, MPC6 and MPC9 with MPC3, MPC5, MPC8 and MPC10 it is clear that the difference is in the on-off frequency in the latter cases. The frequent on-off cycling of the system causes an higher discrepancy between the prediction of the low order model versus the emulator model. The main reason is that the buildings envelope emulator model is made up of hundreds of states while the reduced order model uses only a handful. The consequence is that the high frequency components impact the temperature nodes in a different way on the the emulator and the reduced order models causing an instability in the MPC and a vicious cyle starts where the MPC continues to change the control trajectory since it does not converge with the emulator model. This can also be noticed by the temperature plots,top charts, where MPC3, MPC5, MPC8 and MPC10 compensate more for an expected steeper drop of temperature with respect to MPC2, MPC4, MPC6 and MPC9. The additional energy leads to an overheating during setback times and explains the difference in K_{cost} KPI. Furthermore, when controlling a system, frequent on-off control should be avoided since it increases the wear of the components.

The newly introduced KPI K_{conlen} shown in Table 5.4, should summarize all the content of Figures 5.6,5.7 and 5.8.Calculating the KPI for the overall thermal power supplied by the HP for the different formulations yields Figure 5.9. Looking at this bar chart the same conclusion can be drawn as for the time series analysis since MPC2, MPC4, MPC9 and MPC6 have a control arc length that is half that of MPC3, MPC5, MPC8 and MPC10, meaning a lot of oscillations and control actions from the latter MPC formulations.

With the addition of K_{conlen} KPI is possible to make a comprehensive comparison between all the MPC formulations, where the baseline performs similarly to MPC2, MPC4, MPC9 and MPC6.This make sense since the baseline controller is properly tuned and turns on and off properly, however considering discomfort K_{dis} and cost K_{cost} the MPC outperforms the baseline controller. In conclusion, it seems that increasing the complexity of the problem does not bring any benefit for the chosen case study, but only adds computational burden, makes the MPC less robust and more

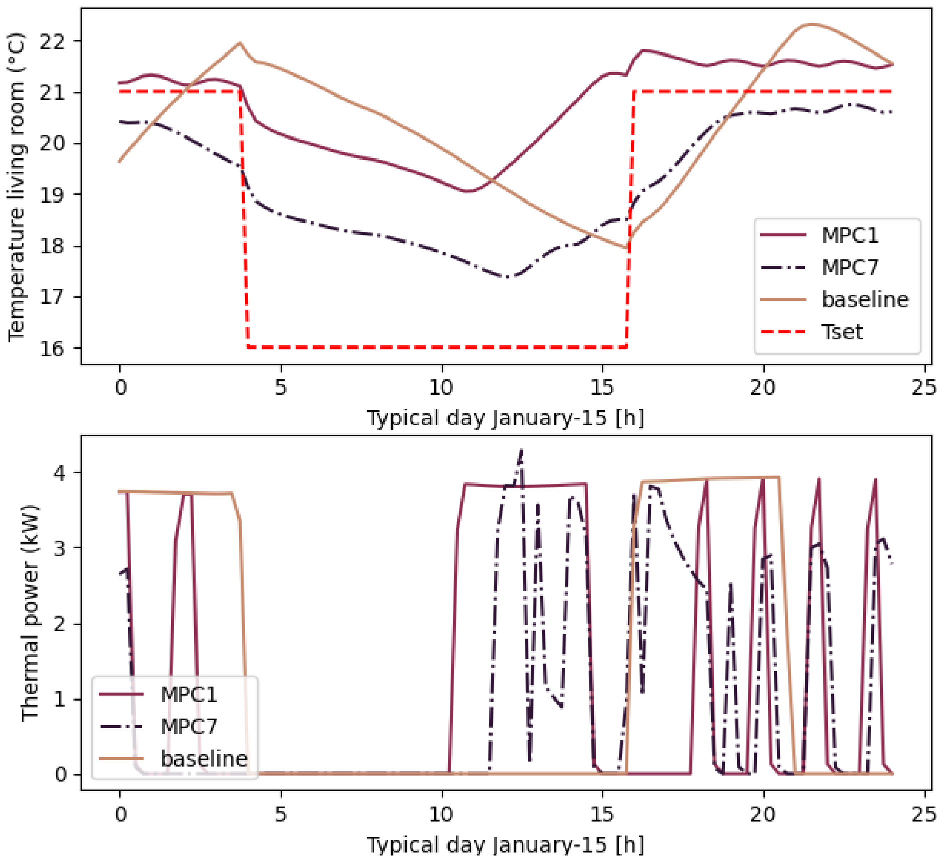

Figure 5.6: results for a typical day 15^{th} of January for MPC7 that did not converge and MPC1 that uses $\dot{Q}$ as control variable: 1) are the temperatures in the living room for baseline; 2) are the total thermal power supplied by the heat pump to the floor heating system.

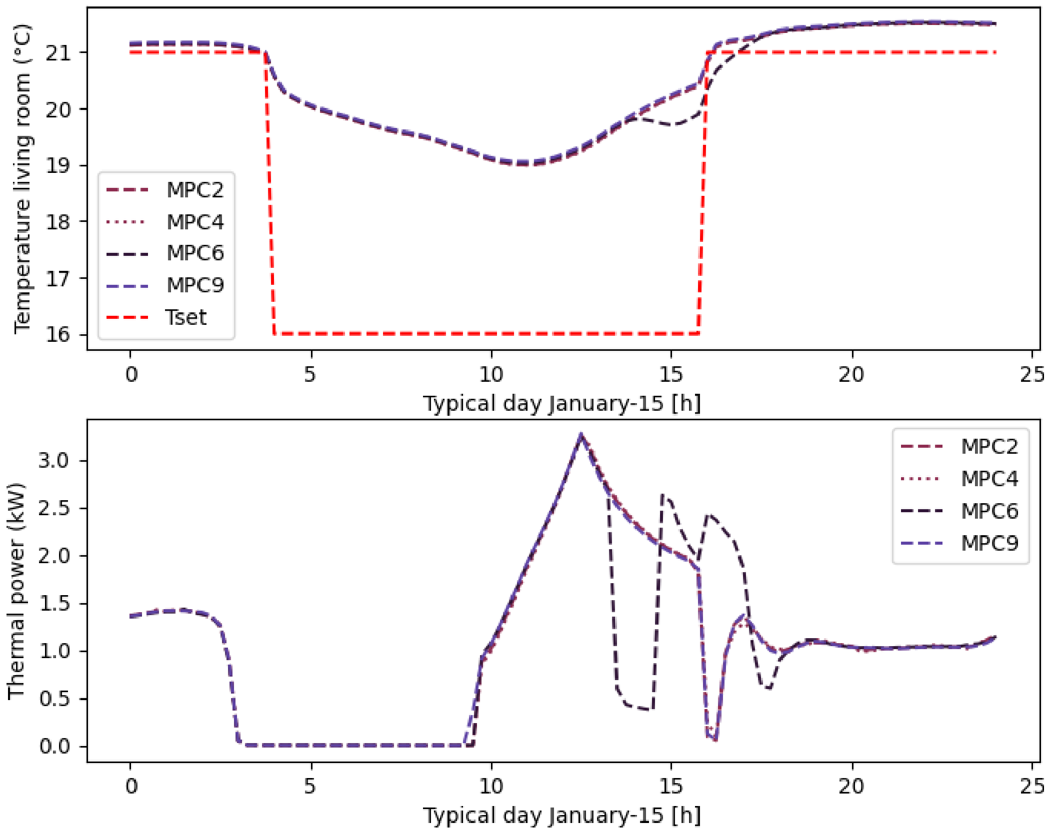

Figure 5.7: results for a typical day 15^{th} of January for MPC2, linear using supply temperature as optimization variable, MPC4 that uses supply temperature and continuous valve control, MPC6 and MPC9 uses supply temperature and integer valve control with the binary constraint: 1) are the temperatures in the living room for baseline; 2) are the total thermal power supplied by the heat pump to the floor heating system.

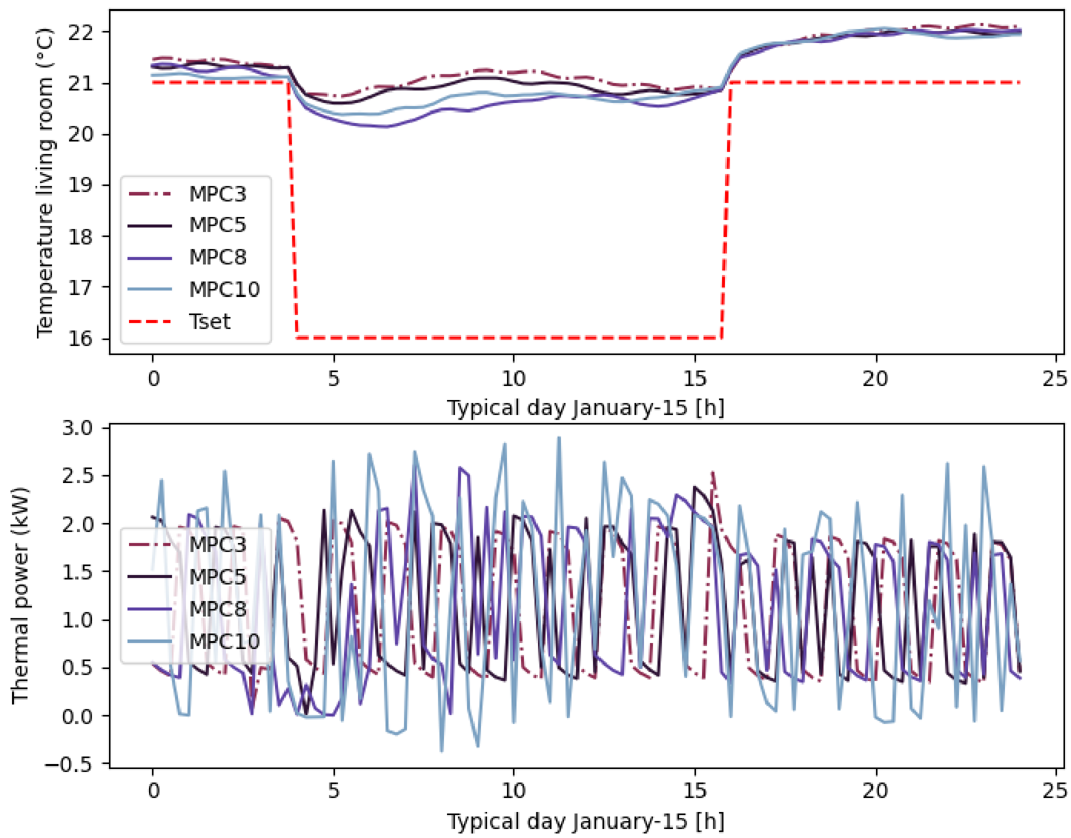

Figure 5.8: Results for a typical day 15^{th} of January for MPC3 and MPC3,using supply temperature and continuous valve control, MPC8 and MPC10 using supply temperature and integer valve control. MPC8 without the binary constraint and MPC10 with the binary constraint 1) are the temperatures in the living room for baseline, 2) are the total thermal power supplied by the heat pump to the floor heating system.

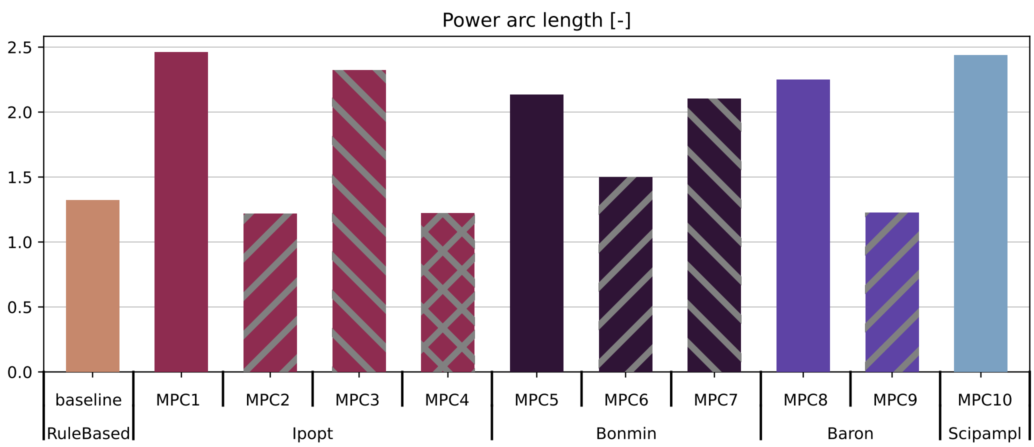

Figure 5.9: Power arc length KPI (K_{conlen}) specific for the month of January KPIs. It allows to estimate the heat pump frequency switching for the different formulations, the KPI description is presented in Table 5.4.

manual tuning is required to find a suitable solution.

5.4.3. Conclusions

This Chapter compared ten combinations of MPC formulations and solvers as shown in Table 5.3 ranging from a Quadratic Programming (QP) formulation, MPC1, to Non Linear Programming (NLP) formulations, MPC2 to MPC4, and Mixed Integer Nonlinear formulations (MINLP), MPC5 to MPC10. The conclusions on the desired objectives are reported in the bullet points below:

- making a linearized formulation of a natively nonlinear problem is a nontrivial task as shown by the big difference in performance between MPC1 and MPC2. In MPC1 the thermal power $u6$ is used to model the temperature in floor heating, while in MPC2 the supply temperature $u2$, with the zone valves always open $u5$. MPC2 allowed for a more detailed formulation of the heat pump COP leading an overall better solution. In this sense, a MINLP formulation could be easier to implement since optimal control variables can correspond to physical control variables that then can be used to estimate the COP of the heat pump. However, the tuning process of the MINLP solver in terms of options, tolerance and initialization to find a suitable solution was not a trivial process,requiring a previous optimization step where a NLP solution was used as initialization;
- in the case study analyzed, no substantial benefit was found in using a more complex formulation in terms of KPIs, since the results are comparable apart from a dramatic increase in computational time for the more complex formulations. Furthermore, as expected, the MINLP formulations are less stable, leading MPC8 and MPC10 to a time out or error in the solution for 30% of the iterations in the evaluation period. The author compared state of the art open source (SCIP,

Bonmin) and commercial (Baron) solvers. I think they are viable options to tackle building HVAC optimal control problems. However, they are not the best solution for the case study under analysis;

- from the overall analysis, it is shown that the initial effort I spent into finding a suitable linear constraint formulation lead to an identical performance with respect to the nonlinear counterparts, while being faster and more robust. In literature there are many examples on how to properly linearize the HVAC system. For example the approach showed in this Chapter can be used in most hydronic based HVAC systems. Therefore, the conclusion is that using a linear formulation for the constraints with a nonlinear objective function and proper initialization method, such as slightly randomized free floating solutions, gives a good balance between the accuracy of the prediction, computational requirements and robustness.

From this analysis the chosen formulation for the parameter extrapolation is MPC2. MPC2 is a linear formulation using only the supply temperature as control variable, while the valves are opened when the temperature is above the minimum HP power in the emulator corresponding to 20% of the nominal capacity. The solver used is IPOPT and in terms of objectives it tried to minimize discomfort and energy consumption. So, the optimal control trajectories shown for the parameter extrapolation analysis discussed in Section 5.5 are calculated using this formulation.

5.5. MPC derived pre-on and pre-off for floor heating scenario

In this Section the optimal control trajectories obtain from the optimal control strategy are used to extrapolate a useful set of pre-on and pre-off parameters that can be directly used in the apartment micro controller.

Section 5.5.1 describes the baseline controller and the reference case study. Section 5.5.2 showcases the general approach used to find the pre-on and pre-off parameters starting from the optimal control trajectories. Finally, Section 5.5.3 shows the results of the baseline controller compared with the results of the improved controller using monthly tuned pre-on and pre-off parameters.

5.5.1. Baseline description

This Section reports the findings in the accepted article [12], where the I am first author. A copy of the manuscript is attached to the end of the manuscript in Appendix C. The goal is to find suitable pre-on and pre-off parameters for the heating system starting from the MPC solution. Before looking at the extrapolation methodology, in Figure 5.10 is reported the control scheme for the heating scenario.

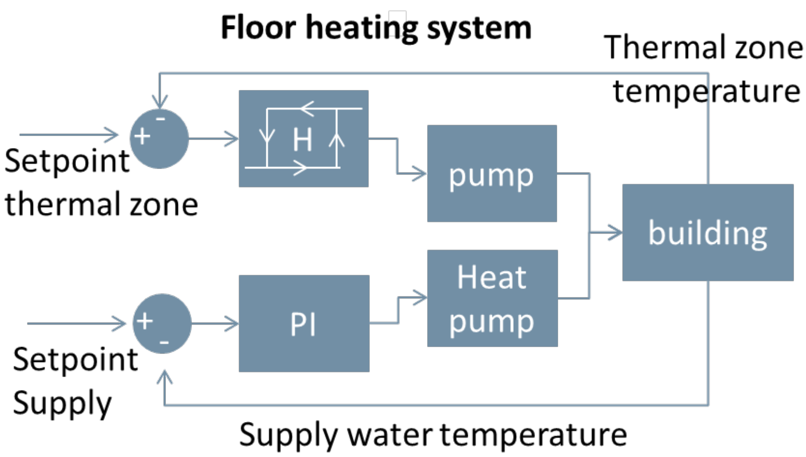

Figure 5.10: control scheme for the heating system in the Modelica model.

The baseline controller is made up of two parts. A thermostat for each thermal zone that has an hysteresis controller with an offset of 0.4 (°C) and a Proportional Integral (PI) controller for the modulation of the supply temperature to the floor heating system. The supply temperature is modulated with a climatic curve as shown in Figure 5.11.

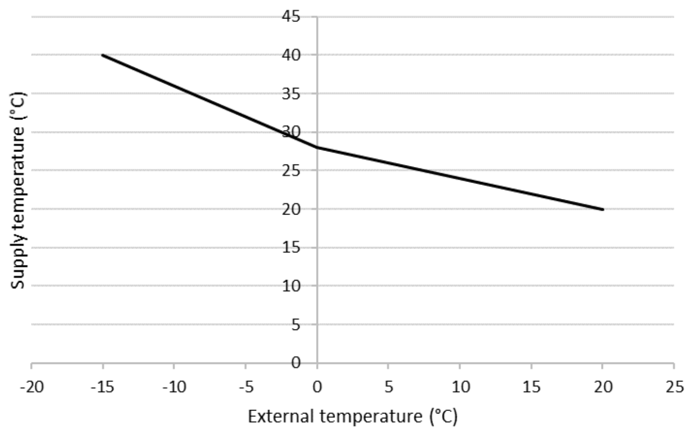

Figure 5.11: Climatic curve used to calculate supply temperature to floor heating system. On y-axis supply temperature and on x-axis external temperature.

The PI parameters were fine tuned to minimize oscillations, overshooting and settling time. Furthermore, a different setpoint was used with respect to the previous section on MPC formulations to increase the variability of occupancy in the apartment differentiating between the thermal zones. Before the living room and bed room were occupied at the same time between 8:00 P.M. and 8 A.M. For the this analysis the setpoint used are reported in Figure 5.12.

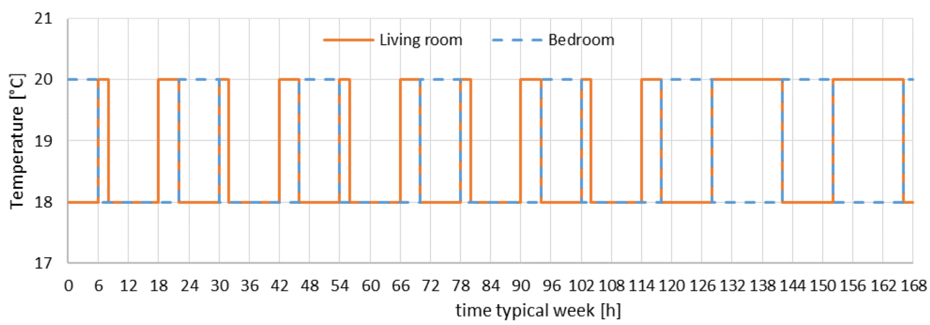

Figure 5.12: New heating setpoint profile for pre on and pre off analysis. Time in hours for a sample week from Monday to Sunday on x-axis. On y-axis the setpoint temperatures for Living room (orange) and for Bedroom (blue dashed line)

In this way the Living room and Bedroom have a different setpoint profile mimicking a working person that comes home at 6 P.M., moves to the

Bedroom at 10 P.M., wakes up at 6 A.M. and goes out of the house at 8 A.M. during the weekdays. During the weekend instead the time is spent in the Living room during from 8 A.M to 10 P.M. and in the bedroom otherwise.

5.5.2. Theoretical approach

The MPC result is a control trajectory that switches on and off the heat pump to guarantee the thermal comfort of the users. To deal with the high thermal inertia of the floor heating system and maintain desirable level of comfort the MPC will turn on the heat pump before a change from setback to setpoint. In the same way, to avoid overheating it will switch it off before the change between setpoint and setback. Depending on the boundary conditions, weather, setpoint and internal gains the time between the setpoint change and the heat pump turning on or off will be different. Theoretically each time the setpoint changes the on and off time will be different. However, to minimize the stress for the network in the Merezzate+ project the communication between the cloud service running the MPC and the local controllers has to be kept at a minimum. For this reason the first try was to find an average pre-on and pre-off parameters for each month of the heating season in Milan, namely from the 15^{th} of October to the 15^{th} of April. These monthly averages were obtained starting from the calculation of the supplied energy to the radiant floor distinguishing between the pre-on phase $Q_{preheaOPT}$ and the normal operation Q_{heaOPT}. These two variables correspond to the orange and red area in Figure 5.13.

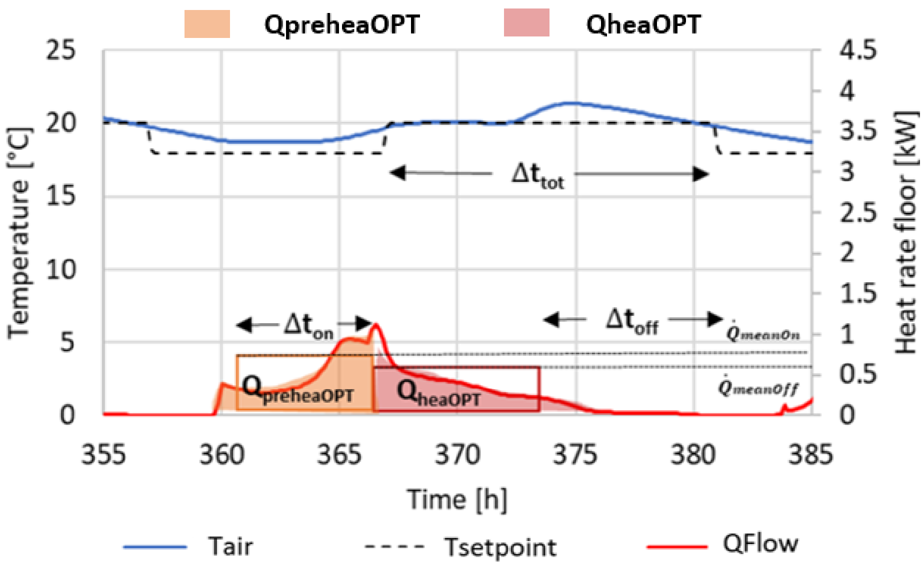

Figure 5.13: Visualization of pre on Δt_{on} and pre off Δt_{off} parameters. On x-axis the time is plotted in hours. On the left y-axis the zone temperature (solid blue line) and setpoint (dashed black line). On the right y-axis the heat rate supplied to the floor heating system is shown (red line). The two highlighted areas are supplied energy to the radiant floor distinguishing between the pre-on phase $Q_{preheaOPT}$ and the normal operation Q_{heaOPT}

The two highlighted areas are equivalent to the rectangles, in which the heights are $\dot{Q}_{meanOn}$ and $\dot{Q}_{meanOff}$ and the two widths are the pre-on parameter Δt_{On} and difference between the total on time before switching off and the pre-off parameter $\Delta t_{tot} - \Delta t_{off}$. Thus, by simply making the equivalence between the two areas the equations for the calculations of pre on and pre off parameters becomes:

$$\begin{aligned} \dot{Q}_{meanOn} &= \frac{Q_{preheaOPT}}{\Delta t_{On}} \\ \dot{Q}_{meanOff} &= \frac{Q_{heaOPT}}{\Delta t_{tot} - \Delta t_{Off}} \end{aligned} \tag{5.2}$$

5.5.3. Pre-on and pre-off results

Calculating the average $Q_{preheaOPT}$ and Q_{heaOPT} for each month the monthly values of Δt_{On} and Δt_{Off} can be found. In the table below are reported the parameters for living room and bedroom:

Table 5.5: average monthly pre on and pre off parameters from 15 of October to 15 of April for living room and bedroom

Period	Pre-on (h) Living room	Pre-off (h) Living room	Pre-on (h) bedroom	Pre-off (h) bedroom
01/01-01/31	1.56	0	4	0.2
02/01-02/28	1.22	0	3.6	0.3
03/01-03/31	0.2	0.2	3	1.7
04/01-04/15	0	1.3	2.2	2.2
10/15-10/31	0	0.6	1	1.9
11/01-11/30	0.8	0.1	2.6	0.8
12/01-12/31	1.4	0.1	3.4	0.2

Looking at Table 5.5 it is interesting to notice how the setpoint difference between Living room and Bedroom drastically affects the pre-on and pre-off parameters. This tells us that when applying this methodology on a real case study several setpoint profiles should be simulated to map the possible user preferences and average out the possible pre-on and pre-off parameters depending on user preference.

In Table 5.6 is shown a KPI comparison between the baseline controller and the controller with the improved parameters:

Table 5.6: KPI results comparison between baseline rule based controller and improved controller with monthly pre on and off parameters

KPI	Baseline	Pre on off
Discomfort Living room (K)	1.104	0.191 (-83%)
Discomfort Bedroom (K)	0.155	0.006 (-96%)
Thermal energy supplied (kWh)	1758	1808 (+2.8%)
Electrical energy consumed (kWh)	437	455 (+4.0%)

The KPIs reported in the table are calculated in the same way as the ones used in BOPTEST described in the MPC section. Looking at Table 5.6 the first difference that jumps to the eyes is the relative decrease in discomfort between the baseline and the improved controller for both Living room and Bedroom. Looking at the absolute numbers though, the Bedroom only shows a marginal improvement from an average of 0.155 (K) to almost 0. The reason is that the two thermal zones are thermally connected to each other trough the walls and also through a constant air exchange between them. This makes so that the Bedroom gets naturally preheated by the floor heating turning on the Living room even in the baseline case with the exception of particularly cold days. In the Living room instead the change is big even in absolute value considering that 1.1 (K) is the average value for the whole heating season, while most of the discomfort occurs in the first few occupied hours due to underheating. In fact, looking at Figure 5.14 it shows that the underheating that can occur in the baseline is higher than 1.1 (K).

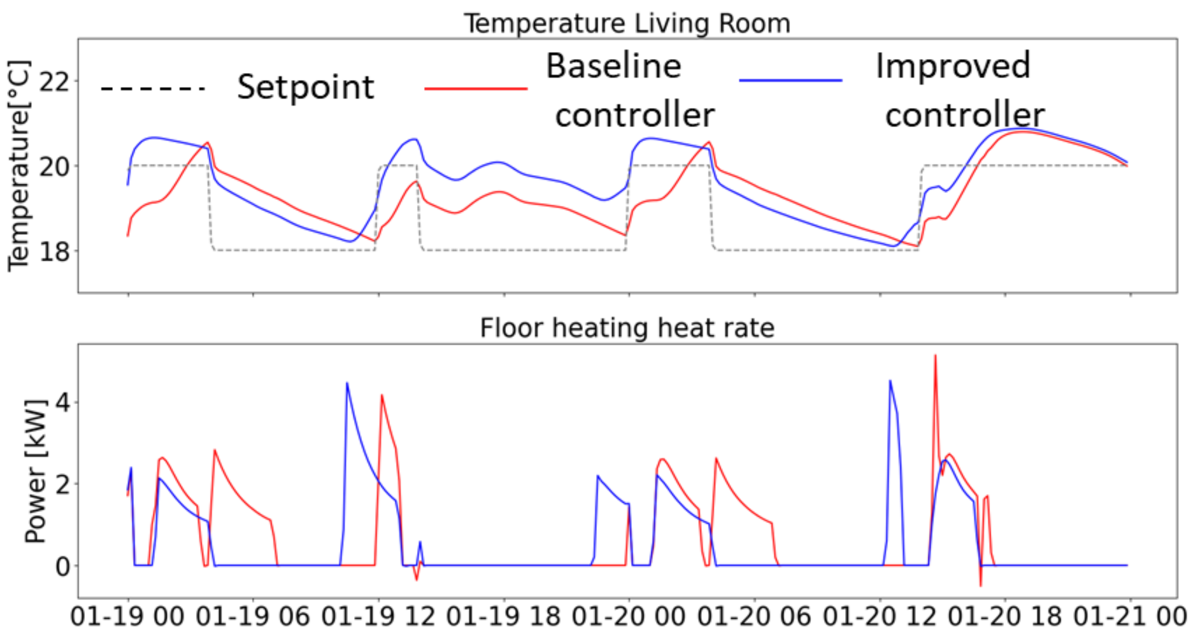

Figure 5.14: On both charts x-axis is two typical days in January. blue line is the improved controller and red line is the baseline, dashed black line is the reference setpoint. In the top chart is plotted the Living room temperature. In the bottom chart is shown the heat rate supplied to the floor heating system

Looking at the thermal and electrical consumption of the heat pump, this did not change too much from the improved control to baseline. This is consistent with the fact that we are dealing with a new building with a well insulated envelope with low losses and the COP of the heat pump is also not particularly affected. Under these conditions the addition of the pre-on and pre-off parameters can be considered a shift of the energy supplied to the floor heating system.

6 | Conclusions

This Chapter reports the results obtained by pursuing the objectives stated in the Introduction section.

- The first objective was to contribute to the development of the latest iteration of the compact Dessicant Evaporative Cooling (DEC) device FREESCOO by carrying out experiments and numerical simulations on the heat exchanger, that is the core component of the device.
  - Two versions of the FREESCOO heat exchanger were tested in the ReLab facility. Around 100 tests for the first heat exchanger and 150 for the second one were conducted. That corresponds to 28 complete cycles for the first heat exchanger and around 43 cycles for the second heat exchanger. Each cycle condition was repeated at least three times to minimize the influence of the previous cycle since the FREESCOO system is always in transient condition.3 external conditions to simulate late spring early autumn and summer T$_wetbulb$ = 20, 23, 26 (°C) and T$_drybulb$ = 28,30 (°C). 3 room conditions T$_room$ = 24, 26, 30(°C) and RH = 60(%) to simulate 2 comfort condition and a ventilation scenario (all supply air is taken from external environment). 12 combinations of flow $\dot{m}_{flow}$ = 40, 60, 80, 100 (%) of the fan nominal value 550 (kg/h) for ADS and RIG, 360 (kg/h) for EVA.3 cycle times for Adsorption (ADS), Regeneration (REG) = 40, 30, 18 (min). Then the experimental data were analyzed and processed to be used for the calibration and validation of the numerical model,

leading to a publication on the transient response of chilled mirrors and capacitive hygrometers.

  – A Modelica library for a 2-D model of the latest iteration of the FREESCOO device was developed and the model calibrated on the available experimental data leading to a NRMSE below 6% with respect to experimental data for the useful adsorption heat and water balance of the silica gel over several cycles in different boundary and working conditions. Then a model of the whole device made up of two heat exchanger, humidifiers and air to water heat exchanger for the regeneration phase was developed and coupled with the Modelica two room apartment case study model.

  – A reduced order model of FREESCOO for optimization purposes was identified starting from the 2-D model output and included in the Modelica library.

  In future work, the Modelica library will be used by SolarInvent to further refine the heat exchanger model and explore new uses for the heat exchanger in addition to being used in the FREESCOO device.

- The second objective was to compare different MPC formulations to address the literature gap. This work tried to partially fill the literature gap by applying a number of MPC optimal control problem formulations and using different optimization solvers to a relatively common HVAC system. The idea was to focus on two issues that could cover a broad range of HVAC systems: 1) nonlinearity arising from the estimation of the heat pump Coefficient of Performance (COP) and 2) binary on-off physical control inputs for distribution circuit valves. Depending on the approach to model these two issues, the resulting optimization problem formulation can be a QP, Non linear

Programming (NLP), or MINLP. The conclusions are listed below.

- making a linearized formulation of a natively nonlinear problem is a nontrivial task as shown by the big difference in performance between MPC1 and MPC2 as shown in Section 5.2. In MPC1 the thermal power $u6$ is used to model the heat rate in the floor heating, while in MPC2 the supply temperature $u2$, with the zone valves always open $u5$. MPC2 allowed for a more detailed formulation of the heat pump COP leading an overall better solution. In this sense a MINLP formulation could be easier to implement since the optimal control variables can correspond to the physical control variables, that then can be used to estimate the COP of the heat pump. However, the tuning process of the MINLP solver to find a suitable solution was not a trivial process (tolerance and initialization options), requiring a previous optimization step where a NLP solution was used as initialization;
- in the case study analyzed, no substantial benefit was found in using a more complex formulation in terms of KPIs, since the results are comparable apart from a dramatic increase in computational time for more complex formulations. Furthermore, as expected, the MINLP formulations are less stable, leading MPC8 and MPC10 to a time out or error in the solution for 30% of the iterations in the evaluation period. The author compared state of the art open source (SCIP, Bonmin) and commercial (Baron) solvers. The author thinks that they are viable options to tackle building HVAC optimal control problems. However, they are not the best solution for the case study under analysis;
- from the overall analysis, it is shown that the initial effort I put into finding a suitable linear constraint formulation lead to an identical performance with respect to the nonlinear counterparts,

while being faster and more robust. In literature there are many examples on how to properly linearize the HVAC system, including this thesis. Therefore, the author concludes that using a linear formulation for the constraints with a nonlinear objective function and proper initialization method, such as slightly randomized free floating solutions, gives a good balance between the accuracy of the prediction, computational requirements and robustness.

Future work could include the addition of this test case to the BOPTEST Github repository together with the MPC framework utilized to facilitate comparisons and future MPC implementations on similar case studies.

- The third objective of the thesis was to extrapolate simplified rules from the optimization process that can improve the rule based controller for the case studies.
  - For the cooling case FREESCOO is a fixed bed transient DEC device that needs to run on an adsorption and regeneration cycle, where the phases times impact the average power output of the system. The ideal scenario to increase the energy performance while keeping comfort would be to match the cooling demand from the building with the average power output of the DEC system. For this reason the adsorption and regeneration cycles times were optimized monthly for the cooling season, leading to a 20% increase in the seasonal thermal COP, without reducing the comfort or increasing the electrical consumption of FREESCOO. In future work the focus will be in trying different tuning periods, such as weekly or daily and also switch the control from an hysteresis controller with nominal flow rate to a proportional integral control that modulates the airflow depending on the error between setpoint and room temperature. This should mitigate the over-

coooling action carried out by the current version of FREESCOO.

– For the heating case, the goal was to use the MPC results to mitigate the impact of floor heating on thermal comfort. Their high thermal inertia caused underheating or overheating issues and consequent discomfort and/or waste of energy in the baseline controller. The optimal control trajectory found by the MPC algorithm took into account the disturbances and buildings dynamics to avoid both underheating and overheating. Using the MPC trajectory, monthly constant pre on and pre off parameters were obtained leading to a decrease in discomfort of 90% for the whole heating season, while not increasing the energy demand. For the future development of this work, different feature extrapolation methods will be considered. Instead of monthly, the pre-on/pre-off parameters could be updated with a different frequency. Furthermore, the function used to find the parameters can be changed from a constant average power to a linear or non-linear relations. Lastly, depending on the sensors available locally or cloud forecast different heuristic metrics will be developed and tested in Merezzate+.

Bibliography

[1] I E A Building Energy Performance Metrics. Supporting Energy Efficiency Progress in Major Economies. *International Energy Agency: Paris, France*, 2015.

[2] Antoine Levesque, Robert C Pietzcker, Lavinia Baumstark, Simon De Stercke, Arnulf Grübler, and Gunnar Luderer. How much energy will buildings consume in 2100? a global perspective within a scenario framework. *Energy*, 148:514–527, 2018.

[3] Mat Santamouris. Innovating to zero the building sector in europe: Minimising the energy consumption, eradication of the energy poverty and mitigating the local climate change. *Solar Energy*, 128:61–94, 2016.

[4] Andrea Invidiata and Enedir Ghisi. Impact of climate change on heating and cooling energy demand in houses in brazil. *Energy and Buildings*, 130:20–32, 2016.

[5] M Mujahid Rafique, P Gandhidasan, Shafiqur Rehman, and Luai M Al-Hadhrami. A review on desiccant based evaporative cooling systems. *Renewable and Sustainable Energy Reviews*, 45:145–159, 2015.

[6] TS Ge, Y Li, RZ Wang, and YJ Dai. A review of the mathematical models for predicting rotary desiccant wheel. *Renewable and Sustainable Energy Reviews*, 12(6):1485–1528, 2008.

[7] Jubair A Shamim, Wei-Lun Hsu, Soumyadeep Paul, Lili Yu, and Hirofumi Daiguji. A review of solid desiccant dehumidifiers: Current

status and near-term development goals in the context of net zero energy buildings. *Renewable and Sustainable Energy Reviews*, 137: 110456, 2021.

[8] Nsilulu T Mbungu, Raj M Naidoo, Ramesh C Bansal, Mukwanga W Siti, and Diambomba H Tungadio. An overview of renewable energy resources and grid integration for commercial building applications. *Journal of Energy Storage*, 29:101385, 2020.

[9] Maryam Gholamzadehmir, Claudio Del Pero, Simone Buffa, Roberto Fedrizzi, et al. Adaptive-predictive control strategy for hvac systems in smart buildings–a review. *Sustainable Cities and Society*, 63:102480, 2020.

[10] Kurt W Roth, Detlef Westphalen, John Dieckmann, Sephir D Hamilton, and William Goetzler. Energy consumption characteristics of commercial building HVAC systems volume III: Energy savings potential. *TIAX LLC Report for US Department of Energy Building Technologies Program*, 2002.

[11] Maria del Mar Castilla, Jose Domingo Alvarez, Francisco Rodriguez, and Manuel Berenguel. *Comfort control in buildings*. Springer, 2014.

[12] Ettore Zanetti, Rossella Alesci, Rossano Scoccia, and Marcello Aprile. Floor heating pre-on/off parameters based on model predictive control feature extrapolation. *CLIMA2022 proceedings*, 2022.

[13] Ettore Zanetti, Marcello Aprile, Dongsuk Kum, Rossano Scoccia, and Mario Motta. Energy saving potentials of a photovoltaic assisted heat pump for hybrid building heating system via optimal control. *Journal of Building engineering*, 27:100854, 2020.

[14] Ján Drgoňa, Javier Arroyo, Iago Cupeiro Figueroa, David Blum, Krzysztof Arendt, Donghun Kim, Enric Perarnau Ollé, Juraj Oravec,

Michael Wetter, Draguna L. Vrabie, and Lieve Helsen. All you need to know about model predictive control for buildings. *Annual Reviews in Control*, 50:190–232, 2020. ISSN 13675788. doi: 10.1016/j.arcontrol.2020.09.001.

[15] Anjukan Kathirgamanathan, Mattia De Rosa, Eleni Mangina, and Donal P. Finn. Data-driven predictive control for unlocking building energy flexibility: A review. *Renewable and Sustainable Energy Reviews*, 135(August 2020):110120, 2021. ISSN 18790690. doi: 10.1016/j.rser.2020.110120. URL `https://doi.org/10.1016/j.rser.2020.110120`.

[16] Peter Rockett and Elizabeth Abigail Hathway. Model-predictive control for non-domestic buildings: a critical review and prospects. *Building Research and Information*, 45(5):556–571, 2017. ISSN 14664321. doi: 10.1080/09613218.2016.1139885.

[17] Bako Ali and Ali Ismail Awad. Cyber and physical security vulnerability assessment for iot-based smart homes. *sensors*, 18(3):817, 2018.

[18] Ettore Zanetti, David Blum, Donghun Kim, Rossano Scoccia, and Marcello Aprile. Performance comparison of different mpc formulations and solvers on air source heat pump hydronic floor heating system. *In submission*, 2022.

[19] Hélène Thieblemont, Fariborz Haghighat, Ryozo Ooka, and Alain Moreau. Predictive control strategies based on weather forecast in buildings with energy storage system: A review of the state-of-the art. *Energy and Buildings*, 153:485–500, 2017.

[20] Gianluca Serale, Massimo Fiorentini, Alfonso Capozzoli, Daniele Bernardini, and Alberto Bemporad. Model Predictive Control (MPC) for enhancing building and HVAC system energy efficiency: Problem

formulation, applications and opportunities. *Energies*, 11(3), 2018. ISSN 19961073. doi: 10.3390/en11030631.

[21] Helton F Scherer, Manuel Pasamontes, Jose Luis Guzmán, JD Álvarez, E Camponogara, and JE Normey-Rico. Efficient building energy management using distributed model predictive control. *Journal of Process Control*, 24(6):740–749, 2014.

[22] Shalika SW Walker, Warody Lombardi, Suzanne Lesecq, and Samira Roshany-Yamchi. Application of distributed model predictive approaches to temperature and co2 concentration control in buildings. *IFAC-PapersOnLine*, 50(1):2589–2594, 2017.

[23] Frauke Oldewurtel, Alessandra Parisio, Colin N Jones, Dimitrios Gyalistras, Markus Gwerder, Vanessa Stauch, Beat Lehmann, and Manfred Morari. Use of model predictive control and weather forecasts for energy efficient building climate control. *Energy and Buildings*, 45:15–27, 2012.

[24] Ján Drgoňa, Michal Kvasnica, Martin Klaučo, and Miroslav Fikar. Explicit stochastic mpc approach to building temperature control. In *52nd IEEE Conference on Decision and Control*, pages 6440–6445. IEEE, 2013.

[25] Yudong Ma, Jadranko Matuško, and Francesco Borrelli. Stochastic model predictive control for building hvac systems: Complexity and conservatism. *IEEE Transactions on Control Systems Technology*, 23 (1):101–116, 2014.

[26] Mehdi Maasoumy, M Razmara, M Shahbakhti, and A Sangiovanni Vincentelli. Handling model uncertainty in model predictive control for energy efficient buildings. *Energy and Buildings*, 77:377–392, 2014.

[27] Jiri Cigler, Jan Siroky, Milan Korda, and Colin Jones. On the selection

of the most appropriate MPC problem formulation for Buildings. *Proc. 11th REHVA World Congress CLIMA 2013*, 2013.

[28] Jan Drgona and Michal Kvasnica. Comparison of MPC strategies for building control. *Proceedings of the 2013 International Conference on Process Control, PC 2013*, pages 401–406, 2013. doi: 10.1109/PC.2013.6581444.

[29] Samuel Prívara, Jiří Cigler, Zdeněk Váňa, Frauke Oldewurtel, Carina Sagerschnig, and Eva Žáčeková. Building modeling as a crucial part for building predictive control. *Energy and Buildings*, 56:8–22, 2013. ISSN 03787788. doi: 10.1016/j.enbuild.2012.10.024.

[30] Maarten Sourbron, Clara Verhelst, and Lieve Helsen. Building models for model predictive control of office buildings with concrete core activation. *Journal of building performance simulation*, 6(3):175–198, 2013.

[31] DH Blum, K Arendt, L Rivalin, MA Piette, M Wetter, and CT Veje. Practical factors of envelope model setup and their effects on the performance of model predictive control for building heating, ventilating, and air conditioning systems. *Applied Energy*, 236:410–425, 2019.

[32] Damien Picard, Ján Drgoňa, Michal Kvasnica, and Lieve Helsen. Impact of the controller model complexity on model predictive control performance for buildings. *Energy and Buildings*, 152:739–751, 2017.

[33] Damien Picard, Maarten Sourbron, Filip Jorissen, Ji Cigler, Lukás Ferkl, Lieve Helsen, et al. Comparison of model predictive control performance using grey-box and white box controller models. *International High Performance Buildings Conference proceedings*, 2016.

[34] Clara Verhelst, David Degrauwe, Filip Logist, Jan van Impe, and Lieve Helsen. Multi-objective optimal control of an air-to-water heat pump

for residential heating. *Building Simulation*, 5(3):281–291, 2012. ISSN 19968744. doi: 10.1007/s12273-012-0061-z.

[35] Matej Pčolka, Eva Žáčeková, Rush Robinett, Sergej Čelikovský, and Michael Šebek. Bridging the gap between the linear and nonlinear predictive control: Adaptations for efficient building climate control. *Control Engineering Practice*, 53:124–138, 2016. ISSN 09670661. doi: 10.1016/j.conengprac.2016.01.007.

[36] Adrian Burger, Clemens Zeile, Angelika Altmann-Dieses, Sebastian Sager, and Moritz Diehl. An Algorithm for Mixed-Integer Optimal Control of Solar Thermal Climate Systems with MPC-Capable Runtime. *2018 European Control Conference, ECC 2018*, pages 1379–1385, 2018. doi: 10.23919/ECC.2018.8550424.

[37] Pierre Bonami, Lorenz T. Biegler, Andrew R. Conn, Gérard Cornuéjols, Ignacio E. Grossmann, Carl D. Laird, Jon Lee, Andrea Lodi, François Margot, Nicolas Sawaya, and Andreas Wächter. An algorithmic framework for convex mixed integer nonlinear programs. *Discrete Optimization*, 5(2):186–204, 2008. ISSN 15725286. doi: 10.1016/j.disopt.2006.10.011.

[38] Pietro Finocchiaro, Marco Beccali, Andrea Calabrese, and Edoardo Moreci. Second generation of freescoo solar dec prototypes for residential applications. *Energy Procedia*, 70:427–434, 2015.

[39] Pietro Finocchiaro. Solarinvent. URL `https://www.freescoo.com/solarinvent/`.

[40] Pietro Finocchiaro, Marco Beccali, and Vincenzo Gentile. Experimental results on adsorption beds for air dehumidification. *International Journal of Refrigeration*, 63:100–112, 2016.

[41] Marek Brand and Svend Svendsen. Renewable-based low-temperature

district heating for existing buildings in various stages of refurbishment. *Energy*, 62:311–319, 2013.

[42] Jacopo Famiglietti, Luisa Gerevini, Giulia Spirito, Marianna Pozzi, Alice Dénarié, Rossano Scoccia, and Mario Motta. Environmental life cycle assessment scenarios for a district heating network. an italian case study. *Energy Reports*, 7:368–379, 2021.

[43] Hao Fang, Jianjun Xia, Kan Zhu, Yingbo Su, and Yi Jiang. Industrial waste heat utilization for low temperature district heating. *Energy policy*, 62:236–246, 2013.

[44] Junpeng Huang, Jianhua Fan, and Simon Furbo. Demonstration and optimization of a solar district heating system with ground source heat pumps. *Solar Energy*, 202:171–189, 2020.

[45] Kang Zhao, Xiao-Hua Liu, and Yi Jiang. Dynamic performance of water-based radiant floors during start-up and high-intensity solar radiation. *Solar Energy*, 101:232–244, 2014.

[46] Drury B. Crawley, Curtis O. Pedersen, Linda K. Lawrie, and Frederick C. Winkelmann. Energyplus: Energy simulation program. *ASHRAE Journal*, 42:49–56, 2000.

[47] William A Beckman, Lars Broman, Alex Fiksel, Sanford A Klein, Eva Lindberg, Mattias Schuler, and Jeff Thornton. Trnsys the most complete solar energy system modeling and simulation software. *Renewable energy*, 5(1-4):486–488, 1994.

[48] Ies-ve building simulation software. `https://www.iesve.com`.

[49] Peter Fritzson and Peter Bunus. Modelica-a general object-oriented language for continuous and discrete-event system modeling and simulation. In *Proceedings 35th Annual Simulation Symposium. SS 2002*, pages 365–380. IEEE, 2002.

[50] Modelica Association. Modelica® - a unified object-oriented language for physical systems modeling. Tutorial, December 2000. URL http://www.modelica.org/documents/ModelicaTutorial14.pdf.

[51] Michael Wetter, David Blum, Jianjun Hu, and USDOE. Modelica IBPSA Library v1. 2019. doi: 10.11578/dc.20190520.1. URL https://www.osti.gov/biblio/1529269.

[52] Michael Wetter, Wangda Zuo, Thierry S Nouidui, and Xiufeng Pang. Modelica Buildings library. *Journal of Building Performance Simulation*, 7(4):253–270, 2014. doi: 10.1080/19401493.2013.765506. URL https://doi.org/10.1080/19401493.2013.765506.

[53] F Jorissen, G Reynders, R Baetens, D Picard, D Saelens, and L Helsen. Implementation and verification of the IDEAS building energy simulation library. *Journal of Building Performance Simulation*, 11(6):669–688, nov 2018. ISSN 1940-1493. doi: 10.1080/19401493.2018.1428361. URL https://doi.org/10.1080/19401493.2018.1428361.

[54] McDowell Timothy P and Muehleisen Ralph T. New standard 140 test suite: check the weather before you simulate. *BS2021 proceedings*, 2021.

[55] Joel AE Andersson, Joris Gillis, Greg Horn, James B Rawlings, and Moritz Diehl. Casadi: a software framework for nonlinear optimization and optimal control. *Mathematical Programming Computation*, 11(1):1–36, 2019.

[56] Michael L Bynum, Gabriel A Hackebeil, William E Hart, Carl D Laird, Bethany L Nicholson, John D Siirola, Jean-Paul Watson, and David L Woodruff. *Pyomo–optimization modeling in python*, volume 67. Springer Science & Business Media, third edition, 2021.

[57] Ampl solver interface. https://ampl.com/REFS/hooking2.pdf.

[58] Stefan Vigerske and Ambros Gleixner. SCIP: global optimization of mixed-integer nonlinear programs in a branch-and-cut framework. *Optimization Methods and Software*, 33(3):563–593, 2018. ISSN 10294937. doi: 10.1080/10556788.2017.1335312. URL `https://doi.org/10556788.2017.1335312`.

[59] Mustafa R. Kılınç and Nikolaos V. Sahinidis. Exploiting integrality in the global optimization of mixed-integer nonlinear programming problems with BARON. *Optimization Methods and Software*, 33(3): 540–562, 2018. ISSN 10294937. doi: 10.1080/10556788.2017.1350178.

[60] Jan Kronqvist, David E Bernal, Andreas Lundell, and Ignacio E Grossmann. A review and comparison of solvers for convex minlp. *Optimization and Engineering*, 20(2):397–455, 2019.

[61] Andreas Wachter. *An interior point algorithm for large-scale nonlinear optimization with applications in process engineering*. PhD thesis, Carnegie Mellon University, 2002.

[62] David Blum, Javier Arroyo, Sen Huang, Ján Drgoňa, Filip Jorissen, Harald Taxt Walnum, Yan Chen, Kyle Benne, Draguna Vrabie, Michael Wetter, and Lieve Helsen. Building optimization testing framework (BOPTEST) for simulation-based benchmarking of control strategies in buildings. *Journal of Building Performance Simulation*, 14(5):586–610, 2021. doi: 10.1080/19401493.2021.1986574. URL `https://doi.org/10.1080/19401493.2021.1986574`.

[63] Henrik Gadd and Sven Werner. Achieving low return temperatures from district heating substations. *Applied energy*, 136:59–67, 2014.

[64] Thierry Stephane Nouidui. Validation and application of the room model of the modelica buildings library. 2012.

[65] Mario Motta. Relab. URL `https://www.relab.polimi.it/`.

[66] ASHRAE Handbook. *HVAC systems and equipment*, volume 39. chapter, 2017.

[67] Ettore Zanetti, Rossano Scoccia, Marcello Aprile, and Mario Motta. Dynamic modelling and comparison between transient step response of capacitive hygrometers and chilled mirrors for delay compensation. *BS2021 proceedings*, 2021.

[68] Ronald W Schafer. What is a savitzky-golay filter? *IEEE Signal processing magazine*, 28(4):111–117, 2011.

[69] IF Macdonald, MS El-Sayed, K Mow, and FAL Dullien. Flow through porous media-the ergun equation revisited. *Industrial & Engineering Chemistry Fundamentals*, 18(3):199–208, 1979.

[70] YS Muzychka and MM Yovanovich. Laminar forced convection heat transfer in the combined entry region of non-circular ducts. *J. Heat Transfer*, 126(1):54–61, 2004.

[71] Fujio Kuwahara, Mitsuhiro Shirota, and Akira Nakayama. A numerical study of interfacial convective heat transfer coefficient in two-energy equation model for convection in porous media. *International journal of heat and mass transfer*, 44(6):1153–1159, 2001.

[72] E Zavaglio, R Scoccia, and M Motta. Rc building modelling for control purposes: A case study. In *Building Simulation Applications, BSA 2017-3rd IBPSA-Italy Conference*, volume 2017, pages 145–152. Free University of Bozen Bolzano, 2017.

[73] Lennart Ljung and Rajiv Singh. Version 8 of the matlab system identification toolbox. *IFAC Proceedings Volumes*, 45(16):1826–1831, 2012.

[74] Michael G Smart and John A Ballinger. Fourier-synthesized weather data for building energy use estimation. *Building and Environment*, 19(1):41–48, 1984.

[75] Oskar Von Stryk. User's guide for dircol–a direct collocation method for the numerical solution of optimal control problems. 1999.

[76] Roger R Labbe. Filterpy documentation. 2018.

A | Appendix A

Performance Comparison of Quadratic, Nonlinear, and Mixed Integer Nonlinear MPC Formulations and Solvers on an Air Source Heat Pump Hydronic Floor Heating System

Ettore Zanetti[a,*], Donghun Kim[b], David Blum[b], Rossano Scoccia[a], Marcello Aprile[a]

[a] *Department of Energy, Politecnico di Milano, Piazza Leonardo da Vinci, Milano MI, Italy*

[b] *Building Technology & Urban Systems Division, Lawrence Berkeley National Laboratory, Berkeley, CA, USA*

Abstract

There is a gap in literature on comparisons between different MPC optimal control formulations and solver choices for the same building HVAC system. Mixed Integer Nonlinear (MINL) formulations are rarely considered, despite being the most physically accurate way to represent HVAC systems. This work compares several MPC formulations, including Quadratic, Nonlinear, and MINL, applied to a case study building and investigates benefits and challenges of MINL MPCs from practical perspectives. Ten different MPC formulations were developed and implemented using Pyomo. Then, a detailed emulator model was developed using open-source Modelica libraries and used with BOPTEST to assess the performance of each MPC. Results show that convergence and control switching behaviors of MINL MPCs are sensitive to formulations, initialization approaches, solver selections, and solver parameters. Thus, they require significant effort for tuning. However, a very well-tuned MINL MPC performed similarly to successful Nonlinear MPC formulations.

Keywords: Building HVAC optimal control, Model predictive control, Optimal control problem formulations comparison, Mixed integer nonlinear optimization

---

*Ettore Zanetti
Email address: `ettore.zanetti@polimi.it` (Ettore Zanetti)

Nomenclature

Symbols

δ Auxiliary temperature variable $[K]$

$\dot{H}$ Enthalpy flow rate $[kW]$

$\dot{Q}$ Heat flow rate $[kW]$

Φ Specific heat rate $[kW/m^2]$

A Flow or surface area $[m^2]$

C Heat Capacity $[kJ/K]$

p_e Electricity price [€]

R Thermal Resistance $[kW/K]$

T Temperature $[K]$

u_i Control variable $[-]$

Acronyms

API Application Programming Interface

BOPTEST Building Optimization Performance Test framework

COP Coefficient Of Performance

HVAC Heating, Ventilation and Air Conditioning

I or IP Integer or Integer Programming

KPI Key Performance Indicator

L or LP Linear or Linear Programming

MEF Major Economic Forum

MIL or MILP Mixed Integer Linear or Mixed Integer Linear Programming

MINL or MINLP Mixed Integer Nonlinear or Mixed Inger NonLinear Programming

MPC Model Predictive Control

NL or NLP Nonlinear or NonLinear Programming

NRMSE Normalized Root Mean Square Error

Q or QP Quadratic or Quadratic Programming

SQP Sequential Quadratic Programming

1. Introduction

HVAC systems account for 20% of the total primary energy consumption in Major Economies Forum (MEF) countries (Metrics, 2015). Therefore, advanced controls for those systems can help reduce environmental impact as well as help renewable penetration by unlocking load flexibility potential in buildings (Roth et al., 2002; del Mar Castilla et al., 2014). For the last decades there has been a lot of research on advanced control, including Model Predictive Control (MPC), for the optimal operation of building HVAC systems (Drgoňa et al., 2020; Kathirgamanathan et al., 2021; Rockett and Hathway, 2017).

For MPC, the optimal control problem can be formulated mathematically in a variety of different ways, even for identical HVAC systems. The primary reasons for the variety include:

- A general optimization problem could have multiple *equivalent*[1] problems, e.g., by introducing slack variables, elimination procedure, hard or soft constraints and the epigraph problem formulation (Boyd et al., 2004).
- There are various approximation techniques, e.g., the McCormick convex relaxation of a bilinear function (McCormick, 1976), piecewise linear approximation for a nonlinear function, and linear programming (LP) relaxation of a mixed integer linear program (MILP), which relaxes the integer constraints.
- MPC itself has different theoretical approaches, such as centralized versus decentralized/distributed or stochastic versus deterministic.

[1] Two optimization problems are called *equivalent* if one solution of a problem is or can be readily found from the other solution.

- The objective and constraints of a MPC can be formulated in different ways regarding the quantification, relative importance, and constraints on energy use, carbon emissions, energy cost, load flexibility, and thermal comfort.

- Each component of an HVAC system can be modeled in several ways, which affects the performance of the prediction accuracy, robustness and computing time. For example, modelling the Coefficient of Performance (COP) of an air to water heat pump ranges from the constant COP approach to the DOE-2 (research group LBL, 1991) like performance mapping as a function of part load ratio, outdoor air temperature and supply water temperature.

- The selection of MPC optimization variables is a control design factor. For example, one may select either controllable inputs that are the same as those of the physical system, such as percent valve position, or that are abstracted from the system model, such as heat flow rates. In the latter case, a strategy is needed to convert optimal solutions to control inputs that are available in the physical system.

The significance of these variations of MPC formulations is that they could change not only the accuracy/physical reliability of a model and computation time, but also the class of optimization problems (e.g., from convex to nonconvex, from NLP to LP or MILP, and vice versa), affecting mathematical properties of global optimality, feasibility, uniqueness of a solution, convergence of numerical optimization algorithms, and MPC closed-loop stability. Consequently, it could considerably impact the overall MPC performance (e.g., energy consumption, comfort, computational time, and the rate of change of control inputs). As a consequence, a significant amount of time could be spent iterating to identify the most suitable optimization formulation for each HVAC system. Despite this importance, there are very few well-documented papers that investigate different MPC formulations. This is especially true for MINL MPC, which is one of the most natural and straightforward ways to formulate optimal control problems for many HVAC applications. This paper tries to partially fill this gap in the literature by providing comparisons of multiple MPC formulations for an HVAC system that has both binary and continuous control variables. In addition, this paper investigates the practical applicability of MINL MPC approaches.

Section 2 reports the case study details, MPC formulations, optimization solvers and the co-simulation setup. Section 3 presents the results for the

MPC formulations comparison. Finally, Section 4 reports the main conclusions of this study.

1.1. Literature review

Equivalent formulations for building applications can be found in many papers. One example is when peak demand is considered in a control objective. This approach replaces the maximum power or demand cost over a prediction horizon with linear constraints and a slack variable, namely the target peak or demand cost (ASHRAE, 2019, Chapter 43). Depending on applications, this approach could convert NLP to LP or MINLP to MILP (Kim and Braun, 2018).

Approximation techniques have also been widely applied to HVAC systems. Risbeck et al. (2017) applied a piecewise linearization technique for optimal scheduling of operations of chillers, pumps, cooling towers, boilers and thermal energy storages. The introduced approach approximates a nonlinear chiller performance map with a set of piecewise linear models, converting MINLP to MILP. Kim et al. (2015) applied a linear programming relaxation approach that relaxes integer constraints for coordinating operations of multiple rooftop units. This approach converts an IP to LP for better computation efficiency. Atam and Helsen (2015) applied a convex relaxation technique to handle the bilinearity that naturally appears in thermal energy systems. The proposed method converts a nonconvex optimization problem to a convex problem to ensure global optimality.

Considering MPC architecture and the theoretical approach, Scherer et al. (2014); Walker et al. (2017) compared centralized and distributed MPC architectures, highlighting that distributed approaches have slightly worse KPI performance but better computational time. Oldewurtel et al. (2012); Drgoňa et al. (2013); Ma et al. (2014); Maasoumy et al. (2014) compared deterministic versus robust or stochastic MPC, showing that a robust or stochastic MPC performs better in scenarios of high uncertainty and is comparable in other cases. Rather than focusing on architecture and theoretical approach, Cigler et al. (2013); Drgona and Kvasnica (2013) instead analyzed the formulation of the MPC problem, focusing on different cost functions and constraints, assessing which formulations are more robust and computationally efficient, but limiting their analysis to LP, QP and MILP.

Considerable effort was also put into analyzing different building envelope thermal modeling approaches. Prívara et al. (2013) compared several black-box and gray-box model structures to model building envelope systems and concluded that black box models are more computationally efficient for larger case studies but become less reliable for longer prediction horizons.

Sourbron et al. (2013) analyzed the effects of grey box model order on the performance of MPC for concrete core activated buildings. Blum et al. (2019) also shows that model order has a strong influence on the model quality. Furthermore, Blum et al. (2019) identified seven factors that play an important role in the accuracy of the building envelope model. Picard et al. (2017, 2016) show that a purely physical driven white box approach can be viable in certain building types. Kim et al. (2016, 2018) pointed out that a typical identification algorithm with any model structure would likely result in a biased model when significant unmeasured disturbances (e.g., unmeasured internal heat gain, in/exfiltration, door/window openings, zonal plug load) presented in a training dataset, and proposed a new identification approach for a typical grey box model structure to mitigate this negative effect.

Drgoňa et al. (2020); Serale et al. (2018) provided comprehensive reviews on building MPC literature. For the papers that they reviewed, many works address the benefit and applicability of their own MPC formulations compared with rule-based controls. Less comprehensive work is available on comparisons between different HVAC modeling approaches, optimization variable choices, and their impacts on the resulting MPC performance. Verhelst et al. (2012) performed an extensive analysis of different COP formulations in the MPC problem leading to LP and NLP problems, highlighting the potential benefit of a nonlinear formulation. Pčolka et al. (2016) compares a linear time invariant MPC, a linear time variant and a nonlinear MPC in a case study for a heat pump and domestic hot water system. It reports that the nonlinear solution is the best, but the linear time variant gets close and remains more robust. In both studies of Pčolka et al. (2016); Verhelst et al. (2012), binary variables were not taken into account to avoid MILNP formulations, although MINLP arises fairly naturally when dealing with HVAC systems. Indeed, very few studies can be found comparing MINLP with other formulations. To the authors' knowledge, only Burger et al. (2018) introduces a custom MINLP solver compared with Bonmin (Bonami et al., 2008) for a solar thermal system. Furthermore, it is hard to cross-compare to different works due to the unique case study system and lack of common metrics.

1.2. Objectives and contributions

This work aims to partially fill this literature gap by presenting comparisons of ten MPC formulations with a greater focus on MINL MPCs, for a relatively common HVAC system that requires control decisions on valve on/off and supply water temperature setpoint. The diversity of formulations is due to two issues that appear in a broad range of HVAC systems: 1) the nonlinearity arising from modeling heat pump COP and 2) the binary on-off physical control inputs for distribution circuit valves. Depending on modeling and approximation approaches to handle them, the resulting optimal control problem formulations become QP, NLP or MINLP. Each formulation encompasses a trade-off between accuracy in the prediction, robustness to find an optimal solution, computational requirements, the rate of change of control inputs, energy consumption, and comfort violation.

The contributions of this paper are:

- Present a well-documented work on how HVAC performance can vary with MPC formulations
- Understand the benefits of increased prediction accuracy from increased model complexity and the corresponding trade-offs
- Introduce a new Key Performance Indicator (KPI) to quantify the rate of change of a control input
- Survey, introduce, and test available optimization solvers of each problem formulation, especially novel MINLP-specific solvers, that were not comprehensively investigated, but could potentially be useful for typical building HVAC optimal control problems
- Share lessons-learned for designing MINL MPC

2. Methodology

2.1. Case study description

The chosen case study is a newly built two-room apartment in Milan, Italy. The HVAC system is a two-circuit radiant floor heating system connected to an air source heat pump. A diagram of the HVAC system is presented in Figure 1.

Each thermal zone is independently controlled via its own on/off valve. The pump works with a constant head tuned to provide the nominal water mass flow rate to each floor heating circuit when a valve is open. Control decisions are the two valves' statuses and the heat pump supply water set point. Despite its simplicity, the case study includes the HVAC hydronic system components that allow for several optimal control models, and lead to three different optimization problem classes to be solved: QP, NLP, and MINLP.

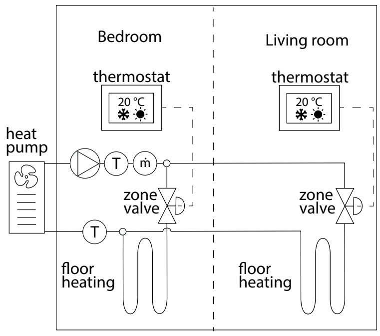

Figure 1: Scheme of the case study HVAC.

The emulator model for the apartment and HVAC system was developed in Modelica using the IBPSA 3.0 (master branch commit 8a0d237) (Wetter et al., 2019), Buildings 8.0 (master branch commit 69bb7cf) (Wetter et al., 2014) and IDEAS 2.2.1 (master branch commit 32860ea) (Jorissen et al., 2018) libraries. The MPC algorithms were implemented using the Python-based optimization modeling language Pyomo (Bynum et al., 2021). Finally the various MPC formulations were co-simulated with the emulator model thanks to the Application Performance Interfaces (APIs) and run-time environment provided by the BOPTEST software framework (Blum et al., 2021), which also provides as output a standard subset of KPIs, including thermal discomfort, energy consumption, cost of the energy and computational time ratio. In this way, it will be possible to consistently compare all MPC formulations on the same emulator, highlight the pros and cons of each approach, and make the emulator publicly available for continued usage and further comparison of control approaches.

2.2. Introduction of optimization solvers

Pyomo allows to easily couple different solvers through the AMPL interface (AMPL, 2003) which is supported by a wide variety of solvers. The QP and NLP solver, IPOPT (Wachter, 2002) was chosen due to the popularity and widespread usage. The MINLP solvers were chosen by looking at the results from (Kronqvist et al., 2019), which analyzed solver performance on a set of 335 convex MINLP problems and included both open source and commercial solvers. The subset of solvers chosen for this study includes some of the best performing and most popular choices for open source and commercial alternatives. BONMIN (Bonami et al., 2008) is an open source project belonging to the project COIN-OR foundation (or Foundation, 2006), as does IPOPT, and it is a MINLP solver mainly used for convex MINLP problems. MINLP solvers divide the optimization problem into a MILP or MIQP problem and NLP sub problems. In our setup, BONMIN uses CBC (Forrest and Lougee-Heimer, 2005) as the MIQP subsolver and IPOPT as the NLP solver. In particular, two algorithms are tested from BONMIN. The first is BONMIN-BB, which uses a variation of the Branch and Bound algorithm to convert the problem. The second one is BONMIN-Hyb, which is a hybrid approach between Branch and Cut and Outer Approximation algorithms, which is faster than BONMIN-BB, but suffers more from the issue of falling into a local minima when the objective function is not convex. As a commercial alternative, Baron (Kılınç and Sahinidis, 2018) was used since, differently from BONMIN, it should be able to guarantee a close to global optimum even when the objective function is not convex. Baron uses a variation of the Branch and Bound algorithm to reduce the MINLP problem into a subset of NLP problems and a MIQP problem. The MIQP solver is CPLEX and the NLP solver is IPOPT. Lastly an open source alternative to Baron, SCIP, is also tested, which is a global solver that uses a variation of the Branch and Bound algorithm. In our setup, SCIP uses CBC as the MIQP subsolver and IPOPT as the NLP solver.

2.3. Emulator model

In Figure 2, a schematic of the apartment is presented, while in Figures 3 and 4, the yearly frequency plot of the dry bulb temperature and global horizontal radiation for the location (Milan, Italy) are shown. Milan can be considered a continental temperate humid climate. The maximum $T_{DryBulb}$ is 32 [°C], the minimum is -7.4 [°C] and the average 11.7 [°C]. In Figure 5, a brief validation of the emulator model is shown, which used experimental data coming from a globe thermometer positioned in the center of the living room, while the boundary conditions were determined from local weather stations and localized forecast services. For an in depth description of the envelope, the reader can access the test case (two zone hydronic apartment) documentation at the BOPTEST repository Two zone hydronic apartment (IBPSA, 2019). In Table 1, a summary of the main features of the case study is reported.

The thermal zones and floor heating system are modelled using the Buildings library. The remainder of the hydronic system is modelled using the IBPSA library apart from the heat pump, where a dynamic performance map model from the IDEAS library is used. The baseline controller in the emulator is an on-off controller with a 1[°C] hysteresis on the room set point temperature. The zone valve fully opens when the hysteresis controller gives

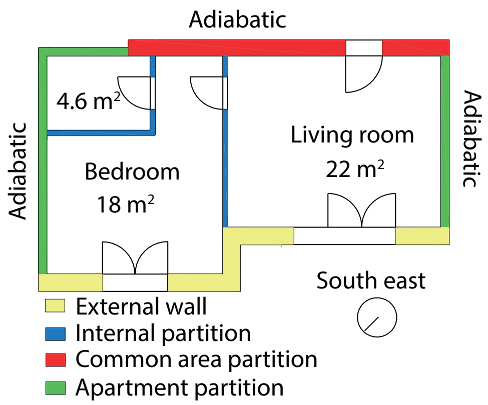

Figure 2: Case study apartment scheme.

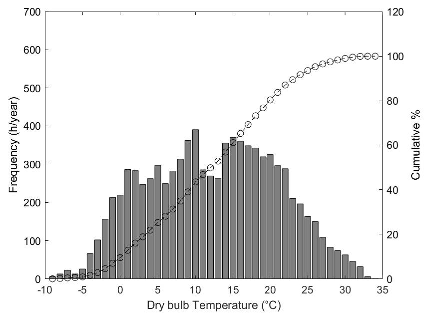

Figure 3: Dry Bulb temperature yearly frequency for Milan typical year weather data.

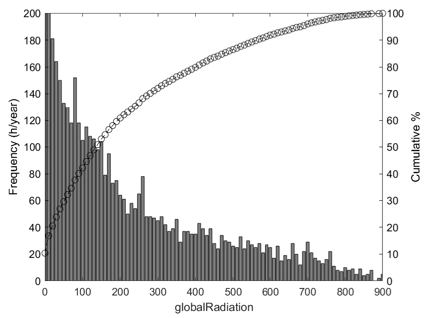

Figure 4: Global horizontal radiation yearly frequency for Milan typical year weather data.

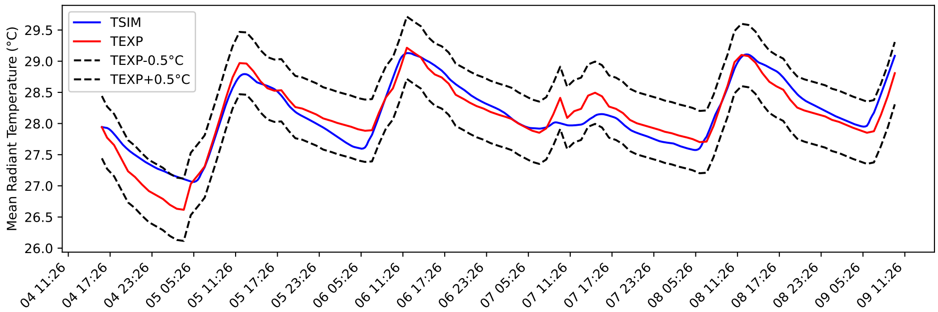

Figure 5: Validation of the living room mean radiant temperature for a week free floating experiment in September. TSIM corresponds to the simulation temperature and TEXP corresponds to the experimental measurement done with a globe thermometer. The dashed line ±0.5 (°C)corresponds to an estimation of the error the instrument, namely ±0.25 (°C) and the other measurements used

Table 1: Apartment properties.

Total floor area	44.5 $[\mathrm{m}^2]$
Total window area	8 $[\mathrm{m}^2]$
External surface to volume ratio	0.25 [1/m]
Average external thermal transmittance	0.46 $[\mathrm{W}/(\mathrm{m}^2\mathrm{K})]$
heat pump nominal capacity	5 [kW]
Occupation period	from 8 p.m. to 8 a.m. for weekdays and unoccupied during the Weekends
Total sensible internal loads	150 [W/zone] when occupied
Total latent internal loads	40 [W/zone] when occupied

an on signal and remains closed otherwise. Each thermal zone has its own thermostat and is controlled independently. The pump works to provide a constant head, tuned to provide each floor heating circuit the respective nominal water mass flow rate. The heat pump supply water set point temperature is calculated via a climatic curve that depends on the external temperature. The baseline results shown in the Results section 3, refer to the emulator running the simulation with this baseline controller. The external Python-Pyomo based MPC is able to override both the zone valve on-off signal, u_i, and the heat pump supply water set point $T_{in,set}$.

2.4. Reduced order model

A grey-box model based on the resistance-capacitance (RC) analogy was identified using the Matlab identification toolbox (Ljung and Singh, 2012) for use within the MPC controller. Looking at Table 1, the apartment can be considered to be well insulated and with heavy construction. Different combinations of resistors and capacitors were tried, leading to a 3C7R scheme that was adopted for each thermal zone. The scheme of the resulting RC circuit for each thermal zone is shown in Figure 6. The three capacities are related to the room temperature T_r, wall temperature T_w and floor temperature T_f. Resistances connect the capacities nodes to each other and furthermore, two resistances connect C_r and C_w to the external temperature T_{ext}. The wall has a resistance that connects also with the sky temperature T_{sky}. The sky temperature allows the low order model to better treat the radiative heat exchange with the external environment, especially in the presence or absence of clouds. Lastly, the capacitors of the rooms are connected to each other through a resistor as a proxy for air exchange between the two thermal zones.

The solar heat source $\Phi_s[W/m^2]$ is the hemispherical global radiation hitting the external wall and window. It is divided between the wall and the floor and multiplied respectively by the opaque area A_{wall} and the windows area A_{win}. a and c are tuning parameters that can be assumed as proxy of absorptance and trasmittance. $\Phi_{int}[W]$ are the internal gains divided between sensible and radiative by the parameter b. The sensible part goes to the room C_r and radiative goes to the wall C_w. Finally, the heat flow rate to the floor heating system is shown in Figure 6 as $\Delta\dot{H} = \dot{H}_{in} - \dot{H}_{out}$. It is modelled in four different ways resulting in different classes of optimization problems:

1. Linear formulation where $\Delta\dot{H}$ itself is treated as an optimization variable (in this case, we let $\Delta\dot{H} := \dot{Q}$).
2. Linear formulation where $\Delta\dot{H}$ is modeled with the supply water temperature T_{in}, return water temperature T_{out} and the nominal value of mass flow $\dot{m}_{fnom}$ (in this case $\Delta\dot{H} := \dot{m}_{fnom}c_w(T_{in} - T_{out})$)
3. Nonlinear formulation where $\Delta\dot{H}$ is modeled with the energy balance in 2., but multiplied by the valve position u_i, and with the continuous relaxation of the integer constraint, i.e., $u_i \in [0, 1]$ (in this case $\Delta\dot{H} := u_i\dot{m}_{fnom}c_w(T_{in} - T_{out})$)
4. Mixed Integer Nonlinear formulation where $\Delta\dot{H}$ is modeled as 3. but without the continuous relaxation.

For formulation 1 the optimal control variable will be the thermal power provided to the floor heating $\dot{Q}$. For formulation 2 the optimal control variables will be the floor heating inlet temperature T_{in}. For formulations

3-4 the optimal control variables are T_{in} and the zone valve status u_i. For the formulations 2-4 using the supply temperature T_{in} as an optimization variable, the return/outlet temperature T_{out} was modeled with the following linear equation to correlate T_{out} with T_{in} and floor temperature T_f as shown in equation 1 .

$$T_{out} = w_f T_{in} + (1 - w_f) T_f \tag{1}$$

w_f is the weighting factor for the identification process. The rationale behind this linear relationship is that the water mass flow rate $\dot{m}_{floor}$ is constant and so if we consider the floor heating system as an heat exchanger w_f would be equivalent to a constant effectiveness. This equation is valid for this case study since the zones valves can only be open or closed and do not provide variable flow control. The authors would like to point out that this approximation might be more problematic for formulation 3., because with the continuous relaxation the valve will be able to modulate the flow and could lead to a larger error between the reduced order model and the emulator model and instability in the MPC.

Since the training of RC models is not the focus of the present work, the identification procedure is briefly reported. All the reduced order model parameters shown in Figure 6, so not including w_f, were trained using two weeks of free floating data, where the boundary conditions were derived from a synthetic profile obtained through a Fourier analysis of the typical year data (Smart and Ballinger, 1984). In this way all major frequency components are present. After identifying all the model parameters, an additional week of data where the heating system is excited by turning it on and off is used to find the weighting parameter w_f. The result of the overall identification process leads to a Normalized Root Mean Square Error (NRMSE) goodness of fit of 82%, defined in Equation 2, in open loop simulation for the whole heating season which for Milan is from the 15^{th} of October to the 15^{th} of April, where the heating system was functional.

$$\text{NRMSE goodness of fit} = 100 \left(1 - \frac{|y_{data} - y_{model}|}{|y_{data} - \overline{y}_{data})|}\right) [\%] \tag{2}$$

2.5. MPC formulations

Besides the modeling approaches, other constraints and objective functions were specified to complete MPC problem formulations. In Table 2, all formulation elements and MPC implementation parameters that were commonly used for the ten different MPCs are shown. Furthermore, Table

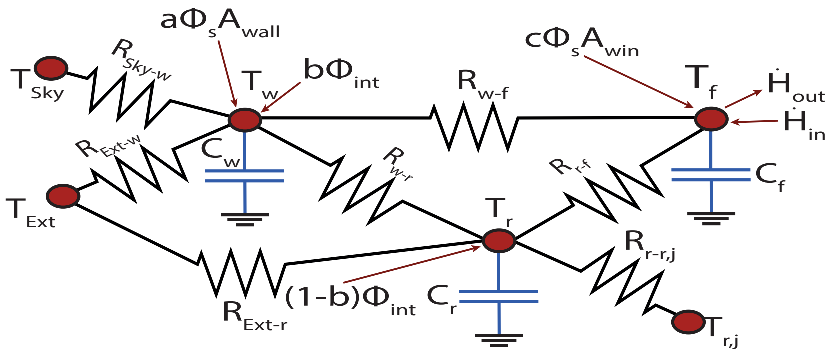

Figure 6: Thermal zone reduced order model, the red dots are the temperatures, the blue parallel lines are the capacitors associated with the temperature states, the resistances are the thermal resistances between the temperatures and the red lines indicate a heat flow into the node.

3 lists all other optimization variables, constraints and objectives. Finally, in Table 4, complete MPC formulations are succinctly summarized with the notations of Table 3.

Table 2: MPC states and disturbances.

Control horizon	24 $[h]$
Time step	15 $[min]$
Solution update	Every time step
Discretization	Direct collocation
States (x)	T_{rliv} $[°C]$: $(-\infty, +\infty)$ T_{fliv} $[°C]$: $(-\infty, +\infty)$ T_{wliv} $[°C]$: $(-\infty, +\infty)$ T_{rbed} $[°C]$: $(-\infty, +\infty)$ T_{fbed} $[°C]$: $(-\infty, +\infty)$ T_{wbed} $[°C]$: $(-\infty, +\infty)$
Disturbances	T_{ext} $[°C]$: $(-\infty, +\infty)$ T_{sky} $[°C]$: $(-\infty, +\infty)$ T_{setliv} $[°C]$: $(-\infty, +\infty)$ T_{setbed} $[°C]$: $(-\infty, +\infty)$ $\dot{Q}_{rad}[kW]$: $[0, max]$ $\dot{Q}_{intliv}[kW]$: $[0, max]$ $\dot{Q}_{intbed}[kW]$: $[0, max]$ $p_e[€]$: $[constant]$

Table 3: List of MPC optimization variables, constraints and objectives.

Variables	$\delta_{liv/bed}$ $[°C]$	$(-\infty, +\infty)$
	T_{in} $[°C]$	$[T_{mix}, T_{inmax}]$
	u_B $[-]$	$u_{liv/bed} : \{0, 1\} \in \mathbb{Z}$
	u_R $[-]$	$u_{liv/bed} : [0, 1] \in \mathbb{R}$
	u_{open} $[-]$	$u_{liv/bed} = 1$
	$\dot{Q}_{liv/bed}$ $[kW]$	$[0, max]$
Constraints	C_{comf}	Comfort constraint $T_{r,liv/bed}(t) - T_{set,liv/bed}(t) + \delta_{liv/bed}(t) \geq 0$
	C_{Qmax}	Maximum heat flow rate $1/(1 - w_f)\dot{Q}_{liv/bed}(t) \leq \dot{m}_f c_w (T_{inmax} - T_{f,liv/bed}(t))$
	C_{Tmin}	Mixing constraint $T_{in} \geq T_{mix} = \dfrac{u_{liv} T_{f,liv} + u_{bed} T_{f,bed}}{(u_{liv} + u_{bed})}$
Objective functions	J_{tot}	Final control objective $min(J_{tot} = \int_{t_0}^{t_f} \sum_{i=1}^{N} k_i j_i(t) dt)\ with\ 0 \leq k_i \leq 1$
	$j_{COP,L}$	Energy cost QP $J_{en} = p_e \dfrac{(\Delta \dot{H}_{liv}(t) + \Delta \dot{H}_{bed}(t))}{COP(T_{ext})(t)}$ [€]
	$j_{COP,NL}$	Energy cost NLP $J_{en} = p_e \dfrac{\Delta \dot{H}_{liv}(t) + \Delta \dot{H}_{bed}(t)}{COP(T_{ext}, T_{in})(t)}$ [€]
	j_{comf}	Temperature mismatch $J_{com} = \delta^2(t)\ [K^2 h]$
	j_{switch}	Switching frequency $J_{swi} = \dfrac{du_{liv}}{dt}^2 + \dfrac{du_{bed}}{dt}^2\ [-]$
	j_B	Binary constraint $J_{bin} = u_{liv}(1 - u_{liv}) + u_{bed}(1 - u_{bed})\ [-]$

Table 2 contains all common elements across the formulations, including dynamic states, disturbances and implementation choices. In Table 2, only the final choice for control horizon and time step is shown. However, four different control horizons were tried for the optimal control problems from 6 up to 72 [h]. The final choice was 24 [h] since a longer prediction horizon did not show significant improvement on KPIs. This time scale aligns with the fact that we are dealing with a heavy construction and a floor heating with a high thermal inertia. Another parametric study was carried out to identify a suitable time step where a MPC solution updates. Bringing it below 15 [min] did not give any significant benefits. To convert continuous optimal control problems into discrete programming problems, a direct collocation method was implemented using the Pyomo problem statement. The six states include all temperatures in both thermal zones and the disturbances as reported in Section 2.4, plus the two room set points and the energy price p_e[€] set to 0.20 [€/kWh].

Table 3 lists all other optimization variables, constraints, and objective functions used in different formulations (each MPC formulation is expressed with a combination of those in Table 4). $\delta_{liv/bed}$ is an auxiliary variable representing a temperature deviation from a setpoint, and is coupled with the constraint C_{comf} and the objective j_{comf}. By looking at the constraint C_{comf}, the value of δ will be higher than zero if the room temperature T_r is lower than the setpoint temperature T_{set}. In this case, it will be penalized by including δ^2 in the objective j_{comf}. This will push the MPC to keep T_r higher than the setpoint temperature.

The other optimization variables, as well as the constraints, are related to the floor heat flow rate models explained in Section 2.4. T_{in} is the supply temperature and can go up to the the maximum temperature of 45 [°C] to avoid high temperatures in the floor, down to a minimum temperature, defined as the adiabatic mixing temperature in constraint C_{Tmin}. The formulation of constraint C_{Tmin} comes from a local energy and mass balance at the return outlet of the floor heating system under the assumption that the nominal flow rate is the same for all circuits. $T_{f,liv/bed}$ is the floor temperature and $u_{liv/bed}$ is the floor heating circuit valve control. u_R represents a continuous relaxation on the valve control, so that the valve can continuously modulate the flow from totally closed to totally opened. u_B indicates the valve controls without the relaxation and are consistent with the actual system and emulator model. u_{open} means the valve controls under the assumption that the valve is always open and the modulation is carried out only at the supply temperature T_{in}. Finally, $\dot{Q}_{liv/bed}$ is used directly as an optimization variable when the heat flow rate is not modeled explicitly. It can go from zero to a maximum value determined by constraint C_{Qmax}. The constraint on the heat flow rate C_{Qmax} imposes the maximum heat flow rate linearly with the floor temperature as a function of the maximum supply temperature T_{inmax} and the weighting parameter w_f. This constraint helps to model the behavior of the floor slab, where, at constant supply temper-

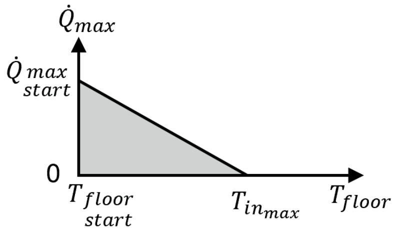

Figure 7: Visual representation of the C_{Qmax} constraint. In grey is highlighted the admissible control area with C_{Qmax} implemented. It reduces as the floor temperature T_f since T_{inmax} is a constant value.

ature, the higher the floor temperature, the lower the heat transfer rate to the floor. Figure 7 is given as a visual representation of the idea.

The last section of Table 4 presents all the components that can make up a complete control objective function. The complete objective function J_{tot} to be minimized is the sum of these different objective components with some weights, denoted as k_i where i corresponds to a specific objective component. The weighting parameters k_i need to be tuned to balance the impact of each objective on the total objective function J_{tot}. To find the best values of k_i, several iterative studies were performed for each MPC formulation and priority was given to the comfort constraint. The objectives $j_{COP,L}$ and $j_{COP,NL}$ are the energy cost and are calculated as the energy price p_e multiplied by the total heat flow rate provided by the heat pump , $\Delta\dot{H}_{liv}(t)+\Delta\dot{H}_{bed}(t)$, divided by the heat pump COP. The COP is a function of the external temperature $COP(T_{ext})$ for $j_{COP,L}$, so the underlying problem remains quadratic. In $j_{COP,NL}$, the COP is a function of the external and supply temperatures $COP(T_{ext}, T_{in})$. Here, the optimization problem becomes nonlinear because a control variable is present in the denominator of a fraction. j_{comf} is the temperature mismatch between room temperature T_r and setpoint T_{set} and works as a comfort proxy. The switching frequency objective j_{switch} is the sum of the squared valve control derivatives. This objectives serves the purpose of penalizing undesirable sudden changes in the control variables. Since the derivative is discretized with forward Euler in the direct collocation method, there is no difference between the formulations that use valve control state as integer u_B and as continuous u_R. Finally, the binary constraint, j_B, forces u_{liv} and u_{bed} to be close to either 0 or 1 to avoid having an objective greater than 0. The reasoning behind this constraint is to approximate a MINLP as a NLP. However, as was found in this study, care should be taken when initializing this optimization problem because the introduction of the binary constraint causes a significant discontinuity in the solution space.

Starting from Tables 2 and 3, several MPC formulations can be defined, ranging from QP to MINLP. Table 4 reports the MPC formulations coupled with the solvers and relative options used for the study.

Table 4: MPC problem statement.

Tag	**Formulation**	**Problem type**	**Solver**	**Tolerance**	**Initialization**	**Post process**	**Subsolvers**
MPC1	$\delta_{liv/bed}$, $\dot{Q}_{liv/bed}$, C_{comf}, C_{Qmax}, $j_{COP,L}$, j_{comf}, j_{switch}	QP	IPOPT	10^{-6}	Free-floating	$\dot{Q}_i$ conversion into u_i and $T_{in,set}$	MA57
MPC2	$\delta_{liv/bed}$, T_{in}, u_{open}, C_{comf}, C_{Tmin}, $j_{COP,NL}$, j_{comf}, j_{switch}	NLP	IPOPT	10^{-6}	Free-floating	conversion of u_i from T_{in} and $T_{in} = T_{in,set}$	MA57
MPC3	$\delta_{liv/bed}$, T_{in}, u_R, C_{comf}, C_{Tmin}, $j_{COP,NL}$, j_{comf}, j_{switch}	NLP	IPOPT	10^{-6}	Free-floating	round u_i and $T_{in} = T_{in,set}$	MA57
MPC4	$\delta_{liv/bed}$, T_{in}, u_R, C_{comf}, C_{Tmin}, $j_{COP,NL}$, j_{comf}, j_{switch}, j_B	NLP	IPOPT	10^{-6}	Free-floating	$T_{in} = T_{in,set}$	MA57
MPC5	$\delta_{liv/bed}$, T_{in}, u_B, C_{comf}, C_{Tmin}, $j_{COP,NL}$, j_{comf}, j_{switch}	MINLP	Bonmin-BB	10^{-4}	MPC3 sol	$T_{in} = T_{in,set}$	CBC, IPOPT
MPC6	$\delta_{liv/bed}$, T_{in}, u_B, C_{comf}, C_{Tmin}, $j_{COP,NL}$, j_{comf} ,j_{switch}, j_B	MINLP	Bonmin-BB	10^{-4}	MPC4 sol	$T_{in} = T_{in,set}$	CBC, IPOPT
MPC7	$\delta_{liv/bed}$, T_{in}, u_B, C_{comf}, C_{Tmin}, $j_{COP,NL}$, j_{comf}, j_{switch}, j_B	MINLP	Bonmin-Hyb	10^{-4}	MPC4 sol	$T_{in} = T_{in,set}$	CBC, IPOPT
MPC8	$\delta_{liv/bed}$, T_{in}, u_B, C_{comf}, C_{Tmin} ,$j_{COP,NL}$, j_{comf}, j_{switch}	MINLP	Baron	10^{-4}	MPC3 sol	$T_{in} = T_{in,set}$	CPLEX, IPOPT
MPC9	$\delta_{liv/bed}$, T_{in}, u_B, C_{comf}, C_{Tmin}, $j_{COP,NL}$, j_{comf}, j_{switch}, j_B	MINLP	Baron	10^{-4}	MPC4 sol	$T_{in} = T_{in,set}$	CPLEX, IPOPT
MPC10	$\delta_{liv/bed}$, T_{in}, u_B, C_{comf},C_{Tmin} ,$j_{COP,NL}$, j_{comf}, j_{switch}, j_B	MINLP	SCIP	10^{-4}	MPC4 sol	$T_{in} = T_{in,set}$	CPLEX, IPOPT

Table 4 shows the ten MPC formulations that were tested. The Tag column reports the formulation names. The Formulation column shows the corresponding optimization variables, constraints, and objectives described in Table 3. Note that the auxiliary variable δ, the temperature constraint C_{comf}, the temperature mismatch j_{comf}, and the switching objective j_{switch} are present in all formulations, apart from MPC2 where j_{switch} is not needed since there is no valve control. The Problem Type column reports the optimization problem type for each MPC formulation, which can be either QP, NLP or MINLP. The Solver column shows the solver chosen, including the MINLP handling algorithm option if present. The Tolerance column is the solver tolerance which was determined through a parametric study as a compromise between quality of the solution and computational time for each solver. The Initialization column defines how the optimization problem variables were initialized. Free-floating initialization means that a simulation runs using the reduced order model subject to the same boundary conditions, as in the forecasts used for the optimal control, with the floor heat flow rate set to zero. In other formulations, a slightly randomized solution of a different MPC formulation is used as initialization as indicated. The Post Process column shows the steps needed to convert the optimal control trajectory into the physical control inputs used in the emulator model. The Subsolvers column refers to the solvers used by the solver indicated in the Solver column. Another parameter not included in the table is the Timeout. It corresponds to the maximum time between each control horizon optimization and was fixed at two minutes for all formulations as a compromise between giving the solvers enough time to converge to a solution and the overall computational time.

Below, a summary for each MPC formulation presented in Table 4 is provided:

- MPC1: This formulation uses heat flow rates directly as optimization variables $\dot{Q}_{liv/bed}$, and $j_{COP,L}$ as the energy objective. In this way, the final constraints are linear in optimization variables, and the objective function is quadratic, making a QP problem. The solver of choice for QP was IPOPT with the MA57 linear subsolver. The tolerance was set to 10^{-6} from the default value of 10^{-8} and the timeout time to 120 $[s]$, and the initialization is free-floating. Some post processing is required to convert the optimal control trajectory into the physical control variables used in the emulator. If $\dot{Q}_{liv/bed}$ is higher than a threshold value, equivalent to the minimum cutoff power of the heat pump set as 20 % of the nominal value 800 [W], the valves $u_{liv/bed}$ will be opened otherwise they remain closed. The supply temperature setpoint is calculated using the previous step return temperature plus the delta given by $\dot{Q}_{liv/bed}$.

- MPC2: This formulation uses the supply temperature as an optimization variable T_{in}, while the circuit valves remain always open u_{open}, and $j_{COP,NL}$ is used for the energy objective. Together with the linear radiant floor heat modeling approach (see point 2.) in Section 2.4, the final constraints are linear in optimization variables, and nonlinear in the objective due to the presence of COP as a function of the supply temperature T_{in}, making it a NLP problem. The solver of choice for the NLP problem was IPOPT with the linear subsolver MA57. The tolerance was set to 10^{-6} from the default value of 10^{-8} and the timeout time to 120 $[s]$, and the initialization is free-floating. A post process is required to convert the optimal control trajectory into the physical control variables used in the emulator. If the supply temperature T_{in} is higher than a threshold value, the valves $u_{liv/bed}$ will open; otherwise, they remain closed. The threshold is calculated as an estimation of the minimum cutoff power of the heat pump set as 20 % of the nominal value, 800 [W]. The minimum heat flow rate $\dot{Q}$ is calculated using the expression in point 2. Section 2.4. Then T_{in} is used as setpoint supply temperature in the emulator.

- MPC3: Compared to MPC2, this MPC does not assume that the circuit valves are fully open. Instead, it relaxes the on/off binary constraints to a real number set u_R as mentioned in 3) in Section 2.4 and in Table 3. The final problem formulation is nonlinear in terms of constraints and optimization variables due to the multiplication between supply temperature and valve control. The objective is also nonlinear due to the presence of COP as a function of the supply temperature T_{in} and the multiplication of two optimization variables in the calculation of the heat flow rate $\Delta\dot{H}$. The added nonlinearity of MPC3 compared to MPC2 makes the problem nonconvex because the solver can change T_{in} or u_R to modulate the heat flow rate, making the process of finding a global optimum harder. Solver settings were identical to MPC2. MPC also needs to convert the optimal control trajectory into the physical control variables used in the emulator. If the circuit valve $u_{liv/bed}$ value is higher than a threshold value, the most common choice would be 0.4. However, the authors found out that playing around with this parameter and reducing it to 0.3 lead to a more stable solution. So in case the valve control is higher than the threshold the valves $u_{liv/bed}$ will be opened, else they remain closed. Then T_{in} is used as setpoint for the supply temperature in the emulator.

- MPC4: This formulation is identical to MPC3, apart from the addition of the binary objective j_B. The idea behind j_B is to force u_R to be either closed $u_R = 0$, or open $u_R = 1$, by penalizing all solutions that modulate the flow rate in a continuous manner. This allows for a smaller control space by reducing the optimal operating range of the zone valves. This will serve as an NLP approximation of a MINLP formulation. In this case $u_{liv/bed}$ will be used directly in the emulator, because $u_{liv/bed}$ in the raw solution when using j_B are very close to 0 or very close to 1, making the rounding process trivial and T_{in} is used as setpoint for the supply temperature.

- MPC5: This formulation is the same as MPC3 but replacing the continuous relaxation (u_R) with the binary constraint (u_B). In this way the final problem formulation is mixed integer nonlinear due to the multiplication between contnious supply temperature and on/off valve control variables, making a MINLP problem. The additional complexity of MPC5 compared to the previous QP and NLP formulations requires a dedicated MINLP solver. The solver of choice for MPC5 was BONMIN-BB. CBC was used as MIQP subsolver and IPOPT as NLP solver. The tolerance was set to 10^{-4} from the default value of 10^{-6} and the timeout time to 120 $[s]$. The initialization is done by taking the solution of MPC3 after rounding the values of $u_{liv/bed}$. The MINLP solution can be directly applied to the emulator with no need for post processing of the solution.In this case $u_{liv/bed}$ will be directly used in the emulator and T_{in} is used as setpoint for the supply temperature.

- MPC6: This formulation is identical to MPC5 apart from the addition of the binary objective j_B and the initialization done with MPC4 solution. The rationale is similar as in the transition from MPC3 to MPC4. However, instead of a single NLP problem, it is extended to all subsets of NLP problems generated by the MINLP solver.In this case $u_{liv/bed}$ will be directly used in the emulator and T_{in} is used as setpoint for the supply temperature.

- MPC7: This formulation is identical to MPC6, where a different MINLP algorithm option was used for the Bonmin solver BONMIN-Hyb. In this case $u_{liv/bed}$ will be directly used in the emulator and T_{in} is used as setpoint for the supply temperature.

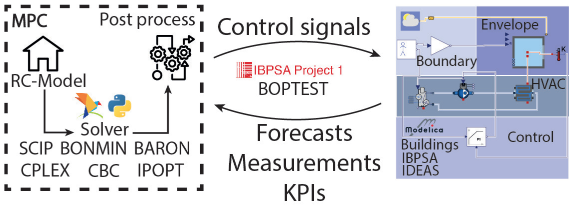

Figure 8: co-simulation setup.

- MPC8: This formulation is identical to MPC5, where a different MINLP solver was used named Baron. The MIQP solver is CPLEX and the NLP solver is IPOPT.In this case $u_{liv/bed}$ will be directly used in the emulator and T_{in} is used as setpoint for the supply temperature.

- MPC9: This formulation is identical to MPC8 with the addition of the binary constraint j_B.In this case $u_{liv/bed}$ will be directly used in the emulator and T_{in} is used as setpoint for the supply temperature.

- MPC10: This formulation is identical to MPC9 with the difference that the MINLP solver of choice was SCIP.In this case $u_{liv/bed}$ will be directly used in the emulator and T_{in} is used as setpoint for the supply temperature.

2.6. Co-simulation setup

All elements shown in previous sections are coupled in a co-simulation, a graphical representation is given in Figure 8. The optimal control routine runs on the Pyomo Python toolbox Pyomo (Bynum et al., 2021) and the detailed emulator model is wrapped in a Docker container using the BOPTEST software (Blum et al., 2021). all simulations were carried out on a Linux Ubuntu 18 laptop with 16GB of RAM and an Intel(R) Core(TM) i7-8650U CPU @ 1.90GHz. all solvers have multi thread capability so up to 8 threads were used for the simulations.

All cases mentioned in Table 4 were directly implemented in Python using a concrete instance modeling feature of Pyomo. The solvers were compiled externally and coupled with Pyomo using the AMPL interface. Finally the Kalman filter from (Labbe, 2018) was used to update the states of the reduced order model at each time initialization.

BOPTEST provides an easy to use API interface that allows the optimization scripts to manipulate the control variables of the detailed model, access sensor data and access forecasts, and the KPIs calculated by BOPTEST.

The control variables are the supply temperature setpoint and the zone valve open or closed signal. The forecasts are the disturbance variables reported in Table 2 and are considered deterministic, which means that the same disturbances will also be used in the emulator model. The measurements are the room temperature, the water supply temperature and the return temperature from each zone, and are used by the Kalman filter to estimate the initial value of room, wall, and floor temperatures for each zone for each prediction horizon. To estimate the performance of each MPC formulation, BOPTEST can calculate many KPIs, though this paper considers the thermal discomfort, computational time ratio, and energy cost. Furthermore, four additional KPIs were used to evaluate the performance of these MPC formulations, namely the total computational time $[s]$ of the MPC solver, the thermal energy used $[kWh]$, the control arc length, and the number of MPC solver time-out or error events [%] that occurred throughout the evaluation period. The equations and descriptions of the KPIs are reported in Table 5, and the descriptions of their variables are reported below the table. Only valid solutions are used to update the MPC control trajectory. Time-out solutions are valid when variables values are within the bounds, however, they may be not fully converged, meaning that constraints may not be completely satisfied. Time-out solutions are considered invalid if outside variables bounds. Solutions with an error in the solver status are discarded. When a solution is discarded, the previous solution current time step is used until a new valid solution is found.

In the discomfort KPI K_{dis} calculation, $T_r[K]$ is the room operative temperature and $T_{r,set}[K]$ the heating setpoint, N is the total number of zones, and t_o and t_f are the initial and final time of the evaluation period. In the computational time ratio KPI K_{timr} $\delta T_k[s]$ is the MPC computational time at step k, M is the number of control steps and $\delta t_k[s]$ is the time interval of control step k. In the cost KPI K_{cost}, $p_{el}[EUR/kWh]$ is the electricity price considered as constant, $Q_{tot}[kWh]$ is the total energy supplied by the heat pump and $A_{tot}[m^2]$ is the total floor area of the apartment. $Q_{tot}[kWh]$ is also used to calculate the thermal energy KPI K_{en}. K_{err} is the ratio between the number of MPC iterations that had either timeout $N_{timeouts}$ or errors N_{errors} and the total number of iterations N_{total}, 2976, for the period considered, the month of January with a timestep of 15 [min]. Lastly, a new KPI is introduced in this manuscript called control arc length K_{conlen}. The idea of this KPI is to quantify the frequency of switching for the control system throughout the evaluation period. K_{conlen} is the ratio between the length of the actual control trajectory. It is calculated on the total heat flow rate provided by the heat pump $\dot{Q}_{hp}$ versus a fictional reference trajectory

Table 5: BOPTEST and MPC specific KPIs.

Icon	Name	Equation	Type
K_{dis}	Discomfort	$\frac{\sum_{z=1}^{N}\int_{t_0}^{t_f} max(T_{r,set}(t) - T_r(t), 0)dt}{N}$ $[Kh/zone]$	BOPTEST
K_{timr}	Computational time ratio	$\frac{\sum_{k=1}^{M}\frac{\Delta T_k}{\Delta t_k}}{M}$ $[-]$	BOPTEST
K_{cost}	Energy cost	$\frac{\int_{t_0}^{t_f} p_{el}\frac{\dot{Q}_{tot}(t)}{COP(t)}dt}{A_{tot}}$ $[EUR/m^2]$	BOPTEST
K_{en}	Thermal energy supplied	$\frac{\int_{t_0}^{t_f}\dot{Q}_{tot}(t)dt}{A_{tot}}$ $[kWh/m^2]$	case study specific
K_{ttot}	Total computational time	[s]	case study specific
K_{err}	Solver errors or timeouts	$\frac{N_{errors} + N_{timeouts}}{N_{total}}$ [%]	case study specific
K_{conlen}	Control arc length	$\frac{\int_{t_0}^{t_f}\sqrt{1+\left(\frac{du}{dt}\right)^2}dt}{\int_{t_0}^{t_f}\sqrt{1+\left(\frac{du_{ref}}{dt}\right)^2}dt}$	case study specific

u_{ref} that consider the control variable u to be constant for the evaluation period. A visual representation is given in Figure 9.

3. Results

Simulation evaluation results for the month of January are shown because similar conclusions were drawn from the rest of the heating season. As mentioned, all MPCs were updated for every 15 [min] time step with the control horizon of 24 [h]. Each MPC was calculated 2976 times for the simulation period and has around 1000 constraints and 600 optimization variables for the linear problems and 1200 optimization variables for the nonlinear problems.

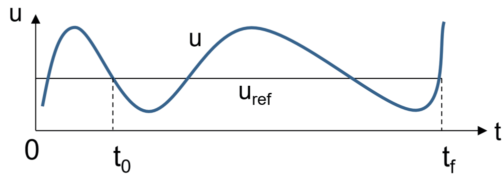

Figure 9: On the y-axis is the value of the control variable u and u_{ref} is the reference value kept as constant. On the x-axis is time with the evaluation period taken from t_0 to t_f.

3.1. KPIs Comparison

Figures 10 and 11 report the KPI results calculated by BOPTEST. From the Discomfort KPI K_{dis} in Figure 10, most of the formulations outperform the rule based controller with more than 90% decrease in discomfort. The main reason is the ability of MPC to predict the step change in zone heating setpoint temperature and compensate for the delayed response of the floor heating system. However, the MPC7 solution using Bonmin with the Hybrid method led to discomfort similar to the baseline controller. The authors managed to make MPC7 work properly, not shown in the chart. However, it required significant manual tuning effort for the weight on comfort constraints and solver internal options (MINLP approximation relaxation, integer tolerance) to guide the solution. This highlights that Bonmin-Hyb is probably not robust enough for this type of problem.

Looking at the computational time ratio K_{timr} in Figure 10 and total computational time K_{ttot} in Figure 11, QP and NLPs (MPC1 - MPC4) required less computing time than MINLPs (MPC5-MPC10) as expected. However, all MPC formulations have a K_{timr} value much lower than one, meaning that MINLPs could be used for a real time application from the computation perspective. Looking at a relative comparison of K_{ttot}, MPC1 (QP) and MPC2 (NLP) take between 15 and 20 [min] to run for all 2976 optimization iterations, so on average from 0.3 to 0.4 [s] per optimization. MPC3 (NLP) and MPC4 (NLP) take between 50 and 60 [min], so on average from 1 to 1.3 [s] per optimization. The remaining MINLP formulations, i.e., MPC5 to MPC10, instead take from 1 [h] 40 [min] up to 2 [d] and 5 [h], so on average from 2 [s] to 64 [s] per optimization. This big variation of computational times shows that MINLP MPCs are sensitive to a formulation, initialization, and solver selection. In fact, the differences between MPC5 and MPC6 are only the initialization approach and the inclusion of j_B, and the difference between MPC9 and MPC10 is only the solver. How-

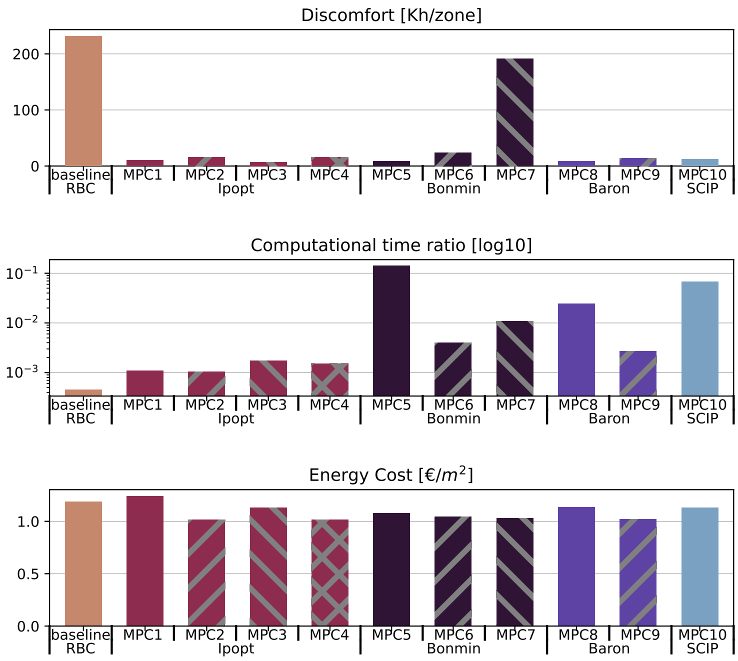

Figure 10: BOPTEST KPIS for the month of January as thermal discomfort K_{dis} (top), computational time ratio K_{timr} in logarithmic scale (middle), and energy cost K_{cost} (bottom). The results are shown for all MPC combinations explained in Table 4.

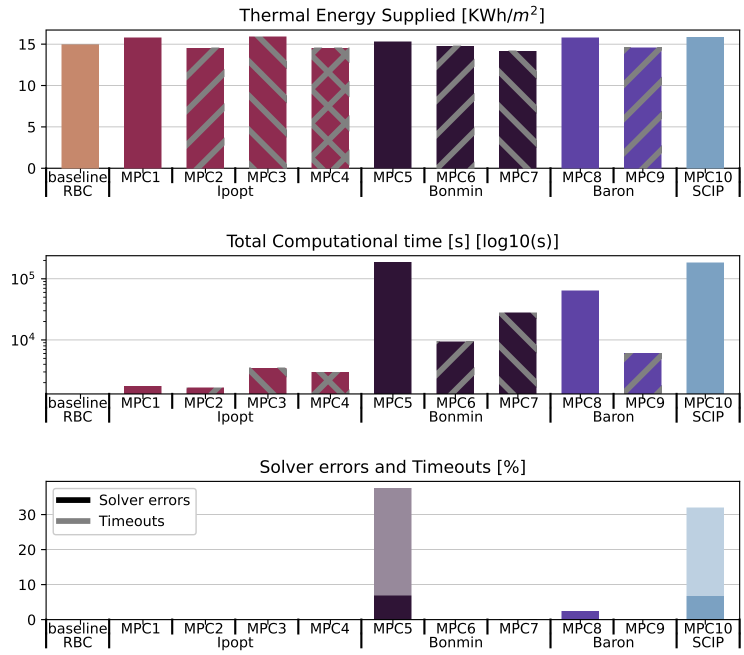

Figure 11: MPC specific KPIs for the month of January, Thermal heating power per square meter K_{en} (top), total computational time K_{ttot} in logarithmic scale (middle), Total number of solver time out or error statuses K_{err} (bottom), the KPI description is presented in Table 5 . The results are shown for all MPC combinations explained in Table 4.

ever, MPC5 and MPC10 result in much longer computational time (a factor of 10) caused by a lot of errors or timeouts for around 30 % of the iterations (see the last subfigure in Figure 11), meaning that the MINLP solvers are struggling to converge. Furthermore, SCIP was not able to find a solution without the j_B binary objective. It is very interesting that all MINLP solvers benefit from the introduction of j_B in terms of solver reliability and time, because the objective seems to be redundant for integer formulations and solvers. This might be explained by the fact that by introducing j_B, each NLP approximation of the MINLP is itself an approximation of a MINLP problem.

The comparisons of energy cost K_{cost} and thermal energy K_{en} are shown in Figure 10 and in Figure 11, respectively. For K_{en}, all formulations and the baseline are within 6 % of each other, with MPC2, MPC4, MPC6, MPC7, and MPC9 being marginally better than the baseline, and MPC1, MPC3, MPC8 and MPC10 being marginally worse. When looking at cost however, MPC1 (QP) is the worst performer with 5 % increase with respect to the baseline[2], while MPC2 (NLP), MPC4 (NLP), MPC6 (MINLP) and MPC9 (MINLP) show the best performance with a 13 % decrease in cost with respect to the baseline. This is due to the fact that MPC1 adopts a simpler COP model, while the other formulations use a more precise performance map allowing a more efficient use of the heat pump. It is not clear from this analysis alone why the MPC2, MPC4, MPC6 and MPC9 seem to outperform the other nonlinear formulations for these KPIs. For that, we consider a more detailed analysis of time series data in Section 3.2.

3.2. Typical day analysis

Figure 12 shows daily temperature and thermal power profiles grouped by similar control patterns based on aggressiveness of switching: medium (left figures): MPC1 and MPC7 with the baseline, smooth (middle figures): MPC2, MPC4, MPC6 and MPC9, aggressive (right figures): MPC3, MPC5,MPC8 and MPC10). The aggressive group's pattern could be explained by the convergence issues as indicated in the last panel of Figure 11 except for MPC3. Although there are cost savings and comfort improvements for those MPCs (see Figure 10), they may not be applicable in practice due to short cycling which increases the wear of components. It is also interesting to see the influence of relaxation schemes for integer con-

[2]The performance of MPC1 (QP) should not be under-evaluated compared to the baseline control because of the significant comfort improvement

straints: The only difference of MPC3 (NLP) compared with MPC2 (LNP) and MPC4 (NLP) that are in the smooth group (middle figures) is in rounding the MPC decision to enforce it to either 0 or 1. This rounding clearly introduces prediction errors and hence pushes MPC3 to solve an unexpected problem at the next time step. The aggressive result of MPC3 indicates that nonlinear MPC could be sensitive to prediction errors at least for this case study. Lastly, the frequent on-off of the system causes a higher discrepancy between the prediction of the low order model versus the emulator model. The main reason is that the Buildings envelope model is made up of hundreds of states while the reduced order model uses only a handful. The consequence is that the high frequency components for the aggressive case impact the temperature nodes in different ways between the emulator and reduced order models, increasing the error of the prediction.

The newly introduced KPI K_{conlen} described in Table 5 can compactly indicate the level of short cycling. Indeed, from Figure 13, which compares K_{conlen}, the same conclusion from the analysis of Figure 12 can be drawn: the smooth group (middle figures: MPC2, MPC4, MPC6 and MPC9) has half the control arc length of the aggressive group (right figures: MPC3, MPC5, MPC8 and MPC10). However, the difference between baseline and MPC1 which use an on-off approach and MPC2,MPC4,MPC6 and MPC9 which modulate the load more is not highlighted. The reason is that the control variable considered is the total heat pump power $\dot{Q}$, which partially masks the behavior of separate control variables, water supply setpoint $T_{in,set}$ and valves on-off u_i. The authors are aware of this simplification and will explore a more comprehensive approach in future work.

From the comprehensive analysis using KPIs of discomfort K_{dis}, cost K_{cost} and on-off switching K_{conlen}, MPC2 (NLP), MPC4 (NLP), MPC6 (MINLP) and MPC9 (MINLP) that are in the smooth group are superior than other MPCs and the baseline, and MPC9 performs the best. However, as pointed out in Section 3.1, MINLP MPC formulations are sensitive to formulations, initialization approaches, solver selections and solver parameters, and the incremental savings of MPC9 are insignificant. Overall, we conclude that increasing the complexity of MINLP-MPC approaches does not bring substantial benefits at least for this case study but only adds computational burden, makes the MPC less robust, and requires more manual tuning efforts. The open-source and commercially available, general purpose MINLP solvers are not yet sufficiently reliable for real time MPC applications for the HVAC system.

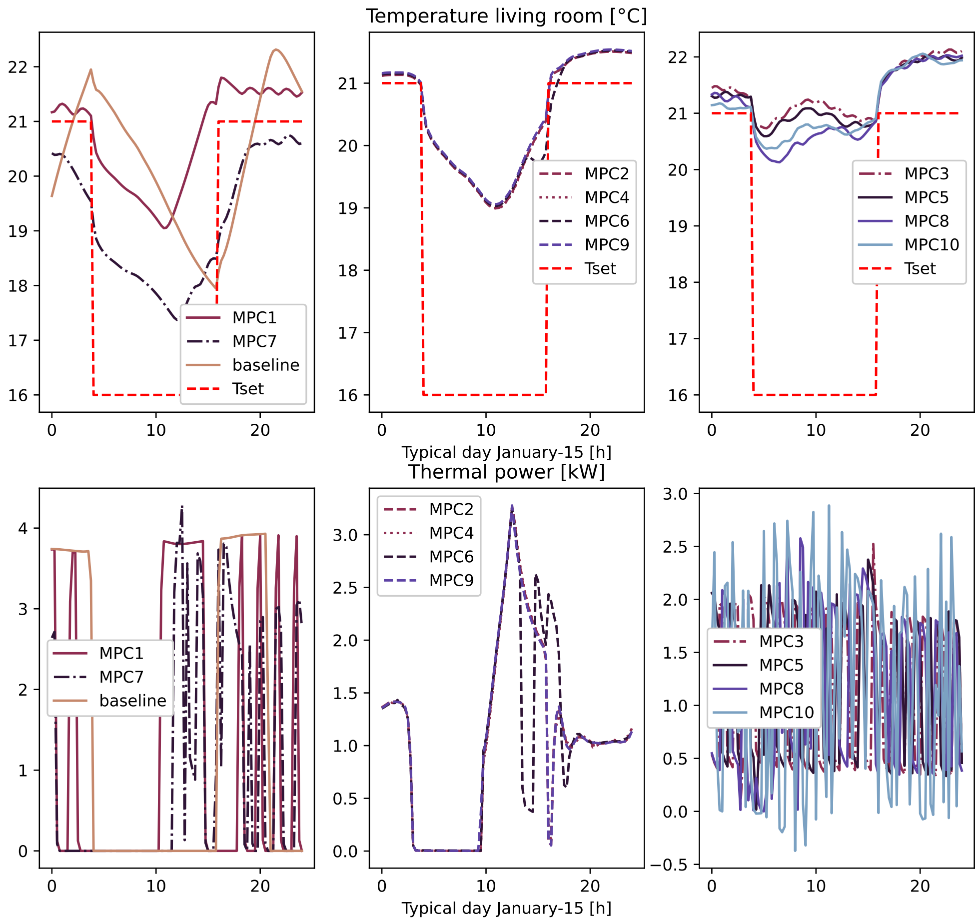

Figure 12: Results for a typical day 15^{th} of January, in the top row charts are the temperatures in the living room for the different formulations,in the bottom row charts are the total thermal power supplied by the heat pump to the floor heating system.

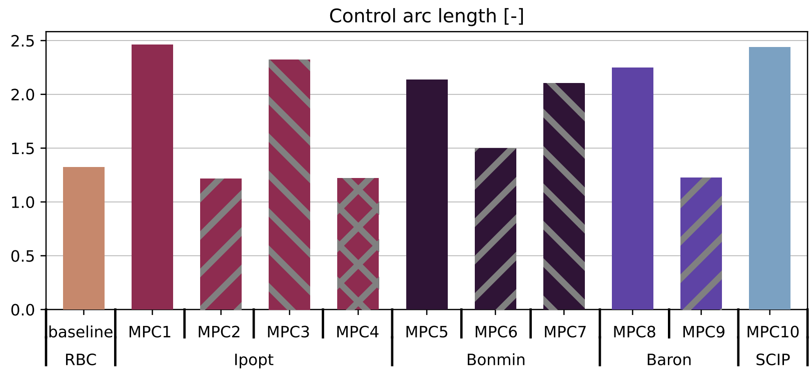

Figure 13: Control arc length KPI K_{conlen} specific for the month of January. It allows for estimating the heat pump switching frequency for the different formulations. The KPI description is presented in Table 5. In this case the total power supplied by the heat pump was used to calculate K_{conlen}

4. Conclusions

This manuscript compared ten combinations of MPC formulations and solvers ranging between a QP formulation (MPC1), NLP formulations (MPC2 - MPC4), and MINLPs (MPC5 - MPC10) with a high focus on the assessment of MINLP MPCs for a residential radiant floor heating system. The performances were evaluated with a detailed emulator model where all MPCs exhibit unmodeled dynamics. The conclusions are summarized as below.

- MPC1 and MPC2 are both linear approximations, for the constraints, of the original MINLP problem. However, there is a large performance gap between the two. MPC1 is the most intuitive way to linearize the heat flow rate by combining valve and temperature into thermal power $\dot{Q}$. However, in this way, the MPC is not able to accurately estimate the heat pump COP as a function of supply temperature, leading to an on-off operation of the system. MPC2, instead, used a less intuitive approach, keeping the valves always open and modulating only the supply temperature in order to maximize COP. Here, the more detailed COP formulation led to an overall better solution.

- MINLP MPC performance is sensitive to formulations, MINLP solvers, solver options and tolerances, and the corresponding tuning process is not trivial. However, a MINLP formulation is natural and more straightforward to implement, since the optimization variables could be consistent with the physical controllable variables and modeling approaches for simulations (e.g. the detailed COP model or use of physical valve positions as optimization variables).

- To make MINLP MPC properly work, it often required solving another, approximated MPC problem. In our case, an NLP MPC was solved for initializing an MINLP MPC.

- For this case study, no substantial benefits of any MINLP MPC formulation was found over an NLP MPC. Meanwhile, MINLP formulations dramatically increased computational time and were less stable, with time outs or errors occurring for over 30% of MPC control steps.

- This paper introduced and compared the state-of-the-art, open source MINLP solvers (SCIP, Bonmin) and commercial solver (Baron). They could be viable options for building HVAC optimal control problems with appropriate tuning, but they were not the best solution for this case study.

- From the overall analysis, it is shown that the initial effort of finding a suitable linear constraint formulation or reduce the unwanted control space (jB), (in modeling the radiant floor heat transfer) leads to identical energy and discomfort performance compared with a very well tuned MINLP MPC, while being faster and more robust. Therefore, the authors conclude that using a linear formulation for the constraints with a nonlinear objective function and proper initialization method, such as slightly randomized free floating solutions, gives a good balance between the accuracy of the prediction, computational requirements, and robustness.

Acknowledgments

This research was supported by the Assistant Secretary for Energy Efficiency and Renewable Energy, Office of Building Technologies of the U.S. Department of Energy, under Contract No. DE-AC02-05CH11231.

References

AMPL, 2003. Ampl solver interface. https://ampl.com/REFS/hooking2.pdf.

ASHRAE, 2019. 2019 ASHRAE Handbook: HVAC Applications. Chapter 43: Supervisory control strategies and optimization. American Society of Heating Refrigerating and Air-Conditioning.

Atam, E., Helsen, L., 2015. A convex approach to a class of non-convex building hvac control problems: Illustration by two case studies. Energy and Buildings 93, 269–281.

Blum, D., Arendt, K., Rivalin, L., Piette, M., Wetter, M., Veje, C., 2019. Practical factors of envelope model setup and their effects on the performance of model predictive control for building heating, ventilating, and air conditioning systems. Applied Energy 236, 410–425.

Blum, D., Arroyo, J., Huang, S., Drgoňa, J., Jorissen, F., Walnum, H.T., Chen, Y., Benne, K., Vrabie, D., Wetter, M., Helsen, L., 2021. Building optimization testing framework (BOPTEST) for simulation-based benchmarking of control strategies in buildings. Journal of Building Performance Simulation 14, 586–610. URL: https://doi.org/10.1080/19401493.2021.1986574, doi:10.1080/19401493.2021.1986574.

Bonami, P., Biegler, L.T., Conn, A.R., Cornuéjols, G., Grossmann, I.E., Laird, C.D., Lee, J., Lodi, A., Margot, F., Sawaya, N., Wächter, A., 2008. An algorithmic framework for convex mixed integer nonlinear programs. Discrete Optimization 5, 186–204. doi:10.1016/j.disopt.2006.10.011.

Boyd, S., Boyd, S.P., Vandenberghe, L., 2004. Convex optimization. Cambridge university press.

Burger, A., Zeile, C., Altmann-Dieses, A., Sager, S., Diehl, M., 2018. An Algorithm for Mixed-Integer Optimal Control of Solar Thermal Climate Systems with MPC-Capable Runtime. 2018 European Control Conference, ECC 2018 , 1379–1385doi:10.23919/ECC.2018.8550424.

Bynum, M.L., Hackebeil, G.A., Hart, W.E., Laird, C.D., Nicholson, B.L., Siirola, J.D., Watson, J.P., Woodruff, D.L., 2021. Pyomo–optimization modeling in python. volume 67. Third ed., Springer Science & Business Media.

Cigler, J., Siroky, J., Korda, M., Jones, C., 2013. On the selection of the most appropriate MPC problem formulation for Buildings. Proc. 11th REHVA World Congress CLIMA 2013 .

del Mar Castilla, M., Alvarez, J.D., Rodriguez, F., Berenguel, M., 2014. Comfort control in buildings. Springer.

Drgona, J., Kvasnica, M., 2013. Comparison of MPC strategies for building control. Proceedings of the 2013 International Conference on Process Control, PC 2013 , 401–406doi:10.1109/PC.2013.6581444.

Drgoňa, J., Kvasnica, M., Klaučo, M., Fikar, M., 2013. Explicit stochastic mpc approach to building temperature control, in: 52nd IEEE Conference on Decision and Control, IEEE. pp. 6440–6445.

Drgoňa, J., Arroyo, J., Cupeiro Figueroa, I., Blum, D., Arendt, K., Kim, D., Ollé, E.P., Oravec, J., Wetter, M., Vrabie, D.L., Helsen, L., 2020. All you need to know about model predictive control for buildings. Annual Reviews in Control 50, 190–232. doi:10.1016/j.arcontrol.2020.09.001.

Forrest, J., Lougee-Heimer, R., 2005. Cbc user guide, in: Emerging theory, methods, and applications. INFORMS, pp. 257–277.

or Foundation, C., 2006. Ipopt. URL: https://github.com/coin-or/.

IBPSA, 2019. Boptest. https://github.com/ibpsa/project1-boptest.

Jorissen, F., Reynders, G., Baetens, R., Picard, D., Saelens, D., Helsen, L., 2018. Implementation and verification of the IDEAS building energy simulation library. Journal of Building Performance Simulation 11, 669–688. URL: https://doi.org/10.1080/19401493.2018.1428361, doi:10.1080/19401493.2018.1428361.

Kathirgamanathan, A., De Rosa, M., Mangina, E., Finn, D.P., 2021. Data-driven predictive control for unlocking building energy flexibility: A review. Renewable and Sustainable Energy Reviews 135, 110120. URL: https://doi.org/10.1016/j.rser.2020.110120, doi:10.1016/j.rser.2020.110120, arXiv:2007.14866.

Kim, D., Braun, J., Cai, J., Fugate, D., 2015. Development and experimental demonstration of a plug-and-play multiple rtu coordination control algorithm for small/medium commercial buildings. Energy and Buildings 107, 279–293.

Kim, D., Braun, J.E., 2018. Development, implementation and performance of a model predictive controller for packaged air conditioners in small and medium-sized commercial building applications. Energy and Buildings 178, 49–60.

Kim, D., Cai, J., Ariyur, K.B., Braun, J.E., 2016. System identification for building thermal systems under the presence of unmeasured disturbances in closed loop operation: Lumped disturbance modeling approach. Building and Environment 107, 169–180.

Kim, D., Cai, J., Braun, J.E., Ariyur, K.B., 2018. System identification for building thermal systems under the presence of unmeasured disturbances in closed loop operation: Theoretical analysis and application. Energy and Buildings 167, 359–369.

Kronqvist, J., Bernal, D.E., Lundell, A., Grossmann, I.E., 2019. A review and comparison of solvers for convex minlp. Optimization and Engineering 20, 397–455.

Kılınç, M.R., Sahinidis, N.V., 2018. Exploiting integrality in the global optimization of mixed-integer nonlinear programming problems with BARON. Optimization Methods and Software 33, 540–562. doi:10.1080/10556788.2017.1350178.

Labbe, R.R., 2018. Filterpy documentation. https://filterpy.readthedocs.io/en/latest/ .

research group LBL, S., 1991. Doe-2. https://doe2.com/DOE2/ .

Ljung, L., Singh, R., 2012. Version 8 of the matlab system identification toolbox. IFAC Proceedings Volumes 45, 1826–1831.

Ma, Y., Matuško, J., Borrelli, F., 2014. Stochastic model predictive control for building hvac systems: Complexity and conservatism. IEEE Transactions on Control Systems Technology 23, 101–116.

Maasoumy, M., Razmara, M., Shahbakhti, M., Vincentelli, A.S., 2014. Handling model uncertainty in model predictive control for energy efficient buildings. Energy and Buildings 77, 377–392.

McCormick, G.P., 1976. Computability of global solutions to factorable nonconvex programs: Part i—convex underestimating problems. Mathematical programming 10, 147–175.

Metrics, I.E.A.B.E.P., 2015. Supporting Energy Efficiency Progress in Major Economies. International Energy Agency: Paris, France .

Oldewurtel, F., Parisio, A., Jones, C.N., Gyalistras, D., Gwerder, M., Stauch, V., Lehmann, B., Morari, M., 2012. Use of model predictive control and weather forecasts for energy efficient building climate control. Energy and Buildings 45, 15–27.

Pčolka, M., Žáčeková, E., Robinett, R., Čelikovský, S., Šebek, M., 2016. Bridging the gap between the linear and nonlinear predictive control: Adaptations for efficient building climate control. Control Engineering Practice 53, 124–138. doi:10.1016/j.conengprac.2016.01.007.

Picard, D., Drgoňa, J., Kvasnica, M., Helsen, L., 2017. Impact of the controller model complexity on model predictive control performance for buildings. Energy and Buildings 152, 739–751.

Picard, D., Sourbron, M., Jorissen, F., Cigler, J., Ferkl, L., Helsen, L., et al., 2016. Comparison of model predictive control performance using grey-box and white box controller models. 2016 International High Performance Buildings Conference proceedings .

Prívara, S., Cigler, J., Váňa, Z., Oldewurtel, F., Sagerschnig, C., Žáčeková, E., 2013. Building modeling as a crucial part for building predictive control. Energy and Buildings 56, 8–22. doi:10.1016/j.enbuild.2012.10.024.

Risbeck, M.J., Maravelias, C.T., Rawlings, J.B., Turney, R.D., 2017. A mixed-integer linear programming model for real-time cost optimization of building heating, ventilation, and air conditioning equipment. Energy and Buildings 142, 220–235.

Rockett, P., Hathway, E.A., 2017. Model-predictive control for non-domestic buildings: a critical review and prospects. Building Research and Information 45, 556–571. doi:10.1080/09613218.2016.1139885.

Roth, K.W., Westphalen, D., Dieckmann, J., Hamilton, S.D., Goetzler, W., 2002. Energy consumption characteristics of commercial building HVAC systems volume III: Energy savings potential. TIAX LLC Report for US Department of Energy Building Technologies Program .

Scherer, H.F., Pasamontes, M., Guzmán, J.L., Álvarez, J., Camponogara, E., Normey-Rico, J., 2014. Efficient building energy management using distributed model predictive control. Journal of Process Control 24, 740–749.

Serale, G., Fiorentini, M., Capozzoli, A., Bernardini, D., Bemporad, A., 2018. Model Predictive Control (MPC) for enhancing building and HVAC system energy efficiency: Problem formulation, applications and opportunities. Energies 11. doi:10.3390/en11030631.

Smart, M.G., Ballinger, J.A., 1984. Fourier-synthesized weather data for building energy use estimation. Building and Environment 19, 41–48.

Sourbron, M., Verhelst, C., Helsen, L., 2013. Building models for model predictive control of office buildings with concrete core activation. Journal of building performance simulation 6, 175–198.

Verhelst, C., Degrauwe, D., Logist, F., van Impe, J., Helsen, L., 2012. Multi-objective optimal control of an air-to-water heat pump for residential heating. Building Simulation 5, 281–291. doi:10.1007/s12273-012-0061-z.

Wachter, A., 2002. An interior point algorithm for large-scale nonlinear optimization with applications in process engineering. Ph.D. thesis. Carnegie Mellon University.

Walker, S.S., Lombardi, W., Lesecq, S., Roshany-Yamchi, S., 2017. Application of distributed model predictive approaches to temperature and co2 concentration control in buildings. IFAC-PapersOnLine 50, 2589–2594.

Wetter, M., Blum, D., Hu, J., USDOE, 2019. Modelica IBPSA Library v1. BS2019 conference proceedings URL: https://www.osti.gov/biblio/1529269, doi:10.11578/dc.20190520.1.

Wetter, M., Zuo, W., Nouidui, T.S., Pang, X., 2014. Modelica Buildings library. Journal of Building Performance Simulation 7, 253–270. URL: https://doi.org/10.1080/19401493.2013.765506, doi:10.1080/19401493.2013.765506.

B | Appendix B

Dynamic modelling and comparison between transient step response of capacitive hygrometers and chilled mirrors for delay compensation

Ettore Zanetti, Rossano Scoccia, Marcello Aprile, Mario Motta
Department of energy, Politecnico di Milano, 20156 Milan, Italy

Abstract

This manuscript presents the results of an experimental study carried out to evaluate the delay of the transient responses of five capacitive hygrometers with respect to four chilled mirrors. Several experiments were carried out changing the values of air flow rate, temperature, and relative humidity in the test chambers in the RELAB research group facility. The results were used to derive different models of the sensors, that can be used to check and eventually reconstruct data from transient operation of desiccant evaporative cooling heat exchangers. The results show that the chilled mirrors are faster for coupled temperature and relative humidity step changes, while for just a relative humidity change the two instruments perform in a similar fashion. This is due to the inherit dependence of relative humidity from dry bulb temperature.

Key Innovations

- Showcase of the transient response for several capacitive hygrometers and chilled mirrors.
- Implementation of transient signal reconstruction for desiccant heat exchanger humidity profiles.

Practical Implications

This manuscript shows a strategy that can be used to reconstruct delayed relative humidity data, due to a slow sensor response time. The readers willing to implement this methodology must pay particular attention to the identification and validation dataset. Furthermore, the choice of the gain factor K and the implementation of a noise rejecting filter are also very important.

Introduction

Desiccant Evaporative Cooling (DEC) systems have seen an increased interest in academia (Yang, Cui, and Lan 2019) and commercial applications (Beccali et al. 2018) for Heating, Ventilation and Air Conditioning (HVAC) applications. The core components of these systems are the direct or indirect evaporative cooler coupled with a desiccant component. Traditionally the process air goes through a desiccant wheel made of silica gel or other desiccant materials, and after being dehumidified and heated up is cooled via the direct or indirect evaporative cooler (Wu et al. 2018). However, in the last years compact systems that perform the evaporative cooling and the desiccant processes at the same time were developed as shown in (Ge et al. 2008) (Beccali et al. 2018). These new heat exchanger designs do not allow a global steady state operation as in the desiccant wheel case; they are cyclic transient systems where the silica gel first dehumidifies the air moisture until saturation and then it is regenerated so that the cycle can repeat. Precisely measuring the humidity for these devices is important since their energy and water balances rely on this property. In a commercial application, where a humidity sensor is needed for control and monitoring, capacitive hygrometers are commonly employed for cost reasons. When switching between the adsorption and regeneration phase of the cycle, the humidity and temperature changes tend to be faster than the capacitive hygrometers response, leading to a delayed measure. Therefore, the objective of this manuscript is to evaluate what is the impact of the of the delay on the humidity measurement, create a model of the humidity sensor and reconstruct the real humidity profile.

In literature there are several examples on high speed capacitive hygrometer sensor element modelling (Kang and Wise 2000; Tetelin and Pellet 2006) and some experimental studies to better calibrate the sensors in dynamic conditions (Högström, Salminen, and Heinonen 2020). However only a handful of examples are available on humidity data reconstruction from capacitive hygrometers due to delays, for atmospheric data (Wildmann, Kaufmann, and Bange 2014),(Dupont 2020) and human breathing data (Bellitti et al. 2019). The concepts developed in these articles will be applied and expanded to the data from experiments carried out at RELAB (Politecnico di Milano) testing facility. Several experiments were carried out for three air flow rates (100-360-550 kg/h), two values of temperatures (20-30 °C) and two (20-60 %) values of relative humidity. Then the data processing and model identification were carried out using the Matlab ® system identification toolbox to derive a suitable model for the humidity sensors. After, the model can be inverted to reconstruct the output-input relationship.

Methods

Experimental setup

Two climatic chambers, in Figure 1, were used to provide the two different temperature and humidity conditions for the tests.

Figure 1: RELAB 50(kW) climatic chambers to simulate external and internal environments.

These climatic chambers and their measurement instrumentation are certified according to the EN 17025. All the instrumentation is connected to the control panel inside the cambers and then the digital signal travels from the acquisition system to the computer interface on the left of Figure 1. The acquisition time step of each climatic chamber is 2 s.

A total of five capacitive hygrometers and four chilled mirrors were tested to measure humidity together with several PT1000 thermo resistances and T type thermocouples for temperature, one thermo flux meter for air flow rate and a differential pressure sensor. One of the capacitive hygrometers, position 1 in Figure 3, has a lighter metal grid tip, while the others have a heavy-duty metal tip. A picture of the tips is shown in Figure 2.

Figure 2: Capacitive hygrometers tips.

In Table 1 a short summary of the characteristics is reported:

Table 1: Instrumentation parameters.

Instrument	Accuracy	Response time t_{90}
Thermocouples Type T	±0.5 °C	< 3 s
Thermal resistors PT1000	± (0.15+0.002*|T/°C|) °C	Air flow 1m/s 10 s
Capacitive hygrometer EE31	± (1.4 + 1%*mv) % RH	Air flow 1m/s <25 s (Heavy sensor tip) 1m/s <15 s (Grid sensor tip)
Chilled mirror OptiDew Mitchell	±0.2 Dew Point °C T	1°C/s
Chilled mirror S8000 Mitchell	±0.1 Dew Point °C	1.5 °C/s
Thermal flux meter Proline t-mass 65	± 1.5% Mass flow rate (kg/s)	Step change < 30 s
KIMO pressure sensor	± 1.5-2%	Negligible

Two capacitive hygrometers and PT1000 are used to control the conditions in the chamber, the other instruments are placed in a 16 (cm) diameter, 4 (m) long insulated plastic tube as shown in Figure 3.

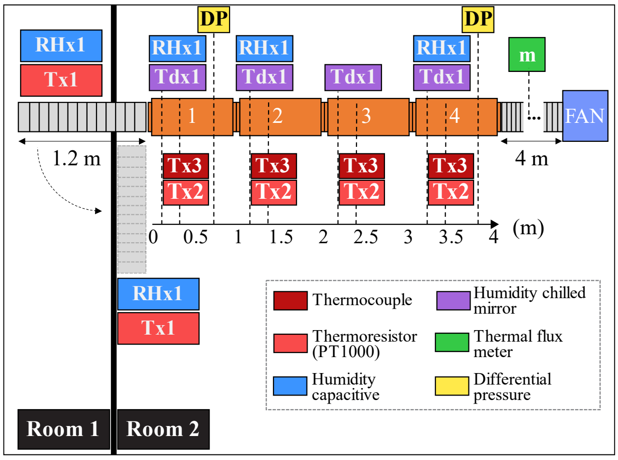

Figure 3: Instruments setup schematics

The x-axis coordinate shows the position with respect to the tube inlet. The designation "xN" tells how many instruments of the same type are present in the same tube section. The tubes are numbered 1 to 4 from the inlet of the first tube.

The climatic chambers are also provided with an absolute barometer used to adjust for ambient pressure together with the differential pressure sensors.

Experimental design

The experiments were designed as a series of step changes between the conditions of the two rooms. As shown in Figure 3, the experimental setup is installed in climatic chamber 2. There is a small aperture between the two chambers where the end of the flexible channel can tightly fit. Two lab technicians were able to move the flexible end of the tube from one measuring point in a chamber to the other in around 1 second, while also sealing or opening the aperture between the two climatic chambers, the fan would suck air inside the duct until a steady state is reached. A total of twelve step change experiments were conducted considering different relative humidity, temperatures, and flow rate as shown in Table 2:

Table 2: Experiments conducted.

Name N(i→j)	T2 (°C)	RH1 (%)	T1 (°C)	RH2 (%)	ṁ (kg/h)
A(1→2)	20±0.2	60±3	20±0.5	20±1.5	100±2
B(2→1)	20±0.2	60±3	20±0.5	20±1.5	100±2
C(1→2)	20±0.2	60±1.5	20±0.5	20±1.5	360±6
D(2→1)	20±0.2	60±1.5	20±0.5	20±1.5	360±6
E(1→2)	20±0.2	60±1.5	20±0.5	20±1.5	550±8
F(2→1)	20±0.2	60±1.5	20±0.5	20±1.5	550±8
G(1→2)	20±0.2	60±1.5	20±0.5	20±1.5	130±2
H(2→1)	20±0.2	20±2.5	30±1.1	20±1.5	100±2
I(1→2)	20±0.2	20±2.5	30±1.1	20±1.5	550±8
L(2→1)	20±0.2	20±2.5	30±1.1	20±1.5	550±8
M(1→2)	20±0.2	20±2.5	30±1.1	20±1.5	360±6
N(2→1)	20±0.2	20±2.5	30±1.1	20±1.5	360±6

The first column indicates the name of the experiment which corresponds to the capital letter, while i→j corresponds to the direction of the step, the tube is moved from chamber i to chamber j. The variable values inside the tables are the mean value of the variable ± two times the standard deviation for each experiment.

Dataset processing

In the first step of the analysis the capacitive hygrometers data are compared with the chilled mirror data. This analysis shows a relative humidity offset between the instruments, Figure 4, even at constant temperature. The capacitive hygrometers tend to overestimate the relative humidity in very dry conditions (T = 20 °C, RH = 20%), while the error gets closer to zero at conditions closer to factory calibration (T = 20 °C, RH = 60%).

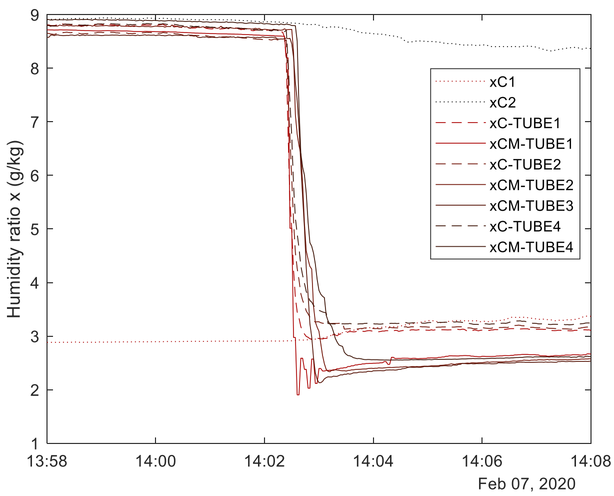

Figure 4: Humidity ratio plot of experiments C and D, dotted lines for the room humidity, dashed lines for the capacitive hygrometers (C) and solid lines for the chilled mirrors (CM)

Therefore, a linear correlation to adjust the capacitive sensors measurements was introduced, by carrying out a linear regression on the mean error in humidity ratio with respect to the relative humidity for all the sensors in all the available experiments as shown in Figure 5.

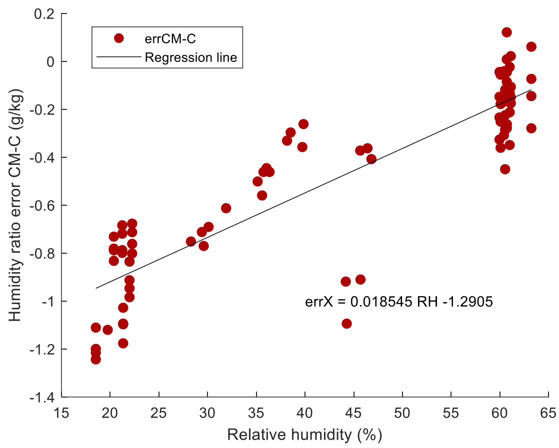

Figure 5: Humidity ratio error between capacitive hygrometer (C) and chilled mirror (CM). The red dots are the mean errors for all the experiments, the black solid line is the regression curve.

The RMSE of the linear regression is 0.17538 (g/kg), while the R^2 is 0.71. The data points between RH = 20% and RH = 60% belong to the experiments shown in Table 2. The other data points were collected in previous unrelated experiments with the same set of instruments in the same climatic chambers.

In Figure 6 the regression curve is applied to the RH measurements.

The second factor to consider is the thermal capacity of the measuring tubes. In experiments H to N there is a 10°C temperature step change, however, the air temperature inside the measuring tubes is affected by their thermal capacity causing a delay in the step experiment. The delay in the temperature change causes an increase in the time response of the capacitive hygrometers. To have a fair comparison with respect to the case at constant temperature, the relative humidity inside the tubes was re-estimated starting from the humidity ratio and the thermocouple temperatures for each part of the tube; under the assumption that the thermocouple is fast enough to catch the real air temperature inside the tubes.

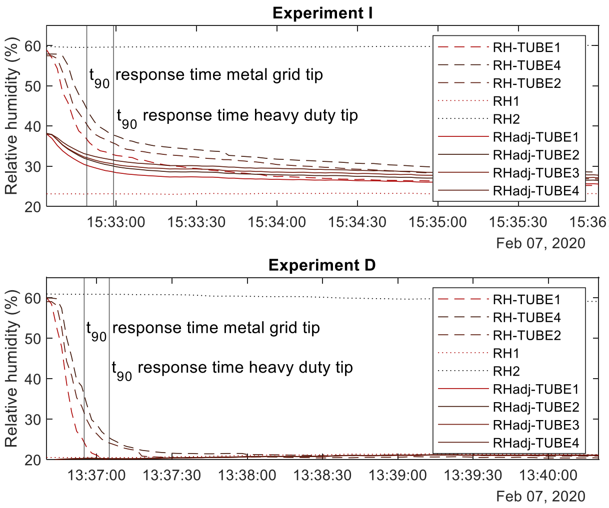

Figure 6: Relative humidity discrepancy due to tubes thermal capacity. RH is the relative humidity measured, RHadj is the adjusted value of the relative humidity.

Looking at Figure 6, once we consider the real relative humidity, *RHadj*, inside the tubes, the t_{90} time response, which is the time that it takes to arrive at 90% of the steady state value, of the capacitive hygrometers is similar in experiments I and D. Furthermore, *RH-TUBE1* time response is faster than *RH-TUBE2 and RH-TUBE4* because of the metal grid tip with respect to the heavy-duty tip.

Changing the flow rate from 100 to 350 and 550 kg/h, which correspond to speeds of 1.1, 4.4 and 6.3 m/s inside the tube does not particularly affect the measurements of the capacitive hygrometers in the experiments at constant temperature A to G, even though for the 100 kg/h experiments we must consider 4 seconds delay for all the air to be displaced inside the tube. Meanwhile in the experiments with a step temperature change, H to N, the smaller flow rate affects the heat exchange inside the tubes leading to a slower thermal response and slower change in the real relative humidity inside the tubes. The chilled mirrors instead could be affected by the change in flow rate if the opening of the sensor is not changed to achieve around ~1 m/s of speed inside the sensor opening. Having a smaller aperture would lead to a slower response time of the sensor, while having a bigger aperture would lead to an initial overshooting of the measurement due to the overcompensation in the internal heat control of the chilled mirror.

Finally, the changes in air properties due the pressure drop inside the tubes is neglected, this is since even at the maximum flowrate, 550 kg/h, the pressure drop is around 19 Pa and therefore the effect can be considered negligible.

Model identification

In (Wildmann, Kaufmann, and Bange 2014) the capacitive hygrometer is modelled as a porous medium where water vapour diffuses using a finite volume approach, the capacitance of the sensor is then function of the moisture content inside the porous media. The equations result in a grey box model where capacitance and diffusivity are the tuning parameters. However, in our case it was not possible to directly acquire the data of the measure capacitance. For this reason, the authors tried several black box models running a batch identification process. Out of all the models tested State Space models (SS) and Autoregressive Regressive eXogeous (ARX) polynomial models resulted in the best performance. The dataset was divided into identification and validation, experiments C, D, M and N were used for validation, a sub dataset of all the others was used for training. A summary of the results inferred from Figure 7 is reported below.

- The plot reports the results of the identification process using different models (empty, filled) and datasets (shape and color). The y-axis reports the model fitness on the validation dataset intended as 100*(1-NRMSE), where NRMSE is the Root Mean Square Error normalized with respect to the norm of the difference between the measured data and the mean of the measured data.
- Higher orders do not improve the accuracy of the model, instead they increase the autocorrelation residuals and the inverse model stability bringing unwanted high frequency components. Therefore, low order models such as one, two and three will be used for the final model.
- Models trained with combined step up and down datasets perform better than only step up or step-down data. The justification is that capacitive hygrometers present a small hysteresis in the adsorption and desorption of water vapour, thus the trained model will correspond to a mean model between the two phases.
- Looking at the empty vs filled shapes state space models seem to perform better with respect to the polynomial models, thus only state space models will be used for the final model.
- Each colour corresponds to a specific identification sub dataset. However, it does not seem that there is a specific correlation between the type of dataset and the quality of the model. This shows that the quality of the experiments is uniform and comprehensive across the overall dataset. However, since capacitive hygrometers have a slight correction of the relative humidity as a function of temperature outside of the 20 °C, shown in (1), the authors preferred to use only experiments from A to G as identification dataset where the temperature is 20 °C, to avoid including the correction correlation in the model.

$$\Delta RH = gRH(T - 20) \tag{1}$$

Where $g = -0.003 \pm 10\%$, RH is the relative humidity measured as a function of the capacitance and T is the measured temperature.

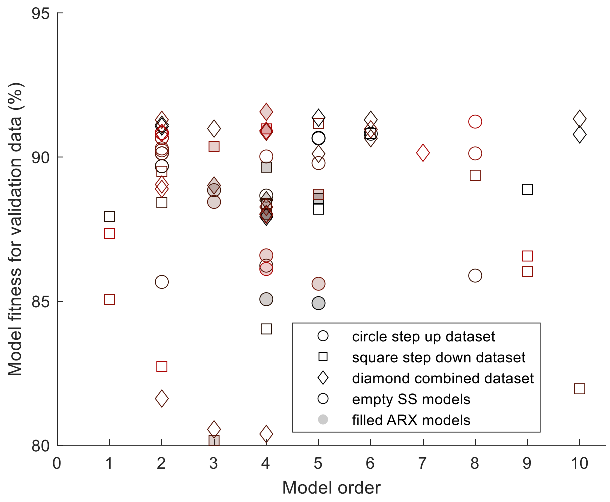

Figure 7: Model fitness (NormalizedRMSE) vs Model order for RH-TUBE2, the colors and shapes correspond to the specific identification set from all the available experiments.

Signal reconstruction

Now a state space model of the form (2-3) can be chosen among the models that have a better performance.

$$\dot{x}(t) = Ax(t) + Bu(t) \quad (2)$$

$$y(t) = Cx(t) + Du(t) \quad (3)$$

Where t is the time, $x(t)$ are the states, $\dot{x}(t)$ their derivatives, u(t) are the inputs and A,B,C and D are the system matrixes. To reconstruct the original signal, the model needs to be inverted to find the relationship output-input. For convenience, the state space model can be converted into a transfer function in the Laplace domain as shown in (4-5) for a single-input single-output SISO model.

$$Y(s) = G(s)U(s) \quad (4)$$

$$G(s) = C(sI - A)^{-1}B + D \quad (5)$$

Where s is the result of the Laplace transform, $Y(s)$ and $U(s)$ are the system output and input in the new coordinates, and I is the identity matrix with the same dimensions as A.

Now the model can be easily inverted according to (6).

$$U(s) = G^{-1}(s)Y(s) \quad (6)$$

Which corresponds to inverting numerator and denominator of the transfer function G.

However, the authors found that the identified models with a good fitting resulted in strictly proper transfer functions, meaning that the order of the denominator is higher than the order of the numerator. This results in an improper inverse transfer function, which cannot be converted back into space-state form and therefore it cannot be directly simulated using only input, but it would require also knowing the derivative of the input (Buchholz and Grunhangen 2008).

There are several ways to avoid estimating the input derivatives (Murray-smith 2011; Buchholz and Grunhangen 2008), the authors tested two typical approaches .

The first one is to append as many high frequency "propening" poles as necessary to make the transfer function proper. This roughly corresponds in coupling the inverted model to a high frequency pass filter. The resulting transfer function, which is the product (7) of the inverted model and the high pass filter, introduces unwanted fast dynamics that can make the system stiff and hard to solve (Murray-smith 2011; Buchholz and Grunhangen 2008).

$$G^*(s) = H(s)G^{-1}(s) \quad (7)$$

Where $H(s)$ is the "propening" transfer function.

The second approach is to invert the original system through a conventional feedback loop and choosing a reasonably high value for the input gain K, as shown in Figure 8. Equation (8) shows the reasoning behind the inversion of the feedback loop.

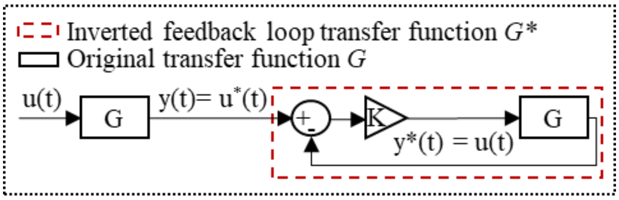

Figure 8: Inverted feedback loop model

$u^*(t)$ corresponds to the humidity read by the sensor, $y^*(t)$ is the output of the feedback loop and corresponds to the reconstructed signal $u(t)$ and G^* corresponds to the inverted transfer function.

$$G^*(s) = \frac{K}{1 - KG(s)} = \frac{K}{1 + K\frac{zeros}{poles}} = \cdots = \frac{Kpoles}{poles + Kzeros} \quad (8)$$

In this way additional poles are added to the denominator making the inverse transfer function proper. This approach is computationally more robust than the previous one, while leading to similar results. The only drawback is the high gain K which makes the inverted model very sensitive to noisy data, therefore care should be taken in the data pre-processing.

Results

From now on all the results will be referred to the capacitive hygrometer RH-TUBE2 in position 2 in the tubes. The identification and model inversion processes are similar for all the humidity sensors.

Sensor model validation

The best model resulted to be a state-space model with two states, the matrix coefficients are reported in (9). To choose this final model the authors screened the models from the results showed in Figure 7. Then took the model with the lowest residual autocorrelation and highest Signal to Noise Ratio (SNR), which where also calculated using Matlab Identification Toolbox.

$$A = \begin{pmatrix} -0.1277 & 0 \\ 0 & -0.00256 \end{pmatrix} \; B = \begin{pmatrix} 0.0019 \\ 0 \end{pmatrix}$$

$$C = \begin{pmatrix} 64.15 \\ -25.66 \end{pmatrix} \; D = (0) \tag{9}$$

The validation with respect to experiments C and D is shown in Figure 9.

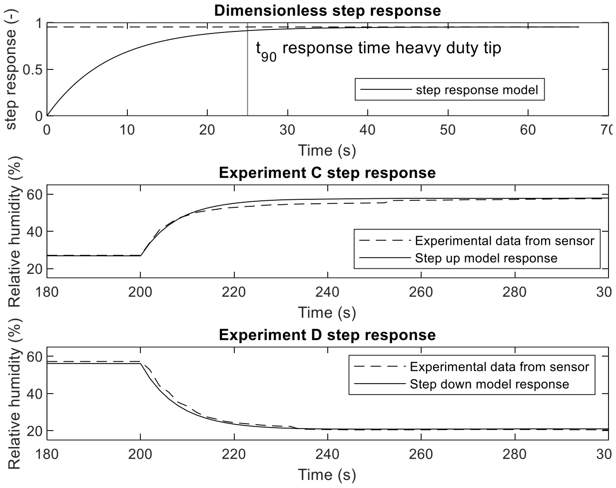

Figure 9: RH-TUBE2 model validation

The plot shows good correspondence between the experimental data and the model output in terms of time response constant, which is slightly smaller than the datasheet value 25 s. The step up and down experiments are also in agreeance with the experimental data, having a Root Mean Square Error (RMSE) of 0.79 % for experiment C and a RMSE of 0.71 % For experiment D, which are well within the instrument tolerance.

Inverse model validation

Once validated the model, it is then converted to a transfer function in accordance to (4-5) and then combined with the gain *K* according to (8) to find the final model. The parameter *K* should be big enough to isolate the poles at the denominator, but not too big to avoid excessive sensitivity to noisy data. After carrying out a sensitivity analysis the gain *K* was chosen to be 40, further increasing the value of *K* does not bring any significant improvement in the results, the impact of K is shown in the signal reconstruction example section. In Figure 10 the validation for the inverted feedback loop model is shown

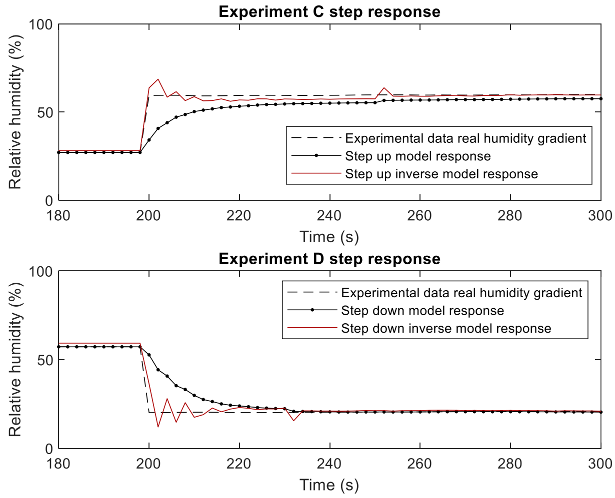

Figure 10: RH-TUBE2 inverse model validation

The inverse model can accurately reconstruct the original data for the step change. However, it does introduce some small nonphysical oscillations in the humidity signal, which can be filtered out with a noise rejecting filter such as a moving average or a Savitzky-Golay filter. Despite the noise introduced the RMSE for both experiments are below the sensor tolerance being 0.9 % for experiment C and 1.4% for experiment D. It is also interesting to notice at 255 s for experiment C and 235 s for experiment D the fact that if the sensor input presents some small noise, it will be amplified by the inverse model. This further confirms the necessity to properly pre-process the data before applying the inverse model.

Signal reconstruction example

Let us assume that the real humidity profile variation in the desiccant heat exchanger cycle is a sinusoidal function of the form (10):

$$RH = 20 \sin\left(\frac{\pi}{60} t\right) + 40\ \% \tag{10}$$

Where *RH* is the real relative humidity and *t* is the time in seconds. By using this as input signal for the model diagram in Figure 8, we obtain:

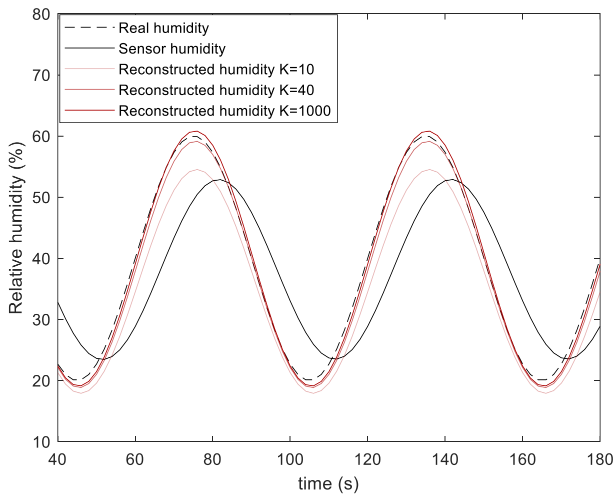

Figure 11: Simulating real humidity profile as sinusoid and reconstruction at different K gain values.

The plot in Figure 11shows that the inverse model can accurately reconstruct the initial sinusoidal humidity signal, the RMSE is 4.2 % for K = 10. 1.2 % for k=40 and 0.97 % for K = 1000 However, if we add ±2% noise, which corresponds to the instrument tolerance, to the real signal the plot in Figure 12 is obtained:

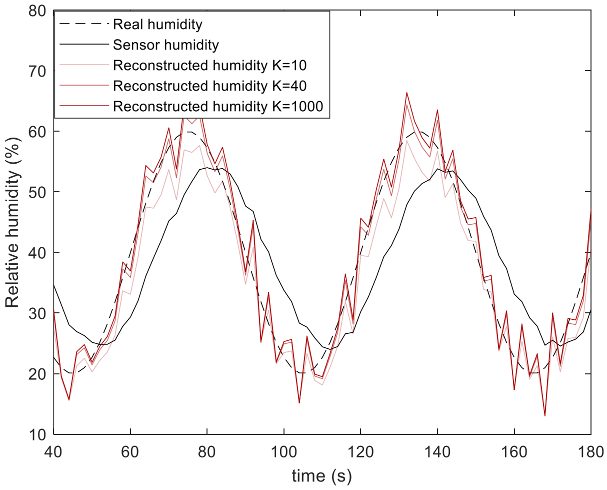

Figure 12: Simulating real humidity profile as sinusoid and reconstruction at different K gain values including ±2% random noise.

In this case the RMSE for K = 10 becomes 4.5 %, 3.9 % for K = 40 and 4.3 for K = 1000. Finally, a Savitzky-Golay filter is added to the noisy signal leading to the final result:

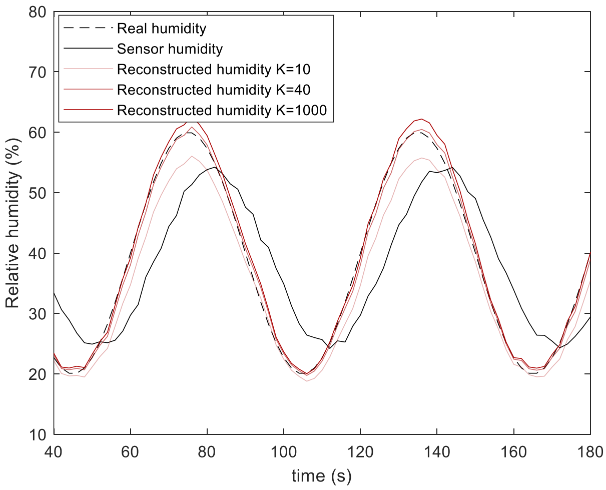

Figure 13: Simulating real humidity profile as sinusoid and reconstruction at different K gain values including ±2% noise and noise rejecting filter.

In this case the RMSE for K = 10 becomes 3.4 %, 1.06 % for K = 40 and 9.6 for K = 1000.

Conclusions

- A total of twelve step humidity change experiments were carried out in the RELAB facility, considering three air flow rates (100-360-550 kg/h), two values of temperatures (20-30 °C) and two (20-60 %) values of relative humidity. A total of five capacitive hygrometers and four chilled mirrors were tested.
- The systematic error of capacitive hygrometers was corrected developing a linear correlation starting from the chilled mirror data.
- A suitable state space model for each sensor was identified and validated against experimental data leading to an average RMSE lower than 1%.
- A feedback loop inversion strategy was applied to reconstruct the original relative humidity profile. The resulting inverted model has an average RMSE lower than 1.5 %.
- The inverted model was tested against a synthetic humidity profile showing a good agreement between the starting profile and the reconstructed one with an RMSE of 1% even in presence of a ±2% random noise.
- The sensitivity analysis on the K value shows the importance in the careful choice of this parameter to balance on one side the quality of the model and on the other the sensitivity to noisy data. Furthermore, a noise rejecting filter is also needed to improve the overall quality of the model output and remove most of the noise amplification.

The developed strategy can now be applied to capacitive hygrometers that are installed in desiccant evaporative air conditioners allowing for an improvement in the transient monitoring of these systems and a more robust humidity driven control without delays.

References

Beccali, Marco, Pietro Finocchiaro, Mario Motta, and Biagio Di Pietra. 2018. “Monitoring and Energy Performance Assessment of the Compact DEC HVAC System ‘Freescoo Facade’ in Lampedusa (Italy).” *Eurosun Conference Proceedings*, 1–8. https://doi.org/10.18086/eurosun2018.04.25.

Bellitti, P, A Bodini, M Borghetti, M Filippini, N Latronico, and E Sardini. 2019. “A Compact Low-Power Wireless System for in Vivo Evaluation of Heat and Moisture Exchanger Performance.”

Buchholz, J, and Wolfgang v. Grunhangen. 2008. *Inversion Impossible ?*

Dupont, JEAN-CHARLES. 2020. “Characterization and Corrections of Relative Humidity Measurement from Meteomodem M10 Radiosondes at Midlatitude Stations.” *Journal of Atmospheric and Oceanic Technology*, 857–71. https://doi.org/10.1175/JTECH-D-18-0205.1.

Ge, T S, Y Li, R Z Ã Wang, and Y J Dai. 2008. “A Review of the Mathematical Models for Predicting Rotary Desiccant Wheel” 12: 1485–1528. https://doi.org/10.1016/j.rser.2007.01.012.

Högström, R, J Salminen, and M Heinonen. 2020. “Calibration of Hygrometers at Non-Static Conditions,” no. Mmc 2019.

Kang, Uksong, and Kensall D Wise. 2000. “A High-Speed Capacitive Humidity Sensor with On-Chip Thermal Reset” 47 (4): 702–10.

Motta, Mario, and Politecnico di Milano. n.d. “ReLab.” http://www.relab.polimi.it/laboratorio/laboratorio/.

Murray-smith, David J. 2011. “Feedback Methods for Inverse Simulation of Dynamic Models for Engineering Systems Applications” 3954. https://doi.org/10.1080/13873954.2011.584323.

Tetelin, Angie, and Claude Pellet. 2006. “Modeling and Optimization of a Fast Response Capacitive Humidity Sensor” 6 (3): 714–20.

Wildmann, N, F Kaufmann, and J Bange. 2014. “An Inverse-Modelling Approach for Frequency Response Correction of Capacitive Humidity Sensors in ABL Research with Small Remotely Piloted Aircraft (RPA),” 3059–69. https://doi.org/10.5194/amt-7-3059-2014.

Wu, X.N., T.S. Ge, Y.J. Dai, and R.Z. Wang. 2018. “Review on Substrate of Solid Desiccant Dehumidification System.” *Renewable and Sustainable Energy Reviews* 82 (February): 3236–49. https://doi.org/10.1016/J.RSER.2017.10.021.

Yang, Yifan, Gary Cui, and Christopher Q Lan. 2019. “Developments in Evaporative Cooling and Enhanced Evaporative Cooling - A Review.” *Renewable and Sustainable Energy Reviews* 113 (May): 109230. https://doi.org/10.1016/j.rser.2019.06.037.

C | Appendix C

Floor heating pre-on/off parameters based on Model Predictive Control feature extrapolation

Ettore Zanetti[a], *Rossella* Alesci[b], *Rossano* Scoccia[c], *Marcello* Aprile[d]

[a] Department of Energy, Politecnico di Milano, Milano, Italy, ettore.zanetti@polimi.it

[b] Department of Energy, Politecnico di Milano, Milano, Italy, rossella.alesci@polimi.it

[c] Department of Energy, Politecnico di Milano, Milano, Italy, rossano.scoccia@polimi.it

[d] Department of Energy, Politecnico di Milano, Milano, Italy, marcello.aprile@polimi.it

Abstract. Floor heating systems are typically characterized by a relatively high thermal inertia, thus they react slowly to setpoint changes. When the system turns on, an under-heating period could occur for a relative long period, vice versa when the setpoint is decreased the floor thermal inertia could lead to overheating. In residential applications, the users try to avoid these discomfort problems by using a constant setpoint, higher than the setback. In this way the average energy consumption as well as the user's bill increases. A smarter solution to mitigate this problem is to include a pre-on period parameter, so that the system will turn on a certain time before the increase in setpoint to avoid the under-heating period and a pre-off period so that it will switch off before overheating. Predictive controllers can be a solution to compensate the slow response of the radiant floor system. However, besides the need for more data, the computational power goes beyond what is available in heating systems micro controllers for residential cases. To avoid these issues, in this paper the optimal control trajectory obtained using a Model Predictive Control (MPC) approach is used to identify the pre-on and pre-off parameters to be periodically updated in the micro controller (e.g. monthly). A simulation work was carried out to compare the performance between a baseline Rule Based Controller (RBC), an improved RBC and a MPC in terms of comfort and energy use. The result is a reduction from an average of 1.1°C to 0.2°C for the worst thermal zone meaning 80% reduction of the discomfort with respect to the baseline and a slight increase of the electrical consumption of the heat pump (less than 5%).

Keywords. Radiant floor, model predictive control, feature extrapolation, pre-heating, KPI.

1. Introduction

HVAC systems account for 20% of the primary energy consumption in MEF countries [1]. Within the perspective of reducing energy consumption and fight climate changes, radiant floor heating applications are becoming more and more used [2]. An important characteristic of standard radiant floor systems is the high thermal inertia which causes a delay between the heat supply and the response in the internal air temperature. For concrete core radiant floors this has been estimated to be 1 to 3 hours [3]. This slow response can create underheating or overheating issues and consequent discomfort and/or waste of energy. In order to assess which are effectively the discomfort periods, the standard EN 12098-1:2017 [4] defines the time and temperature tolerances to guarantee the comfort levels inside the thermal zone.

A solution to compensate the slow response of the radiant floor system and reduce the consequent discomfort could be the use of advanced control strategies such as Model Predictive Control (MPC). The benefit of predictive controllers is that the heat supply can be adjusted in advance thanks to heat demand forecasts [5]. Even if it was proven that MPC can be a good solution to reduce the energy consumption of the HVAC systems, as reported in [6] most buildings today use rule-based controllers to manage the indoor conditions. This is related to the fact that there are different challenges that must be faced to implement MPC in buildings [7] and one of this is the availability of the proper hardware and software infrastructure. For example, model predictive control requires a high computational power that is not available in standard heating systems micro controllers for residential buildings. As reported in [8], MPC can be adopted for complex new commercial buildings while it may not be as solution for residential buildings because it could be too expensive.

This paper proposes a methodology to extrapolate the monthly pre-on and pre-off parameters to be implemented on a micro controller, starting from the results of an optimization problem. This methodology can be deployed as a cloud service, where the pre-on and pre-off parameters can be updated remotely on the micro controller.

This work is part of the Merezzate+ project co-founded by EIT Climate-KIC. The project focuses on sustainability issues from a social, environmental, and economic point of view, adopting measures in the sectors of energy, mobility and circular economy that are the ones with the highest impact on climate change. The project included the construction of around 800 apartments, one of them was chosen as a simulation case study for this work. It is in Milan and is characterized by two rooms and a bathroom. The detailed description is reported in Section 3.

2. Method

An optimal control problem was formulated to obtain the floor heating pre-on and pre-off parameters. In this case, the objective of the optimization problem was to find the control strategy that allows to maximize the comfort of the considered thermal zones.

Starting from the resulting optimal control trajectory, the pre-on and pre-off parameters can be estimated and included in the rule-based controller.

In order to couple the optimization problem with the detailed apartment model at the base of this study, the BOPTEST framework [9] was chosen. It allows to create an API interface between the detailed physics-based model we created using the Modelica Buildings [10] and IBPSA [11] libraries and the optimization problem implemented in a Python code using the Pyomo toolbox [12].

This Section is structured in two sub-sections. In Section 2.1 it has been described the optimization problem and the feature extrapolation. In Section 2.2 it is described the co-simulation environment

2.1 Optimization problem and feature extrapolation

The model predictive control scheme is reported in **Fig. 1**.

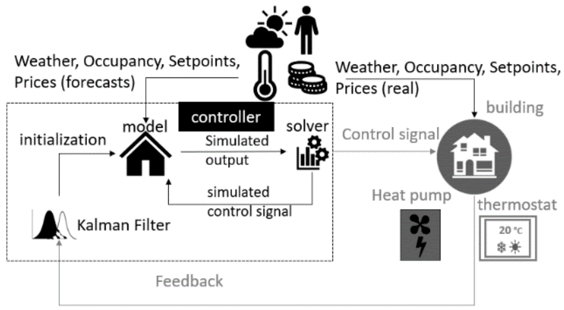

Fig. 1 – Model predictive control scheme.

In order to find the control strategy that allows to achieve the goal, it is necessary to create a simplified model that can capture the correct dynamics of the system. Then, starting from the response of this simplified model subjected to various disturbances (e.g. weather, setpoints, occupation and prices forecasts), the solver calculates the best control trajectory to achieve the "objective function", which is shown in eq. 1. In this case, the forecast is assumed to be deterministic, which means that the forecast adopted during the optimization process is identical to the input of the detailed model of the building. The optimization horizon is 24h and the control signal obtained solving the optimization problem is updated in the detailed model every 15 minutes.

The general form of the objective function can be:

$$\boldsymbol{min\, J_{tot}\,(t)} = \int_{\boldsymbol{t_0}}^{\boldsymbol{t_f}} \sum_{i=1}^{N} k_i J_i(t)\, \boldsymbol{dt} \quad 0 \le k_i \le 1 \qquad (1)$$

Where $J_i(t)$ represents the various objectives and k_i the weighting factor associated with the i-th objective.
In this work, the following combination of objective functions has been adopted:

$$\min \int_{\boldsymbol{t_0}}^{\boldsymbol{t_f}} (k_1 J_1(t) + k_2 J_2(t))\, \boldsymbol{dt} \qquad (2)$$

$$J_1(t) = \left(\left[T_r(t) - \left(T_{setpoint} + \delta\right)\right]^{-}\right)^2 \qquad (3)$$

$$J_2(t) = \frac{\dot{Q}_{hp}(t)}{COP(t)} \qquad (4)$$

Where $J_1(t)$ represents the squared difference between the room air temperature and its setpoint, only in case of under heating. Furthermore, a constant offset δ is added to the setpoint to give a more robust result that will make the parameters work even in a particularly cold day. The value of δ is a tuning parameter that depends on how frequently the pre-on/off parameters will be updated. The solver will try to minimize the differences between these two temperatures to improve the thermal comfort of the users. $J_2(t)$ represents the main electric power needed by the heating system, in this case study represented by a heat pump. In order to minimize this objective, the solver will try to minimize the thermal power $\dot{Q}_{hp}(t)$ but also to maximize the heat pump Coefficient of Performance ($COP(t)$) shifting the heat demand from colder to warmer periods and working at partial load with a lower supply temperature.

The control strategy adopted in this paper tries to maximize the comfort in a specific time interval and to extrapolate some simplified rules to be applied on the energy management system installed in field. The weighting factors adopted in the objective function are $k_1 = 1$ and $k_2 = 0.05$.

The result of the optimization problem described above will be a control that switches on and off the heat pump to guarantee the thermal comfort of the users. Starting from the results of the optimized simulation it is possible to extrapolate some simplified rules that allow to find the pre-on and pre-off parameters to be implemented on a rule-based controller in field. In particular, the pre-on and pre-off parameters are monthly averages. For the months of April and October they take the average only of the days that belong to the heating season, which are respectively the period from the 1st to the 15th for April and the days from the 15th to the 31st for October. They have been obtained starting from the calculation of the supplied energy to the radiant floor distinguishing between the pre-on phase and the normal operation. These two values ($Q_{preheaOPT}$ and Q_{heaOPT}) correspond to the orange and red areas in **Fig. 2**. Then the mean supply heat rate was estimated for the two phases ($\dot{Q}_{meanOn}$ and $\dot{Q}_{meanOff}$). The two areas (orange and red), underneath the thermal power curve, are respectively equal to the areas of the two rectangles, in which the two heights are $\dot{Q}_{meanOn}$ and $\dot{Q}_{meanOff}$ and the two widths are Δt_{On} and $\Delta t_{tot} - \Delta t_{Off}$. Thus, inverting the following formulas, it is possible to obtain the two parameters Δt_{On} and Δt_{Off}:

$$\dot{Q}_{meanOn} = \frac{Q_{preheaOPT}}{\Delta t_{On}} \tag{5}$$

$$\dot{Q}_{meanOff} = \frac{Q_{heaOPT}}{\Delta t_{tot} - \Delta t_{Off}} \tag{6}$$

where Δt_{tot} is the difference of time between the setpoint changes and Δt_{off} is the time difference between the time at which the power goes below a threshold and the lower setpoint change.

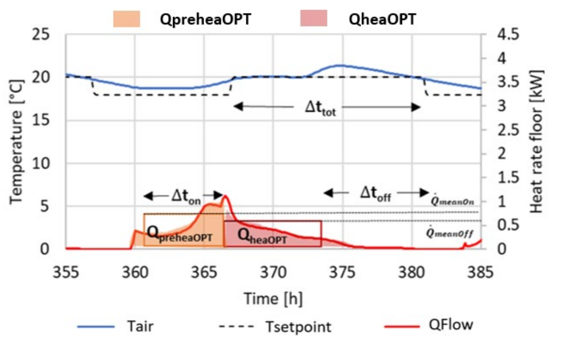

Fig. 2 – Visualization of Δt_{On} and Δt_{Off} calculation procedure.

In this way, starting from the control trajectory it is possible to obtain the two values of Δt_{On} and Δt_{Off} for each pre-on and pre-off and finally calculate the average of these values for each month.

2.2 Implementation

For this work, the Modelica "Buildings" and "IBPSA" libraries were used to develop the detailed model of a three-zone apartment with radiant floor described in Chapter 3.

In particular, for the floor heating modelling, the model called "SingleCircuitSlab" of the "Buildings" library [10] was adopted. It models the radiant slab as a thermal resistance network and uses a fictitious resistance to compute the temperature of the plane that contains the pipes. The same method is implemented in TRNSYS 17 [13]. The rule-based controller used is a tuned PI controller with 0.4 °C hysteresis on the setpoint and a tuned climatic curve on the heat pump supply temperature.
From the detailed model of the building - HVAC system a simplified model was derived through an identification process performed with the MATLAB Identification Toolbox. The simplified model is a grey box, where a thermal electrical analogy is used. This allows to identify a circuit of resistances and thermal capacities (R-C network) to represent the most significant temperatures of the building and HVAC system (**Fig. 3**), starting the identification from the data contained in the detailed model. The methodology followed for the model identification is described in [14]. In summary each thermal zone has a 7R3C circuit and they are all connected to each other.

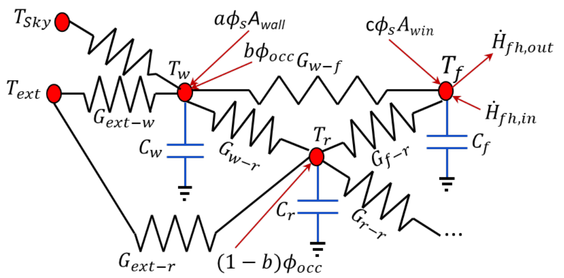

Fig. 3 – R-C network - in red are the temperature nodes T, G_i are the conductances, $\emptyset_i$ are the disturbances (solar, appliances), A_i are the wall and windows area, $\dot{H}$ are the inlet and outlet heat flow rate in the floor and *a,b,c* are the tuning constants.

After this phase, the simplified model and the optimization problem were implemented in Python using the Pyomo toolbox.

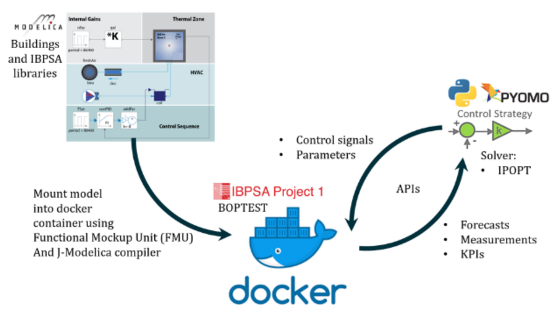

Fig. 4 – Co-simulation environment, on the left the Modelica detailed model and on the right the optimization environment in Python-Pyomo. In between the BOPTEST software is used as a wrapper for the detailed model allowing an API input/output exchange with Python

Finally, the detailed model developed in Modelica interfaces with the optimization problem through the BOPTEST framework. The BOPTEST framework allows a way to easily compile the detailed Modelica model and wrap it around a Docker container. In this way the model can freely run through an easy-to-use API interface, that can be used to obtain sensor signals from the detailed model and provide control trajectories from the optimization routine in Python through APIs.

All these steps are summarized in **Fig. 4.**

3. Case study

The case study chosen for this work is a two rooms one bathroom apartment reported in **Fig. 5**. It is in Milan (Italy) and shares two walls with two adjacent apartments (in green), a wall with the landing (in red) while the rest faces towards outside (in yellow).

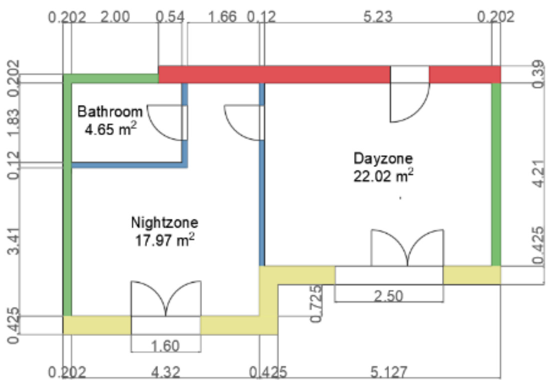

Fig. 5 – Floor Plan of apartment

It is equipped with an air source heat pump, a radiant floor, a DHW tank and PV panels installed on the roof of the building. The heat is used for both space heating and DHW production, giving priority to the latter. The most important characteristics of the above-mentioned system are reported in **Tab. 1**.

Tab. 1 – Characteristics of the system.

Parameter	Value and unit of measurement
Floor area	44.45 m²
Zones height	2.7 m
Number of occupants	1
HP nominal electrical power	1.33 kW*
HP nominal thermal power	4 kW*
PV panels area	5.5 m²
PV panels peak power	0.8 kWp

*Nominal conditions (-7°C, 35°C)

For the simulation of the considered apartment, the occupation profiles were arranged as shown in **Fig. 6** and **Fig**. **7**. The first one is used for all the weekdays, while the other is used to simulate the weekends.

The other input data chosen for these simulations are function of the above-described occupation profiles. In particular, a setpoint temperature of 20°C has been chosen for occupied periods, while a setback temperature of 18°C is applied for the rest of the considered day. In the same way the shading systems of each room are fully closed when it is unoccupied while they are half opened when the considered room is occupied.

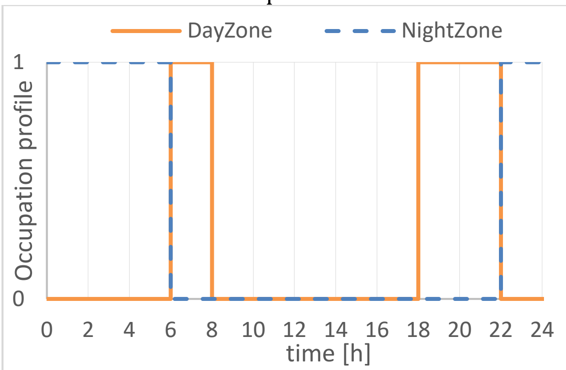

Fig. 6 – Occupation profile weekdays

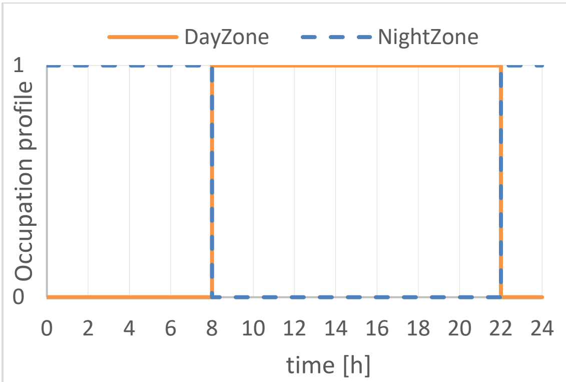

Fig. 7 – Occupation profile weekend

In addition, there are the internal gains related to the presence of people, appliances, and lighting.

Specifically, the sensible internal gain due to the presence of people is defined per person while the others are defined per unit area.

In this case study the following values have been chosen:

$$\dot{Q}_{sens} = 60\frac{W}{pers} \tag{7}$$

$$\dot{Q}_{appliances} = 2.5\frac{W}{m^2} \tag{8}$$

$$\dot{Q}_{lighting} = 4\frac{W}{m^2} \tag{9}$$

In particular, the sensible heat produced by a person respects the standard UNI EN 13779 [15] while the other two values are due to specific assumptions. In fact, since the apartment is small and new, the authors considered to have few and efficient appliances. In addition, they chose led lamps that emit a thermal power of about 80 W for each thermal zone.

In this case, only one user is present inside the apartment as reported in **Fig. 6** and **Fig**. **7**.

All these contributions are different than zero only when the considered thermal zone is occupied. In addition, the lighting contribution is set to zero from 8 a.m. to 5 p.m. thanks to daylight availability.

Finally, the parameters related to the mass exchange with the external environment are summarized in **Tab. 2**. In particular, the value of the air changes related to infiltrations has been chosen considering high quality windows while the value related to mechanical ventilation takes into account the sanitary regulation of the Municipality of Milan [16] which imposes at least 20 m3/h/pers. In this case it was chosen to apply 30 m3/h/pers and 24 m3/h/pers respectively for the DayZone and the NightZone.

Tab. 2 – Infiltration and mechanical ventilation

Air changes	DayZone	NightZone
Infiltrations [1/h]	0.05	0.05
Mechanical ventilation [1/h]	0.5	0.5

4. Results

For this work, three different simulations were performed: a first simulation with a normal rule-based control (baseline), a second simulation based on model predictive control and a final simulation with a rule-based control with pre-on and pre-off parameters obtained averaging the results of the second simulation.

In Section 4.1 are reported the pre-on and pre-off parameters obtained from the calculations described in Section 2.1. In section 4.2 it is possible to observe which are the effects of the activation of the pre-on and pre-off strategies on the air temperature and the thermal power delivered by the heat pump in the three cases, while in Section 4.3 are summarized the Key Performance Indicators (KPI) of the three simulations.

4.1 Monthly pre-on and pre-off parameters

The results of the calculation reported in detail in section 2.1 are summarized in **Tab. 3** and **Tab. 4**. In particular, in the DayZone (**Tab. 3**), the pre-on is not required for the periods that go respectively from the 1st to the 15th of April and from the 15th to the 31st of October.

Tab. 3 – Average values for pre-on and pre-off parameters in the DayZone

Period	Pre-on [h]	Pre-off [h]
1st-31st Jan	1.56	0.00
1st-28th Feb	1.22	0.00
1st -31st Mar	0.20	0.20
1st-15th Apr	0.00	1.30
15th-31st Oct	0.00	0.60
1st-30th Nov	0.80	0.10
1st-31st Dec	1.40	0.10

Tab. 4 – Average values for pre-on and pre-off parameters in the NightZone

Period	Pre-on [h]	Pre-off [h]
1st-31st Jan	4.00	0.20
1st-28th Feb	3.60	0.30
1st -31st Mar	3.00	1.70
1st-15th Apr	2.20	2.20
15th-31st Oct	1.00	1.90
1st-30th Nov	2.60	0.80
1st-31st Dec	3.40	0.20

4.2 Time series analysis

To understand the benefits related to the application of the pre-on and pre-off strategies, in this section a detailed analysis of two days is shown (Friday, 19th of January and Saturday, 20th of January).

In **Fig. 8** and **Fig. 9** are represented the trend of the air temperature with respect to the setpoint respectively in the DayZone and NightZone, while in **Fig. 10** is reported the trend of the thermal power provided by the heat pump to heat up the two thermal zones.

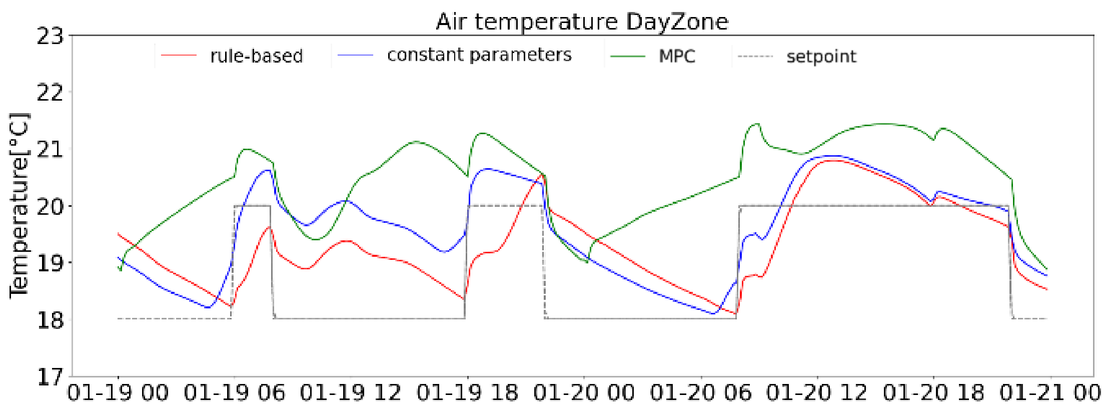

Fig. 8 – DayZone air temperature trend for sample days including weekend

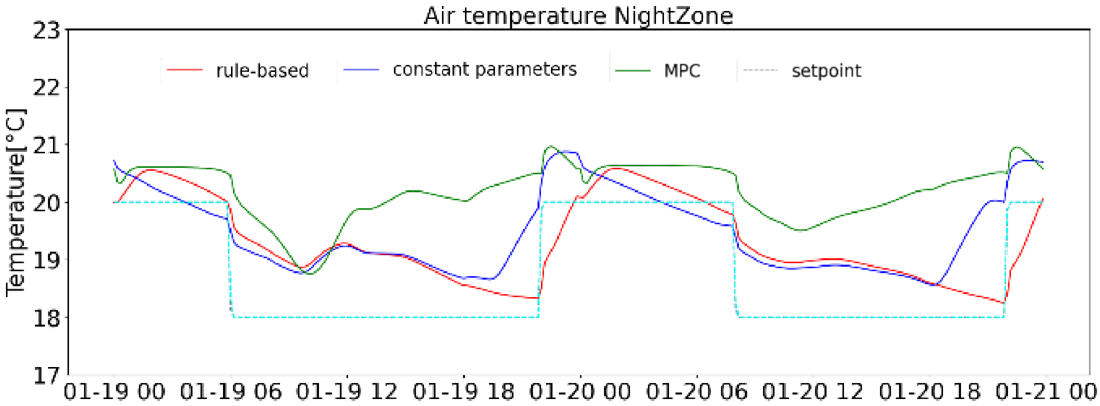

Fig. 9 – NightZone air temperature trend for sample days including weekend

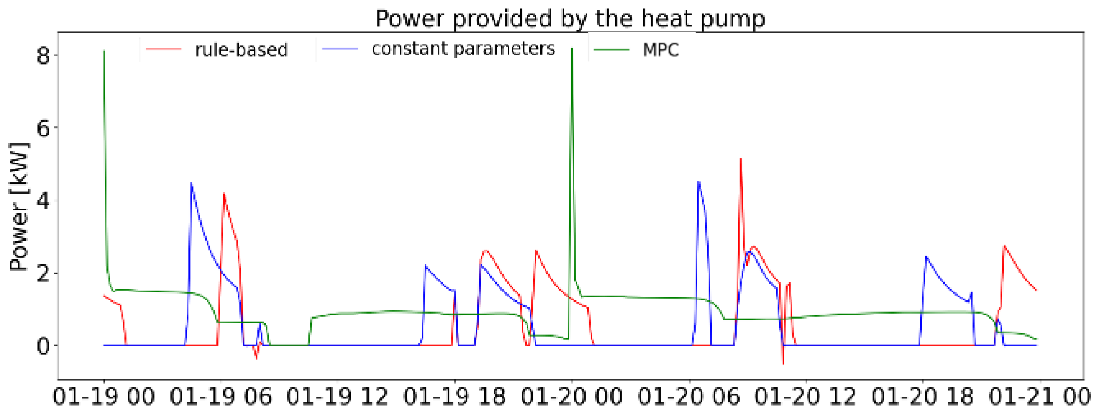

Fig. 10 – Thermal power provided by the heat pump for sample days including weekend

From the first two figures (**Fig. 8** and **Fig. 9**) it can be seen that, while with the normal rule-based control (represented by the red line) the temperature reaches the desired setpoint after about 3 hours, the rule-based control with the pre-on and pre-off parameters (blue curves) is able to follow the change of the setpoint, reducing a lot the periods of discomfort that occur in the baseline case. Finally, from the same graphs it is visible that the temperature obtained with the model predictive control strategies is consistently higher than the setpoint. This is done because the MPC is targeting the setpoint temperature plus δ °C to have a more conservative result when finding the pre-on and pre-off parameters. The big gap between the rule-based and the other controllers can be explained by the fact that in this simulation the baseline rule-based controller turns on the heat pump when the difference between the room and setpoint temperature is lower than minus the hysteresis value. This control strategy will inevitably lead to underheating. So, what expert users usually do is manually insert a pre-on / pre-off parameter based on experience. Less expert users instead will keep the systems always on, leading to a big waste of energy.

Then, from **Fig. 10**, it is clearly visible that the thermal power provided by the heat pump, in the case of application of the pre-on and pre-off strategy (blue line), has been anticipated (shifted towards left) with respect to the normal rule-based control (red line), while MPC keeps the system on for a longer period at a lower mean power. This is due to the fact that, as reported in eq. 1, the objective function not only promote the thermal comfort achievement but also tries to reduce the electric power consumption.

4.3 KPIs analysis

Finally, some Key Performance Indicators (KPI) were defined with the aim of evaluating the overall performance of the advanced control strategies.

In particular, the KPI related to the discomfort of the i-th thermal zone (Dis_{TZi}) is defined as the integral of the difference between the setpoint ($T_{set,i,TZi}$) and the room air temperature ($T_{air,i,TZi}$) for the heating season (from the 15th of October to the 15th of April), subdivided for the number of occupied hours ($n_{occ\ hours}$) in the same period. The integral at the numerator is calculated only in the occupied hours of each day and only when the indoor air temperature is lower than the setpoint temperature minus the hysteresis ($hys = 0.4°C$), as reported below:

$$Dis_{TZi} = \frac{\int_{t_0}^{t_f} \left|T_{set,i,TZi} - hys - T_{air,i,TZi}\right|^{+} dt}{n_{occ\ hours}} \quad (10)$$

Then it is reported the average air temperature ($T_{airAvg,TZi}$) of each thermal zone calculated considering the entire heating season and the related thermal energy need ($E_{th,SH}$) that has to be provided by the heat pump in order to maintain those conditions inside the various thermal zones. They are mathematically expressed as:

$$T_{airAvg,TZi} = \frac{\sum_{j=1}^{N} T_{air,j,TZi}}{N} \quad (11)$$

$$E_{th,SH} = \int_{t_0}^{t_f} \dot{Q}_{th,SH}(t)\, dt \quad (12)$$

Where:

- $T_{air,j,TZi}$ is the air temperature of the thermal zone TZi registered at the j-th time;
- N is the number of elements of the temperature vector during the heating season;
- $\dot{Q}_{th}$ is the thermal power provided by the heat pump for space heating at a specific time.

Finally, it is introduced a KPI which describes the electrical energy consumption of the heat pump ($E_{el,SH}$) for providing heat to the radiant floor (space heating), that is equal to:

$$E_{El,SH} = \int_{t_0}^{t_f} \dot{P}_{el,SH}(t)\, dt \quad (13)$$

Where:

- $P_{el,SH}$ is the electrical power consumption of the heat pump for space heating at a specific time.

The summary of these KPIs is reported in **Tab. 5**.

Analysing the values reported in **Tab. 5** it appears that the value of the discomfort related to the DayZone in the Baseline case is equal to 1.104 K, which is already a low value, but it is still higher than the temperature tolerance, which is fixed to $\pm 0.5K$, as reported in the standard EN 12098-1:2017 [4]. Thus, with the use of the optimized control (PreOnOff Const and PreOnOff Var), the authors were able to respect this tolerance and to obtain a strong percentage reduction of the discomfort, higher than the 80%. For the NightZone, as it is possible to observe from **Tab. 5** the Baseline was already able to respect the above-mentioned tolerance, but the percentage reduction of the discomfort is still important.

In addition, the results in **Tab. 5** show that the optimized rule-based controller, with constant pre-on and pre-off parameters (PreOnOff Const), has comparable performance with respect to the results of the model predictive control (PreOnOff Var).

Tab. 5 – KPI comparison.

KPI	Baseline	PreOnOff Const	PreOnOff Var
$Dis_{DayZone}$ [K]	1.104	0.191 (-83%)	0.006 (-99%)
$Dis_{NigZone}$ [K]	0.155	0.006 (-96%)	0.011 (-93%)
$T_{airAvg,DayZone}$ [°C]	19.7	20.0 (+1.5%)	20.9 (+6.1%)
$T_{airAvg,NigZone}$ [°C]	19.6	19.8 (+1.0%)	20.4 (+4.1%)
$E_{th,SH}$ [kWh]	1758	1808 (+2.8%)	2874 (+63.5%)
$E_{El,SH}$ [kWh]	437	455 (+4.0%)	672 (+53.6%)

The average air temperature increases of the 1-1.5% in the case with monthly constant parameters and of the 4-6% in the case of variable parameters (MPC). The increase of temperature obviously leads to an increase of the thermal energy needs and consequently of the electrical consumptions of the heat pump.

This methodology can be deployed as a cloud service, where the pre-on and pre-off parameters can be updated remotely. In the Merezzate+ project some apartments could be used for testing the methodology. In terms of economic feasibility, it can be used for large residential complexes where the building envelope and HVAC systems can be modelled once and tweaked using data, introducing an economy of scale. For smaller residential buildings archetypes can be built and modelled, where the solution may not be optimal but still better than the baseline.

5. Conclusions

In this paper it is proposed a methodology to extract pre-on and pre-off parameters that can be implemented in micro-controllers of residential buildings. This could help managing the radiant floor heating system and solve the problems of discomfort that could be caused by its slow response.

From the control trajectory obtained solving the optimization problem, some simplified rules were extrapolated. They allow to obtain the monthly pre-on and pre-off parameters to be implemented in the energy management system installed in field thanks to a cloud service.

Then, three simulation that consider respectively a normal rule-based control, model predictive control and a rule-based control with monthly pre-on and pre-off parameters have been performed. Comparing the results of the three simulations it is possible to observe that with both the constant and variable (MPC) pre-on and pre-off parameters, the time in which the air temperature is below the setpoint is strongly reduced and this is also confirmed by the KPI of the discomfort, that undergoes a reduction higher than the 80%. For the future development of this work, the authors will consider different feature extrapolation methods. Instead of monthly, the pre-on/pre-off parameters could be updated with a different frequency. Furthermore, depending on the sensors available locally or cloud forecast different heuristic metrics will be developed.

6. Acknowledgement

The research work presented in this paper receives the support of EIT Climate-KIC through the project "Merezzate+" and REDO sgr spa.

7. References

[1] I. E. A. B. E. P. Metrics. Supporting Energy Efficiency Progress in Major Economies. Int. Energy Agency Paris, Fr., 2015.

[2] Olesen B. W. Radiant Floor Heating In Theory and Practice. no. July, pp. 19–24, 2002.

[3] Zhao K., Liu X., and Jiang Y. Dynamic performance of water-based radiant floors during start-up and high-intensity solar radiation. Sol. Energy, vol. 101, pp. 232–244, 2014.

[4] EN 12098-1:2017 Energy Performance of Buildings - Controls for heating systems Part 1: Control equipment for hot water heating systems - Modules M3-5, 6, 7, 8

[5] Karlsson H. and Hagentoft C. Application of model based predictive control for water-based floor heating in low energy residential buildings. Build Environ, vol. 46, pp. 556–569, 2011.

[6] Drgoňa J. et al. All you need to know about model predictive control for buildings. Annual Reviews in Control, vol 50, pp 190-232, 2020.

[7] Cigler J. et al. Beyond theory: the challenge of implementing Model Predictive Control in buildings. Proceedings of 11th rehva world congress, Clima, Prague, Czech Republic.

[8] Thieblemont H. et al. Predictive control strategies based on weather forecast in buildings with energy storage system: A review of the state-of-the art Energy and Buildings, vol. 153, pp. 485–500, 2017.

[9] Blum D. et al. Building optimization testing framework (BOPTEST) for simulation-based benchmarking of control strategies in buildings. J. Build. Perform. Simul., vol. 14, no. 5, pp. 586–610, 2021.

[10] Wetter M., Zuo W., Nouidui T. S., and Pang X. Modelica Buildings library," J. Build. Perform. Simul., vol. 7, no. 4, pp. 253–270, 2014.

[11] M. Wetter M., D. Blum D., J. Hu J., and USDOE, "Modelica IBPSA Library v1," 2019.

[12] Bynum M. L. et al. Pyomo--optimization modeling in python. Third., vol. 67. Springer Science \& Business Media, 2021.

[13] Thermal Energy System Specialists, LLC. TRNSYS 17 a TRaNsient SYstem Simulation program Multizone Building modeling with Type56 and TRNBuild Vol. 5, Madison USA.

[14] Zavaglio E., Scoccia R., and Motta M. RC Building Modelling for Control Purposes: A Case Study. Build. Simul. Appl. BSA 2017, 2017.

[15] UNI EN 13779 Requisiti di prestazione per i sistemi di ventilazione e di climatizzazione

[16] "Regolamento locale d'igiene, Comune di Milano", December 2012.

8. Data access statement

The datasets generated and analysed during the current study are available in the Zenodo repository, https://zenodo.org/record/6398238#.YkVWfOdByUI

List of Figures

List of Tables

List of Symbols

Variable	Description	SI unit
$\boldsymbol{T}$	Temperature	(°C or K)
$\boldsymbol{RH}$	Relative Humidity	(%)
$\boldsymbol{x}$	Thickness	(m)
$\boldsymbol{k}$	Thermal conductivity	(W/mK)
$\boldsymbol{c}$	Specific heat	(J/kgK)
$\boldsymbol{d}$ or $\boldsymbol{\rho}$	density	(kg/m^3)
$\boldsymbol{C}$	Heat Capacity	(J or kJ)
$\boldsymbol{\Phi}$	heat flux	(W/m^2)
$\boldsymbol{A}$	Area	(m^2)
$\dot{\boldsymbol{H}}$	Enthalpy flow	(W)
$\boldsymbol{\Delta}$	indicates a difference	(-)
$\boldsymbol{u}$	indicated a control or disturbance	(-)
$\dot{\boldsymbol{Q}}$	Heat rate	(W or kW)
$\dot{\boldsymbol{m}}$	Mass flow rate	(kg/s)
$\mathbb{R}$	Real Numbers	(-)
$\mathbb{Z}$	Integer Numbers	(-)
$\boldsymbol{p}$	price	(EUR)
$\boldsymbol{x}$	Humidity ratio	(kg_w/kg_{dair})
$\boldsymbol{h}$	Specific enthalpy	(J/kgK)
$\boldsymbol{h_c}$	Convective heat transfer coefficient	(W/m^2K)
$\boldsymbol{Nu}$	Nusselt number	(-)
$\boldsymbol{Re}$	Reynolds number	(-)
$\boldsymbol{\lambda}$	thermal conductivity	(W/mK)
$\boldsymbol{Pr}$	Prandtl Number	(-)
$\boldsymbol{D}$	Diameter	(m)
$\boldsymbol{W}$	Water uptake	(kg_w/kg_{sigel})
$\boldsymbol{q}$	Specific heat rate	(W/m^2)

List of Acronyms

Acronym	Description
AHU	Air Handling Unit
API	Application Programming Interface
CFD	Computational Fluid Dynamics
COP	Coefficient of Performance
DEC	Desiccant Evaporative Cooling
DH	District Heating
EER	Energy Efficiency Ratio
FREESCOO	FREE Solar COOling
HVAC	Heating Ventilation and Air Conditioning
HX	Heat Exchanger
KPI	Key Performance Indicator
LP	Linear Programming
MEF	Major Economic Forum
MILP	Mixed Integer Linear Programming
MINLP	Mixed Integer NonLinear Programming
MIQP	Mixed Integer Quadratic Programming
MPC	Model Predictive Control
NLP	NonLinear Programming
NMRSE	Normalized Root Mean Square Error
PV	PhotoVoltaic
QP	Quadratic Programming
RC	Resistance Capacitance